

1995

Experimental and Numerical-Modeling Studies of a Field-Scale Hazardous Waste Rotary Kiln Incinerator.

Allen Lee Jakway
Louisiana State University and Agricultural & Mechanical College

Follow this and additional works at: https://digitalcommons.lsu.edu/gradschool_disstheses

Recommended Citation

Jakway, Allen Lee, "Experimental and Numerical-Modeling Studies of a Field-Scale Hazardous Waste Rotary Kiln Incinerator." (1995). *LSU Historical Dissertations and Theses*. 6110.
https://digitalcommons.lsu.edu/gradschool_disstheses/6110

This Dissertation is brought to you for free and open access by the Graduate School at LSU Digital Commons. It has been accepted for inclusion in LSU Historical Dissertations and Theses by an authorized administrator of LSU Digital Commons. For more information, please contact gradetd@lsu.edu.

INFORMATION TO USERS

This manuscript has been reproduced from the microfilm master. UMI films the text directly from the original or copy submitted. Thus, some thesis and dissertation copies are in typewriter face, while others may be from any type of computer printer.

The quality of this reproduction is dependent upon the quality of the copy submitted. Broken or indistinct print, colored or poor quality illustrations and photographs, print bleedthrough, substandard margins, and improper alignment can adversely affect reproduction.

In the unlikely event that the author did not send UMI a complete manuscript and there are missing pages, these will be noted. Also, if unauthorized copyright material had to be removed, a note will indicate the deletion.

Oversize materials (e.g., maps, drawings, charts) are reproduced by sectioning the original, beginning at the upper left-hand corner and continuing from left to right in equal sections with small overlaps. Each original is also photographed in one exposure and is included in reduced form at the back of the book.

Photographs included in the original manuscript have been reproduced xerographically in this copy. Higher quality 6" x 9" black and white photographic prints are available for any photographs or illustrations appearing in this copy for an additional charge. Contact UMI directly to order.

UMI

A Bell & Howell Information Company
300 North Zeeb Road, Ann Arbor MI 48106-1346 USA
313/761-4700 800/521-0600

**EXPERIMENTAL AND NUMERICAL-MODELING STUDIES
OF A FIELD-SCALE HAZARDOUS WASTE
ROTARY KILN INCINERATOR**

A Dissertation

Submitted to the Graduate Faculty of the
Louisiana State University and
Agricultural and Mechanical College
in partial fulfillment of the
requirements for the degree of
Doctor of Philosophy

in

The Department of Mechanical Engineering

by
Allen Lee Jakway
B.S., University of New Orleans, 1985
December 1995

UMI Number: 9618300

UMI Microform 9618300
Copyright 1996, by UMI Company. All rights reserved.

**This microform edition is protected against unauthorized
copying under Title 17, United States Code.**

UMI
300 North Zeeb Road
Ann Arbor, MI 48103

ACKNOWLEDGMENTS

The author would like to express his gratitude to a cast of people who made this research possible. First, the author is grateful to Dr. Vic A. Cundy whose invaluable guidance, determination, encouragement, and personal sacrifice were instrumental in making this project possible. Dr. Arthur M. Sterling also provided clear direction and meaningful advice throughout the author's research effort. Finally, the author's graduate committee, composed of Drs. Robert W. Courter (who helped bring him to L.S.U.), Dimitris E. Nikitopoulos, Tryfon T. Charalampopoulos, and Robert Hammer, has contributed suggestions and advice to enhance the quality of this research.

Additionally, the author would like to thank several other people at L. S. U. for their contributions to this research. First, the friendship, support and technical expertise given by co-workers and co-authors Dr. Christopher B. Leger, Dr. Charles A. Cook, and Mr. Alfred N. Montestruc, are appreciatively acknowledged. Second, the author is extremely grateful for the very capable assistance in assembling and executing research experiments generously supplied by Mr. Rodger Conway, Mr. Daniel Farrell, and Ms. Jodi Roszell. Third, use of computer facilities made available through the Advanced Workstation Laboratory, headed by Dr. Robert McIlhenny and run by Mr. George Ohrberg, is greatly appreciated. Fourth, computer support lent by Ms. Gabriela Segarra, Mr. Alaric Haag, Mr. Myles Prather, and Dr. David Koonce was essential to the completion of this project. Finally, the support offered by Dr. Louis J. Thibodeaux, Director of the Hazardous Substance Research Center South and Southwest at Louisiana State University, is appreciated.

The author is also grateful to several other specialists outside of the L.S.U. community for their support of this combustion and modeling research. First, the author's brief, but highly educational, pilot-scale kiln research effort at the University of Utah was made possible and fruitful by Dr. Warren D. Owens, Dr. David W. Pershing, Dr. JoAnn S. Lighty, and Mr. David Wagner. Second, Drs. Christopher B. Leger of Praxair, Inc. and Joseph D. Smith of The Dow Chemical Company provided insight to the research through their vast experience in modeling rotary kilns. Third, Drs. Louis A. Gritzko, Sheldon R. Tieszen, Russell D. Skocypec, and Mr. Jaime L. Moya of Sandia National Laboratories and Dr. Tim Tong (Arizona State University) hosted a summer internship in Albuquerque N. M. during which the author received a crash course in soot modeling, among other combustion topics, relevant to this research. Fourth, the author gratefully acknowledges the assistance and cooperation of both the Michigan and Louisiana Divisions of The Dow Chemical Company and several of its employees, namely Mr. Tony Brouillette, Mr. Jonathan Huggins, Mr. Scott Mancroni, Mr. J. J. Hiemenz, and Mr. Chuck Lipp, who facilitated the field testing portions of this work.

Of course, none of this research would have been possible without financial resources. Funding of this research was provided by The State of Louisiana Board of Regents, the Department of Mechanical Engineering, The Dow Chemical Company, and The Louisiana Mining and Mineral Resources Research Institute.

Most importantly, the author is grateful to his family and friends for their encouragement, support, and patience while he focused on obtaining the degree associated with this dissertation. This is especially true of Ms. Jennifer Savoie.

TABLE OF CONTENTS

ACKNOWLEDGMENTS	ii
NOMENCLATURE	vii
ABSTRACT	xi
CHAPTER	
1 INTRODUCTION	1
Establishing Common Ground	1
Why Incinerate Waste: The Hierarchy of Waste Handling	4
Description of General Incineration Facilities	7
2 LITERATURE REVIEW	11
Numerical Modeling: An Overview	11
Numerical Kiln Models	15
Zonal Models	16
Navier-Stokes Solvers	19
Summary of Numerical Models	25
Field-Scale Incineration: Experimental Studies	26
Introduction	26
Review of literature	28
Summary of Experimental Field-Scale Incineration Studies	37
3 RESEARCH GOALS AND OBJECTIVES	38
Overall Program Goals	38
Specific Research Objectives	40
Field-Scale Experimental Objectives	40
Numerical Modeling Objectives	41
4 <i>IN SITU</i> VELOCITY MEASUREMENTS FROM AN INDUSTRIAL ROTARY KILN INCINERATOR	42
Implications	42
Introduction	42
Background	43

Apparatus Overview	46
Velocity Probe	46
Pressure Transducer	48
Suction Pyrometer	48
Boom	48
Boom Positioning Rack	50
Experimental Method	51
Results	52
Mean Velocity and Temperature Data	52
Mass Flow Study	59
Numerical Model	63
Summary	64

**5 THREE-DIMENSIONAL NUMERICAL MODELING OF
A FIELD-SCALE ROTARY KILN INCINERATOR 67**

Introduction	67
Physical System	68
Numerical Kiln Model	71
Solution Method	71
Geometry Details	72
Grid Details	74
Fluid Physical Properties	76
Radiation	76
Chemical Reactions	78
Boundary Conditions	81
Results	83
Model Verification	88
Validation I – Comparisons with Experiment (Leger et al., 1991a, 1993a, 1993b) and the Predecessor Model (Leger et al., 1993c)	90
Validation II – Comparisons with experiment Jakway et al. (1995a, 1995b)	93
Validation III – Grid Dependency Study	95
Parametric and Sensitivity Studies	99
Distribution of Unmetered Infiltration Air	99
Effects of Radiation, Soot, and Adiabatic Walls	103
Summary	105

**6 SUMMARY, CONCLUSIONS, AND
RECOMMENDATIONS 107**

Summary	107
Experimental Velocity and Temperature Measurements	107
Numerical Model of Rotary Kiln Incinerator.....	109
Conclusions	110

Recommendations For Further Work	111
Experimental	112
Numerical Modeling	112
BIBLIOGRAPHY	115
APPENDICES	123
A PUBLISHING INFORMATION ON CHAPTER 4	123
Publishing Permission Letters	123
Reviewers Comments	126
B PROBE BOOM CONSTRUCTION	128
C BOOM POSITIONER	139
D DETAILED REVIEW OF MODELING BY LEGER ET AL. (1993C)	140
E KILN WALL HEAT LOSS CALCULATIONS	146
F COMPUTER CODE FOR RADIATION USER SUBROUTINE	147
G GOVERNING DIFFERENTIAL EQUATIONS USED IN THE NUMERICAL MODEL	179
H NUMERICAL MODEL BOUNDARY CONDITIONS AND MISCELLANEOUS SOLUTION INFORMATION	182
Key For The Listing of The Numerical Model Specifications	182
1) TA-on, coarse grid, data from Jakway et al. (1995a, 1995b)	182
2) TA-on, refined grid, data from Jakway et al. (1995a, 1995b)	196
3) TA-off, coarse grid, data from Jakway et al. (1995a, 1995b)	203
4) TA-on, coarse grid, data from Leger et al. (1991a, 1993a, 1993b)	206
5) TA-off, coarse grid, data from Leger et al. (1991a, 1993a, 1993b)	209
VITA	212

NOMENCLATURE

ROMAN SYMBOLS

C	calibration coefficient for velocity probe
D	inside diameter of kiln
D_a	Damkohler number
f_v	volume fraction
F	kiln bed depth
L_m	mean beam length (length)
l_o	characteristic length of large eddies
M	molecular weight
N_A	Avogadro's number
P	static gas pressure
ΔP	differential = dynamic pressure
\bar{R}	universal gas constant
S_l	laminar flame speed
T	temperature
U	fluid mean velocity
U'	fluctuating component of velocity
V	total gas velocity
V_p	volume of a typical soot particle
X	mole fraction of soot particles

GREEK SYMBOLS

α_{ac}	absorption coefficient
α	absorptivity
α_g	absorptivity of gas only
α_p	absorptivity of soot particle only
δ_l	characteristic length of large eddies
ε	rate of κ dissipation
τ_c	characteristic chemical reaction time
τ_m	characteristic mixing time
θ	angle between gas glow and velocity instrument
ρ	gas density
κ	turbulent kinetic energy

CHEMICAL FORMULAS

$\text{Cl}_2\text{C}_2\text{H}_2$	dichloromethane
CH_4	methane
C_xH_y	various combinations of carbon and hydrogen
$\text{C}_6\text{H}_5\text{CH}_3$	toluene
CO	carbon monoxide
CO_2	carbon dioxide
CCl_4	carbon tetrachloride
H_2O	water
N_2	nitrogen
NO_x	various oxides of nitrogen
O_2	oxygen
SO_2	sulfur dioxide

ABBREVIATIONS

atm	atmosphere
BDAT	Best Demonstrated Available Technology
BFC	Body Fitted Coordinate (grid)
CFD	Computational Fluid Dynamics
COV	Coefficient of Variation
CPU	Central Processing Unit
DTRM	Discrete Transfer Radiation Model
DRE	Destruction and Removal Efficiency
FID	Flame Ionizing Detector
GC	Gas Chromatography
Hz	Hertz
LSU	Louisiana State University
MS	Mass Spectrograph
MW	Mega Watts
NTS	Not (drawn) to Scale
OD	Outside Diameter
PDE	Partial Differential Equation
PDF	Probability Density Function
ppm	parts per million
RCRA	Resource Conservation and Recovery Act
r.m.s	root mean square
rpm	revolutions per minute
SCMH	Standard Cubic Meters per Hour
SIMPLEC	Semi-Implicit Method for Pressure-Linked Equations Consistent
TDMA	Thomas TriDiagonal-Matrix Algorithm

tpd	tons per day
THC	Total Hydrocarbon
TA-on	Turbulence Air on (off)
USEPA	United States Environmental Protection Agency
VOST	Volatile Organic Sampling Train
WBPM	Wide Band Property Model
WSGG	Weighted Sum of Grey Gases

ABSTRACT

A comprehensive study of rotary kiln incineration is ongoing at Louisiana State University. Through experimentation at all levels and numerical modeling, the underlying physical processes are searched out and studied with the intent to improve the understanding of how rotary kiln incinerators process waste with the eventual goal of creating a fully predictive numerical model.

The experimental work presented here focuses on mapping combustion gas temperature and, for the first time, velocity fields of a field-scale, industrial incinerator. Measurements are made at multiple points across an upper quadrant of the kiln near its exit using a bidirectional pressure probe, suction pyrometer, and a newly designed, lighter yet stiffer, positioning boom. The kiln is directly fired using natural gas in a steady state mode without waste processing. Results indicate insignificant horizontal variation, but strong vertical stratification, with the highest values of temperature and velocity corresponding to the top of the kiln. Access restraints prevented the lower region from being mapped. Operating conditions were varied by adjusting the amount of ambient air added to the front of the kiln. Increasing this air flow reduced temperatures as expected, but did not have as significant an effect on velocities. The quality of the results is examined by performing mass balances and by comparing with an existing numerical model. Both methods indicate that the experimental results are reasonable.

A new steady state numerical model for the rotary kiln segment of this incinerator is then presented. This model builds on previous LSU work by including radiation and soot in the heat transfer analysis, switching to an adiabatic kiln wall

boundary condition, and including a more accurate geometry and better fitting grid. These changes improve agreement with data taken from this rotary kiln by up to two orders of magnitude compared with previously developed models at LSU. In most instances, prediction is within repeatability limits of the experiments. Grid dependency is demonstrated near the kiln front where gradients are very steep. Near the exit, however, where experimental data are available, both grids produce very similar results. Parametric and sensitivity studies using the developed model are reported.

CHAPTER 1

INTRODUCTION

ESTABLISHING COMMON GROUND

Research in this dissertation centers on the incineration of hazardous wastes. A common ground consisting of both terms and concepts will first be established, allowing the reader to understand better the nature of this work, using a series of questions, along with answers, often asked of scientists. The first question to answer is: "What is waste?" Waste can be defined as anything unwanted and considered worthless by an individual. Under this general definition, grass cuttings may be waste. However, while cuttings may be waste to one person, these cuttings may be a valuable addition to another person's compost pile. Therefore, one must be careful in defining hazardous wastes to avoid these ambiguities.

Today, the regulatory definition of hazardous waste in common use is much more specific than the previous example of grass cuttings. Only materials containing manufactured chemicals that are useless to the owner, and hazardous or toxic to humans, are considered hazardous waste. Further, the limits of the hazardous part of the definition include only wastes which exhibit well defined (CFR, 1991a) characteristic traits of reactivity, ignitibility (i.e. a flash point below 60° C), leachability, corrosivity under ambient conditions, or toxicity.

Issues concerning the management and disposal of hazardous wastes must also be discussed, for the public is becoming more conscious of and knowledgeable about environmental management issues and problems. The most fundamental question

asked by the public is: **"Why is there waste?"** An answer to this question lies in the first of the four natural laws of hazardous waste defined by Thibodeaux (1990) who states the first law as "I am, therefore I pollute." The basis of this statement is that the transformation of any raw material into products creates some residuals or waste. This law holds for chemical manufacturers, food processors, and any other manipulator or transformer of chemical materials, including the human body. Thus, every activity ranging from the obvious production of modern chemicals to preparing a meal produces waste by virtue of changing raw materials into desired products.

Other questions often asked of scientists and industry are: **"Where does the waste come from?"** and **"Where does this waste go?"** Indeed, Congress and the Environmental Protection Agency have reacted to both of these questions by passing legislation from which regulations such as the Community Right-To-Know Act (CFR, 1991b) were developed during the late 1980's. This act requires manufacturers to disclose information regarding storage, treatment, and disposal of chemical materials, including hazardous wastes, to the public. This annual reporting process provides the most comprehensive tracking of quantities, sources, and final fates of wastes ever required in this country.

Because the public is keenly aware of the ultimate fate of wastes, the next question commonly asked is: **"Why don't we just recycle all wastes?"** The second natural law of hazardous waste, which states that "complete waste recycling is impossible," addresses this question (Thibodeaux, 1990). The impossibility of complete waste recycling is a clear consequence of Thibodeaux's first law, that is, some waste is always produced by transforming a material (the waste in this case) into a usable product. Thibodeaux likens the possibility of "one hundred percent recycling" to that of a perpetual motion machine, the existence of which would violate

the second law of thermodynamics. Therefore, waste generation can be reduced by recycling, but not eliminated.

Thibodeaux's second law, then, leads to the obvious question: **"What should be done with the remaining wastes?"** His third natural law answers this, in a fundamental sense, by stating that, "proper disposal of hazardous wastes entails conversion of offensive substances to environmentally compatible or earthen-like materials." The principal idea conveyed by this law is that wastes must be properly and correctly converted into forms that are non-toxic to life. Through regulation, the federal government provides a less philosophical answer to the question through the land disposal bans (CFR, 1991c) promulgated in the late 1980's. Disposal of many hazardous chemicals by landfill, land-farming, and deep-well injection methods was banned by this act, forcing chemical manufacturers to turn to incineration as the only legally acceptable means of waste disposal remaining for certain streams.

Finally, since the first, second, and third laws of hazardous waste suggest that even treatment processes which generate earthen-like, non-toxic materials must generate some wastes, the remaining question which must be addressed by the fourth law is: **"Can some wastes be returned to the environment without harming it?"** The fourth natural law of hazardous waste states that, "small waste leaks are unavoidable and acceptable." During the 1980's, President Reagan stated that, "Trees pollute." Trees do indeed pollute as do all living organisms; however, nature has successfully assimilated these pollutants since the dawn of time because these wastes are typically dilute and are released slowly. Similarly, nature can absorb man-made hazardous wastes as long as the concentrations and/or quantities are low. Scientific efforts to determine the acceptable limits of chemical concentrations that can be naturally degraded without imposing health risks to the public are underway and will be greatly expanded and incorporated into new regulations issued during the 1990's.

In summary, fundamental questions concerning waste generation and waste management are commonly asked by a concerned public. The questions raised address serious problems like why wastes are generated, the inability to completely recycle waste, and the poorly understood assimilative capacity of the environment to manage wastes that are returned to nature. The following discussion addresses the available ways in which wastes, once generated, are best managed and in particular, *why incineration is often the preferred method of waste treatment.*

WHY INCINERATE WASTE: The Hierarchy of Waste Handling

Once a material has been identified as a hazardous waste, there are four primary options for handling this substance. The hierarchy of these four options serves as the basis of the Resource Conservation and Recovery Act (RCRA) passed by Congress in 1976. These management options regarding waste minimization activities are identified in guidance documents published by the United States Environmental Protection Agency (USEPA) (Federal Register, 1993).

First, re-use of the waste as a raw material in some other process is the most desirable waste management choice. An example of this re-use would be a process in which hydrogen chloride is first produced as waste, but then re-used as a raw material in a process to produce calcium chloride, a salable product.

A second alternative is to recover and recycle the portions of the material that still retain some value in the original process. An example of this alternative follows. For a process that generates a waste stream still containing significant concentrations of a usable raw or intermediate material, distillation, evaporation, or other unit operation processes can be applied to the waste stream to separate the valuable fraction from the residuals in the waste stream. The portion that is recovered could then be recycled into the production process, and the residuals subsequently treated and/or disposed. Both of these recycle and re-use activities permit the generator to

capitalize on the valuable aspects of the waste stream while decreasing the amount of residuals which must be treated and disposed.

Two options remain for management of wastes: treatment and disposal. Treatment, the third option for waste handling includes, but is not limited to, incineration, biological degradation, carbon adsorption, and wet air oxidation. These treatment processes remove or chemically change the waste stream pollutants into more innocuous substances which can potentially be released into the environment. The USEPA has further defined various treatment technologies (CFR, 1991d) as the best demonstrated available technology (BDAT) for certain waste streams based on their treatment and residual characteristics. State and federal regulations require many wastes to be treated using the BDAT to meet stringent concentration standards prior to disposal.

For management of wastes, the least preferred option is disposal with or without prior treatment. This option is necessary when all other waste management alternatives have been exhausted or have been dismissed because of technical infeasibility or in some cases, economic unreasonableness. Disposal options include land-farming, deepwell injection, or placement in a secure landfill or salt dome. Under current environmental regulations, use of these disposal options typically requires prior treatment or stabilization of pollutants.

Therefore, several different ways to manage wastes exist, but for any one particular waste there may only be a few methods which are viable or allowable under modern environmental laws. From a performance perspective, incineration is commonly viewed as a state-of-the-art treatment strategy because it is typically capable of delivering 99.99 mass percent or greater conversion of organic pollutants. Also, technical confidence in incinerator design and performance of new units is high, based on many years of safe and effective operation of existing units. Finally,

incineration is explicitly required by the USEPA as the BDAT for many specific hazardous waste streams.

In summary, any comprehensive study of hazardous waste management must address a fundamental set of questions such as: "What is waste?", "Why is there waste?", and "What should be done with the waste?" In the current regulatory sense, hazardous waste typically includes discarded chemical manufactured products that are considered useless to the owner or generator because these streams contain non-recyclable or non-reusable components or exhibit undesirable physical characteristics. As defined by Thibodeaux (1990), the four natural laws of hazardous waste dictate that such wastes and their treatments must result from: (1) human existence; (2) the impossibility of absolutely complete recycling; (3) the need to render wastes ecologically compatible; and (4) phenomena which produce small, acceptable amounts of waste that are assimilated in natural processes. Once wastes are generated, the USEPA often requires that such wastes be incinerated under current environmental regulations which are influenced, in part, by a general public that is becoming more conscious of and knowledgeable about environmental issues. As such, it is important to study incineration to further improve upon performance, to increase cost effectiveness, and to answer many questions that the public may have concerning the design, operation, safety, and environmental impact of incineration units.

A need to study incineration for treatment and disposal of hazardous wastes has now been established. In the next section, incinerator design is discussed. Although there are many different variations in design of incinerators, this dissertation focuses on the treatment of hazardous waste in a rotary kiln incinerator. Descriptions of a general rotary kiln incineration facility as well as a more detailed look at the rotary kiln component follow.

DESCRIPTION OF GENERAL INCINERATION FACILITIES

An incineration facility is designed primarily to react organics with oxygen in a high temperature environment such that these organics are combusted to form carbon dioxide and water, as well as, in the case of halogenated organics, acid gases. Secondly, regulated combustion products such as acid gases and particulate matter are subsequently controlled in downstream equipment such as alkaline scrubbers or baghouses prior to atmospheric discharge. The primary combustor to start the process often takes the form of a rotary kiln which is a horizontally mounted, rotating, cylindrical vessel lined with a high temperature refractory brick. The kiln rotates on external rollers and is slightly angled from the feed end so that solids are slowly moved through the length of the kiln as shown in Figure 1.1. Several variations on this standard design exist. For example, some kilns, called rocking kilns, rock back and forth rather than relying on inclined rotation to move the solid residuals. Other kiln designs have lifting flights or are fixed but have screws or belts that move the solids through the kiln. Solids and combustion gases can flow either co-currently, as shown in Figure 1.1, or counter-currently. Most heat to the kiln is supplied by combustion of the primary waste, but if necessary to sustain adequate combustion, the waste can be supplemented using secondary fuels such as waste oil, natural gas, or coal.

Wastes can enter the kiln in a variety of ways. In the gaseous form, wastes are usually injected through a common burner nozzle. Liquid wastes can be either sprayed into the kiln through an atomizing nozzle or mixed in with solids. Sludges must be either mixed with solids or injected directly into the kiln. And, finally, solids can be fed by screws, conveyers, or rams in either loose or containerized forms.

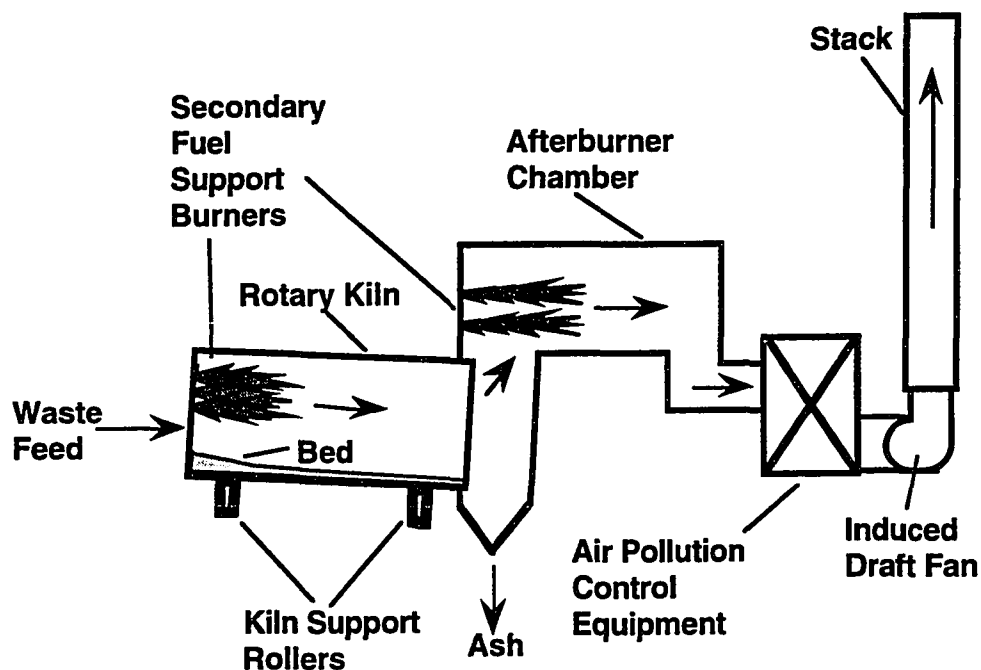


Figure 1.1 General rotary kiln incineration facility

Upon entering the kiln, the waste is subjected to a variety of complicated processes as indicated in Figure 1.2. Solids fall into a pile of accumulated material, called the bed, on the bottom of the kiln. Within the bed, complicated mixing and heat transfer phenomena occur since the bed usually contains a variety of objects which create different and often random bed motions. Containerized packs break open, and are assimilated into the bed. Volatile compounds are desorbed from the bed due to heat transfer which, depending on the design of the kiln occurs by: convection from the gases; conduction from the wall and other solid particles; and radiation from combustion gases, the walls, and other particles. Once in the gas phase, the waste can react with oxygen or any of the free radicals produced in the high temperature flame region.

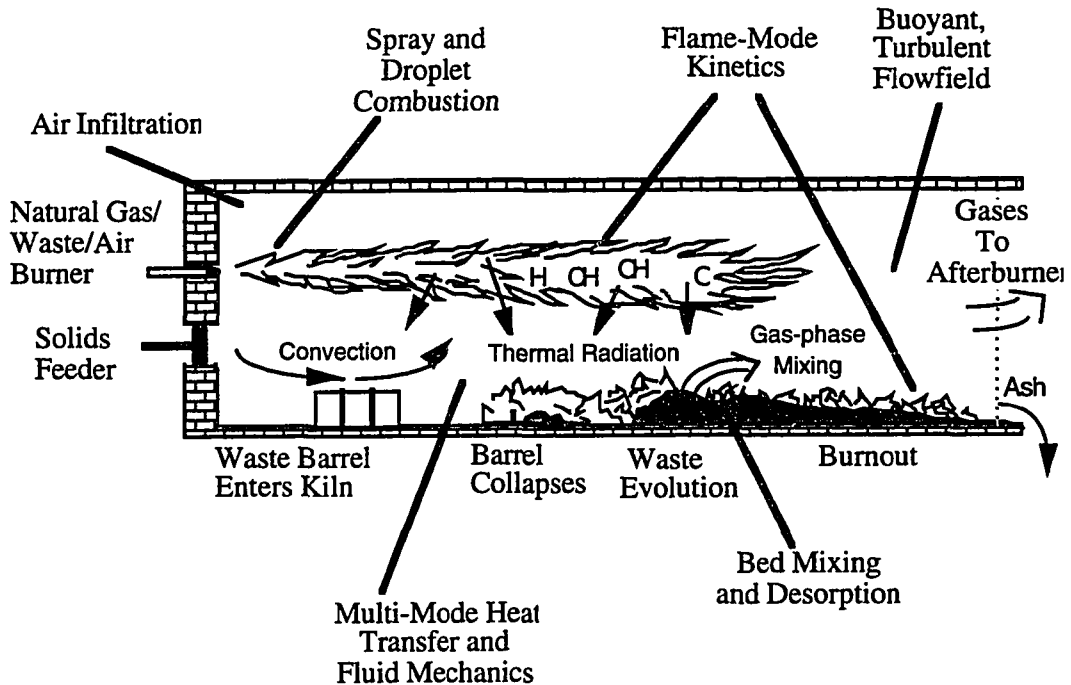


Figure 1.2 Processes occurring in a typical rotary kiln incinerator.

The primary function of the rotary kiln is to remove organics from the contaminated solids. These contaminants vaporize into the kiln gas or pyrolyze to inorganic carbon within the bed of solids. This organic removal results in a reduction of solids' volume and elimination of what is often the most hazardous component of the waste. Inorganic solids remaining after traveling through the kiln are removed from the incinerator and disposed in accordance with environmental standards, usually in an approved and secure landfill. All gases exit the kiln and enter the secondary combustion chamber, or afterburner, for further treatment.

The primary function of the afterburner is to destroy organics in the gas flow. Some kilns are designed to operate at lower temperatures to merely desorb and vaporize the organics. In these desorber systems, the afterburner provides all of the organic destruction of contaminated gases desorbed in the kiln. However, in some

cases, rather than being combusted in an afterburner, the organics and other hazardous compounds are separated from the gas stream by methods such as carbon absorption and partial liquefaction.

Gas and liquid wastes can also be sprayed directly into afterburners. For processes that only produce liquid or gas waste streams, the incinerator often does not have a rotary kiln segment. Incineration facilities that include a rotary kiln, however, provide maximum versatility since these units are able to process gases, liquids, sludges, and solids in bulk or containerized forms. Gases leaving the afterburner are usually quenched in a water spray and then enter downstream gas purification equipment such as wet or dry alkaline scrubbers, electrostatic precipitators, cyclones, or baghouses all of which are designed to remove particulate and/or neutralize acid gas emissions.

Treated gases are drawn through an induced draft fan and out the stack. These fans maintain the entire incinerator train under a slight vacuum to prevent leakage of hazardous vapor contaminants from the facility into the environment. This negative pressure results in air infiltrating into the incineration facility where small gaps exist. Gases discharged from the stack are typically free of 99.99 percent to 99.9999 percent (hence terms such as "four nines" and "six nines") of the original organic mass fed to the incinerator unit. Flue gases discharged from hazardous waste incinerators also must currently meet Federal particulate standards of 0.08 grains per dry standard cubic foot of gas (CFR 1991e).

Reasons why waste creation is inevitable have been reviewed along with an overview of incineration strategy, which can be used to treat selected waste streams. Next, an examination of the background or history of research in the field of rotary kiln incineration and related areas will be presented in the form of a literature review.

CHAPTER 2

LITERATURE REVIEW

This chapter presents a review of literature relevant to the research presented in this dissertation. This review is divided into sections concerning numerical modeling of rotary kiln incinerators and experimental studies of field-scale incinerators since the proposed work will include both experimental and numerical components. Included are works that have elements incorporated directly into the current research or are important in the developmental history of a related area.

NUMERICAL MODELING: AN OVERVIEW

Jones and Whitelaw (1982) present an excellent overview of numerical modeling while focusing on calculation methods for turbulent, reacting flows. They note that turbulence models existing at the time did not correctly predict certain flows. Some examples of flows incorrectly predicted by the then current turbulence models were cases of high temperature re-laminarization of turbulent flows, up-gradient diffusion, and a jet discharging into a quiescent chamber. The authors further note that due to the very nonlinear nature of reaction rates with respect to temperature and species concentration, using mean values of these variables in turbulent fluctuating conditions can lead to errors in reaction rates of up to three orders of magnitude. Probability density functions (PDF) were suggested as a good way to account for fluctuations about the mean, but the authors noted their considerable consumption of computer memory and run time.

The differences between finite rate and "fast" chemistry assumptions for diffusion flames are also reviewed by Jones and Whitelaw (1982). Finite rate chemistry can account for the rate of a global reaction being controlled by different elementary reactions depending on the temperature, pressure, and species concentrations present. To precisely model the chemistry, a complete set of elementary reactions and corresponding kinetic information making up the global reaction (activation energy, pre-exponential factor, and temperature dependence) is needed. However, acquiring this information is not trivial. According to Westbrook and Dryer (1984), the number of elementary steps can approach 100 even for the relatively simple combustion of methane in air. To add even more complexity, the steps used and the corresponding kinetic information for even simple reactions often vary greatly from one researcher to the next. This is pointed out by Westbrook and Dryer (1984) with the following comparison regarding the heat of formation of the formyl radical. The 1971 version of the JANAF Thermochemical Tables (Stull and Prophet, 1971) altered the heat of formation value for the formyl radical from -2.9 kcal/mole (published in the previous edition) to 10.4 kcal/mole. Then in 1976, Benson published a value of 7.2 kcal/mole for the same radical.

Fast chemistry assumptions are divided into either the equilibrium or irreversible reaction cases (Jones and Whitelaw, 1982). Neither case requires kinetic information. The irreversible case requires the user to input a reaction sequence for each reactant, usually a simplified one-step global reaction, specifying the stoichiometry for each reaction step. Whenever all the reactants for a particular reaction are together in one control volume, the reaction is assumed to instantly and irreversibly proceed to completion. Reactants are then created as specified by a particular reaction stoichiometry. In contrast, the equilibrium case requires no formal input of reaction sequences or stoichiometry because a library of thermodynamic and

species information is accessed. This database, used in combination with information on the control volume pressure, temperature and quantities of individual atoms present, can then determine which molecular species and concentrations are present to minimize the Gibbs free energy of the control volume. Both fast chemistry assumptions falter when reaction rates are slow. In the irreversible case, the global reaction assumption ignores sometimes important reaction intermediates.

Jones and Whitelaw (1982) also present several reaction models for premixed flames including the eddy break-up model. This model uses the rate of turbulent mixing rather than kinetics as the reaction rate controller. The authors stress that the eddy break-up model is inappropriate for diffusion flames. Several models that attempt to cover both premixed and diffusion flames are presented but all seem non-workable or valid in only restricted cases. A large number of examples and references are provided throughout the text. In one example, using a PDF to model the mixture fraction, the discrepancy between experimental data and model is traced to insufficient radial turbulent mixing. An attempt to "fix" this by dropping the turbulent Schmidt number to 0.2 was cited as "unjustified" and a failure.

Boris (1989) discusses current directions in Computational Fluid Dynamics (CFD) research. Initially he states that

algorithms for solving partial differential equations (PDE) have reached the point of diminishing returns in terms of trading off computational cost for accuracy. It is now more effective to increase the number of grid points to improve spatial resolution and hence accuracy than to seek greater accuracy through higher-order algorithms. Even increasing the complexity of turbulence and physical sub-models is now less important than resolution improvements.

Boris divides current research into three areas: representational models of the fluid state, algorithms for solving the resulting PDEs, and the computer hardware to run the

algorithms. New fluid state models include cellular-automata, hybrid-cellular-automata, and molecular-dynamics. Also discussed are new approaches for discretizing continuous functions and approaches to decimating the fluid-dynamic equations to a few dynamically significant degrees of freedom.

Algorithmic extensions and new directions discussed include adaptive and unstructured grids, spectral elements, and fully Lagrangian algorithms. On evolving hardware, Boris states that application of CFD technology is and always will be limited by the speed and size of available computers. The speed of single processors is limited by the speed of light and the current requirements of generality. New advances will come in using parallelism, pipelines, and building processors to do specific tasks. An interesting observation is that nature "solves" fluid problems in a fully parallel manner. He notes that to fully utilize the new directions in hardware will require redesigning many of the current solution algorithms.

In discussions related to the research presented in this proposal, Boris states that "fluid-dynamic convection in the absence of strong physical diffusion effects is the most difficult flow process to simulate." Major weaknesses in CFD are the detailed representation and simulation of turbulence and chemical reactions. To resolve small-scale turbulence or full chemical kinetic systems in a multidimensional CFD model imposes unacceptable costs, if it can be done at all. Flows can be solved with either complex geometry and simple physics or with complex physics in relatively simple geometry, but not with both. The example is given: a realistic chemical-reaction mechanism contains many chemical species and perhaps hundreds of reaction rates linking them. Integrating the stiff ordinary differential equations for the evolution of the individual species and fluid temperature in a multidimensional CFD code is theoretically possible. However, two faster and currently usable alternatives exist. First, use the detailed reaction mechanism to calculate bulk

properties, such as final temperatures and pressures across broad zones. Or second, use generalized reaction mechanisms to calculate temperature, pressure and species on a fine spatial resolution. The difference between these two simplifications is the basis for the division of most CFD codes into one of two categories. The first category involves CFD codes that solve relatively inclusive sub-models over coarse zones returning bulk properties called zonal models. The second category of CFD codes are called Navier-Stokes solvers because they solve the Navier-Stokes equations resulting in great flow detail; however, simplified sub-models are usually required. The numerical modeling work presented in Chapter 5 of this dissertation emphasizes analysis of the flow field; therefore, this work utilizes a Navier-Stokes type model code.

NUMERICAL KILN MODELS

Presently, there are two main types of numerical models for incinerator flow fields: those that solve the Navier-Stokes equations and those that divide the flow field into multiple zones, avoiding direct solution of the flow field. The latter uses various models for each zone and does not usually attempt formal solution of the Navier-Stokes equations. Solution of the Navier-Stokes equations is needed for the exact solution of the flow field. However, except for very simple situations, the PDEs are coupled, nonlinear, and very difficult to solve. The zonal models represent the first successful attempts to numerically solve complicated flow fields and are still in wide use today due to their greater flexibility and proven performance. The full Navier-Stokes equation set is still directly solvable for only simple cases, but, by approximating certain terms in the equations through the use of sub-models, the equations can be simplified enough to be solved. An example of this simplification is the κ - ϵ model to evaluate the Reynolds stress term in the time-averaged momentum equations. Also, ingenious methods have been developed to allow the sequential,

though iterative, solution of coupled equations. An example of this is the Semi-Implicit Method of Pressure-Linked Equations or SIMPLE (Patankar, 1980). Although there are a large number of zonal models available, only a few will be presented because the focus of this research uses a Navier-Stokes solver. However, a limited presentation of zonal models follows because these models utilize many of the same sub-models as the Navier-Stokes solvers and provide good insight into the history of numerical flow simulation.

Zonal Models

Jenkins and Moles (1981) present an axisymmetric zonal model to predict gas and refractory temperature profiles in a directly-fired rotary kiln. The authors use a zonal radiation model with exchange areas. Emissivity of the gas is approximated using a three spectral band model consisting of two gray bands and one clear band. The separate effects of soot and other airborne particles on gas emissivity are also included in a three band model. The velocity field is predicted using empirical correlations. The heat release distribution from gas phase reactions is accounted for by analyzing measured gas concentrations of CO and CO₂ in the kiln (see also reference to this work in the experimental section of this literature review) and predicting the amount of reaction required to produce those concentrations. Next, the gas and axial wall temperature profiles are predicted. Model results are then compared with data from a 100 ton per day (tpd) directly heated, coal-fired, cement kiln. Discrepancies in the comparison are explained by the fact that the model does not handle gas phase recirculation, which is calculated as being strong in several regions, nor does it account for CO₂ production and heat transfer from the bed reactions. This approach seems impractical because exact measurements of gas concentrations, which are very difficult to obtain, are needed throughout the kiln in

order to predict refractory and gas temperature profiles which are typically easier to measure.

Clark et al. (1984) present a model for predicting the destruction performance of an incinerator. Analysis includes both the afterburner and stack regions and is compared to a coaxial liquid waste kiln. A zone method coupled with a Monte Carlo technique is used to predict radiant heat transfer. Mixing is handled as macro-scale mass exchange between well-stirred zones. The flow field is obtained by either actual measurement or by estimation techniques using empirical correlations for specific burner types. A large number of possible paths through the system are evaluated, yielding a time/temperature history for each path and a percentage possibility of each path being used. Simple, one-step, first-order Arrhenius kinetics are applied to all paths, giving a fractional decomposition for each path. These results are then averaged over a large number of paths to obtain an average destruction efficiency. The authors claimed that the model correctly predicts trends in destruction efficiency even though it may deviate from measured values by several orders of magnitude. Due to the poor agreement and the sparse experimental data, the results appear inconclusive.

Clark and Seeker (1986) present another model designed to predict the ultimate destruction of waste. This model again assumes complete combustion of waste with no intermediates. Single temperatures for the gas and walls of the kiln as well as the secondary combustion chamber are calculated and used. Plug flow is assumed, and mean residence times are computed. Inputs include the heating value for the fuel and waste. Two percent of the volatile carbon is assumed to become soot, which the authors site as typical, but no references or experimental studies were provided. The radiation model uses a speckled wall approach along with a composition and temperature dependent grey gas. The results match two different kiln data sets fairly well, but both kilns have incomplete operating data. One kiln

required the addition of unreported leak air amounting to more than half of the total air entering the incinerator. A big advantage is that the model code can be run in less than 30 seconds on a personal computer having only 256 k bytes of memory.

Owens et al. (1991) compare their model to data from a directly-fired, pilot-scale rotary kiln. The experimental study focused on four independent variables including bed fill fraction; kiln rotation rate; kiln wall temperature, which was fixed by the natural gas firing rate; and water content of the clay sorbent. The kiln is operated in a batch mode, that is, solids do not flow axially through the system. For their model, a one dimensional approximation is made by dividing the kiln into axial zones within which the gas and solids are assumed to be well mixed and isothermal. Heat transfer is modeled by a thermal resistance network for an indirectly-fired kiln which is assumed to approximate the conditions of low temperature operation in their directly fired kiln. Heat transfer between zones is neglected. The mean beam length radiation model is used along with a grey gas and wall approximation. The model calculates the transient heating of the bed including the effects of bed slumping rates. Solids heating is treated in three stages: initial heating to the boiling point of water, isothermal vaporization of the water, and final heating of the bed above the boiling point after all the water has evolved from the bed. Scaling laws are presented, but different laws are required depending on whether radiation or convection is assumed to dominate the heat transfer or if moisture is present. Wall and gas temperatures are treated as constants and must be inserted to the program before solution can begin. This is a major weakness of their model in that a prior knowledge of the combustion gas and kiln wall temperatures are required.

Chen and Lee (1994) present a one-dimensional, steady state model of a rotary kiln incinerator. A single burner support flame is modeled as a uniform temperature cylinder. Solid pelletized waste is included and allowed to combust via a

surface area, Arrhenius-style pyrolytic reaction. Inert and reactive components of the waste are included, and the pellets are allowed to shrink in size; however, the waste is never named. A surface flame is assumed to exist on top of the bed of solids. Equations are solved using an iterative process coupled to a Newton-Raphson method. The authors state as one of their primary items of focus "to fit all experimental data exactly"; however, neither experimental data nor percent error is ever shown or discussed in the whole work. No kiln details are given with all analyses conducted on a dimensionless basis. Sensitivity studies are carried out on surface emissivity, feed particle size, and the surface flame. A study is performed on radiation indicating that interactions between axial zones can be very important; however, the authors claim that with mole fractions of CO_2 and H_2O in the gas stream less than 10 percent, radiation transfer to adjacent zones will only be reduced by 20 percent, and as a result, radiation exchange with the gas phase can be neglected. They add, however, that in large scale kilns (greater than 2.4 m) or a soot laden kiln, radiation exchange with the gas phase becomes much more important.

Navier-Stokes Solvers

Gillis and Smith (1988) present a three-dimensional numerical model for predicting flow in industrial furnaces. The SIMPLE algorithm and a vectorized Thomas algorithm are used to solve the Navier-Stokes equations. The model can only be utilized in Cartesian or polar coordinates. Perhaps the biggest limitation of the model is that it does not include chemical reactions. The authors compare three turbulence models and examine the assumption of constant eddy diffusivity, the Prandtl mixing length model, and the κ - ϵ model. The κ - ϵ turbulence model uses transport equations for " κ ," the turbulent kinetic energy, as well as " ϵ ," the dissipation rate of turbulent kinetic energy. The model was compared to what the authors describe as a "proven" 2-D axisymmetric numerical model and to a 1/20th

scale pilot testing facility. Because the model does not handle reactions, only air is flowed through the test facility. The κ - ϵ turbulence model is shown to be superior in matching the actual non-reacting furnace flow field. The experimental flow field was not matched exactly, but the model did correctly predict some of the measured flow features and produced a logical flow field. A grid dependence study was executed by examining grids of 17,500; 48,125; and 102,375 nodes. The solution from the grid consisting of the least nodes is greatly different from the others. The two larger cases are closer, but the largest showed several small eddies not developed in the middle case near the highly turbulent burner inlet area. This suggests that further grid refinement may produce more changes in the calculated flow field.

Wang, Chen, and Farmer (1989) apply a finite difference type solution to the Navier-Stokes equations to solve the flow field of a reactive ramjet dump combustor. A term is added to an extended κ - ϵ turbulence model to include the effect of temperature on eddy breakup. Kinetics for an Arrhenius form, finite rate, one step, global reaction of hydrogen and oxygen are generated from the results of a 28 step reaction model. The resulting source term equations are modified by an algorithm called PARASOL (Pade' Rational Solution) before the species equations are solved. Modifications to the solution procedure are designed to allow for solutions across shock waves and in hypersonic flows. The final system of linear algebraic equations are solved by a modified Stone's method using a Cray XMP computer. Even though the reaction scheme seems to work well, the authors caution that global kinetic rate constants such as used in this study are only valid for conditions which have been validated with experimental data. The model matches well for this axisymmetric problem, but it is unclear if this model can be used for three-dimensional problems.

Smith, Sowa, and Hedman (1990) use a comprehensive two dimensional coal combustion model called Pulverized Coal Gasification and Combustion (PCGC-2). A

κ - ϵ model is used that is modified to account for the presence of particles. Reaction rates are assumed to be limited by molecular scale mixing. Probability density functions are used to account for the turbulent fluctuation about the mean values. Radiation is accounted for by a six-flux model that includes anisotropic and multiple scattering from the particles. The usefulness of the model is summarized by the authors as being:

...capable of predicting qualitative information in the combustion and gasification applications that are used as case studies in this paper. In most cases sufficient quantitative information is predicted within the measurable accuracy of the data to justify engineering decisions based on the simulation.

Nasserzadeh et al. (1991) used a commercially available code, FLUENT V 2.95 to model a 500 tonne/day municipal solid-waste incinerator. Modeling was divided into two geometric parts. The first part included the moving grate incinerator which consisted of hoppers, six rollers, and the refuse bed on top of the rollers with a 7,980 node three-dimensional grid. Symmetry was sited to allow only one half of the geometry to be modeled; however, the use of Cartesian coordinates required sloped surfaces to be modeled with a stepped wall approximation. Results from this model were used as boundary conditions for the 10,260 node grid of the other half of the furnace and the shaft and boiler sections. Symmetry was again cited to cut the modeling effort in half. Still, modeled geometry had to be simplified and stair-stepped walls were utilized. Gases were assumed ideal, turbulence was resolved using the κ - ϵ model, and reaction rates were determined by the limiting choice between Arrhenius kinetics and a turbulent eddy-dissipation model. A two step reaction mechanism was employed with C_xH_y and air as reactants, CO as the intermediate, and CO_2 and H_2O as the products. The values of refuse density, molecular weight, heat of combustion, stoichiometric ratio, viscosity (gas), and heat capacity that are used as boundary

conditions are given. The amounts of raw refuse and amounts gasified on top of each roller were patched into the calculations based on experiments conducted at the facility (see this reference in the experimental section of this chapter). No other model details were given or referred to and no facility dimensions were provided. The resulting flow field is said to be nearly two-dimensional. Predicted velocities range from 0 m/s to 7 m/s with temperatures up to 2,000 K. Predicted temperatures leaving the boiler are in the 800 K to 900 K range, very close to the measured values of around 950 K. This is interesting because radiation modeling is never mentioned. Explanation of presented data and model results is incomplete, making comparisons difficult. Gas speciation data were recorded at the exit of air pollution equipment which is downstream of the boiler. The solution domain of the model ends at the boiler exit and therefore does not include the sampling location. The authors state that the CO prediction is low, but their figures appear to show it more than an order of magnitude high. A “mismatch of conditions” is mentioned but not explained as a partial reason for differences between experimental and model results. Even so, the authors state “the two-step kinetic model, for the prediction of CO formation, has performed well.” The possibility of grid dependence of the solution is not mentioned.

Nasserzadeh et al. (1994) uses the above model to examine residence times in the incinerator. Fluent V 2.95 is again used. The only change is that tracking of particles using a Lagrangian type model is included. Neutrally buoyant particles are injected at several locations of the incinerator and tracked. Results show the existence of several recirculation zones. Residence time distributions are calculated showing residence times ranging from 1.6 to 3.4 seconds for entrance from a secondary air inlet to 45 to 70 seconds for entrance from roller number six. No discussion of model validity is made though the authors state that any “possible errors in the results ... are likely to be due to” among other things “the possible existence of some computational

dead time on the small difference cell.” The authors go on to state “Nevertheless, the modeling results obtained here, are generally satisfactory.” Proposed design modifications to improve residence times by eliminating or reducing recirculation regions are tested. Model predictions showed that a proposed baffle addition would nearly double gas residence times. Model predicted improvements are also cited for changing the way secondary air is injected into the incinerator, but no quantification is offered.

Leger et al. (1993c) used FLUENT V 3.0 to examine the flow field inside a field-scale rotary kiln. This incineration facility is detailed in Cundy et al. (1989a) and Montestruc (1989) and is briefly described in both the “Background” section of Chapter 4 and the “Physical System” section of Chapter 5 of this dissertation. Leger created a three-dimensional grid of $17 \times 20 \times 36$ (12,240) control volumes. Air was assumed to infiltrate the kiln through the two kiln rotary seals and the solids loading chute door. Air infiltrating through the rotary seals was included by modeling all of the front and rear kiln-wall perimeter control volumes as inlets. Each burner inlet to the kiln was represented by only a single control volume. Due to the coarseness of the grid and the use of uniform grid spacing, the areas of the burners, solids loading door, and external mixing air inlets did not match the actual areas. To account for this, the inlet velocities were adjusted to maintain the correct mass flow rates. Radiation was not included, and the walls were modeled as isothermal at 800 K. Ideal gas was assumed, and gas composition was included in the specific heat calculations. A more complete description of the model used in Leger et al. (1993c) is given in “Appendix D” of this dissertation. The primary finding by Leger et al. (1993c) was the importance of buoyancy in creating the characteristic, vertically stratified temperature and species profiles observed in experimental data at the kiln exit. The highly three-dimensional nature of the flow field is pointed out as is the unexpected existence of a

recirculation zone in the lower region of the kiln's exit. Quantitative agreement with experimental data is off by as much as two orders of magnitude; however the authors suggest that the model generates reasonable results in spite of the many "gross" underlying assumptions, rough grid, and crude sub-models that are used. Leger et al. suggest that the model is a useful tool for formulating rough comparisons of different kiln operating conditions and design modifications.

Khan et al. (1993) also used FLUENT V 3.0 to examine the same field-scale kiln on which the work of Leger et al. (1993c) and this dissertation are based. Only the major differences between Khan et al. (1993) and Leger et al. (1993c) are discussed here. Khan used a $27 \times 30 \times 40$ control volume grid, (32,400 total nodes) and then checked for grid dependence using a $30 \times 33 \times 75$ grid (74,250 total nodes). Each burner inlet to the kiln was modeled using four inlet control volumes. Again, the modeled areas of the burners, door, and air inlets did not match the actual areas because of the coarse grid and uniform grid spacing used. To compensate for this, the inlet velocities of the burners and air inlet nozzles were reduced to maintain the correct mass flow rates. The velocity of air infiltrating through the door was calculated to be 14.4 m/s using the inviscid Bernoulli equation with a pressure drop of 0.124 kPa. Rotary seal infiltration air was assumed to have an inlet velocity of 1.5 m/s. With the control volume size and leak air inlet velocities fixed, the mass flow of leak air into the kiln could only be controlled by altering the number of control volumes designated as inlets. This means that the physical inlet geometry was artificially altered in order to account for the different leak air rates at each different operating condition. Two different heat transfer wall boundary conditions were studied: an adiabatic wall and a constant heat flux wall at 1400 W/m^2 (about 5 percent of the combustion energy). Turbulence was accounted for by the κ - ϵ turbulence

model, and the specific heat was assumed to be that of air. Three conspicuous differences between the model setup and the field-scale facility are:

1. The burners are placed on the wrong side of the kiln;
2. Infiltration air from the loading chute door is placed too low in the kiln;
and
3. Metered air for both the kiln and afterburner is input through the kiln burners.

The results of interest are that the maximum temperature at the kiln exit was 2,344 K, the flow field was virtually unaffected by the difference of adiabatic versus constant heat flux wall boundary conditions, the solution was grid dependent, and recirculation existed in the top rather than the bottom of the kiln as in Leger et al. (1993c). Khan et al. (1993) compared these methane only (no waste) modeling results to experiments in which methane, along with liquid carbon tetrachloride (CCl₄) waste, was continuously burned, as published in Cundy et al. (1989a, 1989b, 1989c). The results of the model qualitatively match the field results to the extent that the model correctly shows the existence of vertical stratification at the kiln exit, with little to no stratification in the other two planes.

Summary of Numerical Models

Numerical models using Navier-Stokes solvers are relatively new and are quickly improving; however, the zonal models are still in wide use due to their proven performance and greater adaptability. Navier-Stokes solvers are not yet able to handle situations involving vastly different phenomena in the same problem, such as solids mixing in a bed along with full spectrally dependent radiation in the gas flow field above the bed. Zonal models, which handle various detailed sub-models

relatively well, only calculate bulk flow properties, have trouble with large property discontinuities at boundaries between zones, and rely on the assumption that properties are uniform within zones. All of the models reviewed are limited to steady state operation and depend on the ability to make simplifying assumptions such as plug flow of solids and/or gases. For both solver types, sub-model development is needed. In particular, turbulence and radiation sub-models need improvement. Currently no model correctly predicts the quantitative aspects of an incinerator flow field.

FIELD-SCALE INCINERATION: EXPERIMENTAL STUDIES

Introduction

Every facility that burns waste must first acquire a permit from the USEPA or state/local regulatory agencies. To obtain a permit, proof of the incinerator's ability to achieve required performance standards must be established and documented. This proof is obtained by presenting satisfactory results from a "trial burn" for incinerators, cement kilns, and boilers that burn hazardous wastes. Facilities processing non hazardous wastes must submit results from a similar, but slightly less stringent, "compliance test". Although the results of these trial burns are available to the general public through facility permit applications, these documents are not usually helpful to researchers for several reasons. First, information about results of pre-trial tests and any design changes that may have been made to achieve the final test burn results are not ordinarily included in public documents. Rather, public test burn documents usually contain data about the final feed, operating conditions, and stack exhaust measurements and only minimal information about the kiln or afterburner regions. Second, permits containing the final test results are lengthy, contain much extraneous information, and are difficult to read. A typical example is the Trial Burn Report submitted by Eastman Kodak in 1985 that contained 1,800

pages of documentation in eight volumes (Bastian and Wood, 1987). Such information from the public record is generally of little value to researchers and the scientific community.

Very few non-trial burn, scientific studies of field-scale incinerators have been undertaken. Although there are several reasons for this void, the primary reason is that researchers generally cannot gain access to incinerators that are suitably designed and fitted for detailed studies. To further exacerbate the situation, current regulations discourage post-trial burn modifications such as installing extra inlets or additional access ports that could be useful for sampling and/or viewing. Finally, many incinerator facilities are just not accessible for testing because of the placement of equipment and utilities, and large incineration facilities are too expensive to build solely for experimentation purposes.

The two main groups of owners of hazardous waste incinerators are the private sector and the federal government. The federal government and many private companies generally will not allow details of their proprietary processes published for reasons of competitiveness, national security, and/or public reaction which is increasingly set against incineration. Additionally, academic research at privately owned hazardous waste incinerators is usually not conducted because business demands dictate that unit downtime to conduct research experiments is economically unreasonable. For example, one facility 'roughly' estimated that for twelve hours of experimental tests, costs in excess of \$60,000 were incurred, not including lost revenues (Lipp, 1992).

Another reason for the lack of useful experimental data at the field-scale is the large amount of manpower generally necessary to safely and expediently complete a test run. For example, field-scale tests conducted by Louisiana State University researchers typically require ten workers in addition to five plant personnel (Huggins,

1994). Even pilot-scale facilities tend to require four or more people to conduct tests. Finally, the difficulty and sometimes unavailability of methods to extract data from various points within a large rotating kiln with temperatures in the 600° C to 2,000° C range contribute to the lack of experimental data found in the literature.

Given these reasons, it is not surprising that only a few groups have done experimental work with field-scale incineration units. The first group to present data on field-scale units was Jenkins and Moles (1981) with data from a 100 tpd cement kiln. Next, R. W. Wood (1987) presents detailed results from a hazardous waste incinerator trial burn. Then, Nasserzadeh et al. (1991) present data from a 500 tonne/day municipal solid-waste incinerator. Finally, a group at Louisiana State University has been studying a directly fired hazardous waste kiln since 1986. Each of these studies are reviewed next.

Review of Literature

Jenkins and Moles (1981) present data taken from the 100 tpd cement kiln at the Barnstone Works in Nottinghamshire. The kiln is 1.7 m in diameter by 45.7 m long and directly heated by coal. The authors explain that gas samples were collected "... through water-cooled probes using an integral sample cooling unit which rotated with the kiln." Highly detailed two-dimensional axial contour plots were constructed for CO₂, CO, O₂, and temperature fields along with an axial wall temperature profile. Gas temperatures as high as 2,000° C were measured. Gas temperatures were measured using both suction pyrometers and venturi-pneumatic pyrometers, while wall temperatures were gathered using sheathed thermocouples. Clinkering and decarbonizing reactions took place in the solids bed during data collection. Recirculation of the gases was observed in the kiln and a Craya-Curtet parameter, m , equal to 3.5 was calculated indicating stronger recirculation than claimed as the industry average; $m = 0.8$ to 1.6. The Craya-Curtet parameter indicates the onset of

recirculation areas in systems with a primary jet issuing into a larger area, and ranges from zero to infinity. Modeling work presented in Jenkins and Moles (1981) is discussed in the modeling section of this chapter.

Although most public information, such as trial burn and permit application information, is usually not useful for research purposes, R. W. Wood (1987) presents a rare summary of a trial burn report that includes the pre-trial burn data and resultant operational modifications suggested by those tests. This trial burn report is the culmination of tests performed from 1980 to 1984 on Eastman Kodak's rotary kiln incinerator located at the Kodak Park film, paper, and chemical manufacturing site in Rochester, New York. Data recorded during the tests include temperature from a single point at the kiln exit and the middle of the afterburner, O₂ level in the afterburner, CO concentration and GC/MS/FID analysis of the stack gas. Operating parameters measured during the tests included type of waste and waste feed container, kiln temperature, rate of rotation, and air inlet rates. The general finding of these tests was that longer residence times at higher operating temperatures improve the destruction and removal efficiency (DRE) of the wastes under study in this incinerator. To achieve longer residence time and higher temperatures which in turn lead to higher DREs, it was necessary to reduce the rate of air infiltrating the kiln. A new kiln exit seal was installed resulting in a temperature drop between the kiln exit and the quench of 100° F compared to the previous 400° F temperature drop.

Nasserzadeh et al. (1991) present data from the 30MW, 500 tonne/day municipal solid-waste incinerator located in Sheffield, England. The incinerator is designed to handle 10 tonne/hr of raw waste in each of the facilities' two grates, and its boiler provides heat for 10,000 homes. A typical analysis of the Sheffield refuse is broken down into 8 categories by both weight and volume with the two largest categories being paper and vegetable putrescent matter. Temperatures recorded at a

point in the boiler exit range from 875° C to 1,025° C over 40 minutes. A water-cooled probe was used to gather speciation data at the exit of the electrostatic precipitator located downstream of the boiler. Measured CO ranged from 110 to 190 ppm, while O₂ ranged from 8 to 12 volume percent. Data is also presented for NO_x, SO₂, and CO₂.

The group located at Louisiana State University is continuing research started in 1986 on a hazardous waste, rotary kiln incinerator located at Dow Chemical Company in Plaquemine, Louisiana. This incineration facility is detailed in Cundy et al. (1989a) and Montestruc (1989) and is briefly described in both the “Background” section of Chapter 4 and the “Physical System” section of Chapter 5 of this dissertation. Initial studies on this kiln consisted of three sets of experiments (Cundy 1989a, 1989b, 1989c), each carried out on a different day. For all experiments, liquid CCl₄ was directly injected, along with natural gas and air, through one burner nozzle, while natural gas and air were injected through another nozzle. To the greatest extent possible, the operating parameters were kept constant over all three test days.

In the first paper, Cundy et al. (1989a) discuss insights gained by studying incineration practices in Germany, and then details the incinerator facility under study, including its geometry and operation, along with sampling methods and locations. Data were obtained from the exit of the rotary kiln using a 7.8 m long stainless steel, circulating water-cooled probe, detailed in the paper. Gas temperature was measured by a suction pyrometer protected by a ceramic radiation shield at the end of the probe. The gases from the suction pyrometer were analyzed for CO₂ and O₂. A shorter 3.8 m probe, otherwise identical in design, was used to extract the same type of data from the middle of the afterburner.

At the kiln exit only horizontal traverses were possible. Relatively little variation was observed moving from the kiln centerline to near the burner side of the

kiln: 1.4 percent increase in O₂, 16.7 percent decrease in CO₂, and 3.7° C decrease in temperature. With the addition of extra mixing air supplied at the burner face, the above values increased to 10.3 percent, 46.7 percent, and 17.4° C respectively. Axial variation was also minimal with no change in O₂ concentration, a 33 percent increase in CO₂ concentration, and a 15° C temperature decrease at the downstream location. Gas samples were collected in glass bottles for later GC/MS analysis. The experiment was duplicated so that data could be recorded first in the kiln and then in the afterburner.

In the next experiments, Cundy et al. (1989b) took simultaneous measurements at fixed locations in the kiln, afterburner, and stack. Stack testing included volatile organic sampling train (VOST) analysis recorded over 20 minute intervals along with batch sampling. Continuous total hydrocarbon (THC) data were recorded only at the kiln. A new access port allowed measurements to be obtained from the previously inaccessible upper region of the kiln; hence, vertical profiles were obtained for the first time. These data were compared to previous data (Cundy et al., 1989a) taken in the lower kiln region. Separate test days were required for data collection from the top and bottom regions of the kiln. These experiments showed the presence of a strong vertical stratification at the kiln exit that was greater than expected and greater than stratification in the horizontal plane. Specifically, in the upper kiln as compared to the lower kiln region the O₂ mole fraction was 360 percent less, the CO₂ mole fraction was 3,150 percent greater, and the temperature increased by 570° C. The addition of mixing air at the burner face of the kiln reduced these differences.

In the final paper of the series, Cundy et al. (1989c) present data from another experimental set while providing a summary of the two previous test sets (Cundy et al., 1989a, 1989b). This newest set involved taking data at five locations in a section

of the transition between the kiln and the afterburner. Because this location was an expansion, recirculation region, few hypotheses could be inferred from the data. This test did demonstrate, however, the relatively uniform conditions that occur in such an expansion recirculation region.

Experiments conducted by the Louisiana State University team after the steady CCl_4 feed experiments focused on batch feed waste processing. The complexity of these experiments increases dramatically as the number and type of data collected per experiment increases.

In Cundy et al. (1989d) the first batch waste processing experiments are presented along with some preliminary data. Before the run, 18.9 liters of toluene ($\text{C}_6\text{H}_5\text{CH}_3$) were poured into 53 liter (3.2 kg) polyethylene packs containing 22.7 kg of montmorillonite clay granules, with an average diameter of 0.635 cm. One pack was inserted into the kiln by a hydraulic ram every five minutes. Continuous THC and temperature data, measured at 30 second intervals, are presented only for the upper kiln location at several operating conditions. When the pack was inserted into the kiln, the kiln exit temperature dropped initially, due to the opening of the loading chute doors leading into the kiln, and then a double peak in temperature occurred before the profile gradually returned to baseline values. The authors relate these peaks to the initial pack breakdown and bed motion. As expected, the THC concentration measured at the exit of the kiln showed an opposite behavior, that is, the THC increased during drops in temperature. Addition of external mixing air increased the magnitude of the excursions from baseline. Visual observations indicate that periods of high THC correspond to periods in which the kiln is obscured by highly-luminous, particle-laden flames. Conversely, periods of low THC correspond to improved visibility, often to the front of the kiln. A large part of this paper discusses complementary work using pilot-scale facilities at the University of Utah.

These pilot-scale studies confirmed trends observed at the field-scale and indicated that the multiple spikes in various parameters were associated with toluene evolution resulting from pack break-up and bed motion dynamics. The paper recaps the continuous data from Cundy et al. (1989a, 1989b, 1989c) and discusses several numerical models of kiln processes under development. Several innovative methods of approximating CCl_4 reaction rates are also presented.

Lester et al. (1990) continue the discussion on the toluene batch runs introduced in Cundy et al. (1989d). Data recorded in the transition section downstream from the kiln exit and closest to the back wall had a temperature 300°C less than that in the upper kiln. This point was theorized to be in the streamline from the bottom of the kiln. For the first time, VHS video data were recorded simultaneously from the lower port in the transition section, with a view of the front face of the kiln, while the probe was inserted in the upper port. Several color reproductions taken from this recording are presented showing periods of intense sooting, large turbulent flame zones, and the general non uniformities that exist in the flow. Several pictures include the natural gas support flame which radiates a bright yellow-orange. The pictures indicate the intense changes that can occur in a matter of seconds in the flow field during pack break-up and subsequent toluene evolution. The authors also learned from the video data that even after five minutes, pack combustion was not complete. Efforts to demonstrate repeatability were only partially successful due largely to the randomness of initial pack break-up and subsequent mixing with the existing bed.

In Cundy et al. (1991a) information on batch processing of packs is presented similar to Lester et al. (1990) and Cundy et al. (1989d), except the packs contained xylene instead of toluene. Using information gained from the previous experiment (Lester et al., 1990), one pack was inserted every ten minutes to ensure the complete

processing of each pack before introduction of the next pack. The experiments were performed on two different days to allow sampling from both the lower and upper areas of the kiln exit. Four to eight packs were inserted for each combination of the independent variables which were rotation rate at 0.25 or 0.1 rpm and external mixing air injection (on or off). Continuous CO₂, CO, O₂, temperature, and THC were recorded for the first time at the kiln exit. These data were recorded once per second. To reduce the effect of instrument noise and to consolidate the large number of data points in the presentation, ten second "boxcar" (Willard et al., 1981) averages were applied. Within each operating condition, the random effects of bed motion and pack break-up resulted in differences between each pack's combustion. These random variations within a set operating mode made it hard to compare between different operating conditions. To reduce this randomness effect, the data were ensemble averaged for all runs conducted at the same operating conditions. Vertical stratification was again noted between the upper and lower kiln sampling locations. No THC was detected in the lower kiln while peaks over 150 ppm were recorded in the upper kiln. The O₂ concentration dipped as low as 9 percent in the upper region versus a minimum of 15 percent in the lower region. Similarly, temperature peaks were 300° C higher, and CO peaks were almost an order of magnitude greater in the upper kiln. Material balances on carbon showed 90 percent mass closure with external mixing air on and 50 percent mass closure when the external air was off. Color pictures from VHS data are presented and correlated with the continuous data.

In Cundy et al. (1991b), data from batch processing of dichloromethane (Cl₂C₂H₂) are presented for the lower and upper regions of the kiln exit, and these data are compared to the xylene runs discussed above in Cundy et al. (1991a). In addition to the CO₂, CO, O₂, temperature, and THC data recorded continuously, grab sample data from the kiln are also presented for both xylene and dichloromethane

processing. The O_2 and CO_2 concentrations, along with the temperature showed similar profiles; however, the temperature response was flatter and did not show short duration excursions as clearly as the O_2 and CO_2 concentrations. Peaks in THC coincided very closely with peaks in the CO trace. Deviations from baseline kiln O_2 , CO_2 , and temperature values during waste combustion were much larger for xylene than dichloromethane. These differences were related to the different reaction stoichiometry and thermodynamics of the two wastes.

In the next series of papers, Leger et al. (1991a, 1993a, 1993b) present the most complete set of data taken by this research group. For the first time, continuous CO_2 , CO, O_2 , THC, and temperature measurements were simultaneously recorded at the kiln exit and afterburner along with continuous CO, O_2 and THC data at the stack. Several permanent facility temperature and pressure readings were continuously recorded, and gas batch samples were taken for GC/MS analysis. Toluene, inserted via packs at ten minute intervals, was the test waste. Experiments were again performed on different days to obtain data from both the upper and lower kiln exit locations. Video data was not recorded during data collection from the lower kiln since only the lower port offered a good view of the kiln and the probe and camera could not both fit in the lower access port. A summary of these papers follows.

Leger et al. (1991a), the first paper in the series, sets the stage for the other papers by listing the experimental matrix, showing the sampling locations, the kiln operational parameters and instruments used to gather data. Continuous, unaveraged oxygen data are presented for all packs at all locations to highlight the randomness and similarities between packs. Individual excursions were traced from the kiln to the stack with only minimal smoothing due to axial flow mixing. A large flow of air, infiltrating around the hydraulic ram during pack insertion, is noted by observing blowing debris during pack feeding. The argument is made that even though the

magnitudes of the individual responses at the two kiln sampling locations were greatly different, their trends were the same. The authors further suggest that this indicates that measurements taken at only one point in the kiln exit may be a good qualitative indicator of events or phenomena occurring elsewhere in the kiln.

In Leger et al. (1993a) all the data, including the previously presented oxygen data (Leger et al., 1991a), is presented in ensemble averaged form. GC analysis are overlaid with continuous data. The two data sets matched well about half the time, and the error for the other half was attributed to a possible sampling leak causing dilution in the sample bottles used for the GC analysis. A thermocouple was inserted into the bed in the front (loading) area of the kiln, but the positioning pipe became bent by the kiln's rotary motion. This caused uncertainty regarding whether or not the thermocouple was in the bed. Video data, not presented, indicated that the bed was in a slipping rather than the usual slumping motion. This different bed motion was attributed possibly to the presence of the thermocouple probe in the bed. No difference between "fast" and "slow" data was observed, and this was thought to be due to the slipping bed motion. This result suggested the interesting possibility that bed motion, and thereby evolution rates, could be controlled by placing objects in the bed.

In Leger et al. (1993b) the previously presented data, Leger et al. (1991a, 1993a), are manipulated generating leak air rates, evolution curves, mass closure calculations, and characteristic times for evolution. The amount of air infiltrating into the incinerator was calculated to be between 2.8 and 3.5 times the amount of metered air which is in the range estimated from previous experiments. Mass closure was calculated to be 0.88 with a standard deviation of 0.18 over 32 values, which is very good for a large industrial system.

Summary of Experimental Field-Scale Incineration Studies

The study by Jenkins and Moles (1981) presented several highly detailed contour maps of CO₂, CO, O₂, and temperature inside a coal-fired cement kiln. However, Jenkins and Moles did not present a parametric study nor was any waste incineration involved. Wood (1987) presented a rare summary of a trial burn report which included the pre-trial results and resulting operational modifications from these early tests. However, the only variable recorded for this kiln is the temperature at only one point just past the kiln's exit. For both of the above groups, no recent experimental data has been published. Nasserzadeh et al. (1991) present a large array of data, but the waste feed is not uniform and all the data is taken downstream of the boiler. The research team at Louisiana State University has been consistently publishing detailed information on field-scale, rotary kiln incinerators. No information on the velocity fields inside a full size rotary kiln, necessary to validate numerical models, exists today.

In the preceding literature review several gaps or shortcomings in the collection of published work on incineration have been pointed out. The next section entitled "Research Goals and Objectives" will indicate which areas were researched to fill in some of the aforementioned gaps in incineration knowledge. The last part of the goals section pinpoints what was done in each of the general areas of research by delineating itemized research objectives.

CHAPTER 3

RESEARCH GOALS AND OBJECTIVES

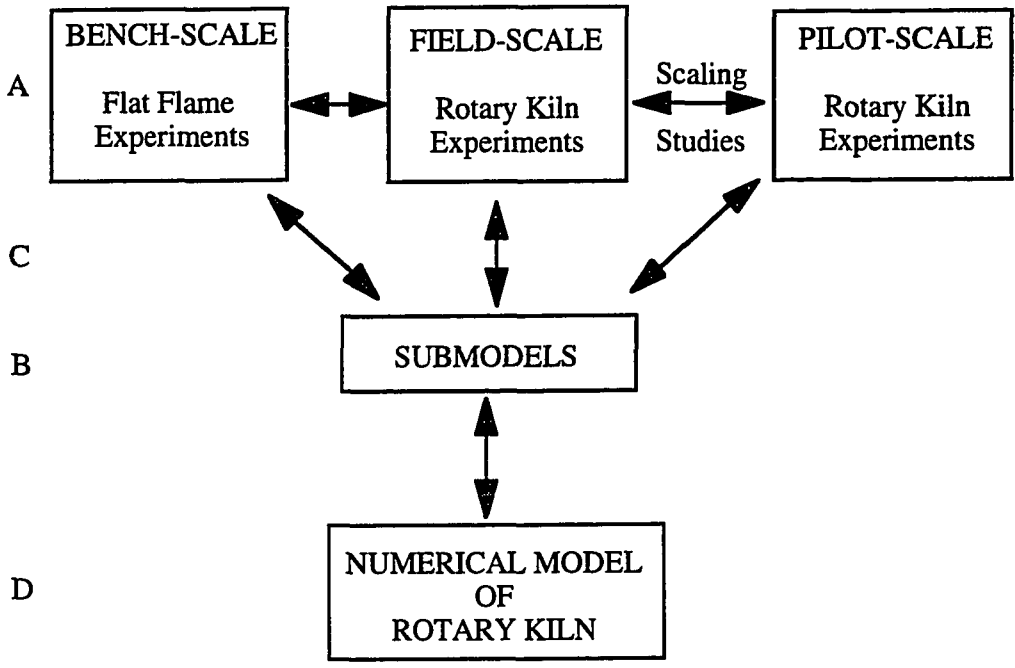
OVERALL PROGRAM GOALS

The overall objective of the Louisiana State University incineration group is to develop a rudimentary, but reliable predictive capability for rotary kiln incineration. This ultimate goal cannot be achieved in a single step. The components of the group's research include:

- A) Collecting data from bench-scale, pilot-scale, and field-scale facilities.
- B) Developing sub-models to describe observed phenomena.
- C) Evaluating sub-models against experimental data.
- D) Combining sub-models into a rudimentary global model capable of predicting the gross aspects of system performance.

The overall project organization structure and the associated project objectives incorporate the components listed above and are shown in Figure 3.1.

Although development of a single comprehensive model is outside of the scope of this research, this dissertation does present the results of investigation in the areas of numerical modeling and field-scale experimentation that have contributed toward achievement of the group's overall goals. Chronologically, pilot-scale studies were carried out first. Since the model is attempting to match a field-scale kiln and



Bench-Scale

Determine Reaction Pathways

Field-Scale

Determine the effects of operational parameters[§] on:

- gas temperature^{1,2,3,4}
- gas speciation^{2,3,4}
- gas velocity¹
- bed evolution rates
- bed temperature

Pilot-Scale

Determine the effects of operational parameters[£] on:

- gas temperature[¥]
- gas speciation[¥]
- bed evolution rates
- bed temperature profiles

Notes on completed projects:

[§]Operational Parameters

- rpm: 0.1 or 0.25
- TA: on or off

[£]Operational Parameters

- rpm
- fill fraction
- burner firing rate

¹ Measured across upper quadrant of kiln exit

² Measured at two locations in the kiln exit

³ Measured at one point in afterburner

⁴ Measured in stack

[¥] Measured at one point beyond the kiln exit in the transition section leading to the afterburner

Figure 3.1 Overall Project Organization Structure and Associated Objectives

proven scaling laws do not exist, pilot-scale data cannot be used directly. However, the pilot-scale studies are needed to provide information to guide the much more expensive and involved field-scale experiments. Pilot-scale work that this author participated in includes the following: Owens et al., 1990a, 1990b, 1991, 1992; Silcox et al., 1990. The field-scale effort presented in this dissertation is aimed at providing information on velocity and temperature fields in an incinerator. Field-scale research that this author participated in, but preceding the work presented in this dissertation, includes the following: Cundy et al., 1989e, 1990, 1991a, 1991b, 1991c, 1991d; Sterling et al., 1990a, 1990b; Lester et al., 1991; Cook et al., 1992; Leger et al., 1991a, 1991b, 1993a, 1993b. Research in these two areas of field and pilot-scale experimentation is required to provide data needed to support the numerical modeling effort. Numerical modeling research not presented here includes Jakway et al., 1993a, 1993b, 1995a. The central focus of the modeling research is development of a rudimentary three-dimensional numerical model of a field-scale rotary kiln incinerator. The new research presented here centers on obtaining field-scale data and using this data to develop and validate a numerical model of a field-scale unit. The general objectives of the field-scale experimentation and numerical modeling research are explicitly enumerated in the following section.

SPECIFIC RESEARCH OBJECTIVES

Field-Scale Experimental Objectives

1. To design, build, and test a probe capable of measuring the temperature and, for the first time, velocity inside a directly fired rotary kiln incinerator;
2. To design a test procedure and matrix which will provide an accurate map of the velocity and temperature fields at a cross-sectional plane at the exit of the kiln for various operating conditions;

3. To perform experimental tests on a field-scale facility while recording continuous data from the kiln for several different operating cases;
4. To create velocity and temperature maps of the cross-section of the kiln exit;
5. To determine the effects of turbulence air addition on the temperature and velocity fields.

Numerical Modeling Objectives

6. To further develop the Leger et al. (1993c) numerical model of a directly-fired, field-scale rotary kiln by:
 - A) more accurately matching the geometry of the kiln and its inlets
 - B) improving the geometrical representation of the transition section
 - C) improving the numerical grid
 - D) accounting for radiation effects
 - E) adding soot to the radiation model
7. To compare the kiln exit flow field predicted by the numerical model with experimentally measured flow field data.

The following two chapters detail the methodologies used to achieve the objectives listed above. Chapter 4 presents the design work and results of the field-scale experiments. Chapter 5 presents the numerical model and compares results to data from Chapter 4 and previous experimental work. Chapter 6 summarizes results given in this dissertation, presents conclusions, and offers recommendations for future endeavors.

CHAPTER 4

IN SITU* VELOCITY MEASUREMENTS FROM AN INDUSTRIAL ROTARY KILN INCINERATOR

IMPLICATIONS

Previous experimental work has shown that incinerator flows can be highly stratified in both temperature and chemical species. This latest work shows that the exit of a rotary kiln incinerator can also be highly stratified in velocity and presents evidence that regions of reverse flow may exist. It is, therefore, important to consider the general velocity field when interpreting other measurements taken from the rotary kiln section of an incinerator. This is particularly important if single point sampling is used to characterize the incineration process, so that stagnant areas and regions of reverse flow can be identified. This work presents a device and methodology for measuring velocities in high-temperature, particulate-laden turbulent flows.

INTRODUCTION

At Louisiana State University, an ongoing research program is focused toward obtaining a better understanding and characterization of the physical and chemical processes associated with rotary kiln incineration. In this particular study, temperatures and, for the first time, velocities were mapped over a significant portion of the exit region of a directly-fired, field-scale, rotary kiln incinerator under

* Reprinted with permission from *The Journal of the Air and Waste Management Association*. November 1995. All Rights Reserved.

controlled experimental conditions. These measurements provide more insight into the complex heat transfer and fluid dynamics occurring inside the rotary kiln incinerator chamber. They also provide a means to develop and validate numerical models of these phenomena. Instrumentation used to obtain these data is discussed, the data are presented and discussed, and comparisons with a numerical model are provided.

BACKGROUND

This study was performed at the Dow Chemical Company rotary kiln incinerator located in Plaquemine, Louisiana. This facility has been described by Cundy et al. (1989a). Access to this kiln for experimental measurements is through an off-axis view port located at the back of the transition section between the exit of the rotary kiln incinerator and the entrance to the afterburner (see Figure 4.1). The refractory brick is 33 cm thick at this port, thus limiting boom movement. View port geometry, along with its location relative to the kiln, precludes access to all of the kiln exit; however, a new boom, developed to support the measuring devices, allowed a complete quadrant of the kiln exit to be mapped. Design of this boom will be discussed later.

Three off-axis primary burners are located on the kiln's front face, each of which may be fired using a combination of waste and/or conventional make-up fuel (typically natural gas). A large pack/drum loading chute is also located on the front face. Two tangentially oriented air nozzles on the kiln front face provide external air to increase turbulence and promote better mixing. Operation with and without the use of this turbulence-enhancing mixing air is denoted as TA-on (turbulent air on) or TA-off (turbulent air off) respectively.

This particular kiln has been the focus of study at Louisiana State University since the mid-1980's (Cundy et al., 1989a, 1989b, 1989c, 1991a, 1991b; Lester et al.,

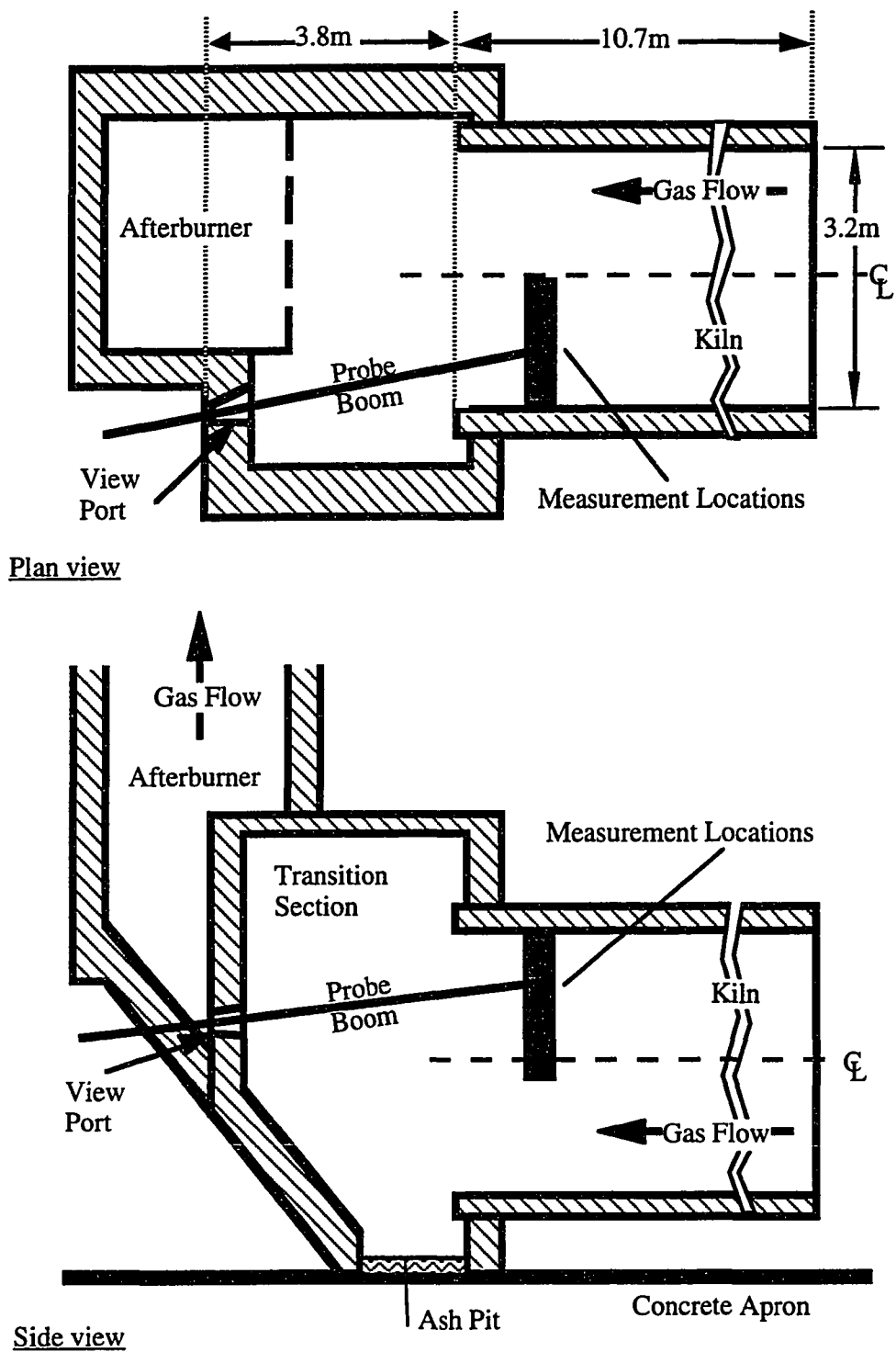


Figure 4.1 Schematic of rotary kiln incinerator and sampled area; Dow Chemical Company, Plaquemine Louisiana facility. Not drawn to scale (NTS).

1990; Leger et al., 1991a, 1993a, 1993b; Cook et al., 1992). Gas temperatures and compositions have been obtained from inside the kiln, afterburner, and stack. Experiments have been conducted under a variety of operating and feed conditions. The significant vertical gradients in temperature and chemical composition at this kiln's exit, characterized by a highly reactive combustion region (high temperatures and high levels of combustion products) in the upper kiln and a less reactive environment (low temperatures and chemical compositions close to that of ambient air) in the lower kiln, have been discussed at length. The gradients were observed in both steady waste feed experiments and transient pack feed runs, persisting even when the turbulence-enhancing mixing air was added.

Leger et al. (1993c) developed a fully three-dimensional numerical model of the flow field inside this rotary kiln incinerator. The model reproduced the experimentally-observed vertical stratification and further predicted the existence of a recirculation region in the lower area of the kiln exit. A parametric study using the model showed that the location and quantity of unmetered air infiltrating the kiln have a major influence on the flow inside the kiln. Overall, the study demonstrated that a relatively simple numerical model of a rotary kiln incinerator can provide valuable insight into the process, especially when used in conjunction with experimental data.

Results of these experimental and numerical studies have helped to provide a better picture of the incineration process in this rotary kiln incinerator; however, the picture is far from complete. A velocity map with corresponding temperatures at the kiln exit is needed to improve understanding of the flow dynamics, and to assist both in interpreting past data and further development of the model. This is also an important step in generalizing results from the kiln under study to other rotary kiln incinerators.

APPARATUS OVERVIEW

Velocity Probe

Any probe used inside an operating incinerator must be sturdy, since field conditions often involve difficult physical layouts and rough handling, not to mention low velocities and high temperatures, both of which fluctuate rapidly, along with an oxidizing and corrosive environment inside the kiln. These limitations ruled out the use of laser optical methods, hot wire anemometry, and typical narrow-bore Pitot-static tube instruments commonly used to measure velocity. Robustness is the critical criterion for probe design in this work environment.

McCaffrey and Heskestad (1976) developed such a probe for use in flame and fire applications. This robust, bidirectional probe is sensitive for use in low velocity flows (as low as 0.3 m/s) and is relatively insensitive to the flow orientation. Kent and Schneider (1987) used the bidirectional probe to determine velocities in large pool fires. Measured velocities from their work ranged from an average of 4.6 m/s to 12.6 m/s with temperatures of 460 K to 1,025 K. The probe was modified for use in the current work by installing an extra tube, as shown in Figure 4.2, thereby providing a combination of structural support and air cooling for the probe.

Velocity measurement using this probe is based on the differential between static and stagnation pressures. Under the Ideal Gas Law and Bernoulli assumptions, the free stream velocity, V , and the measured pressure differential between stagnation and static pressures, ΔP , can be related as follows:

$$V = \frac{\Delta P}{|\Delta P|} \sqrt{\frac{2 R T |\Delta P|}{M P C^2}} \quad (4.1)$$

where \bar{R} is the universal gas constant; T is the absolute temperature of the gas; the term $\Delta P / |\Delta P|$ gives the correct sign to V ; M is the molecular weight of the gas; C is a calibration constant; and P is the static pressure in the kiln. For the experiments presented here, the gas is assumed to be air, and the static pressure is assumed to be atmospheric since the kiln is operated at only very slight negative pressures. For Reynolds Numbers (based on the probe instrument head outer diameter) greater than 600 and less than 4000, Kent and Schneider (1987) determined the calibration constant, C , to be 1.07. Kent and Schneider (1987) also found the probe to be relatively insensitive to its alignment with the flow, producing errors no higher than

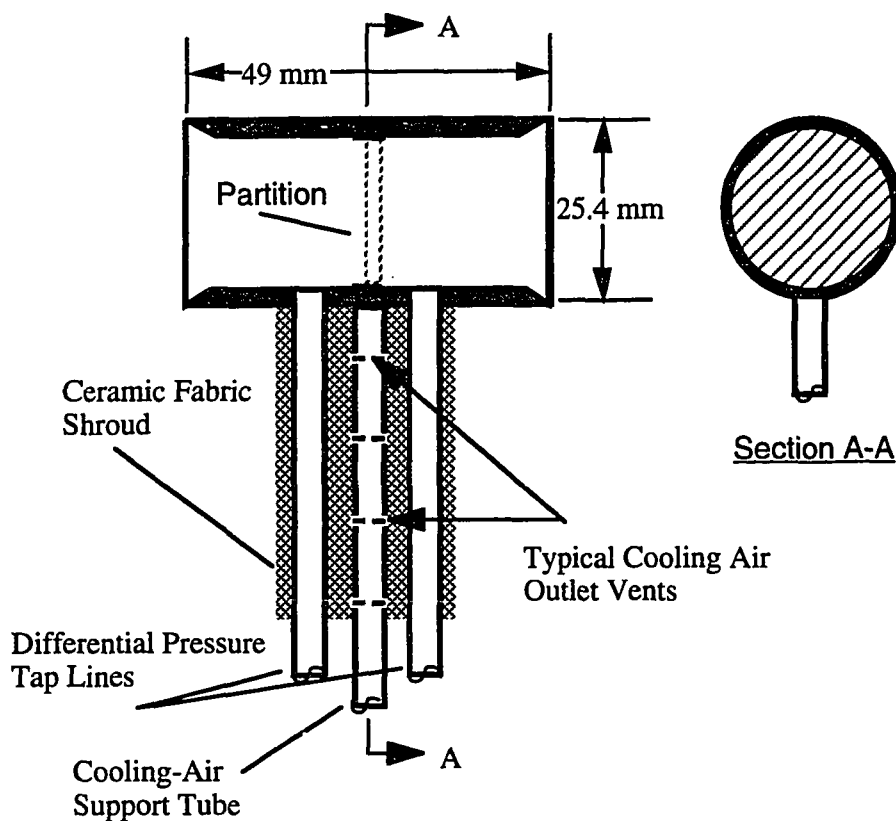


Figure 4.2 Bidirectional velocity probe schematic. NTS

10 percent for angles up to $\pm 50^\circ$ (where 0° represents probe alignment parallel to flow streamlines).

Pressure Transducer

The pressure differential, ΔP , was measured using an MKS Instruments Inc. model 220CO-00001A2BS pressure transducer. This instrument is rated from 0.0 inch to 0.5 inches water column (0.0 cm to 1.27 cm), with an accuracy of ± 0.005 inches water column (± 0.13 mm) and was factory calibrated.

Suction Pyrometer

To minimize radiation-induced error, a suction pyrometer was used to measure gas temperatures. The pyrometer is a 1.59 mm diameter, sheathed and grounded, type K thermocouple housed in a 9.53 mm OD Monel tube. This pyrometer was attached to the boom and placed in close proximity to the velocity probe, but not so close as to affect the free-stream velocity. Gas flow through the pyrometer was provided by an eductor using high pressure air for the driver. A suction flow rate of approximately 2.3 standard cubic meters per hour (SCMH) was maintained throughout the test program. Exhaust gas from the eductor was routed back into the incinerator downstream of the kiln exit.

Boom

The boom supports the velocity probe and suction pyrometer in the kiln and protects the associated tubing from the kiln's environment. The access port to the kiln is located 3.8 m downstream from the exit of the rotary kiln incinerator (see Figure 4.1). Hence, a relatively long and stiff boom was required in order to reach into the incinerator while maintaining confidence in the measurement location. A circulating-water-cooled boom used in previous experiments (Cundy et al., 1989a, 1989b, 1989c, 1991a, 1991b; Lester et al., 1990; Leger et al., 1991a, 1993a, 1993b; Cook et al., 1992) was considered for use in this study; however, because of the large

droop associated with the previous boom design and the inability to easily modify the boom to accommodate the velocity instrument head and associated tubing, this was ruled out. Consequently, we designed a light, stiff, and robust boom cooled with circulating water. A schematic of this boom is shown in Figure 4.3. The new boom design incorporates the following improvements:

- A removable probe-tip plate allows the boom to be used with different probes
- Two concentric aluminum jackets direct water flow and provide stiffness to the boom
- An air annulus between the inner and outer aluminum water jackets reduces the weight of the boom and isolates the hot return water from the cooler supply water
- The use of aluminum on all parts which are not directly exposed to the kiln environment reduces the weight of the boom
- A thicker walled tube incorporated along the base of the boom provides added support where the bending moment is highest

The velocity probe tip was aligned as close to co-axial with the expected kiln flow as possible. Tip deflection was measured outside the kiln to be 11.4 cm when the boom was filled with water and cantilevered. This same deflection was assumed to occur when the boom was fully inserted into the kiln, as the return cooling water, in general, was heated only 17° C, exiting the boom around 33° C. Construction details of this boom and a comparisons to the previous boom are given in “Appendix B” of this dissertation.

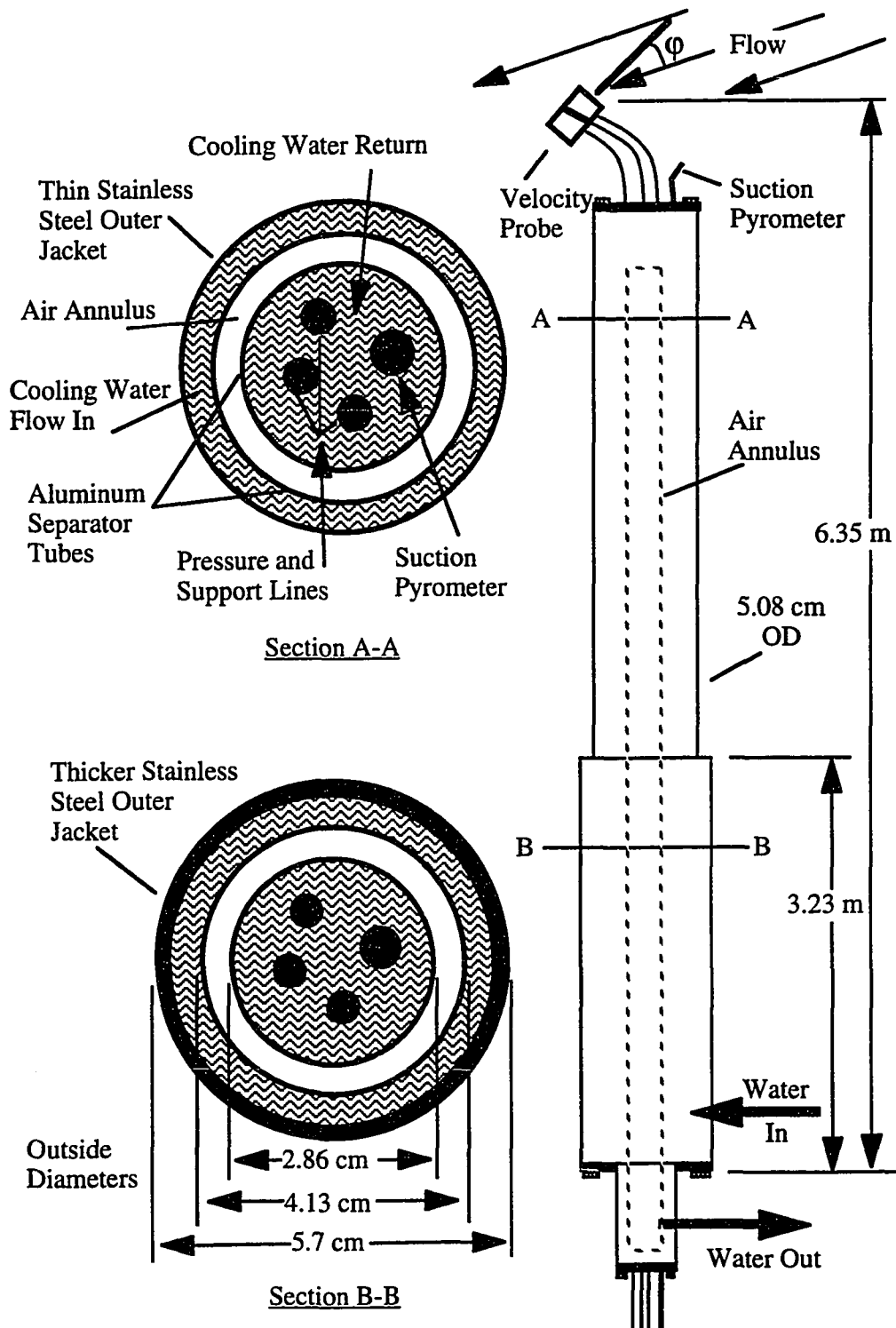


Figure 4.3 Circulating-water-cooled boom with bidirectional velocity probe tip. NTS

Boom Positioning Rack

For these experiments, a positioning rack was designed to securely hold the boom during measurement periods and to insure repeatability of position inside the kiln. The rack was attached to a handrail near the view port through which the probe was inserted. "Appendix C" of this dissertation shows a general view of this positioning rack.

EXPERIMENTAL METHOD

In the tests reported here, natural gas, air, and steam were fed to the kiln at the rates shown in Table 4.1. Rates are given as mean and standard deviations from data recorded every minute by permanent facility equipment. Kiln rotation rate was set to 0.25 rpm. No waste was fed to the kiln, nor was there a solids bed in the kiln during these experiments.

Table 4.1 System Input Parameters.

Measured Parameter	TA-off			TA-on		
	Air ¹	Fuel ¹	Steam ²	Air ¹	Fuel ¹	Steam ²
Kiln						
Upper Burner	990±8.2	225±0.268	22±1.4	990±10	225±0.165	22±0.20
Middle Burner	240±4.5	--	0	240±4.8	--	0
Lower Burner	990±7.4	279±0.287	21±2.5	990±6.9	279±0.176	22±2.7
Sludge Lance	--	--	37±0.40	--	--	37±0.35
Turbulence Air	0	--	--	2300	--	--
Afterburner						
Burner A	990±3.5	238	4.5±0.07	990±3.2	238	4.5±0.13
Burner B	710±13	255±0.388	0	710±8.3	255±0.280	0

¹ SCMH - Standard Cubic Meters /Hour:

(1 atm and 21.1° C for air)

(1.022 atm and 21.1° C for natural gas)

² kg/hr

At the beginning of the experiment, the two pressure lines from the pressure transducer were connected together and vented to the atmosphere in order to establish a zero pressure differential. This procedure was repeated throughout the experiment to monitor zero drift in the pressure transducer. Corrections for zero drift were made during post run data analysis. The pressure transmission lines connecting the differential pressure cell to the velocity probe were periodically purged with high-pressure, dry nitrogen to insure clear and dry lines. A sampling matrix was established prior to the experiment. During the experiment, the probe was positioned as close as possible to the predetermined locations using the positioning rack. The actual locations were recorded using locators on the boom and the boom positioning rack.

Temperature and differential pressure data were recorded for 90 seconds at most locations. For two locations during each operating condition (TA-on and TA-off), the data were recorded for 240 seconds, corresponding to the time required for one complete kiln revolution. Temperature data were recorded at 1.0 Hz while differential pressure data were recorded at both 0.3 and 1.0 Hz. After data were recorded at each probe location, the boom was moved, the zero differential pressure reading was recorded, and position, pressure differential, and temperature measurements at the new location were taken.

RESULTS

Mean Velocity and Temperature Data

Figure 4.4 presents a view of the kiln exit cross section showing the locations where measurements were obtained. Table 4.2 lists the location coordinates along with the corresponding velocity and temperature data.

Measurement locations were approximately the same for both TA-on and TA-off operating conditions. Location coordinate error was estimated to be ± 0.2 m in a

Table 4.2 Measurement Locations And Measured Mean Velocity And Temperature.

Location §	X (m)	Y (m)	Z† (m)	Velocity (m/s)		Temperature (K)	
				TA-off	TA-on	TA-off	TA-on
1	0.08	1.45	9.80	7.0 ± 0.7	7.1 ± 0.7	1340 ± 7	1289 ± 4
2	0.53	1.47	9.64	5.8 ± 0.7	6.6 ± 0.6	1328 ± 9	1274 ± 5
3	0.35	1.21	9.64	**	6.0 ± 0.7	1313 ± 10	1266 ± 6
4	0.05	0.79	9.67	4.1 ± 0.7	4.1 ± 0.8	1225 ± 12	1188 ± 6
5	0.52	0.80	9.51	3.7 ± 0.8	4.2 ± 0.8	1219 ± 7	1188 ± 4
6	1.26	0.82	9.38	4.2 ± 0.7	4.5 ± 0.8	1266 ± 7	1200 ± 8
7	0.32	0.34	9.53	2.9 ± 0.8	3.4 ± 0.9	1139 ± 14	1115 ± 11
8	0.04	0.00	9.64	1.9 ± 1.1	2.7 ± 0.8	978 ± 13	977 ± 16
9	0.52	-0.01	9.49	2.2 ± 1.1	**	975 ± 14	973 ± 12
10	1.20	-0.02	9.33	1.5 ± 1.4	1.3 ± 1.8	1001 ± 24	962 ± 38
11	0.05	-0.17	9.60	2.0 ± 1.0	2.1 ± 1.2	956 ± 26	851 ± 16
12	0.32	-0.18	9.53	2.0 ± 1.2	2.2 ± 1.0	945 ± 14	859 ± 34

- § X, Y, and Z measurements have an approximate error sphere of 0.2 meters
† Distance from front (burner) face of the kiln
** Data omitted because of problems/instabilities in the velocity measurements

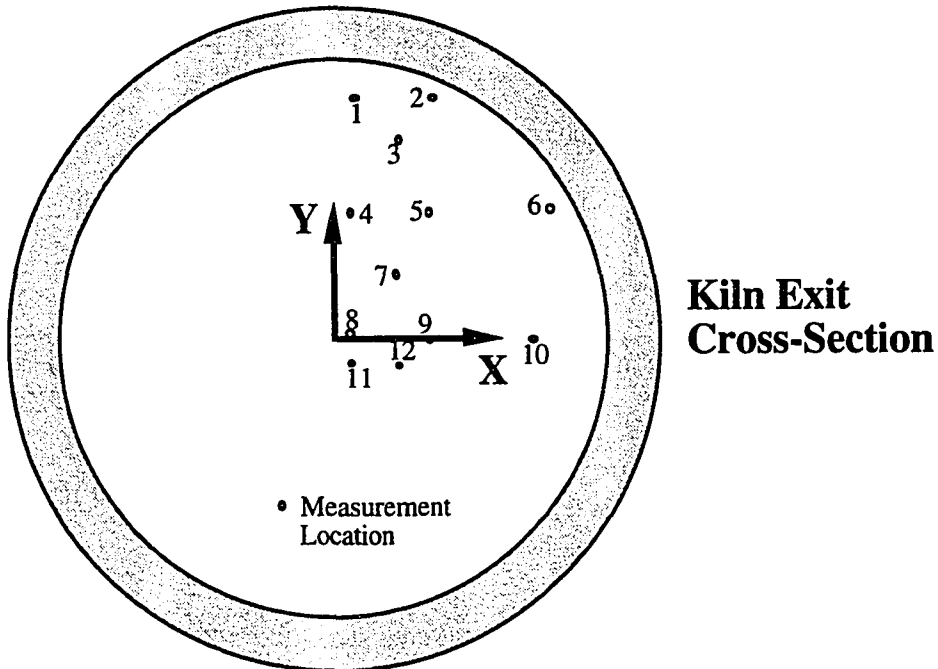


Figure 4.4 Measurement locations.

sphere surrounding the boom tip. Plans were to map a greater portion of the kiln exit; however, slag build-up in the access window hindered boom movement. Still, a complete quadrant of the upper kiln exit was mapped. Temperatures shown are average values from the 1 Hz data. Velocities were calculated at 1 second intervals using a factory calibration of the pressure transducer, the recorded zero drift, and the velocity equation (Equation 4.1). A velocity mean and standard deviation were then calculated for each location. Small-scale, turbulent fluctuations were not measurable due to the characteristic slow response time and insensitivity to flow orientation associated with the velocity probe. Raw velocity and temperature data are presented in Figure 4.5 for the operating condition of TA-on at three different locations along with a typical zero reading. In this figure, location 2 illustrates the relatively low fluctuations about the mean, common in the upper region of the kiln, while locations 10 and 12 demonstrate the wider fluctuations typically observed close to the center of the kiln. Location 10 presents conditions suggestive of intermittent regions of reverse flow. Difficulties with the velocity instrumentation were encountered at two locations—location 3 during TA-off operation and location 9 during TA-on operation—and therefore, the data associated with these locations are not reported. Probe-based Reynolds Numbers ranged from 1000 in the upper region to 300 near the centerline. Calibration work by Kent and Schneider (1987) shows a drop in the calibration constant from ~ 1.07 to ~ 1.02 between Reynolds Numbers of 600 to 300 along with an increase in uncertainty. However, the resulting error in calculated velocities near the centerline, up to 5 percent, was ignored in the present study.

Figures 4.6 and 4.7 show the velocity and temperature data as a function of vertical position along with fitted lines (to be discussed later). Strong vertical stratification is evident in temperature and velocity during both TA-on and TA-off operating conditions. Velocities and temperatures increase significantly from kiln

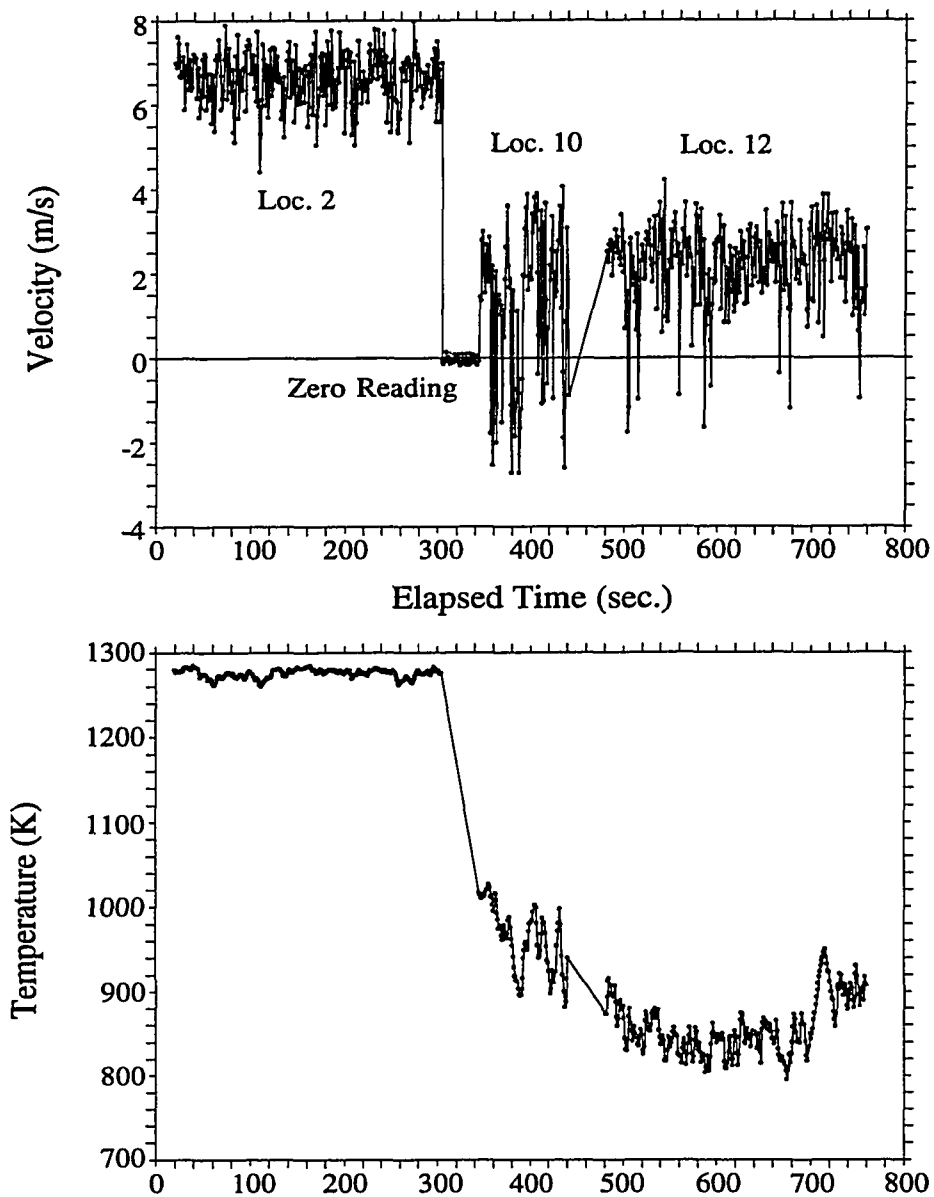


Figure 4.5 Sample raw data from three locations: TA-on.

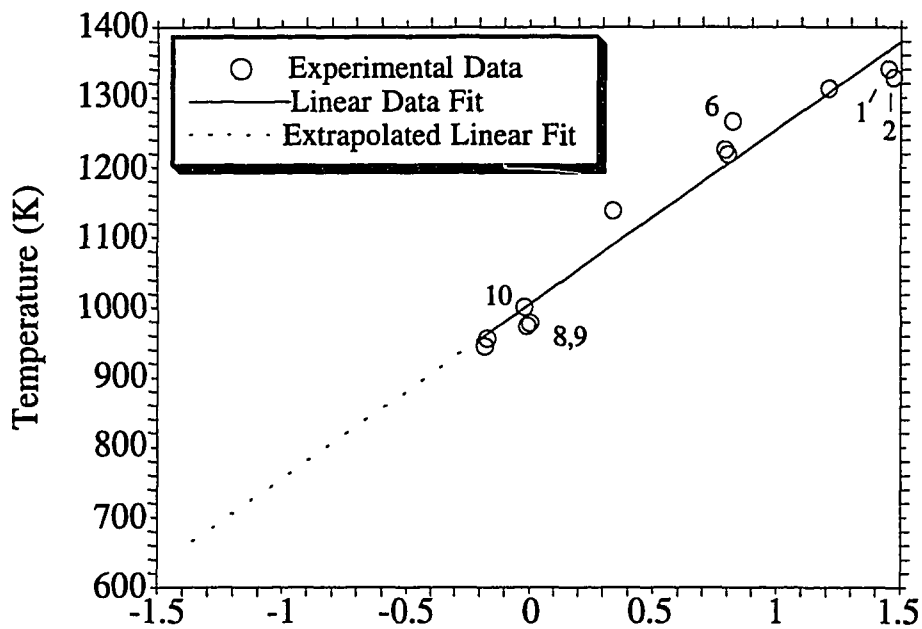
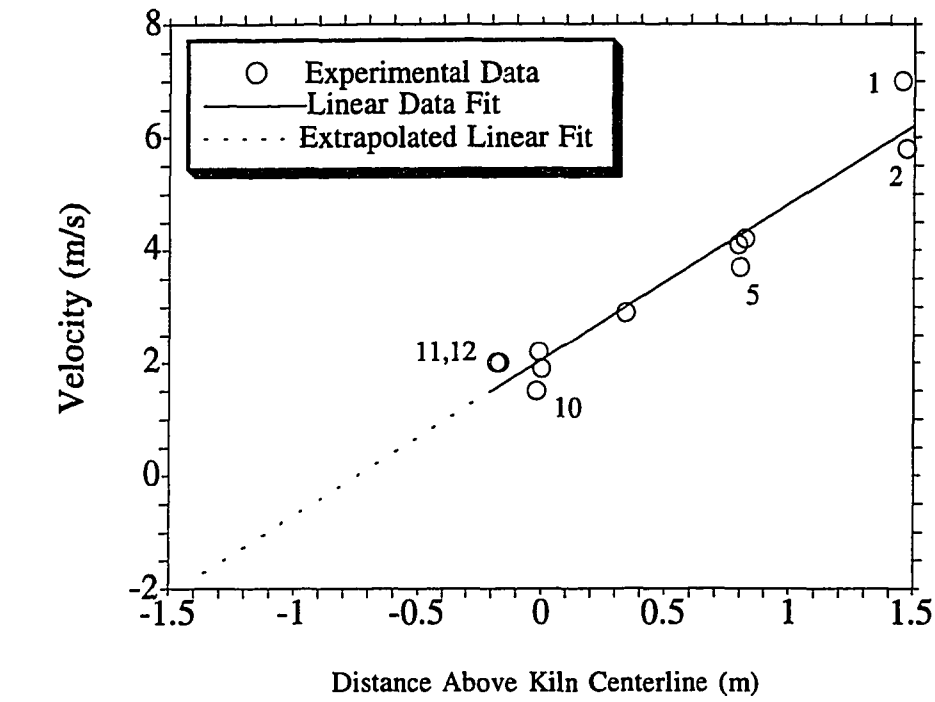


Figure 4.6 Experimental data with curve fits used in mass flow calculations: TA-off.

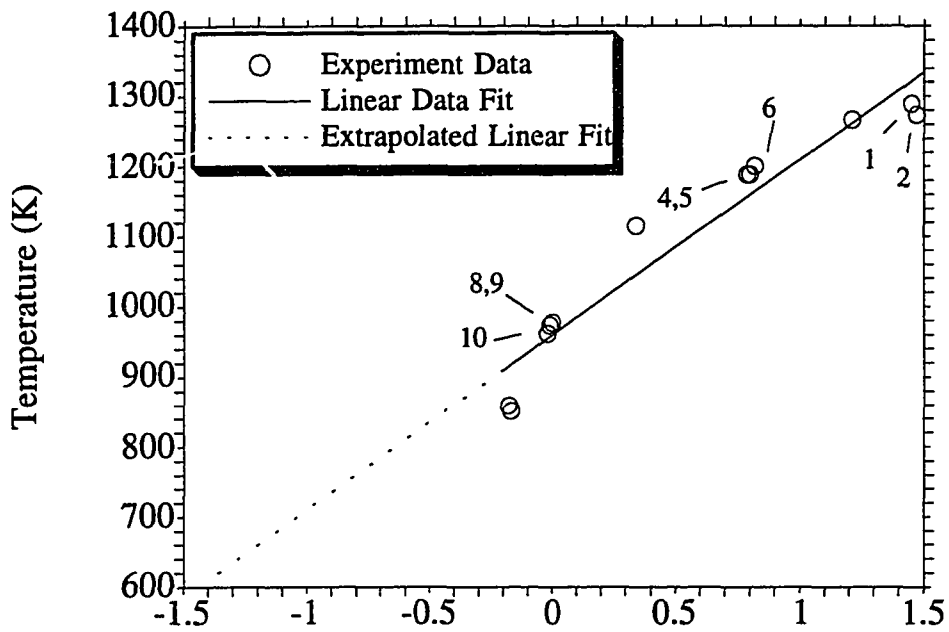
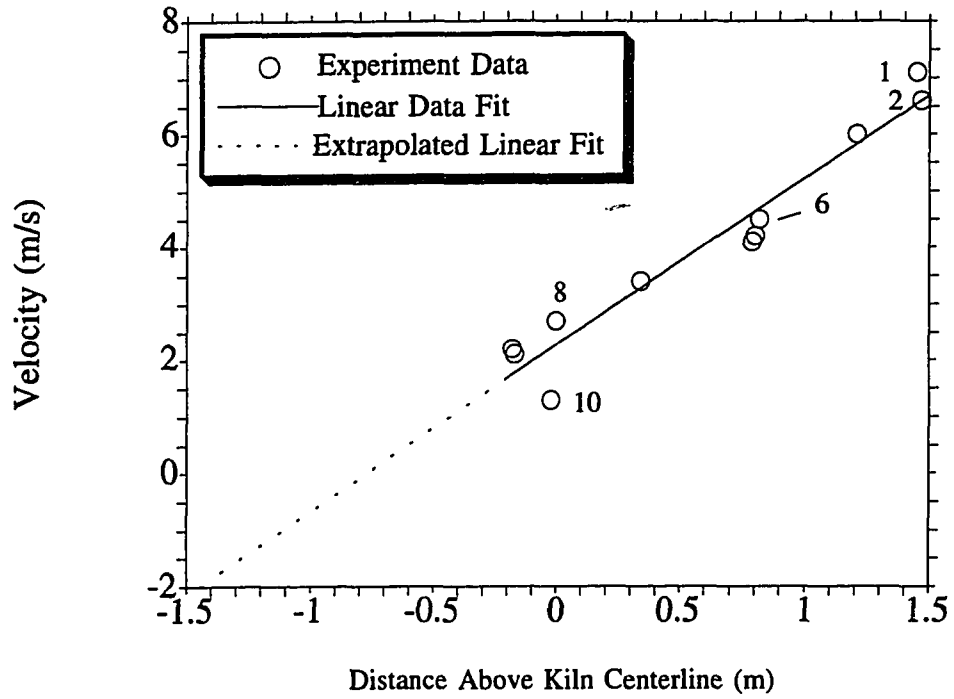


Figure 4.7 Experimental data with curve fits used in mass flow calculations: TA-on.

centerline to the upper regions of the kiln. In contrast, closely spaced and even overlapping data for a given vertical position indicate the lack of stratification in the horizontal direction. An exception to this lack of horizontal variation is that, for both operating conditions, the velocity at location 2 is lower than at location 1. One possible explanation is that location 2 may be close enough to the wall for wall effects to reduce the velocity. Proximity to the wall may also account for the generally higher temperature measured at location 6 and lower temperature at location 2. A study of the data recorded for one complete revolution of the kiln indicates no variance in velocity or temperature with kiln angular location. These results are consistent with previous observations in this kiln (Cundy et al., 1989a, 1989b, 1989c, 1991a, 1991b; Lester et al., 1990; Leger et al., 1991a, 1993a, 1993b).

When turbulence air is turned on, the amount of metered, ambient air entering the front of the kiln approximately doubles. This is the only independent input parameter that differs between the two cases. Thus, it is expected that the temperatures should be lower and the velocities higher in the TA-on case. During TA-on conditions, average temperatures are indeed lower, but only by approximately 45° C, and velocities show an even smaller difference with one of the averaged velocities actually lower for the TA-on case. Reasons for this small effect on velocities are the following: first, a large amount of unmetered air infiltrates the incinerator (5.5 and 3.2 times the metered air flows for the TA-off and TA-on cases respectively); second, less unmetered air infiltrates the incinerator during the TA-on conditions; and third, lower gas temperatures result in higher gas densities.

Previous numerical modeling (Leger et al., 1993c) for conditions similar to this experiment suggested the existence of reverse flow at the kiln exit. During this experiment, short-duration reverse flow was observed near the kiln centerline; however, quantification was not obtained. The pressure transducer was initially

calibrated to read only positive pressure differences. We planned to interchange the pressure taps when reverse flow was encountered, so that a positive pressure difference could be maintained, thus allowing quantification of any reverse flow. This swapping was accomplished by changing valve settings on a five-valve manifold, a process that took 15 to 30 seconds. Unfortunately, the reverse flow had a shorter than expected duration (typically 5 seconds or less) and was infrequent. After the experiment, it was determined that the instrument remained linear into the near reverse pressure range. This information was used to calculate the negative velocities shown in Figure 4.5. Combining the trend of decreasing velocity with elevation together with the appearance of short periods of reverse flow at some of the lower sampling points suggests that, had lower regions been sampled, substantial reverse flow may have been detected.

Mass Flow Study

This paper presents, for the first time, velocities measured inside an operating incinerator using the bidirectional probe assembly of Figure 4.3. Since this is the first time the probe has been used in a confined combustion environment, the data obtained need to be examined and checked for reasonableness. This check is accomplished by comparing the mass flow at the exit plane of the incinerator calculated in two ways. The first technique uses the measured velocities and temperatures to calculate the mass flow, while the second method is based on a mass balance across the kiln. The mass balance method uses the metered inputs along with an estimate of unmetered air infiltrating into the system. Since the second method does not involve the measured velocities, it provides an independent check of the experimental data.

I – Kiln Mass Flow from Experimental Velocity and Temperature Measurements

To calculate a kiln mass flow rate using the measured data, the individual point values of temperature and velocity shown in Table 4.1, and graphed in Figures 4.6 and

4.7, were first transformed into smooth surface functions. Because of the lack of horizontal variation, the surface equations were assumed to vary with "y" only, where "y" is the vertical direction measured from kiln centerline. Utilizing linear approximations for the y-dependency of temperature and velocity along with the ideal gas approximation, the local mass flux was calculated. By integrating this local mass flux over the area of the kiln's upper quadrant, where the experimental values were taken (29 percent of the total cross-sectional area), the total mass flow rate through this region of the kiln was obtained. Results of these calculations indicate mass flow rates of 2.5 kg/s and 2.9 kg/s for the TA-off and TA-on conditions respectively. If the lack of horizontal variation observed in this quadrant of the kiln is true of the other upper quadrant as well, then the above calculated flows can be doubled to yield the mass flow in the entire upper 58 percent of the kiln: 5.0 kg/s and 5.7 kg/s for the TA-off and TA-on conditions respectively.

To determine the total mass flow through the rotary kiln incinerator, the linear curve fits to the temperature and velocity data are assumed to extend to the bottom of the kiln. These straight-line extrapolations are shown as dashed lines in Figures 4.6 and 4.7 (Note that this extrapolation implies the existence of reverse flow in the lower region of the kiln.) Using this approximation, along with horizontal symmetry, the total net mass flow out of the kiln was calculated to be 4.5 kg/s and 5.2 kg/s for the TA-off and TA-on conditions respectively.

The assumption that the velocity and temperature data trends extend linearly to the bottom of the kiln is rather bold. Preliminary numerical modeling suggests, however, that linear extrapolation is usually appropriate. If this linear extrapolation method is indeed valid, the resulting net mass flow rates across the entire exit plane (4.5 kg/s and 5.2 kg/s for the TA-off and TA-on respectively) being less than the net mass flows out the upper half of the exit plane (5.0 kg/s and 5.7 kg/s for the TA-off

and TA-on respectively) indicates that there must be recirculation in the lower region of the kiln, and that the majority of the flow out of the kiln takes place in the upper region, as expected.

II – Kiln Mass Flow from Mass Balance

The mass flow rate calculated from the experimental data can be compared with that found from a mass balance on the system. To perform a mass balance, all inlet and exit flows need to be quantified. Information on all metered inlets to the incinerator is available and has previously been presented in Table 4.1. However, there is also a considerable amount of unmetered air infiltrating the incinerator. This infiltration results from the operation of the incinerator at a slight vacuum (1.1 cm negative water column during TA-off operation and 1.0 cm negative water column during TA-on operation), which is done to prevent fugitive emissions. This unmetered air infiltration rate must be determined in order to complete the mass balance.

Unmetered air infiltrates this system from the front and rear rotary seals of the kiln, around the perimeter of the solids loading chute at the front face of the kiln, and through the pressure relief hatch near the front of the incinerator. Additional air infiltrates the system through various instrumentation ports and other small openings. Although the amount of unmetered air entering through any one of these sources is not known, their combined effect can be calculated in two different ways. The first way, termed the Oxygen Method, uses the metered flow rates into the incinerator, the measured dry oxygen concentration at the stack (13.3 percent for TA-off and 13.5 percent for TA-on operation), and the assumption that the natural gas is pure methane which reacts completely to water vapor and carbon dioxide (Cook et al., 1992; Leger et al., 1993b).

A second way of calculating the unmetered air infiltration rate, the Mass Balance Method, involves performing a mass balance across the whole incinerator on a dry basis. Performing the mass balance on a dry basis allows use of the measured stack flow rate (24,551 SCM_H for TA-off and 24,755 SCM_H for TA-on operation), which was recorded on a dry basis. Again using the assumptions of pure methane completely combusting to water vapor and carbon dioxide, the unmetered air infiltration rate can be determined (Cook et al., 1992; Leger et al., 1993b). Results of these calculations are shown in Table 4.3.

Table 4.3 Calculated incinerator air infiltration, (SCM_H).

	TA-off	TA-on
Oxygen Method	21,400	19,890
Mass Balance Method	21,630	19,550

This table shows that the two methods of calculating unmetered infiltrating air compare very favorably. An average is used in subsequent calculations. Comparison of these data to those in Table 4.1 also shows that the unmetered air infiltrating the incinerator can be as much as 5.5 times the amount of metered air fed into the incinerator. This in-leakage is commonly included when calculating the amount of metered air needed to insure complete combustion in an incinerator.

The problem now reduces to one of proportioning the unmetered infiltration air in order to determine the mass flow in the rotary kiln incinerator. Obviously, this is a difficult process requiring a considerable degree of estimation. Leger et al. (1993c) reasoned that 55 percent of the total unmetered air infiltrating this system entered at the front face of the kiln. Using this estimate, the mass flow leaving the exit plane of the kiln was calculated to be 5.1 kg/s for the TA-off case and 5.5 kg/s for the TA-on case.

These mass flow values differ by 13 and 8 percent respectively from the values calculated above using the experimentally determined temperature and velocity. Thus, the data appear reasonable.

Numerical Model

A second way to examine the reasonableness of the experimental data is by comparison to a numerical model. Leger et al. (1993c) constructed a three-dimensional numerical model of the same rotary kiln incinerator studied in this work. The model is a finite difference type utilizing the SIMPLEC algorithm. The main weakness of this model is that radiation heat transfer is not included. While Leger et al.(1993c) modeled the same incineration facility utilized in the present study, the model inputs do not exactly match the present experimental conditions. For TA-off, the modeled kiln inputs differ from the operating conditions (previously presented in Table 4.1) in the following ways: the kiln natural gas flow was 27 percent lower, the metered air to the afterburner was 8 percent higher, and the unmetered infiltrating air was 25 percent lower. However, incinerator operating conditions for the TA-on case were nearly identical to those of the present study. Given the similarity between the model inputs and the operating conditions of this paper, useful comparisons can be made between the modeling and experimental results.

As an expected result of the omission of radiation heat transfer, the temperatures are over predicted for both the TA-off and TA-on cases. Model predicted velocities at the kiln exit for the TA-off case ranged from a high of 7.7 m/s at the top, to 0.7 m/s at centerline, to - 1.5 m/s at the bottom of the kiln, in an approximately linear fashion. For the TA-on case, velocities were 8.6 m/s at the top, 1.0 m/s at centerline, and - 1.3 m/s at the bottom of the kiln, again varying in an approximately linear fashion.

These modeled velocities are close to the measured values, but are slightly higher at the top of the kiln and marginally lower at the centerline of the kiln. The model also confirms the uniformity of the flow field in the horizontal direction. At a distance one quarter from the top, the maximum deviation from the predicted mean values of velocity and temperature taken horizontally across the kiln are respectively 10 and 14 percent for TA-off, and 13 and 1.2 percent for TA-on operation. The small size of these deviations predicted by the model improves confidence in the assumption that the lack of horizontal variation of velocity and temperature in the quadrant sampled extends to the other quadrants of the kiln exit.

SUMMARY

A new device for measuring velocities and temperatures inside a directly-fired, full-scale, rotary kiln incinerator has been developed, constructed, and tested. Temperatures and, for the first time, velocities were mapped across an upper quadrant of a rotary kiln incinerator during steady state burning of natural gas. The experimental results and ensuing analysis provide the following conclusions.

- Stratification of both temperature and velocities is evident in the vertical but not horizontal direction.
- The highest velocities and temperatures were recorded at the top of the kiln.
- The effect of the turbulent air jets on velocities and temperatures at the exit of the rotary kiln incinerator is largely mitigated by the large amount of unmetered air infiltrating at the front of the kiln.
- Temperature values and data stratification trends generated by this new device agree with previous experimental findings on the same incinerator under similar operating conditions.

- Mass flow rates calculated using the experimental results compare favorably with mass flow rates calculated by a mass balance across the kiln.
- Numerical modeling also produces results that compare favorably with those generated by the new experimental device.
- The need to sample a complete vertical traverse of the rotary kiln incinerator to determine the amount of air infiltrating at the front of the kiln and the possible existence of reverse flow at the exit of the kiln is reinforced.

Prior to obtaining the velocity and temperature data reported in this paper, there were virtually no means to quantify the mass flow inside rotary kilns. This led to uncertainty about the distribution of unmetered infiltration air and the flow dynamics at the locations of previous sampling efforts. Because the limited access of this incinerator did not allow a complete mapping of the kiln exit, the amount of unmetered air entering the kiln is still uncertain. However, the results do help to provide confidence that the estimated infiltration air distribution of Leger et al. (1993c) is realistic. Further, the results indicate that, with adequate access, this probe assembly could completely characterize the mass flow field of this rotary kiln incinerator or other similar combustion devices. Limitations include material compatibility with kiln environment, pressure transducer limitations, and calibration constant applicability limits (not a theoretical limit, but so far determined only for the Reynolds Number range of 300 to 4000 according to Kent and Schneider (1987)). In addition, the relatively good agreement between the measured and calculated kiln mass flow rates suggests that the experimental techniques used and the assumptions imposed (horizontal symmetry at the exit region of the kiln, along with linear velocity and temperature profiles) are reasonable. While this may seem a circular argument, it should be noted that, primarily due to the complexity of the system, never before has

the flow field of an operating rotary kiln incinerator been quantified. With each piece of new information, the picture of what takes place inside a rotary kiln incinerator becomes clearer, and the ability to test previous assumptions becomes possible. While the measurements reported in this paper only covered a portion of the kiln exit region, they have added considerably to our understanding of the complicated process of rotary kiln incineration.

CHAPTER 5

THREE-DIMENSIONAL NUMERICAL MODELING OF A FIELD-SCALE ROTARY KILN INCINERATOR

INTRODUCTION

The second-generation numerical model of a field-scale, direct-fired, rotary kiln incinerator presented in this paper represents a continuation of work initiated by Leger et al. (1993c), hereafter referred to as Leger's model. The work is part of a comprehensive rotary kiln incineration research program undertaken over the past ten years at Louisiana State University. The overall goal of this program is to obtain a better understanding of hazardous waste incineration in rotary kiln facilities.

Leger et al. (1993c) have provided a comprehensive overview of recent attempts to model rotary kiln incineration processes. This overview points out that incinerators are typically over designed and operated far below capacity, and that there is a scarcity of field-scale data, proven numerical models, or empirical relations for design or optimization studies. The lack of experimental data is due, in part, to strict incineration regulations requiring field-scale units to operate within a narrow range of previously established compliance conditions with virtually zero tolerance for excursion from these limits. Recent modeling studies conducted at LSU have, therefore, aimed toward development of a comprehensive and reliable numerical model of rotary kiln incineration. This model can then be used to investigate, among other issues, the effects of system geometry, overall configuration, and waste composition

as well as optimal operating parameters, and failure modes, all currently nearly impossible to do in the field.

The approach taken by Louisiana State University has been to develop this model in stages, relying on experimental data to characterize and verify predicted kiln behavior under various operating conditions. The current stage of model development focuses only on the rotary kiln section of the incinerator during operation without waste processing. This stage, a second generation model which is presented here, builds on its predecessor (Leger et al., 1993c) by providing a more accurate representation of the facility geometry and including the effects of radiation and soot in the heat transfer analysis. A grid dependency study is provided for the first time, and sensitivity and parametric studies are also presented. Waste is not yet included in the model because even baseline conditions (operation with natural gas support flames only in the kiln) have yet to be fully understood and modeled. Even so, the model in its current stage of development, can be used for limited design and operation studies as demonstrated in the following sections.

PHYSICAL SYSTEM

The incinerator under study (Figure 5.1a shows a general skematic) is owned and operated by The Dow Chemical Company. It is a direct-fired, hazardous waste, rotary kiln incinerator located in Plaquemine, Louisiana. A more complete description of the facility is available elsewhere (Cundy et al., 1989a; Montestruc, 1989; Jakway et al., 1995a, 1995b); only a brief description is provided here.

The kiln is 10.7 m in length and its inside diameter is 3.2 m. Gases exiting the cylindrical kiln pass into a rectangular transition section which directs the flow into a vertical afterburner. Gasses then pass through air pollution control systems and the stack. As shown in Figure 5.1b, the front face of the kiln is highly non-symmetric,

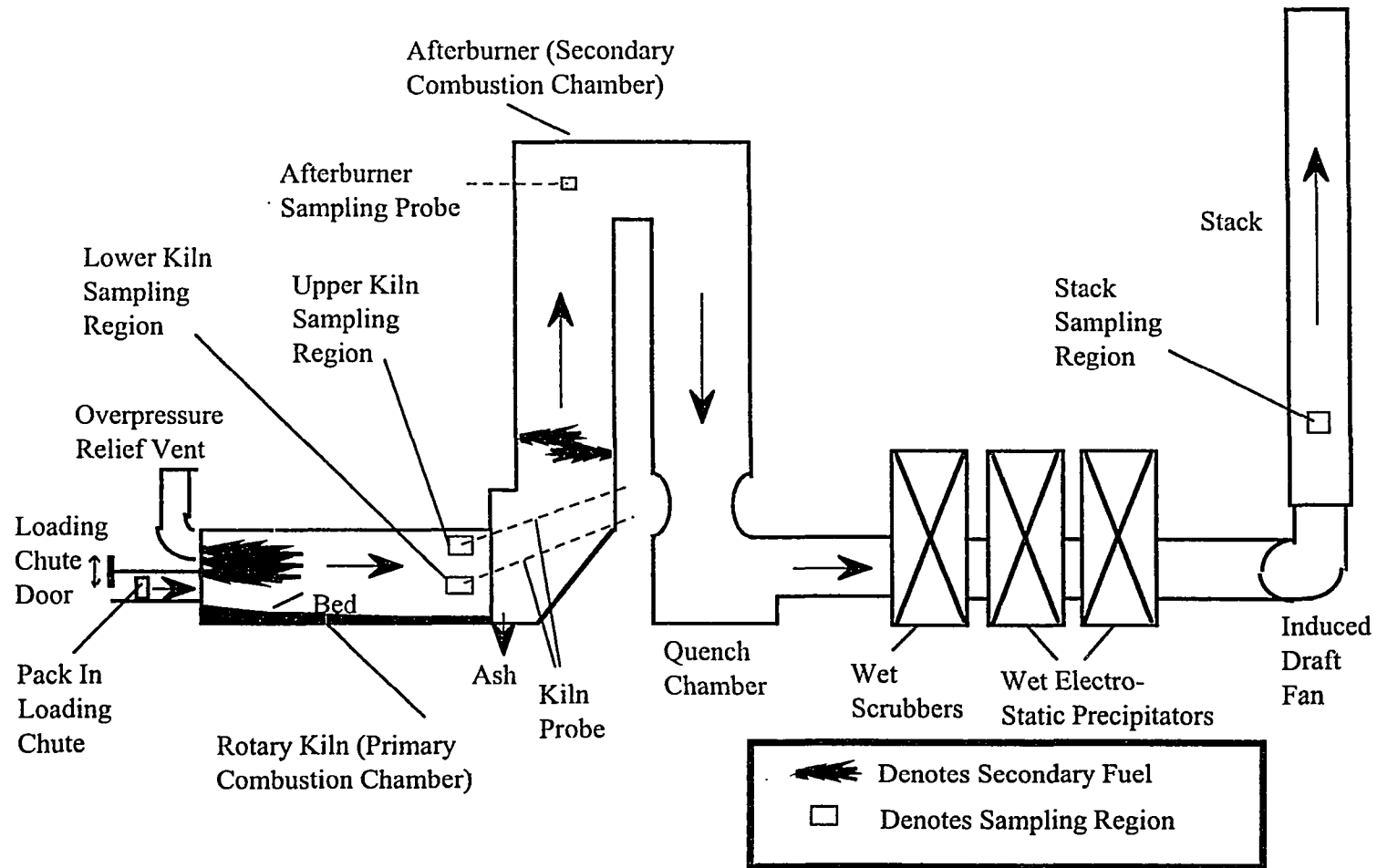


Figure 5.1a Schematic of Dow Rotary Kiln Facility Showing Approximate Sampling Locations.

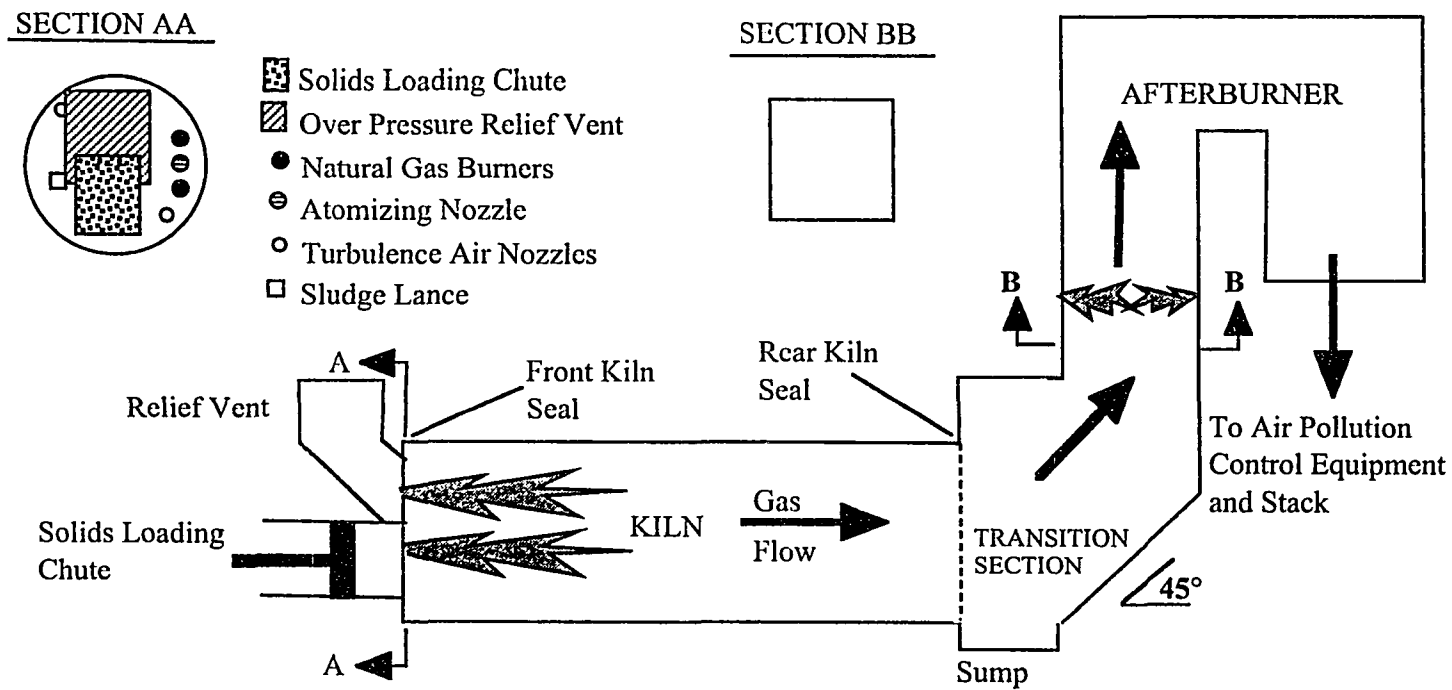


Figure 5.1b Side View Schematic of Rotary Kiln, Transition, and Afterburner Sections of The Incinerator Studied In This Work.

with an off-axis solids loading chute as well as off-axis and angled natural gas burners and secondary air nozzles (termed turbulence air nozzles). Turbulence air nozzles are designed to assist combustion by introducing a jet of high velocity ambient air, thereby increasing turbulence and mixing in the kiln. The system is designed to operate with (TA-on) or without (TA-off) secondary turbulence air.

The kiln is operated at a slight vacuum to prevent fugitive emissions; this also allows substantial amounts of unmeted air to infiltrate into the system. Infiltration is known to occur at the front and rear kiln rotary seals, around the edges of the solids loading door and pressure relief hatch, and through various instrument ports. Infiltration amounts have been calculated as high as 5.5 times the metered air flowing into the incinerator system (Leger et al., 1993b; Jakway et al., 1995a, 1995b). A fuel-rich mixture of natural gas and air is typically injected from the upper and lower kiln burners, which also have a low steam feed to cool the burners.

NUMERICAL KILN MODEL

The model described here contains a number of improvements and new features not contained in Leger's model. In this section the general solution method is presented, followed by brief discussions of the geometry, the grid, and methods used to calculate important physical properties. Radiation (added for the first time) and the chemical reaction rate mechanism are then discussed. This section concludes with a discussion of boundary conditions.

Solution Method

The commercial software package, FLUENT version 4.25, produced by Fluent Inc. (Fluent, 1993), is used as the primary source code for the model. This package employs a control-volume-based, finite-difference solution technique to allow full characterization of the flow field. The Reynolds-averaged Navier-Stokes equations coupled with the Reynolds-averaged governing differential equations of continuity,

energy, and species (listed in “Appendix G” of this dissertation) are solved in a discretized form. The standard κ - ϵ turbulence model is employed. To obtain values at control volume interfaces needed for flux calculations, the power law interpolation scheme is utilized. The pressure-linked continuity and momentum equations are solved using the Semi-Implicit Method for Pressure-Linked Equations Consistent (SIMPLEC) solution algorithm. Specific details regarding convergence parameters such as multigrid and underrelaxation factors are available in “Appendix H” of this dissertation.

Geometry Details

The model focuses on, and is considered valid only for, the rotary kiln segment of the incinerator. However, the section immediately downstream of the rotary kiln (the transition section, Figure 5.1) must be included in the model because it exchanges radiation with the kiln, shifts the flow centerline horizontally by 0.7 m, and, for modeling purposes, prevents influx of undefined material at the outlet boundary which would otherwise occur due to recirculation at the kiln exit. This second generation model represents the transition section geometry more accurately than the previous attempt (Leger et al., 1993c), which did not include the horizontal flow shift or the 45° inclination (shown in Figure 5.1).

The outflow boundary condition used in this model requires the flow leaving the solution domain to be fully developed; however, the flow leaving the transition section is far from fully developed. To remedy this situation, a fictitious chimney was added at the exit of the transition section having the same cross-section as the afterburner shown in Figure 5.1. To reduce the height needed to achieve a fully developed exit flow from the solution domain, the chimney’s exit area was reduced or “necked” (see Figure 5.2), eliminating a region where recirculation tended to form. The necked chimney results in a nearly fully developed flow field, without inflow, at the

solution domain exit. Thus, while the kiln and transition section shown in Figure 5.2 are accurate representations of the actual geometry, the chimney section is fictitious and is included only for modeling purposes. It's important to note that the chimney necking does not affect the kiln flow, which is the focus of this study, since the area of the afterburner that is removed by the necking is well downstream from the kiln, and the flow field removed by the altered geometry is essentially a region of separated flow.

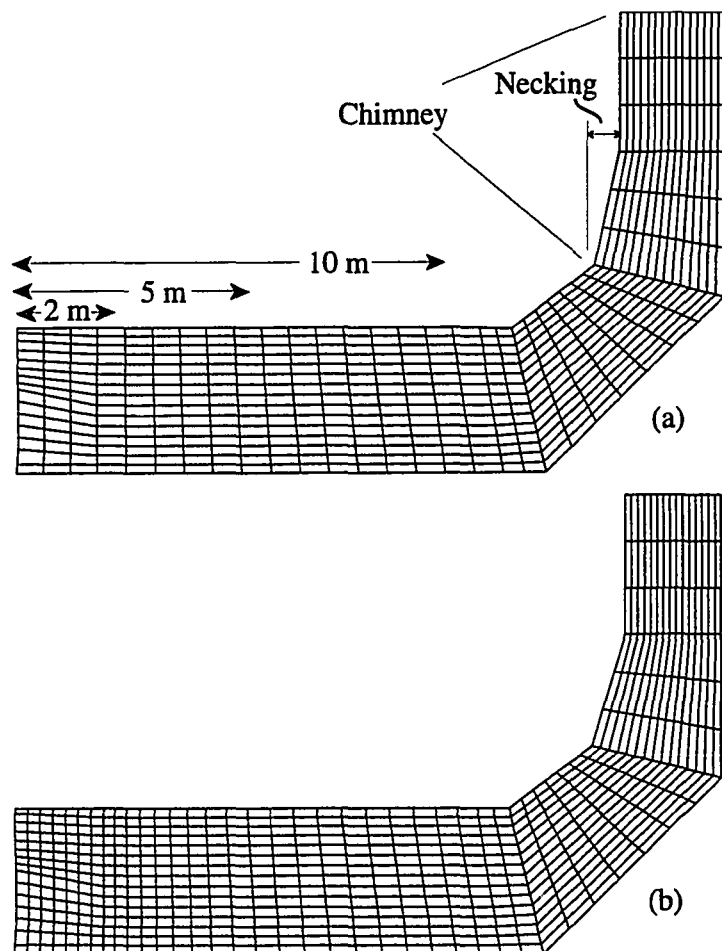


Figure 5.2 Side view of numerical model grid center line: a) initial coarse grid, b) refined grid.

Grid Details

Clearly, the system under consideration is neither rectangular nor cylindrical, but a mix of geometries throughout; the longitudinal kiln walls are cylindrical, and the solids loading chute as well as the transition and afterburner sections are rectangular. In addition, the system has no symmetry which could otherwise be used to simplify the solution technique.

In all previous attempts to model this incinerator system (Leger et al., 1993c; Khan et al., 1993), rectangular coordinates were used. This resulted in a relatively large number of control volumes positioned outside the fluid region to create stair-stepped approximations of the cylindrical kiln walls. In the current model, a non-orthogonal, curvilinear grid is used to match the geometry of the cylindrical walls exactly (termed a body fitted coordinate grid, BFC) without using any unnecessary control volumes. Figure 5.3 shows this grid for cross-sections at two axial locations.

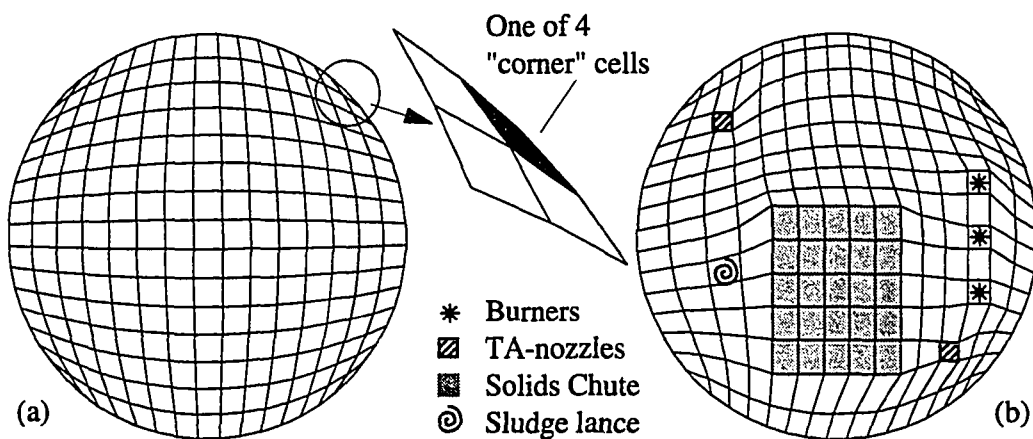


Figure 5.3 Axial cross-section of grid used for rotary kiln showing internal control volumes at: a) typical uniform section downstream from front face; b) front face.

In the previous modeling attempts (Leger et al., 1993c; Khan et al., 1993), the coarseness of the grid and the use of uniform grid spacing required the position of inlet streams (natural gas, steam, and mixing air) to be slightly shifted from actual locations. In addition, the nozzle flow areas were also different from actual areas found in the field; hence, gas velocities differed from known values so that the mass flow rates would match. The non-uniform grid spacing utilized in the current model alleviates this problem thereby allowing gas inlets to be placed and sized precisely. The only exception is the rotary seal gaps at the front and rear of the kiln which are too small to be correctly sized with the coarse grid employed.

The grid used in the model consists of 17×17 control volumes per axial cross-section (15×15 internal control volumes and a boundary control volume at the ends of each row and column of internal control volumes). There are 34 grid cross-sections in the axial flow direction for a total of 9,826 control volumes. Figure 5.3b shows the grid used at the front face of the kiln and highlights the grid distortions used to position and size the inlets accurately. Because of the limited number of control volumes, burners and turbulence air nozzles are represented by single square control volumes. Perimeter cells on the kiln front face are set as inlet cells to account for air infiltrating through the front rotary seal. Two intermediate grid cross-sections are used to make the transition from the distortions of the front face (Figure 5.3b) to the uniform cross-sections shown in Figure 5.3a.

A side view of the centerline grid is shown in Figure 5.2a. This figure also illustrates the necked chimney, which, when combined with the elongation of the chimney control volumes in the flow direction, significantly reduces the total number of control volumes necessary to satisfy the exit boundary condition. Figure 5.2b is a refined version of the grid discussed in a later section.

Fluid Physical Properties

Natural gas feeding the support flames contains a minimum of 95 percent methane by volume and, therefore, is modeled as pure methane. Fluid physical properties are calculated as indicated in Leger et al. (1993c), with the exception of the pure component heat capacities. These are calculated using third order polynomials (listed in "Appendix H" of this dissertation) in temperature fit to data from the JANAF tables (Stull and Prophet, 1971). Maximum error in the resulting heat capacity polynomials is 2.6 percent over the range of 300 K to 3,000 K.

Radiation

Radiation heat transfer is calculated by the Discrete Transfer Radiation Model (DTRM) discussed by Murthy and Choudhury (1992). Heat transfer in the DTRM is accomplished by following the path of radiation as it travels from one surface to another. Eight paths are traced from each surface control volume. Increasing the number of paths to sixteen changed the maximum gas temperature by only 0.3 percent; however, both CPU time and computer storage requirements were significantly increased. As the path from one surface to another is traced, adsorption and emission from participating media are included.

In all experiments that Louisiana State University conducted at this facility, the support flames in the kiln have been orange colored (Lester et al., 1990) and fuel rich, with equivalence ratios at the burners ranging from 2.2 to 2.9 on a molar basis. Therefore, it was concluded that a substantial amount of soot was formed near the burners. As the majority of radiation from flames laden with soot originates from soot particles (J. De Ris, 1978), it is important to include soot in the heat transfer model. Fluent, however, does not currently account for the radiation effects of soot; instead, a special version of the Fluent software was obtained which allowed modification of certain subroutines, including the calculation of absorption

coefficients. The remainder of this sub-section focuses on the subroutines developed to include the radiation effects of soot by modifying the absorption coefficients used in the standard Fluent software package. The numerical codes for the subroutines are given in “Appendix F” of this dissertation.

Effects of gas composition and soot particles on absorptivity, α , are calculated separately and then combined using the technique of Felske and Charalampopoulos (1982):

$$\alpha = \alpha_p + \alpha_g - \alpha_p \alpha_g \quad (5.1)$$

where α_p is the absorptivity of soot particles alone with no participating gas media, and α_g is the absorptivity of gases alone without soot. The Weighted Sum of Gray Gasses, (WSGG) model is used to calculate α_p , with values for the coefficients given by Felske and Charalampopoulos (1982). In calculating α_g , the spectral nature of the gas absorptivity is included using the Wide Band Property Model (WBPM) of Edwards (1981). This model also accounts for arbitrary concentrations of carbon dioxide and water vapor, and compensates for overlapping radiation bands.

The absorption coefficient, α_{ac} , is related to absorptivity, α , and the mean beam length, L_m , on the basis of Beer’s Law (Incropera and DeWitt, 1985):

$$\alpha = 1 - \exp(-\alpha_{ac} L_m) \quad (5.2)$$

The source temperature used in the WBPM is calculated as the volume-based average of all gas-domain control volumes in the upper two thirds of the kiln, as experimental measurements and the model indicate that this is where the majority of the carbon dioxide, water vapor and soot are located. To calculate L_m , the relation of Gorog et al.

(1981) is used. This relation is valid for an infinite circular cylinder of diameter D radiating to its walls and a bed of materials in the bottom of a cylinder of depth F , through a gas of finite optical thickness.

$$L_m = 0.95(1 - F/D)D \quad (5.3)$$

For this work, the bed depth is set to zero, so that L_m is $0.95D$.

Chemical Reactions

I – Reaction Rate Limits

To determine the reaction rate limit, the Damkohler number, D_a , defined as the ratio of the characteristic mixing time, τ_m , to the characteristic chemical reaction time, τ_c , is calculated as follows (Glassman, 1987):

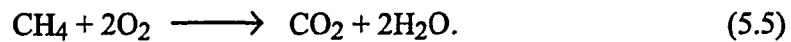
$$D_a = \frac{\tau_m}{\tau_c} = \frac{l_o \cdot S_l}{U' \cdot \delta_l} \quad (5.4)$$

where l_o is the characteristic length of large eddies, S_l is the laminar flame speed, U' is the magnitude of turbulent fluctuations, and δ_l is characteristic thickness of the premixed flame. Several assumptions are required to make this calculation. The inside diameter of the burner chamber, 0.25 m, is used for l_o , and Glassman (1987) recommends 40 cm/s for S_l . Thus τ_m is approximately 0.4 s. To calculate U' , the relation $U' = U \cdot (U'/U)$ is used, where U is the fluid mean velocity in the flame region, typically 7 m/s as estimated by the current numerical model, and U'/U is the turbulent intensity, estimated at 10 percent. Glassman (1987) uses typical hydrocarbon flame lengths, δ_l , on the order of 1 mm. These values combine to yield τ_c at approximately 0.003 s.

Because the characteristic time of chemical reaction is much less than the characteristic time of mixing (Damkohler Number approximately 130) the rate of reaction for this work is assumed to be turbulent mixing rate limited. Consequently, the eddy break-up model of Magnussen and Hjertager (1977) was chosen to determine the reaction rate.

II – Methane Reaction Model

Methane combustion is modeled by the one step global reaction (Leger et al., 1993c):



III – Soot Reaction Model

The simple methane reaction model does not allow for soot formation; however, calculation of soot absorptivity detailed earlier requires the soot volume fraction, f_v . Therefore, for modeling purposes soot is assumed to enter the kiln at the burner nozzles. Soot is added at the expense of N_2 instead of CH_4 in order to maintain the correct overall flow rate and heat input to the incinerator. Bard and Pagni (1981) have shown that between 0.5 and 3.1 percent of the volatile carbon is converted to soot in a variety of fuels; Clark et al. (1986) use a value of two percent for all fuels in their modeling work. While there is a degree of uncertainty, a value of one percent soot conversion was chosen for this modeling work. In the highly turbulent flame zone, soot is assumed to flow with the local gases. The soot volume fraction, defined as the volume of soot per unit of gas volume, can be calculated as:

$$f_v = \frac{V_p N_A X P}{\bar{R} T} \quad (5.6)$$

where V_p is the volume of each soot particle, N_A is Avogadro's number, \bar{R} is the universal gas constant, X is the mole fraction of soot particles, and P is the control volume pressure which is assumed atmospheric. To calculate the volume of a soot particle, some assumptions about shape and size must be invoked. Even though as soot agglomerates it can take a variety of shapes such as clusters, straight chains, or irregular, random structures (Charalampopoulos and Chang, 1991), soot is often assumed spherical for modeling purposes. Bard and Pagni (1981) give values ranging from 27 nm to 47 nm for the mean radius of soot in pool fires generated from a variety of fuels; Wagner (1981) suggests a radii in the range of 20 nm to 30 nm; Charalampopoulos and Chang (1988) graph soot radii as a function of height above a flat flame burner, with values ranging from 16 nm to 36 nm for premixed propane in oxygen with an equivalence ratio of 1.8. A 25 nm spherical radius was chosen for the present work.

An average soot particle contains 10^6 carbon atoms (Wagner, 1981) and only one percent of the fuel carbon atoms are assumed to contribute to soot production. Hence, soot particle mole fractions are typically very small. This is important since transport equations in Fluent are solved in terms of mole fractions using single precision FORTRAN variables. To circumvent precision problems, the transport equations are solved in terms of the mole fraction of individual carbon atoms which form the soot particle, termed "soot carbon atoms," rather than the entire soot particle. The mole fraction of soot needed for Equation 6 can then be accurately calculated from the mole fraction of soot carbon atoms within the double precision code developed for this work, rather than the primary, single precision Fluent code. For the present modeling work, the soot carbon atoms are assigned a molecular weight of 12 and a specific heat for carbon atoms in the solid phase. The specific heat used is

third order in temperature, calculated from curve fits given in Gardner (1984) for the temperature range of 300 K to 2,500 K. Because of their minimal importance in the overall flow field calculations, the gas thermal conductivity and molecular viscosity terms are not altered to reflect the presence of soot.

No mechanism for soot combustion is included. Instead, soot downstream of the first one-third of the rotary kiln is assigned an absorptivity of zero (corresponding to soot burnout). This distance is based on typical visual observations at the incinerator facility (Lester et al., 1990). Radiation exchange with carbon dioxide and water vapor is included throughout the incinerator.

Boundary Conditions

Since 1987, the incineration research group at Louisiana State University has performed a number of field-scale tests using this incinerator (Jakway et al., 1995b). Several of these tests will be used to verify the model (Leger et al., 1991a, 1993a, 1993b; Jakway et al., 1995a, 1995b). Operational conditions recorded during these tests are used to determine the inlet boundary conditions for the model. A complete list of conditions used in the current work, including inlet speciation, temperature, and three-component velocities are provided in “Appendix H” of this dissertation.

The refractory brick walls of the kiln, transition, and chimney sections are assigned an emissivity of 0.8 (Gorog et al., 1983), and the surfaces of all inlets to the rotary kiln are assigned emissivities of 0.01. The maximum rotation rate during field-scale testing was 0.25 rpm, generating a velocity at the inner wall of 0.042 m/s. Since this wall velocity is very small, it is believed to have a negligible effect on the flow field in the kiln; hence, the simulated kiln walls do not rotate. Previous modeling by Leger et al. (1993c) assumed that the 33 cm thick refractory brick walls of the rotary kiln behave isothermally. However, a heat balance shows that an adiabatic condition

is more realistic, with less than one percent of the heat generated within the kiln lost to the atmosphere. More detail available in "Appendix E" of this dissertation.

The large amount of unmetered infiltration air creates unique challenges when modeling this kiln system. While the total amounts of air infiltrating the incinerator have been calculated (Montestruc, 1989; Leger et al., 1993b; Jakway et al., 1995a, 1995b), neither the amount nor the temperature of the individual sources of the infiltrating air are known. Therefore, values are assumed using general reasoning found in Leger et al. (1993c). Table 5.1 shows the assumed distribution, as percent of total infiltration, and entering temperature of the infiltration air. Inlet locations listed in Table 5.1 are shown in Figure 5.1. The row labeled " Σ Kiln Front" represents the total percentage of infiltration air thought to enter at the kiln front face: the sum of air infiltrating at the solids loading chute, the over pressure relief vent, and the kiln front seal. A major departure from distributions used in the previous model (Leger et al., 1993c) is the addition of the inlet location labeled "downstream of sump" which includes all infiltration that takes place from the afterburner to the stack. The BASE distribution refers to the most likely air infiltration distribution. The other

Table 5.1 Temperature and Division of Infiltration Air.

Inlet Location	Mass Distribution					Temp (K)
	BASE (%)	FRONT ⁻ (%)	FRONT ⁺ (%)	SUMP ⁻ (%)	SUMP ⁺ (%)	
Solids Loading Chute	30	15	40	30	40	400
Relief Vent	5	0	15	5	10	400
Front Kiln Seal	23	10	25	23	25	500
Σ Kiln Front	58%	25%	80%	58%	75%	-
Rear Kiln Seal	18	18	10	18	5	500
Sump Area	10	10	5	0	15	350
Downstream of Sump	14	47	5	24	5	-

distributions (FRONT⁻, FRONT⁺, SUMP⁻, and SUMP⁺) will be discussed in later sections. Infiltration air temperatures were assumed the same for all cases.

Relatively cold and heavy air infiltrating the relief vent is assumed to fall into the solids loading chute (refer to Figure 5.1) where it then enters the kiln. Based on the refractory arrangement around the front kiln seal, infiltration air at this location is assumed to enter axially in the positive flow direction, while at the rear rotary seal the air is assumed to enter radially. Relatively cool air infiltrating into the transition section through various avenues is assumed to sink to the bottom of the ash sump and slowly rise as it is heated. Therefore, in the model, infiltration air enters at the sump location vertically. Considering all inlets at the front of the kiln, and using the BASE distribution, the overall equivalence ratio in the kiln is approximately 0.3.

RESULTS

Convergence is based on residual values. For all results shown in this paper, enthalpy residual is a maximum of 2.6×10^{-6} and the maximum of all other solved variable residuals is 4.3×10^{-5} . Results presented in this section are generated using flow boundary conditions derived from Jakway et al. (1995a, 1995b) for the TA-on operating condition and the BASE distribution of infiltration air from Table 5.1. In Figures 5.4 through 5.9, different views of the kiln velocity and temperature distributions are presented. Vector head size and tail length are scaled to the relative magnitude of the velocity. Part (a) of each figure shows results when the previously described grid, referred to as the coarse grid, is used in the model. Part (b) of each figure presents results based on a more refined grid to be discussed later.

Figure 5.4a shows a side view at the incinerator grid centerline displaying velocity vectors at every other axial cross-section. Shaded areas are of special interest and are shown in greater detail in the inserts of the figure. The lower right-hand shaded area details the region of reverse flow predicted at the lower exit of the kiln.

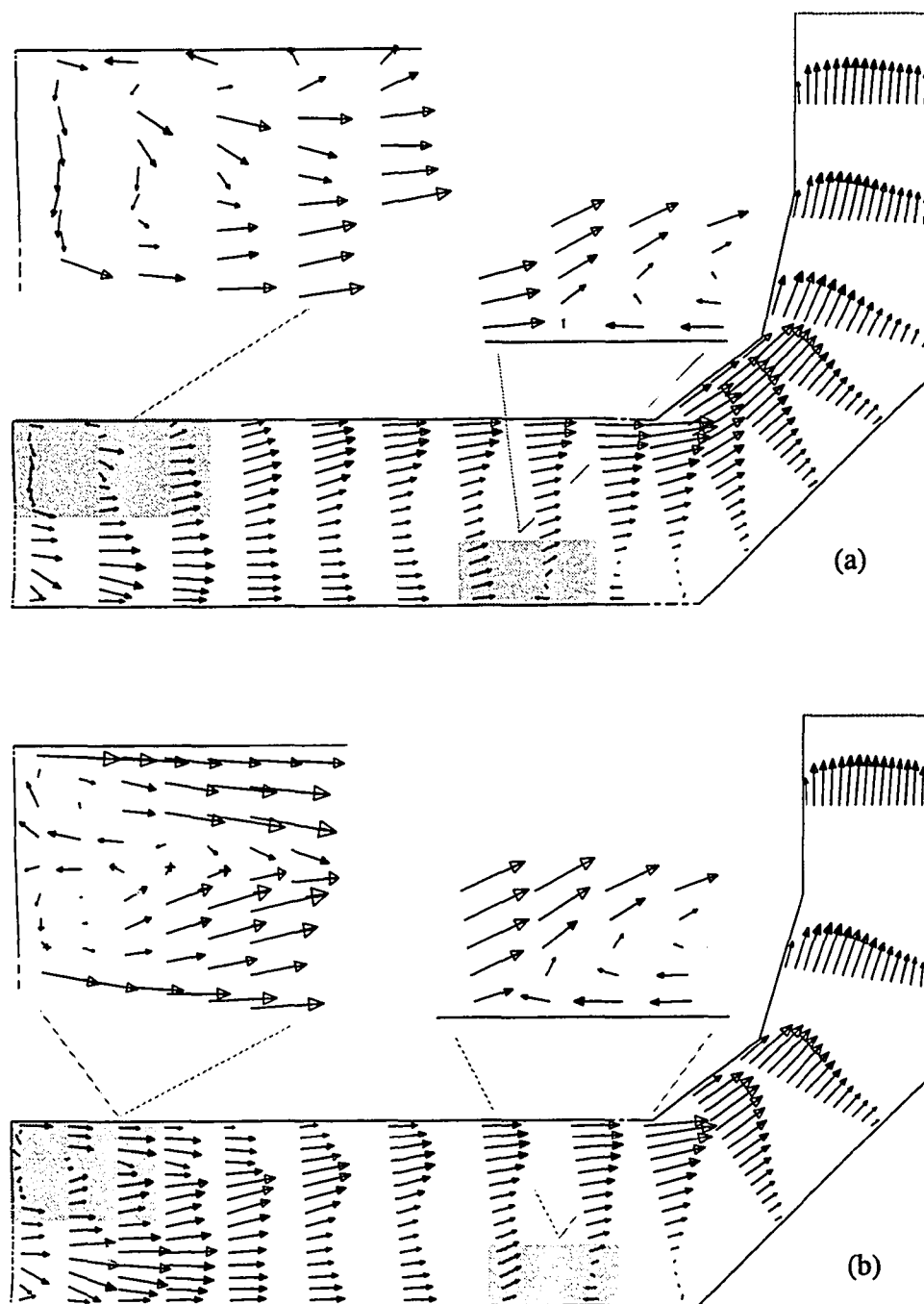


Figure 5.4 Side view of center line velocity vectors generated by coarse grid (a) and refined grid (b).

The upper left-hand shaded area details the high velocity gradients above and adjacent to the burners. Upon reaching the exit of the kiln, velocities have become highly stratified in the vertical direction, with the highest velocities at the top of the kiln. Velocities at the exit of the chimney are relatively uniform and directed outward, indicating that the geometry and grid design produce exit flows beneficial to convergence.

Figure 5.5a shows the velocity field at an axial cross-section two meters from the front of the kiln using trans-axial velocity vectors and contours of axial velocity. Strong outward flow generated by the burners is visible on the right hand side of Figure 5.5. This flow is also directed upward due to the buoyancy of the high-temperature combustion gas in this area. Heavier, cool air infiltrating primarily from the loading chute causes the down and outward flow in the central lower region. An area of reverse flow (flow toward the burner face) is present on the non burner side of the kiln. Maximum trans-axial velocity is 2.0 m/s.

Figure 5.6a shows the axial cross-section of the velocity field at five meters (about halfway) from the kiln front face. Reverse flow is absent, and the maximum trans-axial velocity is 2.2 m/s. A strong counter-clockwise flow pattern pervades nearly the entire cross-section. Both Figures 5.5 and 5.6 demonstrate the lack of symmetry in this highly 3-D flow field.

After the flow has traveled ten meters down the kiln, i.e. near the kiln exit where velocity, temperature, and speciation data have been recorded, the flow is almost entirely in the axial direction. Trans-axial velocities (not shown) have a maximum of 1.1 m/s, with most less than 0.7 m/s. Contours of axial velocity, shown in Figure 5.7a, indicate the flow field is relatively uniform in the horizontal direction, maximum velocity is at the top, and a region of reverse flow exists in the lower part of the kiln.

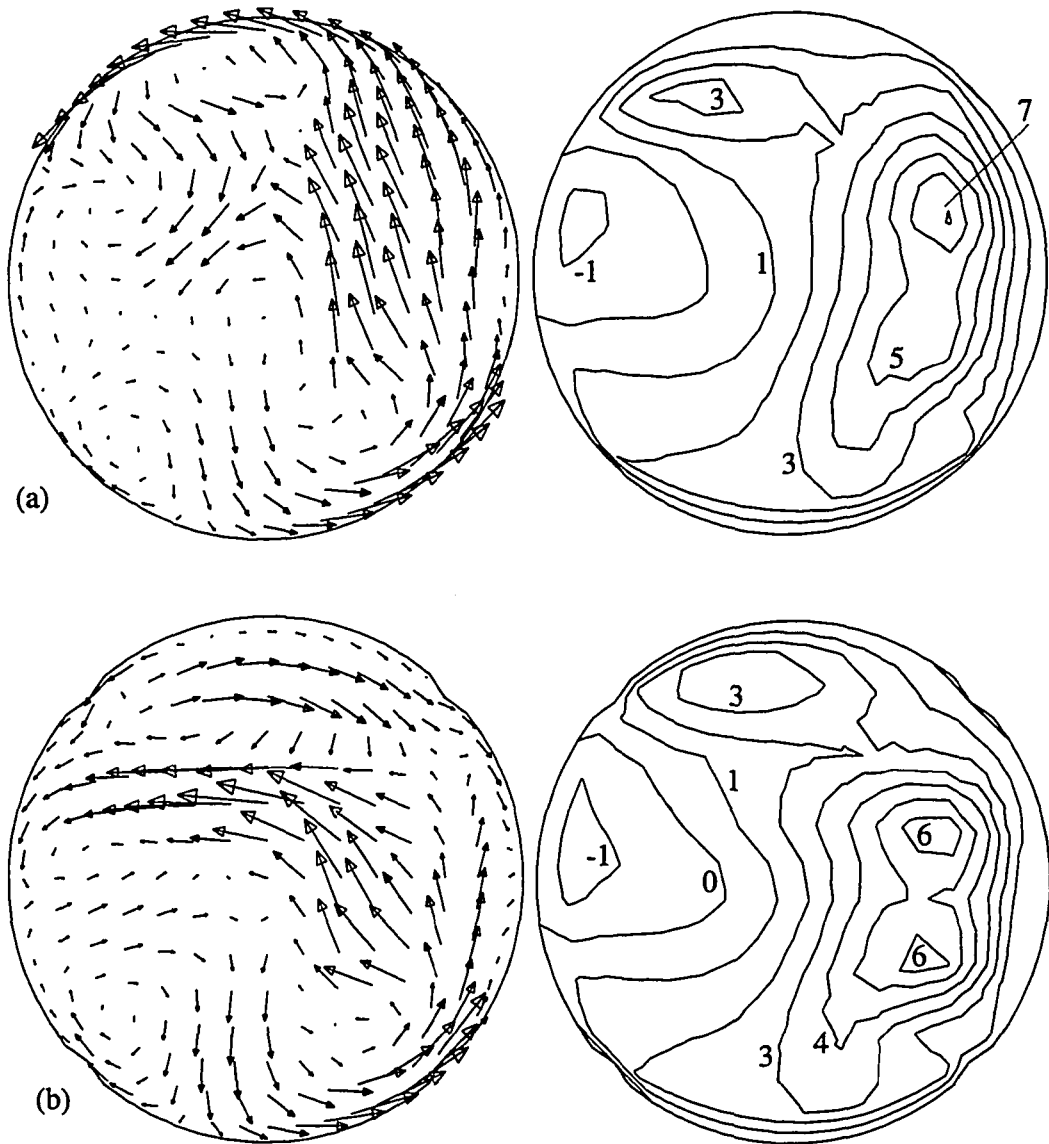


Figure 5.5 Axial cross-sections 2 meters downstream from the kiln front face showing velocity vectors in trans-axial directions and contours of axial velocity (m/s) for: a) the coarse grid, b) the refined grid.

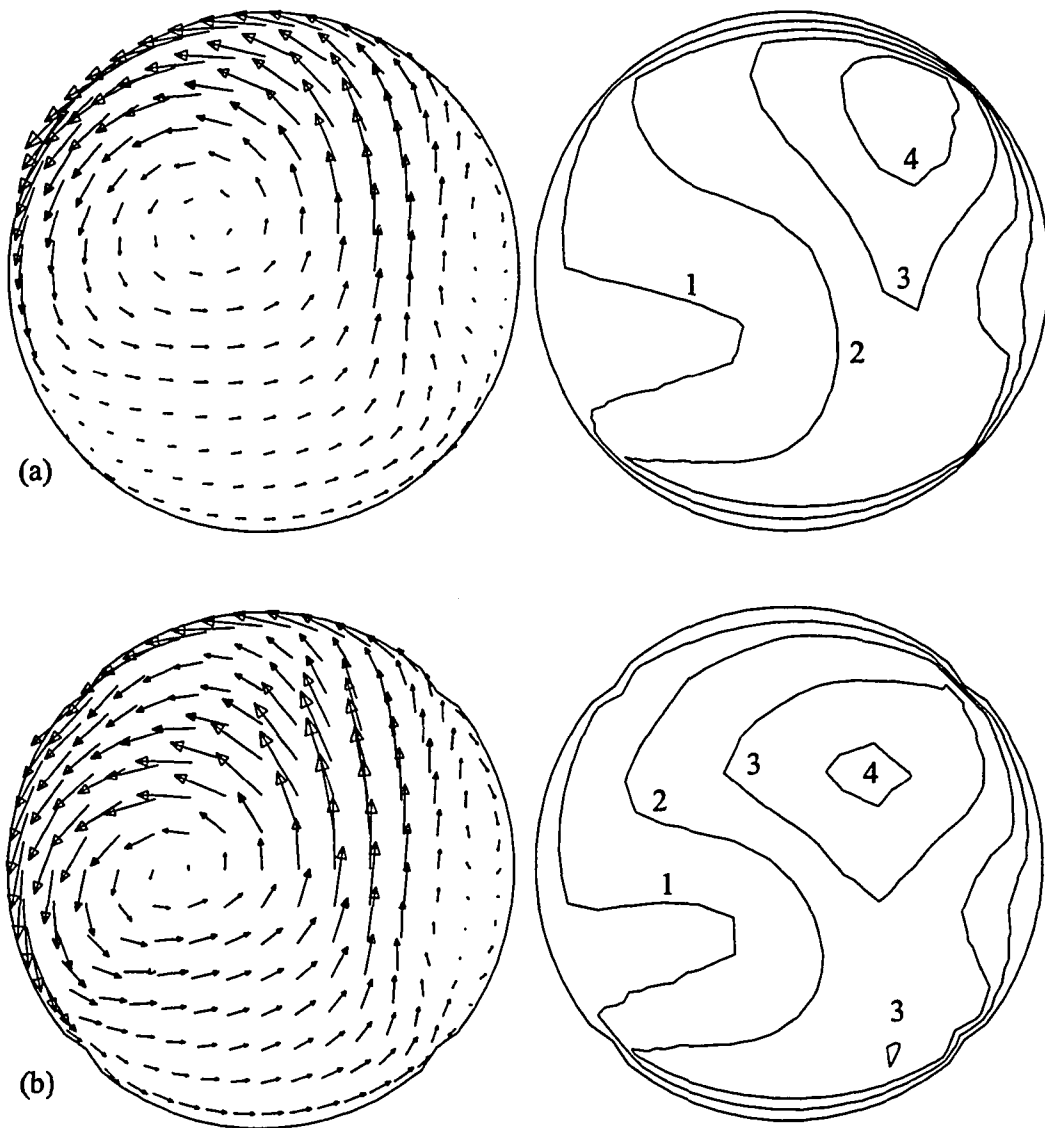


Figure 5.6 Axial cross-sections 5 meters downstream from the kiln front face showing velocity vectors in trans-axial directions and contours of axial velocity (m/s) for: a) the coarse grid, b) the refined grid.

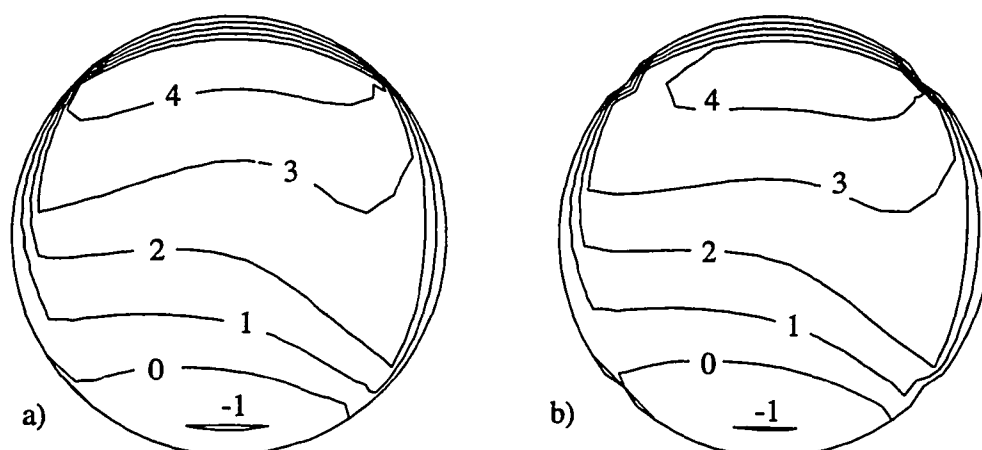


Figure 5.7 Axial cross-sections 10 meters downstream from the kiln front face showing contours of axial velocity (m/s) for: a) coarse grid and b) refined grid.

Figure 5.8 shows a side view of temperature contours along the grid centerline of the kiln. Effects of the relatively cool infiltration air are seen at the lower front, primarily from the loading chute, and at the rear of the kiln in the sump area. Considering this figure along with Figure 5.6a, the high temperature zone is seen to originate on the burner side of the kiln. Similar to the velocity field at the exit of the kiln, temperature gradients are almost exclusively in the vertical direction as shown in Figure 5.9.

MODEL VERIFICATION

The previous section provided an overview of the capabilities of the model and a general description of the kinds of information available from the model. Verification is divided into three parts: first, the current model is compared to the experimental data of Leger et al. (1991a, 1993a, 1993b) and the corresponding previous model (Leger et al., 1993c) of these data; next, the current model is compared to experimental data from Jakway et al. (1995a, 1995b); and finally, a grid dependency study is presented.

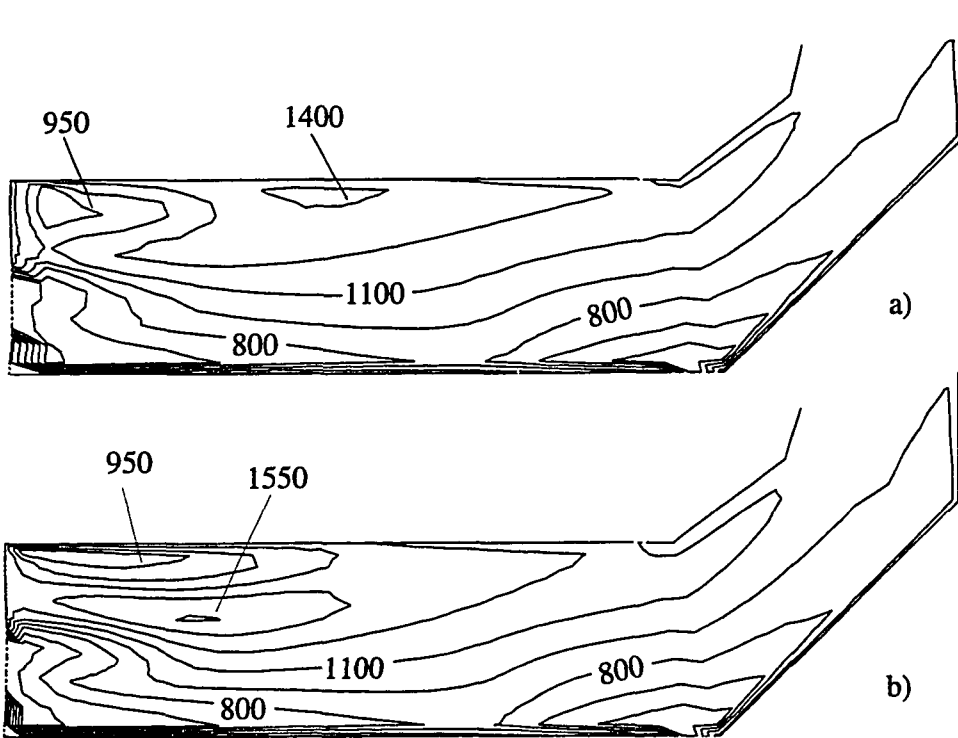


Figure 5.8 Side view of center-line temperature (K) contours: a) coarse grid and b) refined grid.

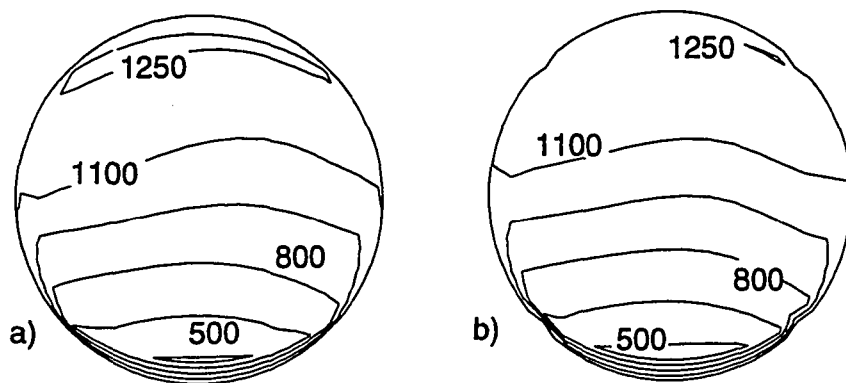


Figure 5.9 Axial cross-sections 10 meters downstream from the kiln front face showing contours of temperature (K) for: a) coarse grid and b) refined grid.

Validation I – Comparisons with Experiment (Leger et al., 1991a, 1993a, 1993b) and the Predecessor Model (Leger et al., 1993c)

The kiln is being modeled as a steady state system; however, maintaining day-to-day repeatability at field-scale facilities is sometimes difficult. To quantify the variation between experiments conducted by Leger et al. (1991a, 1993a, 1993b), the coefficient of variation (COV, ratio of standard deviation to the mean) was calculated for all metered and calculated flows within each experimental set (TA-off and TA-on). The COV ranged from 0.0002 for natural gas at a kiln burner to 0.3 for air to a burner in the secondary. A COV of one was calculated for steam fed to a kiln burner, but this is not considered significant as this feed represented only 0.06 percent of the total flow in the rotary kiln. Considering the scale of the experiments and the relative low values of the COVs, operating conditions for each experimental set were considered to be reproducible. Therefore, operating conditions for all experiments within each experimental set presented in Leger et al. (1991a, 1993a, 1993b) were averaged together to generate the flow boundary conditions used in modeling the respective TA-off and TA-on set.

Data chosen for comparison are the gas temperature and dry mole fractions of CO₂ and O₂ obtained during TA-off and TA-on experiments from an upper and lower (just below the centerline) location near the exit plane of the kiln (the only experimental locations where data were obtained). Figure 5.10 shows experimental data from Leger et al. (1993c) labeled as 'Expt. Fast' and 'Expt. Slow' representing results from operating at fast, 0.25 rpm, and slow, 0.1 rpm, kiln rotation rates respectively. Recall that, at these slow rotation rates, rotation rate of the kiln should not effect the flow field when solid waste is not processed; hence, experimental data differences are more likely an indication of experimental repeatability than changes due to different rotation rates. Figure 5.10 also contains results from the current

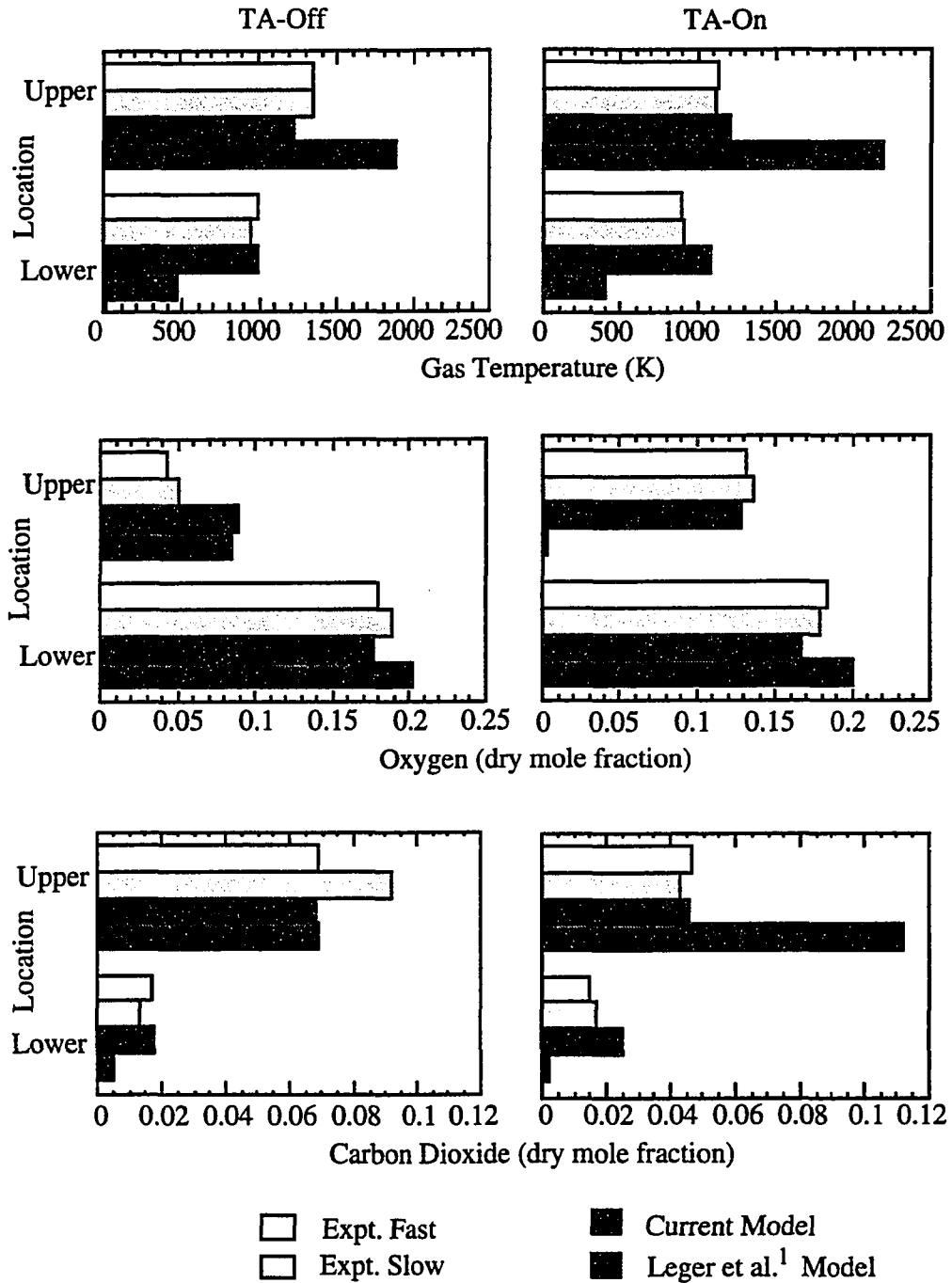


Figure 5.10 Comparison of current model to model by Leger et al. (1993c), and experimental data from Leger et al. (1991, 1993a, 1993b) at 1m before kiln exit.

model and Leger's model. The remainder of this discussion focuses on a comparison between the two models, and how each compares to the experimental data.

For TA-off operation, model improvement is most marked in the prediction of temperature. Compared to experimental data, Leger's model over predicted temperature at the upper location by 550 K, and under predicted temperature at the lower location by 500 K. The current model improves these predictions greatly with the upper temperature under predicted by only 110 K and the lower temperature over predicted by only 30 K. Both models predict the O₂ dry mole fraction to be nearly twice as high as that measured in the upper kiln; in the lower kiln, both predictions nearly match the experimental data. Both models predict CO₂ concentrations equally well at the upper location; however, at the lower location, Leger et al. (1993c) under predict the value by a factor of three, and the current model over predicts experimental measurements by only 20 percent.

Even larger improvements are noted during TA-on operation. Leger's model over predicted the upper location temperature by 1,090 K (nearly twice the measured value), while it under predicted the lower location temperature by 500 K (nearly half the measured value). In comparison, the current model over predicts temperatures by only 90 K and 180 K at the upper and lower kiln exit locations respectively. Leger's model under predicted the dry O₂ mole fraction in the upper kiln by nearly two orders of magnitude; similarly, the dry CO₂ mole fraction was over predicted in the upper kiln by nearly a factor of 3. The current model closely matches experimental data for both O₂ and CO₂. In the lower kiln, both the current model and Leger's model reasonably match the measured O₂ mole fraction; however, Leger's model under predicted CO₂ by nearly an order of magnitude, whereas the value predicted by the current model is only 1.5 times the observed value.

Improvement over Leger's model in temperature prediction is attributed to the combination of treating the wall as adiabatic rather than isothermal and including radiation with participating CO₂, water vapor, and soot. Better agreements with experiment in species concentrations are most likely due to an increase in vertical mixing induced by a less-stratified temperature distribution in the current model. Predictions by the current model in all cases, except the upper region TA-off O₂ prediction, are within the repeatability limits of the experiments. Whereas Leger's model was capable of only qualitative predictions, the current model quantitatively predicts accurate results at the kiln exit when no waste is processed.

Validation Test II – Comparisons with experiment Jakway et al. (1995a, 1995b)

Although Jakway et al. (1995a, 1995b) do not report gas speciation, a mapping of the velocity and temperature distribution near the same exit location of the kiln is presented. Data were obtained at 12 locations across an upper quadrant axial cross-section of the kiln, about one meter before the kiln exit. For these experiments, turbulence air was the only parameter varied. Maximum metered and calculated flow COV for Jakway et al. (1995a, 1995b) over a time of 2 hours was 0.3, again for steam to one of the afterburner burners. Non steam COV's ranged from 0.0006 for natural gas to the lower kiln burner to 0.1 for the total stack dry air flow rate.

Model results are compared to experimental data in Figures 5.11, TA-off, and 5.12, TA-on. In both Figures, solid lines represent predicted velocity and temperature distributions; experimental velocity and temperature data are graphed as open circles. All data are plotted against vertical distance from the center-line of the kiln. Multiple data points for an elevation indicate values from different horizontal locations. The lack of horizontal gradients measured at this location supports the

model's prediction of relatively flat contours, and hence, only the centerline values for the model are shown.

As shown in Figures 5.11 and 5.12, the model qualitatively predicts the experimental trends quite well, and in many instances, provides good quantitative results. For the TA-off case (Figure 5.11), the temperature just below the kiln

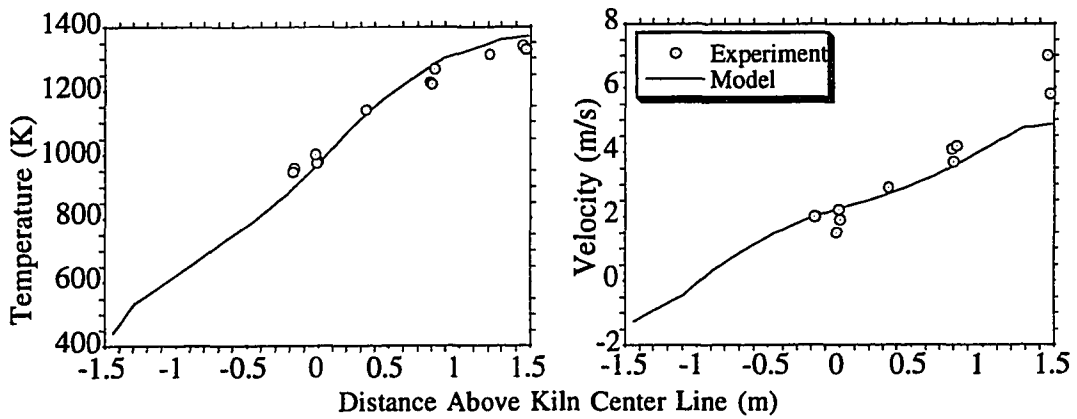


Figure 5.11 Comparison to current model with coarse grid 1m before kiln exit, using TA-off data from Jakway et al. (1995a, 1995b).

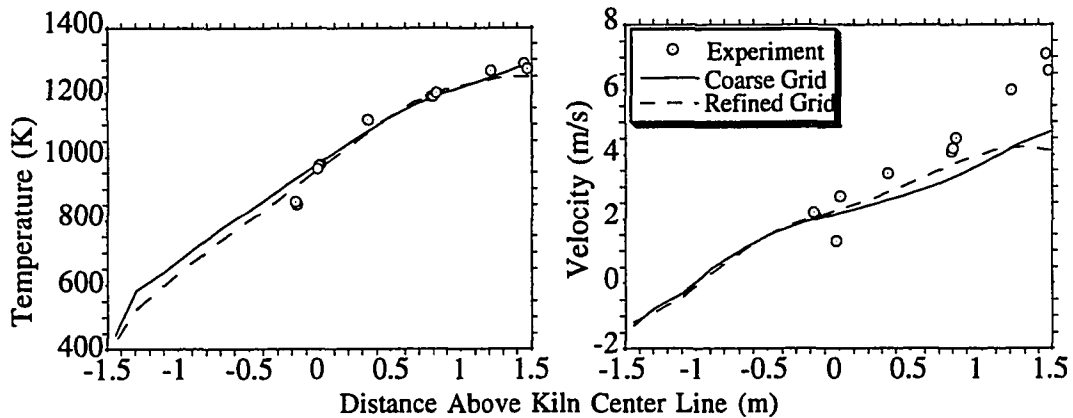


Figure 5.12 Grid dependency comparison using TA-on data from Jakway et al. (1995a, 1995b) at 1m before kiln exit.

centerline is under predicted by 5 percent, and over predicted by only 3 percent near the top of the kiln. For the TA-on case (Figure 5.12), the temperature is over predicted near the kiln centerline by about 8 percent. Model-predicted velocities match well for the TA-off case (Figure 5.11) except at the uppermost location where the error is 24 percent. Most of the predicted velocities tend to be slightly lower than experimental values when the turbulence air is activated (Figure 5.12) reaching a maximum difference of 31 percent, again at the very top of the kiln. The discrepancy between predicted and experimental data at the upper locations is, as yet, unexplained.

Validation Test III – Grid Dependency Study

To examine the effect of the grid on the numerical results, the same general geometry was fitted to a grid of 12,427 control volumes, a 27 percent increase over the baseline coarse grid used in all model results presented thus far. The only change in the geometry was to increase necking of the chimney, thereby further reducing the cross-sectional area by 10 percent and improving the solution domain exit flow. The new control volumes are added as 9 extra axial cross-sections. Perhaps more important than the addition of control volumes is their placement. While the cross-sections of the baseline coarse grid are uniformly spaced in the axial direction, the refined grid makes use of non-uniform spacing to concentrate the axial grid cross-sections at the front of the kiln where spatial gradients in the flow variables are the greatest. This dense grid is gradually expanded to a less dense spacing at the kiln exit as shown in Figure 5.2b. The grid used on the axial cross-sections is unchanged; however, to achieve final convergence, one control volume in each of the four “corners” (highlighted in Figure 5.3a) is changed from an interior volume to a volume in the kiln wall. This is necessary because of the high degree of skew (departure from orthogonal intersections) present in these control volumes. Resulting reduction in the

cross-sectional area of the internal kiln is only 0.026 m^2 or 0.33 percent; therefore, effects on the flow field are assumed negligible.

Comparison between the coarse and fine grids of Figure 5.2 is performed using TA-on flow boundary conditions derived from the experimental data of Jakway et al. (1995a, 1995b). Part (b) of Figures 5.4 through 5.9 contain data generated by the model using the refined grid which can be compared to Parts (a) of each figure, representing the baseline coarse grid results. Consider first Figure 5.4, where a side view of the velocity vectors are shown. For clarity, vectors are shown at every other axial cross-section in Figure 5.4(a) and every third axial cross-section in Figure 5.4(b). Again, the highlighted regions show areas where more complex flow patterns develop. The primary differences between the velocities generated by the two grids appears in the upper highlighted zone near the front of the kiln. The refined grid produces a flow structure resembling a pair of counter-rotating eddies at the front wall of the kiln, which is not present in the coarse grid results. Otherwise this figure indicates that the two grids produce very similar velocity fields.

Cross-sectional views of the developing velocity fields are compared in Figures 5.5, 5.6, and 5.7, again comparing parts (a) for the baseline coarse grid with parts (b) for the fine grid. At 2 m from the front face, axial velocity contours are very similar for both grids as are the trans-axial velocities in lower half of Figure 5.5. However, major differences in trans-axial velocities are visible in the upper region. A primary difference is that, just above the centerline, the refined grid generates a strong right-to-left flow not present in the coarse grid solution. Maximum trans-axial velocity is 2.3 m/s for the refined grid. Interestingly, despite the major trans-axial velocity differences noted above near the front of the kiln, Figure 5.6 indicates that at 5 m from the kiln front face the flows generated by both grids are very similar. Maximum trans-axial velocity is 1.3 m/s for the refined grid. At 10 m from the kiln

front face (Figure 5.7), both grids generate nearly identical velocity fields with the refined grid predicting a maximum trans-axial velocity of only 0.6 m/s.

Temperature contours can be compared by referring to Figure 5.8. Similar to the velocities, the greatest difference in temperature fields occurs in the upper part of the front half of the kiln. The zone inside the 1,550 K contour of the fine grid solution corresponds to a region in the flow where the hot burner gases are transported across from the burner side of the kiln (Figure 5.5). Overall maximum gas temperature is 120 K greater in the fine grid solution. However, similar to the velocity predictions, Figures 5.8 and 5.9 show that nearly identical temperature fields are generated for each grid by the time the flow reaches the kiln exit.

Figure 5.12 compares velocity and temperature data to model results using both the coarse and fine grids. As previously noted, differences generated in the front portion of the kiln are damped by the time the flow reaches the kiln exit, with both grids producing nearly identical velocity and temperature profiles at the exit of the kiln. Temperature prediction just below the kiln centerline is improved from 8 percent high to a value of 6 percent high. Velocity prediction is somewhat improved across the upper half of the kiln cross-section except at the very top where predictions are up to 40 percent low. The root mean square (r.m.s.) error, the standard error of the estimate, also compares relative fits of the experimental data to estimates from the model. The r.m.s. errors for temperature are 35 K and 30 K while velocity r.m.s. errors are 1.26 m/s and 1.35 m/s for the coarse and refined grids respectively, again indicating the closeness of the results generated by both grids near the kiln exit.

The different results generated with the refined grid show that the baseline coarse grid solution is indeed grid dependent. This is especially noticeable in the upper front region of the kiln where the refined grid predicts several new eddies. The

appearance of new eddies (Figure 5.4) is not unexpected; as grids are refined, more detail is possible and new small eddies can form, especially in areas with large shear such as near the burners. However, Figure 5.5 shows that changes in the flow field generated by the refined grid are not confined to the generation of several small eddies, and a 120 K increase in maximum temperature within the kiln is significant. It is, however, noteworthy that even though there are significant changes produced by the refined grid, these changes are starting to damp-out by the middle of the kiln (Figure 5.6) with both grids producing nearly identical flow fields by the exit of the kiln as evidenced by Figures 5.7, 5.9, and 5.12. The detail provided by a refined grid will no doubt become more important with the eventual addition of waste processing and a more complete set of chemical reactions, especially if the influence of kinetics is included. These model refinements will have to be included in next-generation models. At this time, and for the limited experimental data available, the use of either grid produces reasonable qualitative and quantitative results at the kiln exit.

Attempts were made to further refine the grid; however, these were unsuccessful. Complications were partially attributed to the highly non-orthogonal grid skew at 'corners' making convergence extremely difficult. This skew increases dramatically as the number of control volumes defining circular cross-sections increase. Additional difficulties were attributed to the relatively low inlet flow rates involved in this work, making the influence of the boundary conditions quite weak on internal control volumes far downstream from the front face of the kiln. As control volumes are added, the internal control volumes become even further removed from their influence, making convergence more difficult. Changing to a higher order differencing scheme caused rapid divergence as did attempts at using the re-normalized group turbulence model and solving thermal and velocity fields separately (Fluent, 1993). Radiation did not seem to interfere with convergence. Working with multigrid,

sweep, block correction, and underrelaxation parameters was required to achieve convergence of the refined grid used in this work; however, an appropriate combination of these parameters could not be developed to prevent divergence when more nodes were added. Future efforts may involve relaxing geometry restrictions at the front face of the kiln to reduce the grid skew at this location.

PARAMETRIC AND SENSITIVITY STUDIES

The effects of various unmetered infiltration air distributions are discussed in the first part of this section. Following this, sensitivity to each of the three main improvements to the current model (addition of radiation, improved boundary conditions, and addition of soot) are discussed. All studies are conducted using the baseline coarse grid with flow boundary conditions for the TA-on case from Jakway et al. (1995a, 1995b).

Distribution of Unmetered Infiltration Air

Figures 5.11 and 5.12 show that while the model matched velocity data reasonably well, improvement is still possible. The distribution of unmetered infiltration air entering the incinerator represents the single largest unknown; therefore, it was expected that reasonable changes to this distribution might improve the velocity prediction. The TA-on operating condition was chosen for this parametric study because it produced the greatest error in velocity prediction. The following parametric studies were undertaken to quantify the importance of the unmetered air distribution.

For the first parametric study, the total amount of infiltration air assigned to the front of the rotary kiln was varied. Infiltration at the other inlets was redistributed so that the overall amount of infiltration air into the incinerator was held constant at the experimentally determined value. The amount of infiltration air allowed at the front of the kiln was bracketed around the BASE distribution (58

percent at the kiln front - see Table 5.1) with 25 percent and 80 percent termed FRONT⁻ and FRONT⁺ distributions respectively. Table 5.1 shows how the individual infiltration sources were proportioned for each case.

Results are shown graphically in Figure 5.13 along the centerline 1m before the exit of the kiln. As expected, the FRONT⁻ distribution, where the flow of cold infiltration air to the front of the kiln is greatly reduced, produces generally lower velocities and much higher temperatures than the BASE distribution. Surprisingly, the results of the FRONT⁺ distribution, where the flow of the cold infiltration air to

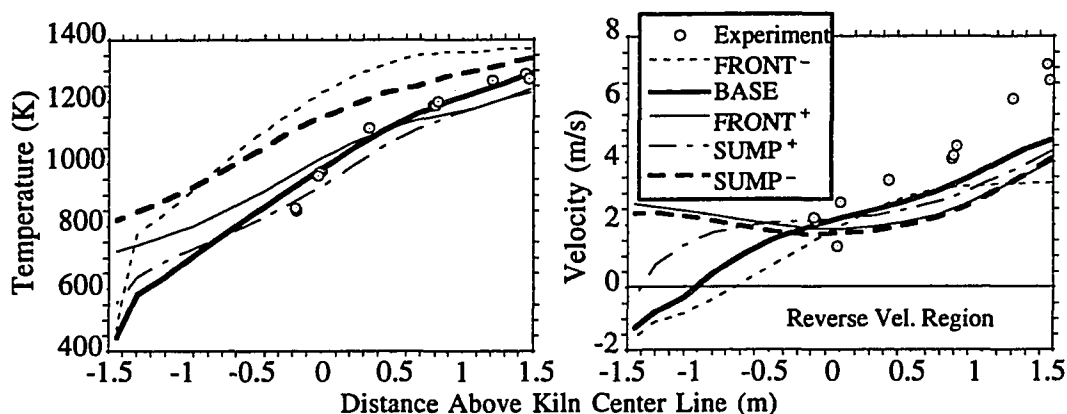


Figure 5.13 Infiltration air parametric study using TA-on data from Jakway et al. (1995a, 1995b) and the coarse grid. Results shown for cross-section 1 m before kiln exit.

the front of the kiln is increased, also produced lower velocities in the upper region of the kiln exit. This occurs because the increased influx of cold air moves along the bottom of the kiln, eliminating the region of reverse flow that occurs at the kiln exit with the BASE distribution. Also, while the gas temperatures are slightly lower in the upper kiln for the FRONT⁺ case, gas temperatures in the lower kiln actually increase. This temperature increase in the lower kiln owes to a lack of mixing with cooler air from the sump, which occurs when recirculation is present. Neither of these two

distributions produce results that match the velocity data better than the BASE distribution.

Several other distributions were studied, but are not shown. Of these, only one produced even marginal improvement in the velocity prediction. In the previous distributions (BASE, FRONT⁻, FRONT⁺), infiltration through the front and rear seals is assumed to occur uniformly around the periphery of the seals. In one study, 50 percent of the infiltration air assigned to the front kiln seal was allowed to enter the kiln through the bottom of the front seal, with 20 percent on the sides and the remaining 10 percent entering in the upper region of the seal. Such a distribution might occur if the kiln was misaligned. This distribution produced an increase in velocities on the order of 5 percent near the top of the kiln exit region. Still, overall model velocities were up to 30 percent below measured values and temperature predictions worsened. Increasing the total amount of front seal infiltration air by 10 percent, at the expense of the loading chute infiltration air, and maintaining the unbalanced front seal distribution noted above, produced only negligible changes. Therefore, it is concluded that changing the distribution of infiltration air at the kiln front face has little effect on improving the match with experimental data at the exit of the kiln.

However, varying the infiltration air allowed at the kiln front face led to an important observation: increasing the amount of infiltration air entering the front of the kiln by just over 20 percent of the total air infiltrating the kiln completely eliminated the region of reverse flow at the kiln exit. Early experiments probing the exit region of this rotary kiln incinerator showed that the lower kiln exit area contained relatively low temperature gases very close in composition to ambient air (Cundy et al., 1989a). This was unexpected and produced speculation that this lower area was relatively uninvolved in the combustion and waste destruction process, at least for the

experiments conducted. That this area might actually be a recirculation region was first suggested in the numerical modeling work of Leger et al. (1993c). Recirculation zones are important in incineration because they reduce the effective volume of the incinerator, thereby decreasing the residence time of most gases. Low temperature recirculation zones are especially undesirable as little to no destruction of waste takes place in these zones.

Given these observations, a second parametric study was conducted with the objective to examine the effect that infiltration air has on the kiln exit recirculation region. Two new distributions were tested, SUMP⁻ and SUMP⁺ shown in Table 5.1. The SUMP⁻ distribution has the same front distribution as the BASE case, but the sump inlet is reduced to zero flow with its flow entering downstream of the sump. Figure 5.13 shows that the region of reverse flow at the exit of the kiln is eliminated in this case, similar to the result using the FRONT⁺ distribution, but without increased flow from the front of the kiln. To further examine the importance of the sump inlet flow to the exit recirculation region, the SUMP⁺ distribution was developed. This has nearly the same distribution of air at the front of the kiln as the FRONT⁺ case, but the flow to the sump area is increased. This re-establishes the recirculation region originally eliminated by the FRONT⁺ distribution. Changes to the other infiltration inlets of similar magnitude had only minor effects on the flow field at the exit of the kiln. None of the infiltration distributions generated velocity predictions at the exit of the kiln that were better than the original BASE distribution.

In summary, the BASE distribution of infiltration air produces results which match the experimentally measured velocity and temperature data most accurately. The parametric studies performed show that reverse flow at the exit of the kiln may be affected by controlling the amounts of infiltration air leaking into the front of the kiln and at the sump. If reverse flow is predicted for one set of inlet conditions, for

example the BASE case, then reverse flow might be eliminated by either increasing the flow of cold air to the front of the kiln, as evidenced by case FRONT⁺, or by lowering the infiltration in the transition and kiln exit areas, as in the SUMP⁻ case. This study also underscores the need to record velocities across a *complete* cross section of the kiln in order to improve validation of numerical models. The extra data would allow the total amount of air infiltrating at the front of the kiln to be quantified; questions about the existence and location of reverse flow regions would also be clarified.

Effects of Radiation, Soot, and Adiabatic Walls

As discussed previously, radiative heat transfer, including the effects of soot, has been added to the current model, and an adiabatic wall boundary condition replaces the isothermal wall of Leger's model. Additional differences between the two models, termed base differences for this discussion, include the grid, use of power law and SIMPLIC in the solution method, a more accurate geometry, corrected heat capacities, and slight changes in the infiltration proportioning and temperatures. The sensitivity of the model to these changes is determined in a series of sub-studies in which the changes are executed in succession.

Initially, the effect of the base differences is examined. Leger's model, with its isothermal walls, produced a maximum gas temperature of 2,350 K, which is above the adiabatic flame temperature of 2,220 K for a stoichmetric mixture (Glassman, 1987). However, the current model, including the base differences noted above but without radiation and using the same 800 K isothermal wall boundary condition as in Leger's model, predicts a more realistic maximum gas temperature of 2,190 K.

Next, the individual effect of the radiation model is characterized. This is done without incorporation of soot in order to determine the sensitivity of the current model to the radiation model alone. Kiln interior walls were again assumed isothermal

at 800 K. When the radiation model is enabled under these conditions, along with the base differences, the maximum gas temperature inside the rotary kiln is reduced from 2,190 K (as noted above) to 1,720 K. This overall reduction in temperature is considered good because it is thought to represent the fuel rich, soot laden flame temperature better, even though flame temperature measurements were not conducted. This result is also not unexpected since, at these high temperatures, radiation should be of first-order importance.

The effects of the isothermal kiln wall assumption are determined by changing the kiln wall boundary condition from isothermal to adiabatic. In this sub-study the base differences are included, and the radiation model is enabled, although soot is not yet included. Changing to the adiabatic wall boundary condition increases the wall temperatures throughout. The maximum wall temperature increases from 800 K (isothermal condition) to 1,430 K at about 2 m from the front face of the kiln. Even near the exit of the kiln, wall temperatures are predicted to be as high as 1,000 K. This indicates not only that a single temperature cannot characterize the wall, but also that the temperature chosen for Leger's model, 800 K, was probably too low. The change to adiabatic walls with the corresponding increase in wall temperatures throughout is accompanied by an increase in the maximum gas temperature of about 120 K.

Finally, the heat transfer effects of soot are resolved. As in the previous case, the adiabatic wall boundary condition is used and the radiation model enabled, along with all the base differences noted previously. With the addition of soot effects in the radiation model, the maximum gas temperature, which occurs in the combustion zone, decreases by 130 K to 1,730 K. This is reasonable as soot tends to increase radiative heat transfer, thereby lowering nearby gas temperatures. Correspondingly, the wall temperature immediately adjacent to this maximum gas temperature zone increases to

a maximum of 1,490 K. However, wall temperatures decrease everywhere else in the kiln.

Results of this section are summarized in Table 5.2. Each of the three major changes (the inclusion of radiation heat transfer, soot particles, and the change to an adiabatic wall boundary condition) from the predecessor model (Leger et al., 1993c) produce reasonable and desirable changes. These improvements, coupled with a better geometric representation of the kiln along with the more flexible curvilinear coordinate system employed, combine to yield the substantial improvements over Leger's model displayed in Figure 5.10.

Table 5.2 Results of Modifications to Previous Model of Leger et al. 1993c.

	Max. Wall Temp. (K)	Max. Gas Temp. (K)
Leger et al. 1993c	800	2350
+ Base Differences	800	2190
+ Radiation	800	1720
+ Adiabatic Wall	1430	+ 120
+ Soot	1490	1730

SUMMARY

A numerical model for rotary kiln incineration has been developed. This model builds on its predecessor (Leger et al. 1993c) by successfully adding radiation and soot to the heat transfer analysis. Heat transfer is also improved by switching to an adiabatic wall boundary condition and including a more accurate geometry and better fitting grid. These changes result in an improvement in matching experimental data taken from a field-scale rotary kiln of up to two orders of magnitude compared to the predecessor model (Leger et al., 1993c). In most instances, prediction is within

repeatability limits of the experiments. The primary exception is in the prediction of velocity; while matching experimental data at the kiln centerline, error at the top of the kiln is as high as 40 percent. A grid dependency study showed the flow field to be dependent on the grid, especially at the upper front of the kiln where gradients are very steep. Still, near the exit of the kiln where the limited experimental data were available, both grids produced very similar results. Attempts at further refinement were not successful.

The parametric study on the effect of infiltration air distribution underscores the need to record velocities across a complete cross section of the kiln in order to validate numerical models of rotary kilns. This would allow the total amount of air infiltrating at the front of the kiln to be quantified as well as answering some of the questions about the existence and location of reverse flow regions. The sensitivity study demonstrates the importance of the individual improvements in the heat transfer analysis.

This complicated model of rotary kiln incineration is evolving in stages, and while the results reported herein represent considerable improvement over the first-generation work of Leger et al. (1993c), the model cannot yet be used to simulate waste processing. Even so, the model in its current stage of development, can be used for limited design and operation studies.

CHAPTER 6

SUMMARY, CONCLUSIONS, AND RECOMMENDATIONS

SUMMARY

The major accomplishments of the research that has been presented in this dissertation are summarized in this section. Conclusions and recommendations follow.

Experimental Velocity and Temperature Measurements

A new device for measuring velocities and temperatures inside a directly-fired, full-scale, rotary kiln incinerator has been developed, constructed, and tested. Using this device, velocities were measured for the first time inside a field-scale rotary kiln incinerator. Combustion gas velocities and temperatures were measured at multiple points across a quadrant of the rotary kiln segment of a hazardous waste incinerator near its exit. Measurements were made using a bidirectional pressure probe and suction pyrometer. To accommodate the new bidirectional probe and gain access to the upper portion of the kiln, a lighter and stiffer positioning boom was designed. To ensure precise and accurate placement of the probe tip, a positioning device was designed and attached to the incinerator. The kiln was directly fired using natural gas in a steady state mode. Results indicate strong vertical stratification of both velocity and temperature, with the highest values corresponding to the top of the kiln. Access restraints prevented the lower region of the kiln from being mapped. Horizontal variations in both temperature and velocity were insignificant. Operating conditions were varied by adjusting the amount of ambient air added to the front of

the kiln. Increasing the flow of ambient air into the front of the kiln reduced the measured temperatures as expected, but did not have as significant an effect on measured velocities possibly due to the mitigating effect of the large amount of unmetered air infiltrating at the front of the kiln. Temperature values and data stratification trends generated by this new device agree with previous experimental findings on the same incinerator under similar operating conditions.

Prior to obtaining the velocity and temperature data of this paper, there were virtually no means to quantify the mass flow inside rotary kilns. This led to uncertainty about the distribution of unmetered infiltration air and the flow dynamics at the locations of previous sampling efforts. Because the limited access of this incinerator did not allow a complete mapping of the kiln exit, the amount of unmetered air entering the kiln is still uncertain. However, the results do help to provide confidence that the estimated infiltration air distribution is realistic. Further, the results indicate that, with adequate access, this probe assembly could completely characterize the mass flow field of this rotary kiln incinerator or other similar combustion devices. Limitations include material compatibility with kiln environment, pressure transducer limitations, and calibration constant applicability limits (not a theoretical limit, but so far only determined for the Reynolds Number range of 300 to 4000). In addition, the relatively good agreement between the measured and calculated kiln mass flow rates suggests that the experimental techniques used and the assumptions imposed (horizontal symmetry at the exit region of the kiln, along with linear velocity and temperature profiles) are reasonable. While this may seem a circular argument, it should be noted that, primarily due to the complexity of the system, never before has the flow field of an operating rotary kiln incinerator been quantified. With each piece of new information, the picture of what takes place inside a rotary kiln incinerator becomes clearer, and the ability to test

previous assumptions becomes possible. While the measurements reported in this paper only covered a portion of the kiln exit region, they have added considerably to our understanding of the complicated process of rotary kiln incineration.

Numerical Model of Rotary Kiln Incinerator

A steady state numerical model for the rotary kiln segment of a direct-fired hazardous waste incinerator has been developed. This model builds on work previously conducted at Louisiana State University by including radiation and soot in the heat transfer analysis, by switching to an adiabatic wall boundary condition, and including a more accurate geometry and better fitting grid. These changes improve agreement with data taken from a field-scale industrial rotary kiln, operating with a natural gas support flame, but no waste processing, by up to two orders of magnitude compared to previously developed models at Louisiana State University. In most instances, prediction is within repeatability limits of the experiments. The primary exception is in the prediction of velocity; while matching experimental data at the kiln centerline, error at the top of the kiln is as high as 40 percent. Grid dependency is demonstrated, especially at the upper front of the kiln where gradients are very steep. However, differences between predictions by the two grids have lessened greatly by the middle of the kiln, with both grids producing nearly identical flow fields by the exit of the kiln where the limited experimental data are available. Attempts at further refinement were not successful.

The parametric study on the effect of infiltration air distribution underscores the need to record velocities across a complete cross section of the kiln in order to validate numerical models of rotary kilns. This would allow the total amount of air infiltrating at the front of the kiln to be quantified as well as answering some of the questions about the existence and location of reverse flow regions. The sensitivity

study demonstrates the importance of the individual improvements in the heat transfer analysis.

This complicated model of rotary kiln incineration is evolving in stages, and while the results reported herein represent considerable improvement over the first-generation work, the model cannot yet be used to simulate waste processing. Even so, the model in its current stage of development can be used for limited design and operation studies.

CONCLUSIONS

Field-scale experimentation results presented in this dissertation expand the general knowledge of incineration. Previous experimental work has shown that incinerator flows can be highly stratified in both temperature and chemical species. This latest work shows that the exit of a rotary kiln incinerator also can be highly stratified in velocity and presents evidence that regions of reverse flow may exist. It is, therefore, important to consider the general velocity field when interpreting other measurements taken from the rotary kiln section of an incinerator. This is particularly important if single point sampling is used to characterize the incineration process, so that stagnant areas and regions of reverse flow can be identified. This work presents a device and methodology for measuring velocities in high temperature, particulate laden, turbulent flows. This dissertation also provides the research community with the proven design of a lightweight and yet stiff boom that can be used in many high temperature applications.

Successful numerical modeling as presented in this body of work depends on four things. First a representation of the geometry needs to include all aspects that significantly affect areas of interest. At the same time consideration needs to be given to possible simplifications to the geometry so that applying a grid will be easier. The numerical grid should accurately represent the chosen geometry, produce

a converged solution, and be refined enough so that the major aspects of the flow field are not grid dependent. All physical phenomena that are important to the final solution need to be included and correct boundary conditions applied. Finally, model results need to be compared back to data taken from the actual facility being modeled until confidence in the model is attained. The current model improves on its predecessor by addressing all of these requirements. The geometry is more accurate at the front face where the burners are located and in places in the transition section that have a bearing on the main kiln flow field. However, simplifications are made in the geometry of the transition and afterburner sections by eliminating regions of recirculation that do not have direct bearing on the main flow in the kiln. A grid that more accurately matches the combination of cylindrical and rectangular geometries and utilizes non-uniform grid spacing is generated. Radiation, including the effects of soot, is added and the thermal boundary condition at the walls is improved. Grid independence is attempted but not fully attained. Finally, these improvements combine to generate a model that does an exceptional job of quantitatively, as well as qualitatively, matching all of the available experimental data except velocity data at the top of the kiln. This current model is an improvement over previous models of this facility; however, questions remain about grid dependence, and waste modeling is not included yet.

RECOMMENDATIONS FOR FURTHER WORK

Research results presented in this dissertation represent a substantial forward movement toward the twin goals of obtaining a better understanding of processes occurring in hazardous waste rotary kiln incinerators and achieving the capability to correctly predict incinerator performance. This work also points to the progress that remains to be achieved. Following is a list of specific recommendations for additional projects based on the work presented here.

Experimental

- 1) The steady state velocity field of the rotary kiln discussed in this document needs to be more completely mapped. In particular, a complete vertical traverse is needed so that the total amount of air infiltrating at the front of the kiln can be calculated. Sampling in the lower kiln region is needed to give information on any recirculation regions. This may involve designing another probe that can reach the lower region of the kiln given the existing limited access. One possibility is to make the boom with a bend or even a dogleg in it.
- 2) Data on the chemical species present should also be mapped along with the temperature and velocity. This can be done by analyzing gases withdrawn by the suction pyrometer.
- 3) A device and or methodology for quantifying soot would add a significant piece of information to any future incineration data gathered. This would also greatly help with attempts to include soot in numerical modeling.
- 4) Recording the transient response of the velocity field at several locations to loadings of pack or drums of solid waste would be a step forward and would allow reinterpretation of some previous data. This was attempted with packs of clay sorbent and diesel fuel, but thermocouple problems led to inconclusive results. Dichloromethane or toluene would be good choices for the hazardous waste because temperature and speciation data have been recorded during previous batch experiments using these chemicals.

Numerical Modeling

- 5) To design a geometry and grid combination that will have enough refinement to not have any effect on correct prediction considering the large size of the incinerator, the small scale at which chemical reactions and turbulence are

important, and the current computing limitations, is presently impossible. However, refinement of the grid to the point that only very small and localized changes occur upon further grid refinement (beyond that presented in this document) should be attained.

- 6) A more accurate picture of the chemical reaction process needs to be included to improve the current methane-only flame modeling and before waste processing can be successfully modeled. In particular, intermediates such as carbon monoxide and the high temperature dissociation of water vapor and carbon dioxide need to be included. Also, while the radiation effects of soot were included in the current model, results could be improved by an accurate modeling of its formation and destruction.
- 7) The ultimate goal is to be able to predict conversion of hazardous waste fed to the incinerator. To do this will require the ability to model the combustion of wastes. As relatively detailed experimental data have been recorded for the destruction of packs containing clay sorbent and toluene, these would be good materials to initially model.
- 8) Modeling the conversion of toluene absorbed onto clay sorbent and fed to the incinerator in drums or packs is a batch process and is therefore unsteady. A completely unsteady model could be attempted or several evolution rates could be considered to be steady, yielding rough snap-shots of the transient process.
- 9) Drum or pack processing will also require models for the initial container destruction, mixing of the new solid material with the existing bed of solids, heat transfer with the bed, kiln wall, and overhead gases and flames. An initial simplifying move could be to use previously estimated evolution rates of the waste as a boundary condition. Reaction schemes may require the

inclusion of a pyrolytic series. Visual observations indicate airborne soot to be optically thick, reducing viewing to approximately 1 meter at times, and often surviving through the rotary kiln and transition sections of the incinerator during batch processing of toluene and dichloromethane.

- 10) Improved predictive capabilities of new sub-models such as for turbulence or chemical reactions should be examined for possible inclusion in the model. However, these need to be weighed against any penalties in convergence, CPU time, or computer memory requirements. The same is true for advances in equation solution technology such as higher order differencing schemes.
- 11) Further data during the processing of waste, including temperature, speciation and velocity, need to be collected to aid in the construction of this numerical model.

BIBLIOGRAPHY

- Bard, S. and P. J. Pagni, "Carbon Particulate in Small Pool Fire Flames," *Journal of Heat Transfer*, Vol. 103, pp. 357-362, (1981).
- Bastian, R. E. and R. W. Wood, "Eastman Kodak Company Chemical Waste Incineration - Organic Compound Destruction," in Proceedings of the Conference On Rotary Kiln Incineration of Hazardous Waste, Hazardous Waste Research Center-Department of Mechanical Engineering-Center for Energy Studies, Louisiana State University, Baton Rouge, Louisiana, (1987).
- Boris, J. P., "New Directions in Computational Fluid Dynamics," *Annual Review of Fluid Mechanics*, 21: p. 345-385, (1989).
- Charalampopoulos, T. T. and H. Chang, "In situ Optical Properties of Soot Particles in the Wavelength Range from 340 nm to 600 nm," *Combustion Science and Technology*, Vol. 59, pp. 401-421, (1988).
- Charalampopoulos, T. T. and H. Chang, "Effects of Soot Agglomeration on Radiative Transfer," *Journal of Quant. Spectrosc. Radiat. Transfer*, Vol. 46, No. 3, pp. 125-134, (1991).
- Chen, Y. Y. and D. J. Lee, "A Steady State Model of a Rotary Kiln Incinerator," *Hazardous Waste and Hazardous Materials*, Vol. 11, No. 4, pp. 541-559, (1994).
- Clark, W. D., M. P. Heap, W. Richter, and W. R. Seeker, "The Prediction of Liquid Injection Hazardous Waste Incinerator Performance," ASME/AIChE National Heat Transfer Conference, Niagara Falls, New York, (1984).
- Clark, W. D., W. R. Seeker, and C. C. Lee, "Engineering Analysis of Hazardous Waste Incineration; Energy and Mass Balance," 12th Annual Hazardous Waste Research Symposium, Cincinnati, Ohio, (1986).
- Code of Federal Regulations, 40: Part 261, Subpart C. July 1, (1991a).
- Code of Federal Regulations, 40: Part 372. July 1, (1991b).
- Code of Federal Regulations, 40: Part 268, Subpart C. July 1, (1991c).

- Code of Federal Regulations, 40: Part 268.42, Subpart D. July 1, (1991d).
- Code of Federal Regulations, 40: Part 264.343 (c). July 1, (1991e).
- Cook, C. A., V. A. Cundy, A. M. Sterling, C. Lu, A. N. Montestruc, C. B. Leger and A. L. Jakway, "Estimating Dichloromethane Evolution Rates from a Sorbent Bed in a Field-Scale Rotary Kiln Incinerator," *Combustion Science and Technology*, Vol. 85, pp. 217-241, (1992).
- Cundy, V. A., T. W. Lester, A. M. Sterling, J. S. Morse, A. N. Montestruc, C. B. Leger, S. Acharya, and D. W. Pershing, "Rotary Kiln Injection I. An Indepth Study -- Liquid Injection," *Journal of the Air Pollution Control Association (JAPCA)*, Vol. 39, No. 1, pp. 63-75, (1989a).
- Cundy, V. A., T. W. Lester, A. M. Sterling, J. S. Morse, A. N. Montestruc, C. B. Leger, and S. Acharya, "Rotary Kiln Injection III. An Indepth Study -- Kiln Exit/Afterburner/Stack Train and Kiln Exit Pattern Factor Measurements During Liquid CCl₄ Processing," *Journal of the Air Pollution Control Association*, Vol. 39, No. 7, pp. 944-952, (1989b).
- Cundy, V. A., T. W. Lester, A. M. Sterling, J. S. Morse, A. N. Montestruc, C. B. Leger, and S. Acharya, "Rotary Kiln Injection IV. An Indepth Study -- Kiln Exit, Transition and Afterburner Sampling During Liquid CCl₄ Processing," *Journal of the Air Pollution Control Association*, Vol. 39, No. 8, pp. 1073-1085, (1989c).
- Cundy, V. A., T. W. Lester, C. Leger, G. Miller, A. N. Montestruc, S. Acharya, and A. M. Sterling, "Rotary Kiln Incineration -- Combustion Chamber Dynamics," *Journal of Hazardous Materials*, Vol. 22, pp. 195-219, (1989d).
- Cundy, V. A., T. W. Lester, R. Conway, A. L. Jakway, C. B. Leger, A. N. Montestruc, S. Acharya, A. M. Sterling, W. D. Owens, J. S. Lighty, W. D. Pershing, and G. D. Silcox, "An Indepth Study of Incineration - Rotary Kiln Performance Characterization," Proceedings of the Third Annual Symposium on Hazardous Waste Research, Hazardous Waste Research Center, Louisiana State University, Baton Rouge, Louisiana, (1989e).
- Cundy, V. A., T. W. Lester, R. Conway, C. Cook, A. L. Jakway, C. B. Leger, C. Lu, A. N. Montestruc, S. Acharya, A. M. Sterling, D. A. Walker, F. S. Larson, R. J. Moore, D. Xian-Xue, J. S. Lighty, and W. D. Owens, "An Indepth Study of Rotary Kiln Incineration," Proceedings of the Fourth Annual Symposium on Hazardous Waste Research, Hazardous Waste Research Center, Louisiana State University, Baton Rouge, Louisiana, (1990).

- Cundy, V. A., A. M. Sterling, T. W. Lester, A. L. Jakway, C. B. Leger, C. Lu, A. N. Montestruc, and R. B. Conway, "Incineration of Xylene/Sorbent Packs. A Study of Conditions at the Exit of a Full-Scale Industrial Incinerator," *Environmental Science and Technology*, Vol. 25, No. 2, pp. 223-231, (1991a).
- Cundy, V. A., C. Lu, C. A. Cook, A. M. Sterling, C. B. Leger, A. L. Jakway, A. N. Montestruc, R. Conway, and T. W. Lester, "Rotary Kiln Incineration of Dichloromethane and Xylene: A Comparison of Incinerability Characteristics Under Various Operating Conditions," *Journal of the Air & Waste Management Association*, Vol. 41, No. 8, pp. 1084-1094, (1991b).
- Cundy, V. A., C. Cook, A. M. Sterling, C. Lu, A. N. Montestruc, C. B. Leger, and, A. L. Jakway, "Rotary Kiln Incineration - Batch Processing of CH_2Cl_2 on Sorbent Contained in Plastic Packs," Proceedings of the 2nd International Congress on Toxic Combustion By-Products Formation and Control, Salt Lake City, Utah, (1991c).
- Cundy, V. A., A. M. Sterling, C. Lu, C. A. Cook, C. B. Leger, A. L. Jakway, A. N. Montestruc, R. Conway, and T. W. Lester, "Rotary Kiln Incineration: A Field-Scale Study of System Dynamics Under Various Operating Conditions," Invited paper, Fifth Annual National Symposium on Incineration of Industrial Wastes, (unpublished paper available at conference), Simon-EEL, Inc., Houston, Texas, (1991d).
- De Ris, J., "Fire Radiation - A Review," 17th Symposium International on Combustion, pp. 1003-1016, (1978).
- Edwards, D. K., Radiation Heat Transfer Notes, Hemisphere Publishing Corp., Washington, (1981).
- Federal Register, p. 31, 114, Friday May 28, (1993).
- Felske, J. D. and T. T. Charalampopoulos, "Gray Gas Weighting Coefficients for Arbitrary Gas-Soot Mixtures," *International Journal of Heat and Mass Transfer*, Vol. 25, No. 12, pp. 1849-1855, (1982).
- Fluent User's Guide, Version 4.2*; Fluent Inc.: Lebanon, NH, June (1993).
- Gardner, W. C. Jr., Combustion Chemistry, Springer-Verlag, New York, NY (1984).

- Gillis, P.A. and P. J. Smith, "Three-Dimensional Fluid Dynamics Modeling in Furnace Geometries," Western States Section of The Combustion Institute, pp. 1-12, (1988).
- Glassman, I., Combustion, second edition, Academic Press, Inc., (1987).
- Gorog, J. P., T. N. Adams, and J. K. Brimacombe, "Heat Transfer from Flames in a Rotary Kiln," *Metallurgical Transactions B*, Vol. 14B, pp. 411-424, (1983).
- Gorog, J. P., T. N. Adams, and J. K. Brimacombe, "Radiative Heat Transfer in Rotary Kilns," *Metallurgical Transactions B*, Vol. 12B, pp. 55-70, (1981).
- Huggins, Jonathan. Personal Communication, March 18, (1994).
- Incropera, F. P. and D. P. DeWitt, Fundamentals of Heat and Mass Transfer, 2nd Ed., John Wiley and Sons, (1985).
- Jakway, A. L., V. A. Cundy, and A. M. Sterling, "3-D Numerical Modeling of a Field Scale Rotary Kiln Incinerator," presentation at The ASME Winter Annual Meeting, Open Forum on Fire and Combustion, American Society of Mechanical Engineers, (unpublished paper available at conference) New Orleans, Louisiana, November 28-December 3, (1993a).
- Jakway, A. L., V. A. Cundy, A. M. Sterling, and C. B. Leger, "A 3-Dimensional Detailed Numerical Model as a Design Tool for Rotary Kiln Incinerators," The 3rd International Congress on Toxic Combustion By-Products, (unpublished paper available at conference) Cambridge, Massachusetts, June 14-16, (1993b).
- Jakway, A. L., V. A. Cundy, A. M. Sterling, C. A. Cook, and A. N. Montestruc, "Insitu Velocity and Temperature Measurements from an Industrial Rotary Kiln Incinerator," *Proceedings of the 14th International Incineration Conference*, Seattle, Washington, May 8-12, (1995a).
- Jakway, A. L., V. A. Cundy, A. M. Sterling, C. A. Cook, and A. N. Montestruc, "In Situ Velocity Measurements from an Industrial Rotary Kiln Incinerator," accepted to the *Journal of the Air and Waste Management Association*, Nov., (1995b).
- Jenkins, B. G. and F. D. Moles, "Modeling of Heat Transfer from a Large Enclosed Flame in a Rotary Kiln," *Transactions of the Institute of Chemical Engineers*, Vol. 59, pp. 17-25, (1981).

- Jones, W. P. and J. H. Whitelaw, "Calculation Methods for Reacting Turbulent Flows: A Review," *Combustion and Flame*, 48: pp. 1-26, (1982).
- Kent, L. A. and M. E. Schneider, "The Design and Application of Bi-Directional Velocity Probes for Measurement in Large Pool Fires," *ISA Transactions*, Vol. 26, No. 4, pp. 25-32, (1987).
- Khan, J. A., D. Pal, and J. S. Morse, "Numerical Modeling of a Rotary Kiln Incinerator," *Hazardous Waste and Hazardous Materials*, Vol. 10, No. 1, p. 81, (1993).
- Leger, C. B., V. A. Cundy, A. M. Sterling, A. N. Montestruc, A. L. Jakway, and W. D. Owens, "Field-Scale Rotary Kiln Incineration: Oxygen Responses at the Kiln, Afterburner, and Stack," *Remediation*, Vol. 1, No. 3, pp. 275-291, (1991a).
- Leger, C. B., V. A. Cundy, A. M. Sterling, C. A. Cook, A. L. Jakway, and A. N. Montestruc, "Rotary Kiln Incineration - Batch Processing of Toluene on Sorbent Contained in Plastic Packs," *Proceedings of the 84th Annual Meeting of the Air and Waste Management Association*, Vancouver BC, (1991b).
- Leger, C. B., "A Study of Selected Phenomena Observed During Rotary Kiln Incineration," Ph.D. Dissertation, Louisiana State University, (1992).
- Leger, C. B., V. A. Cundy, A. M. Sterling, A. N. Montestruc, A. L. Jakway, and W. D. Owens, "Field-Scale Rotary Kiln Incineration of Batch Loaded Toluene/Sorbent. I. Data Analysis and Bed Motion Considerations," *Journal of Hazardous Materials*, Vol. 34, pp. 1-29, (1993a).
- Leger, C. B., C. A. Cook, V. A. Cundy, A. M. Sterling, A. N. Montestruc, A. L. Jakway, and W. D. Owens, "Field-Scale Rotary Kiln Incineration of Batch Loaded Toluene/Sorbent. II. Mass Balances, Evolution Rates, and Bed Motion Comparisons," *Journal of Hazardous Materials*, Vol. 34, pp. 31-50, (1993b).
- Leger, C. B., V. A. Cundy, and A. M. Sterling, "A Three-Dimensional Detailed Numerical Model of a Field-Scale Rotary Kiln Incinerator," *Environmental Science and Technology*, Vol. 27, No. 4, pp. 677-690, (1993c).
- Lester, T. W., V. A. Cundy, A. N. Montestruc, C. B. Leger, S. Acharya, and A. M. Sterling, "Dynamics of Rotary Kiln Incineration of Toluene/Sorbent Packs," *Combustion Science and Technology*, Vol. 74, pp. 67-82, (1990).

- Lester, T. W., V. A. Cundy, A. M. Sterling, A. N. Montestruc, A. L. Jakway, C. Lu, C. B. Leger, D. W. Pershing, J. S. Lighty, G. D. Silcox, and W. D. Owens, "Rotary Kiln Incineration. Comparison and Scaling of Field-Scale and Pilot-Scale Contaminant Evolution Rates from Sorbent Beds," *Environmental Science & Technology*, Vol. 25, No. 6, pp. 1142-1152, (1991).
- Lipp, Chuck. Personal Communication, August 3, (1992).
- Magnussen, B. F. and B. H. Hjertager, "On Mathematical Modeling of Turbulent Combustion With Special Emphasis on Soot Formation and Combustion," Sixteenth International Symposium on Combustion, pp. 719-729, the Combustion Institute, (1976).
- McCaffrey, B. J. and G. Heskestad, Brief communications: "A Robust Bidirectional Low-Velocity Probe for Flame and Fire Application," *Combustion and Flame*, Vol. 26, pp. 125-127, (1976).
- Montestruc, A. N., "Flame Zone Sampling From an Industrial Rotary Kiln," Masters Thesis, Louisiana State University, (1989).
- Murthy, J. Y. and D. Choudhury, "Computation of Participating Radiation in Complex Geometries," National Heat Transfer Conference, San Diego, CA, ASME TN-020, (1992).
- Nasserzadeh, V., J. Swithenbank, and B. Jones, "Three-dimensional Modeling of a Municipal Solid-Waste Incinerator," *Journal of Institute of Energy*, Vol. 64, pp. 166-175, (1991).
- Nasserzadeh, V., J. Swithenbank, C. Schofield, D. W. Scott, and A. Loader, "Effects of High Speed Jets and Internal Baffles on the Gas Residence Times in Large Municipal Incinerators," *Environmental Progress*, Vol. 13, No. 2, pp. 124-133, (1994).
- Owens, W. D., G. D. Silcox, J. S. Lighty, X. X. Deng, D. W. Pershing, T. W. Lester, V. A. Cundy, C. B. Leger, and A. L. Jakway, "Hydrocarbon Evolution From Contaminated solids: Effects of Moisture and Operating Parameters in a Rotary Kiln Environment," Poster Session, 23rd Symposium (International) on Combustion, Orleans, France, (1990a).
- Owens, W. D., G. D. Silcox, J. S. Lighty, X. X. Deng, D. W. Pershing, V. A. Cundy, C. B. Leger, and A. L. Jakway, "Thermal Analysis of Rotary Kiln Incineration: Comparison of Theory and Experiment," Poster Session, 23rd Symposium (International) on Combustion, Orleans, France, (1990b).

- Owens, W. D., G. D. Silcox, J. S. Lighty, X. X. Deng, D. W. Pershing, V. A. Cundy, C. B. Leger, and A. L. Jakway, "Thermal Analysis of Rotary Kiln Incineration: Comparison of Theory and Experiment," *Combustion and Flame*, Vol. 86, pp. 101-114, (1991).
- Owens, W. D., G. D. Silcox, J. S. Lighty, X. X. Deng, D. W. Pershing, V. A. Cundy, C. B. Leger, and A. L. Jakway, "The Desorption of Toluene from a Montmorillonite Clay Adsorbent in a Rotary Kiln Environment," *Journal of the Air and Waste Management Association*, Vol. 42, No. 5: pp. 681-690, (1992).
- Silcox, G. D., D. W. Pershing, B. R. Keyes, W. D. Owens, J. S. Lighty, X. X. Deng, V. A. Cundy, C. B. Leger, and A. L. Jakway, "Heat Transfer, Mass Transfer, Vaporization, and Combustion in Rotary Kilns," 1990 Summer National Meeting, AIChE, San Diego, CA., (1990).
- Smith, P. J., W. A. Sowa, and P. O. Hedman, "Furnace Design Using Comprehensive Combustion Models," *Combustion and Flame*, Vol. 79, pp. 111-121, (1990).
- Stanisic, M. M., *The Mathematical Theory of Turbulence*, Springer Verlag, New York, (1985).
- Sterling, A. M., V. A. Cundy, T. W. Lester, A. N. Montestruc, A. L. Jakway, C. B. Leger, C. Lu, and R. Conway, "Fundamental Kiln Processes," Fourth Annual National Symposium - Incineration of Industrial Wastes, (unpublished paper available at conference), Toxcon Engineering Company, Inc., Houston, Texas, (1990a).
- Sterling, A. M., V. A. Cundy, T. W. Lester, A. N. Montestruc, A. L. Jakway, C. B. Leger, C. Lu, and R. Conway, "Rotary Kiln Incineration - The LSU In Situ Field Testing Program," Proceedings of the 83rd Annual Meeting of the Air and Waste Management Association, Pittsburgh, PA., (1990b).
- Stull, D. R. and H. Prophet, "JANAF Thermochemical Tables," NSRDS-NBS 37, National Bureau of Standards and Supplements, Washington, (1971).
- Thibodeaux, L. J., "Hazardous Material Management in the Future," *Environmental Science and Technology*, Vol. 24, No. 4, pp. 456-459, (1990).
- Wagner, H. G., "Soot Formation -- An Overview," in *Particulate Carbon: Formation During Combustion*, edited by D. C. Siegla and G. W. Smith, Plenum Publishing Corporation, (1981).

- Wang, T., Y. Chen, and R. Farmer, "Numerical Study of Reactive Ramjet Dump Combustor Flowfields with a Pressure Base CFD Method," AIAA/ASME/SAE/ASEE 25th Joint Propulsion Conference, AIAA, pp. 1-11, (1989).
- Westbrook, C. K. and F. L. Dryer, "Chemical Kinetic Modeling of Hydrocarbon Combustion," *Prog. Energy Combustion Science*, Vol. 10, pp.1-57, (1984).
- Willard H. H., L. L. Merritt Jr., J. A. Dean, and F. A. Settle Jr., Instrumental Methods of Analysis, sixth ed., Wadsworth Pub. Co., Belmont CA, pp. 854-856, (1981).
- Wood, R. W., "Eastman Kodak Company Rotary Kiln Performance Testing," in Proceedings of the Conference On Rotary Kiln Incineration of Hazardous Waste, Hazardous Waste Research Center-Department of Mechanical Engineering-Center for Energy Studies, Louisiana State University, Baton Rouge, Louisiana, (1987).

APPENDIX A

PUBLISHING INFORMATION ON CHAPTER 4

PUBLISHING PERMISSION LETTERS



LOUISIANA STATE UNIVERSITY

AND AGRICULTURAL AND MECHANICAL COLLEGE

Mechanical Engineering Department • Baton Rouge, LA 70803-6413
504/388-6489 • FAX *5924

September 8, 1995

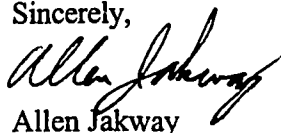
Mr. William Tony
Managing Editor
Journal of the Air & Waste Management Association
Third Floor
One Gateway Center
Pittsburgh, PA 15222

Dear Mr. Tony,

I request a letter from your office granting permission to include a paper that has been accepted to your publication in my Dissertation. The title of the paper is "***In Situ*** Velocity Measurements From An Industrial Rotary Kiln Incinerator" authored by Jakway, Cundy, Sterling, Cook, and Montestruc. Your office has labeled it Manuscript # 114. The dissertation will be microfilmed by University Microfilms, Inc., which may supply single copies on demand. A copy of this letter and your reply will be included in the Dissertation.

Thank you for your time and consideration.

Sincerely,


Allen Jakway

cc: Dr. Vic A. Cundy of Montana State University
Dr. Arthur M. Sterling of Louisiana State University

REVIEWERS COMMENTS

The comments of the two reviewers given below were transcribed from a fax dated 6/8/95 to Dr. Sterling (the author designated for correspondences) from Dr. Koutrakis (an editor for the Journal of the Air & Waste Management Association).

Dear Dr. Koutrakis:

Re: Manuscript No. 114

Generally I find this paper to be well written and of excellent technical quality. It is good to see hard experimental data in this area instead of the typical "theoretical" calculations. The presentation is clear and concise, particularly the drawings and graphs. I have two suggestions for minor changes/additions. These recommendations are for the purpose of clarity and reflect concerns about how similar research efforts have been misinterpreted by regulatory officials and extrapolated into regulatory requirements.

The first suggestion is to clearly refer to the device as a "rotary kiln incinerator". There are a number of industries that use rotary kilns for a variety of industrial purposes. Simply referring to the system as a "rotary kiln" in a number of locations could lead to an inappropriate extrapolation of the data in the report to other rotary kiln technologies.

The second suggestion is that the summary should contain a comment or two regarding the limitations of the measurement technique. Specifically both the temperature and Reynolds number may limit the applicability of this work to devices that fall inside of the range specified earlier in the paper. It is particularly difficult to see how this technique could be utilized in facilities with Reynolds numbers >2000. Since many rotary kiln incinerator and other rotary kiln furnaces have high Reynolds numbers this is of significance.

I hope these suggestions are helpful. Please feel free to contact me if there are any questions.

Dear Dr. Koutrakis

I have read Allen Jakway's paper and completed my review. I recommend it for publication.

The paper was clearly written and well organized. The description of the boom for the velocity probe and suction pyrometer was particularly good and needed as well. The tables and figures were clear and well organized.

The technical content of the paper was good also. As a practicing engineer I prefer English units over the metric units shown.

As a suggestion for further study, I think the industry would be interested in some analysis and the temperature profile of gas flows near the surface of the refractory.

Thank you for allowing me the opportunity to review this paper.

The comments of these two reviewers have been incorporated into the version of the paper that appears in this dissertation as Chapter 4 with the exception of the paper remaining in SI units.

APPENDIX B

PROBE BOOM CONSTRUCTION

COMPARISON TO PREVIOUS BOOM

The new 6.31 m kiln probe with the four tube bidirection velocity probe instrument head attached weighs only 33.2 kg empty and 39.3 kg when filled with water (includes 3.18 kg of external piping for both conditions). This represents an operational, i.e. when full of water, mass decrease of 12.9 kg or 25% from that of the previous probe design. The new probe droops only 11.4 cm when filled with water and cantilevered 4.65 m, a big improvement over the previous probe's approximately 38.1 cm droop over 6.1 m, especially in conjunction with the old probe's approximately 30 cm permanent droop (due to a brief stoppage of the water flow at one time.)

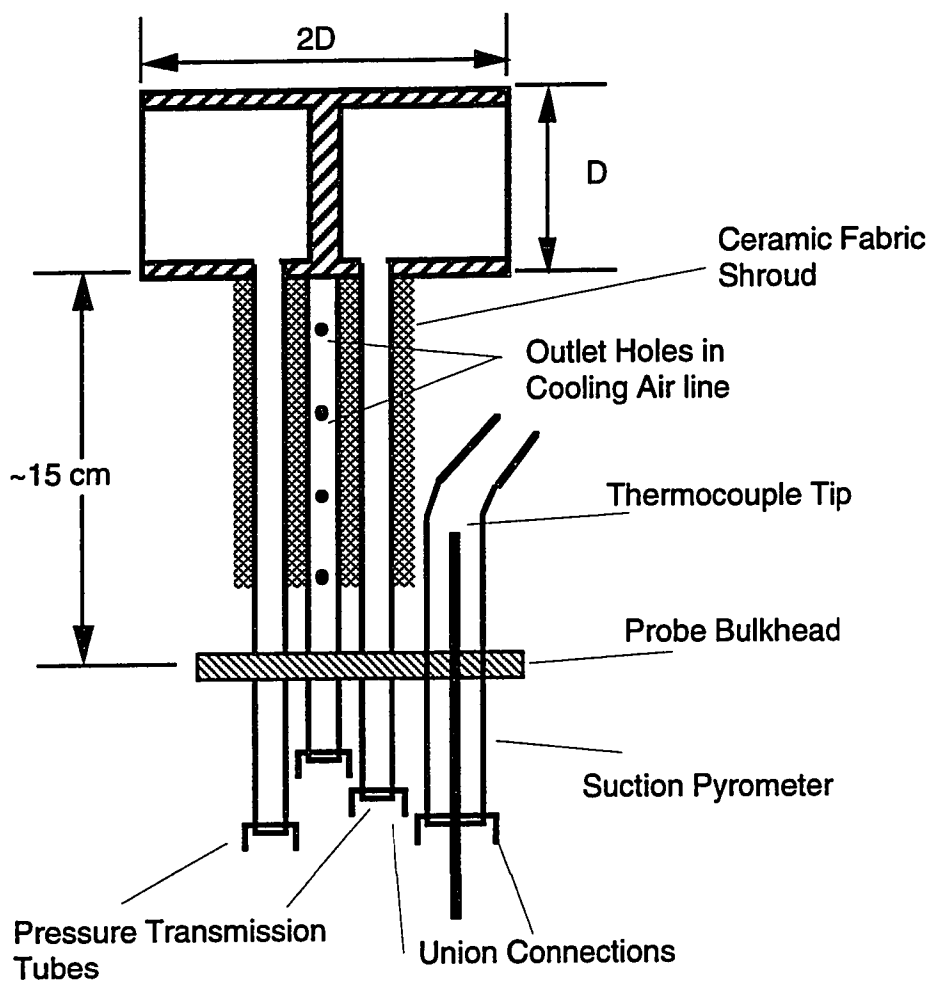
CONSTRUCTION FIGURES

- Figure B.1 Schematic of instrument head with bidirectional velocity probe.
- Figure B.2 Construction schematic of hot end of boom.
- Figure B.3 Construction schematic of cold end of boom.
- Figure B.4 Part #1: Aluminum cooling water end piece.
- Figure B.5 Parts #2 and 3: Aluminum end caps.
- Figure B.6 Part #5: Boom coupling for Instrument head.
- Figure B.7 Part #6: Steel cooling water end piece.

Figure B.8 Parts #8 and 9: Nipples for water connection.

Figure B.9 Part #7: Air gap spacer.

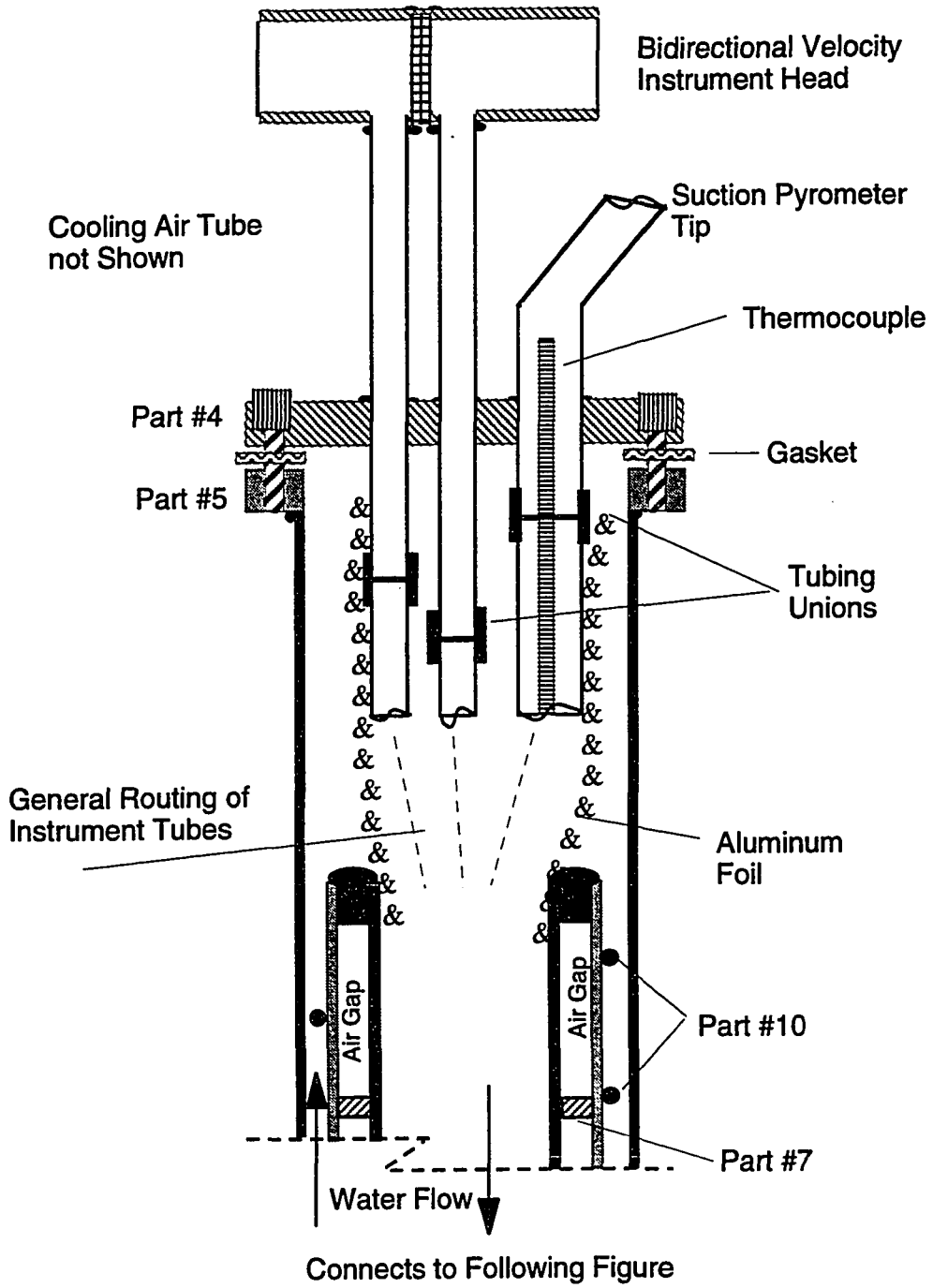
Figure B.10 Part #4: Instrument head connector to boom.



Notes

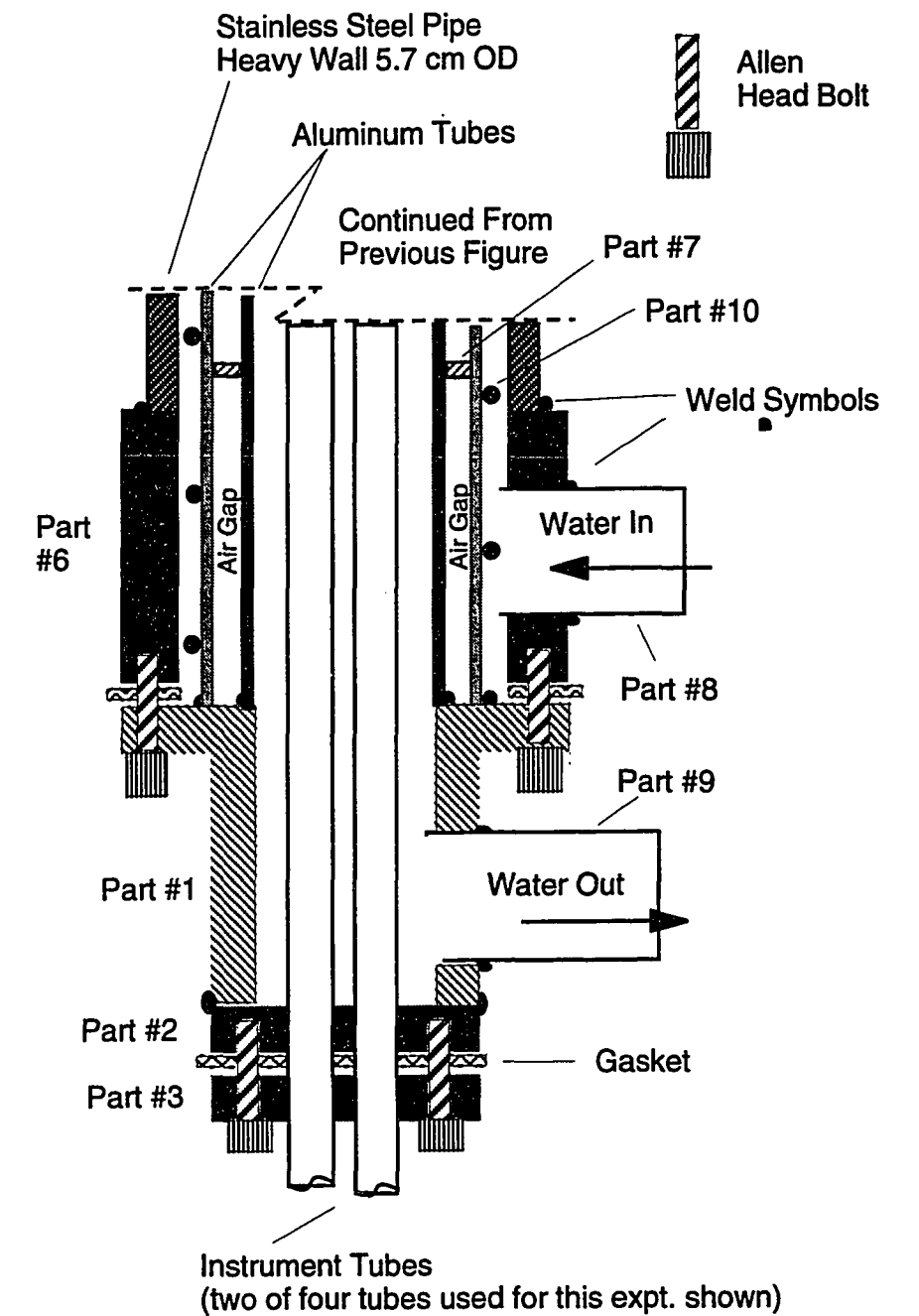
- 1) Suction pyrometer is positioned in same plane as cooling air line (not as shown), pointing away from instrument head.

Figure B.1 Schematic of Instrument head with bidirectional velocity probe.



Note Wrap aluminum foil around instrument tubes so that when assembled, the cooling water flows to the bulkhead (part#4).

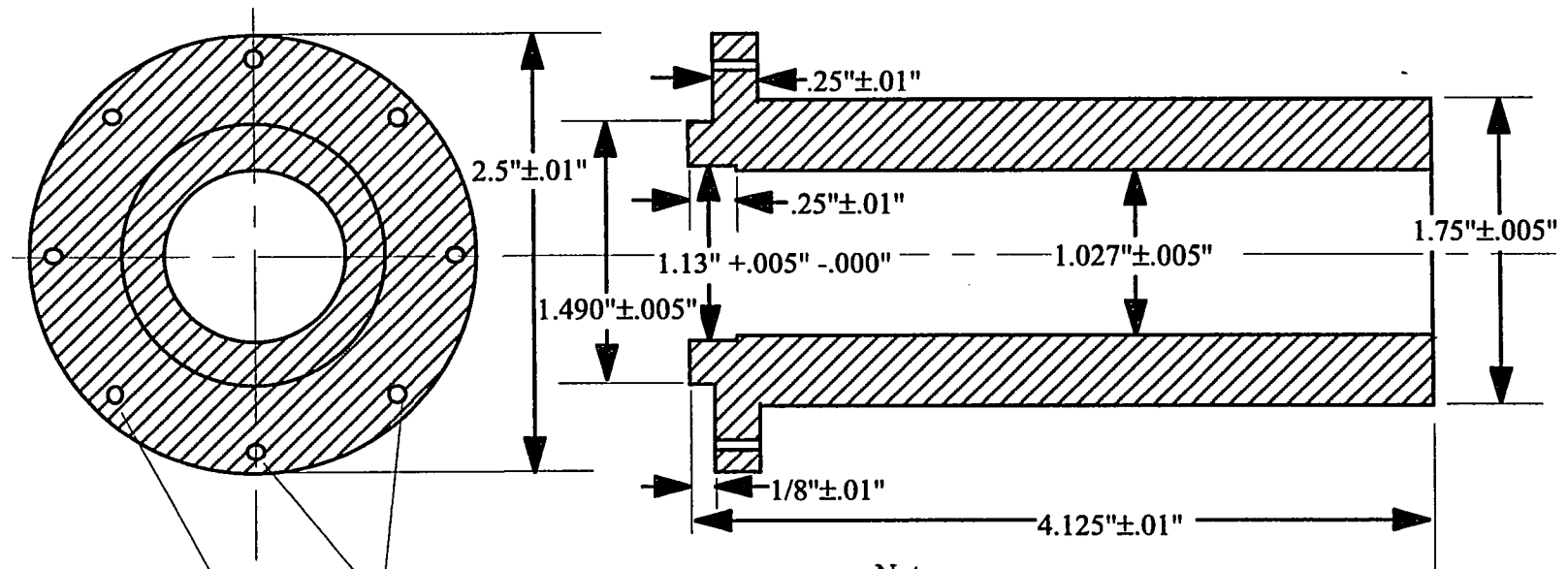
Figure B.2 Construction schematic of hot end of boom.



Note

Part #10 is a wire wrapped helically around the outer air gap tube and tack welded occasionally so that it retains its helical placement.

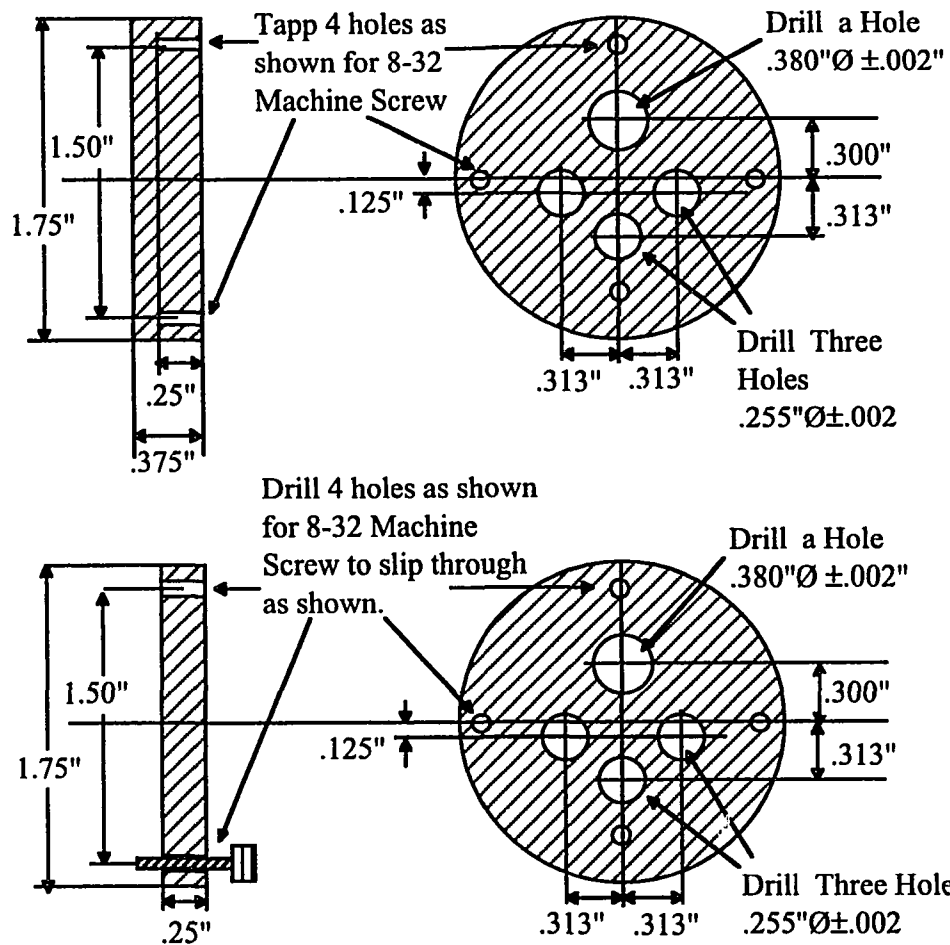
Figure B.3 Construction schematic of cold end of boom.



Drill 8 holes for 8-32 Allen head machine screws to fit as shown on 1.06" radius from centerline.

- Notes
- 1) Part to be made of Aluminum 5056-O
 - 2) Screw holes on Part #1 must line up with tapped holes on Part #6.

Figure B.4 Part #1: Aluminum cooling water end piece.



Part #2 Inner Cap

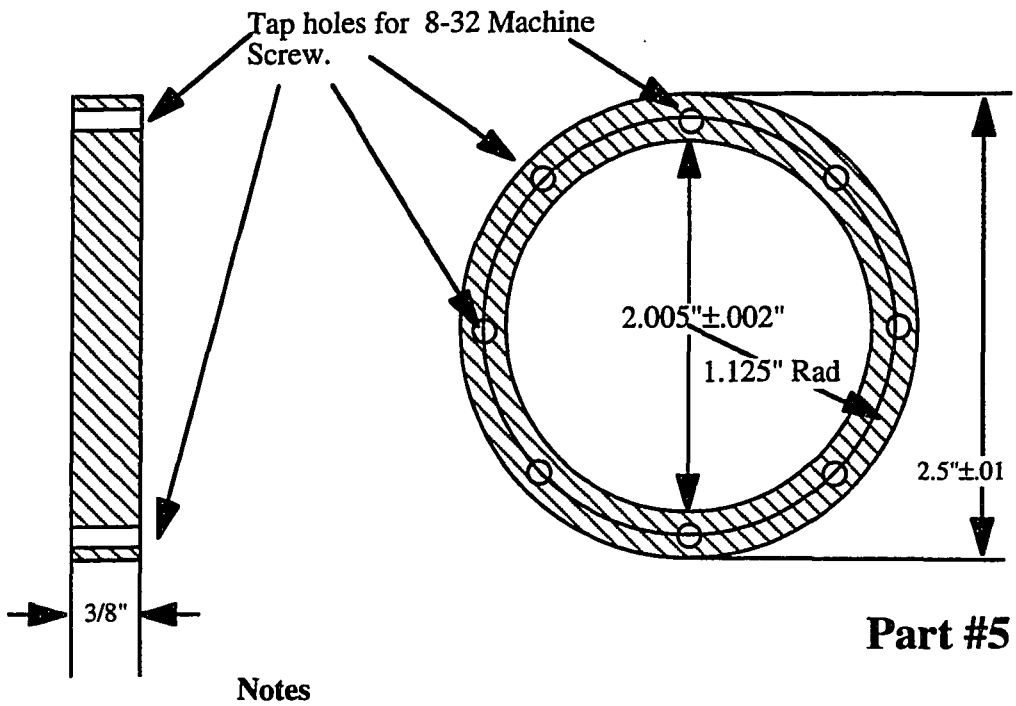
1/2" 8-32 Allen head machine screw 

Notes

- 1) Parts to be made of Aluminum 5056-O
- 2) Screw holes on Part #2 must line up with tapped holes on Part #3.
- 3) The inner cap will be welded to Part #1.

Part #3 Outer Cap

Figure B.5 Parts #2 and 3: Aluminum end caps.



- 1) Both parts to be made from 304 Stainless Steel
- 2) Screw holes on part #4 must line up with tapped holes on part #5.

Figure B.6 Part #5: Boom coupling for Instrument head.

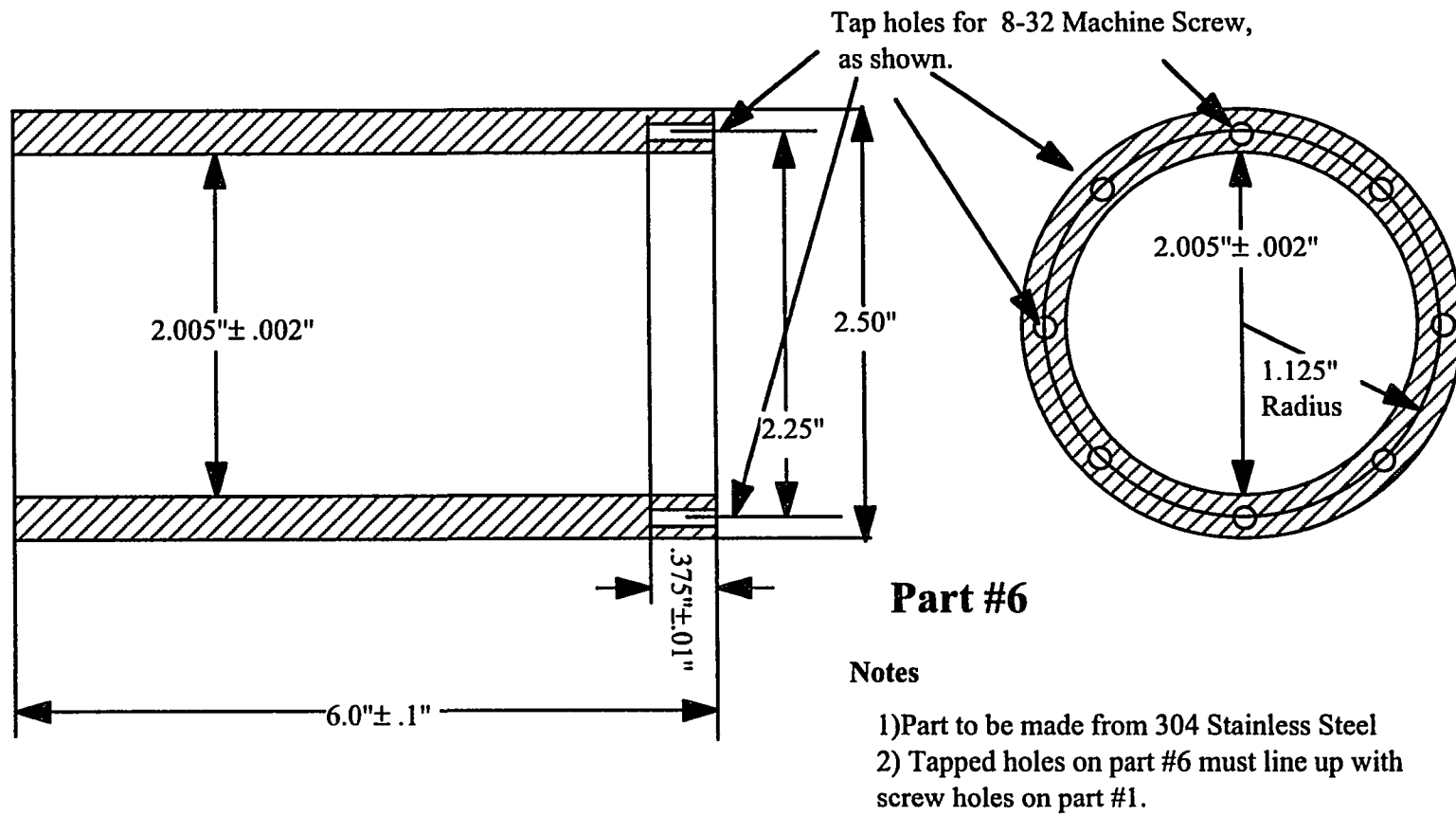
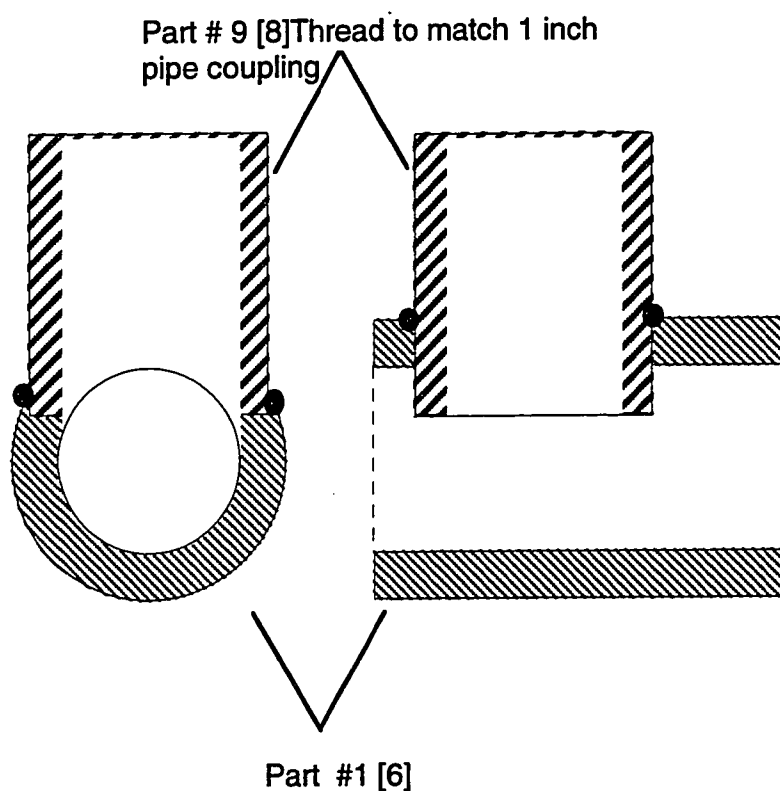
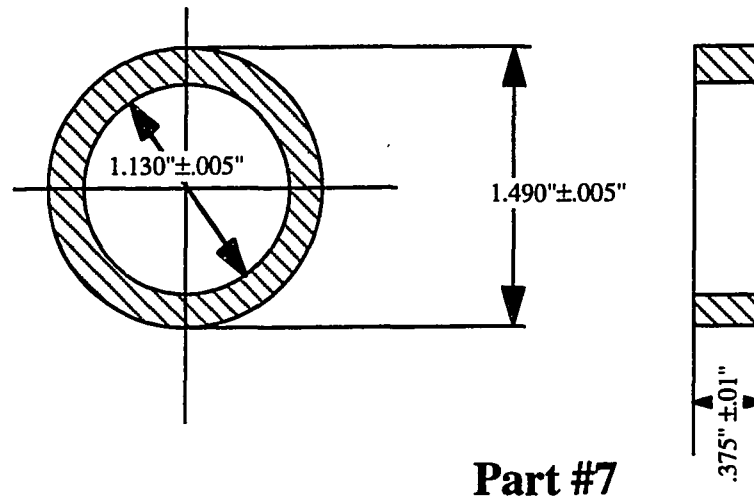


Figure B.7 Part #6: Steel cooling water end piece.

**Notes**

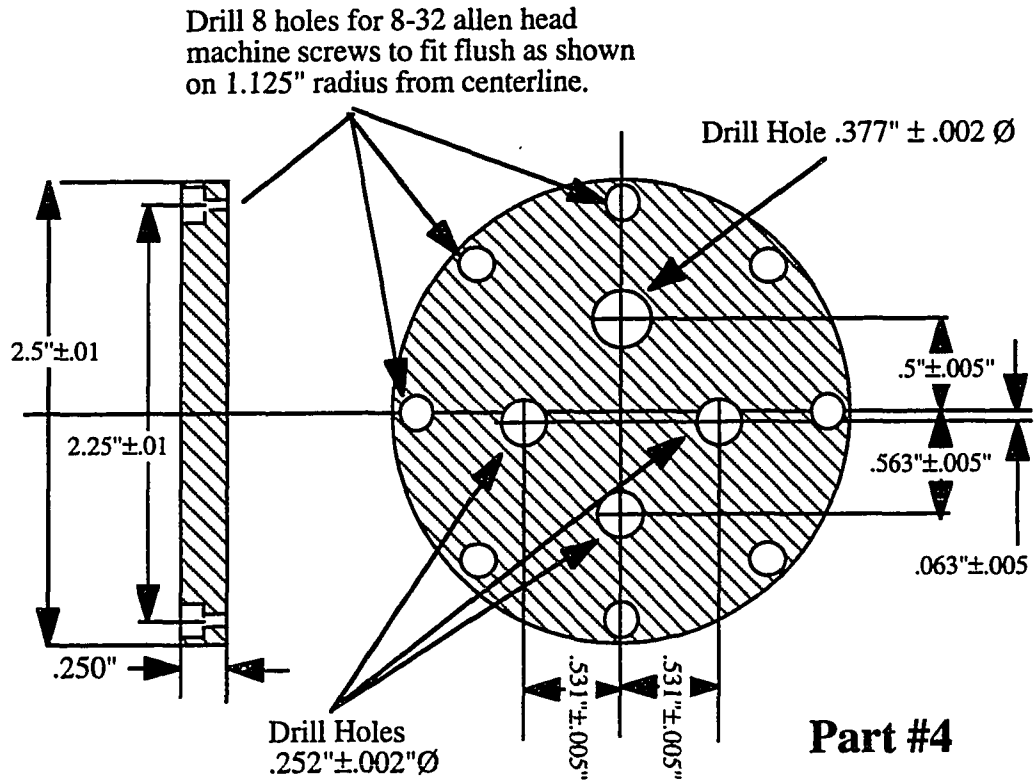
- 1) Part #9 to be made of weldable aluminum
- 2) Part #8 same as part #9 except made of 304 stainless steel

Figure B.8 Parts #8 and 9: Nipples for water connections.

**Notes**

- 1) Part to be made of Weldable Aluminum
- 2) Place at intervals as required to maintain air gap spacing

Figure B.9 Part #7: Air gap spacer.



Notes

- 1) Part to be made from 304 Stainless Steel
- 2) Screw holes on part #4 must line up with tapped holes on part #5.

Figure B.10 Part #4: Instrument head connector to boom.

APPENDIX C

BOOM POSITIONER

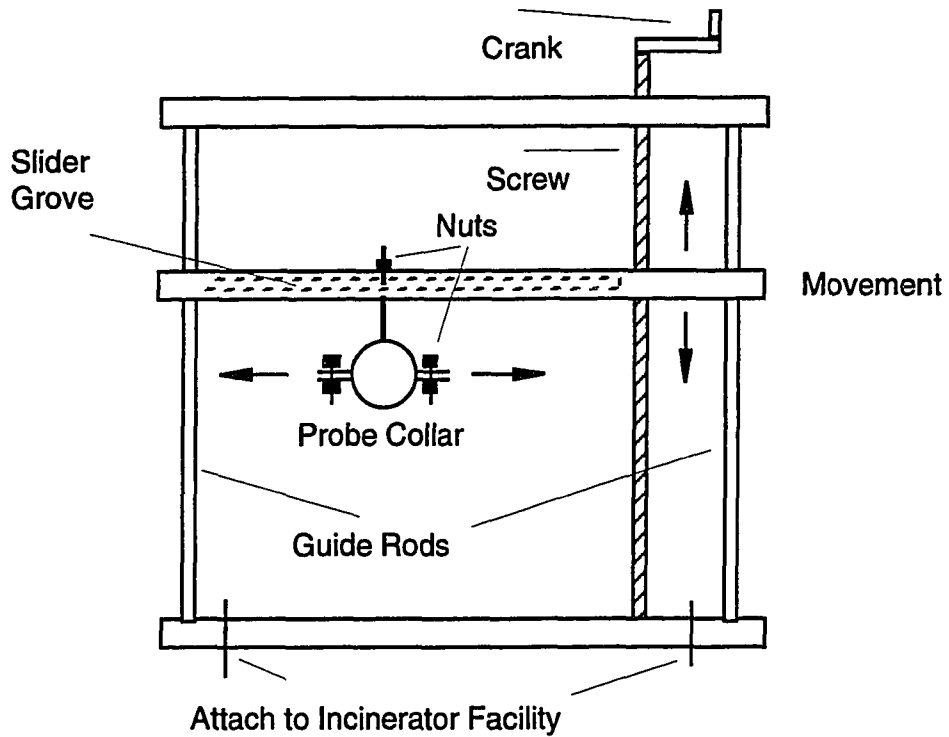


Figure C.1 Boom positioner.

APPENDIX D

DETAILED REVIEW OF MODELING BY LEGER ET AL. (1993C)

INTRODUCTION

The model presented in Chapter 5 of this dissertation is based on the first generation model of Leger et al. (1992 and 1993c), utilizing many of the same assumptions and methods of solution. Because of this, Leger's model is reviewed in detail below.

GEOMETRY

Only the rotary kiln section of the incinerator was modeled. A rough approximation of the transition section between the kiln and the afterburner was included in the model only to enhance numerical stability and convergence.

GRID

Leger created a three-dimensional, uniform grid with 12,240 control volumes as shown in Figures D-1 and D-2. Cartesian coordinates were used because the off-axis burners, non-centered rectangular solids loading chute, and rectangular geometry of the transition and afterburner sections would have been awkward to handle in cylindrical coordinates, the only alternate coordinate system available. Also, using cylindrical coordinates would force the finest area of the grid to be at the centerline of the kiln, a non-optimum location for this modeling problem. The consequences of using Cartesian coordinates were that the kiln's cylindrical wall was stepped, and the nozzles square. Also, one-fourth of the control volumes were not in the flow region,

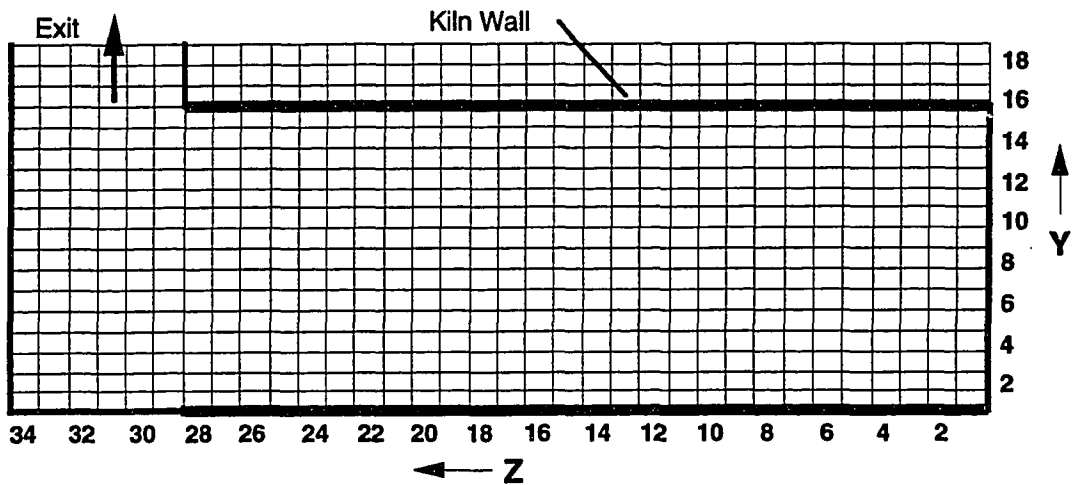


Figure D.1 Side view of computational grid centerline used in Leger et. al (1993c).

but were instead needed to form the cylindrical geometry and exit chimney. Due to the coarseness of the grid, the burner and turbulence air inlets were modeled by single control volumes. Grid coarseness combined with using uniform control volume spacing resulted in incorrectly positioned and sized inlets. A grid dependence study was attempted, but file size and solution divergence problems were never resolved and hence, this study was incomplete.

BOUNDARY CONDITIONS

In the model presented in Leger et al. (1993c), the walls of the rotary kiln did not rotate and were assumed to be isothermal at 800 K.

The air leaking into the incinerator, termed "leak air", has been estimated, by Montestruc (1989) and Leger et al. (1993b) respectively, to range from 1.5 to 3.5

The air leaking into the incinerator, termed "leak air", has been estimated, by Montestruc (1989) and Leger et al. (1993b) respectively, to range from 1.5 to 3.5 times the metered air flows into the system. Air is known to leak into the kiln at the

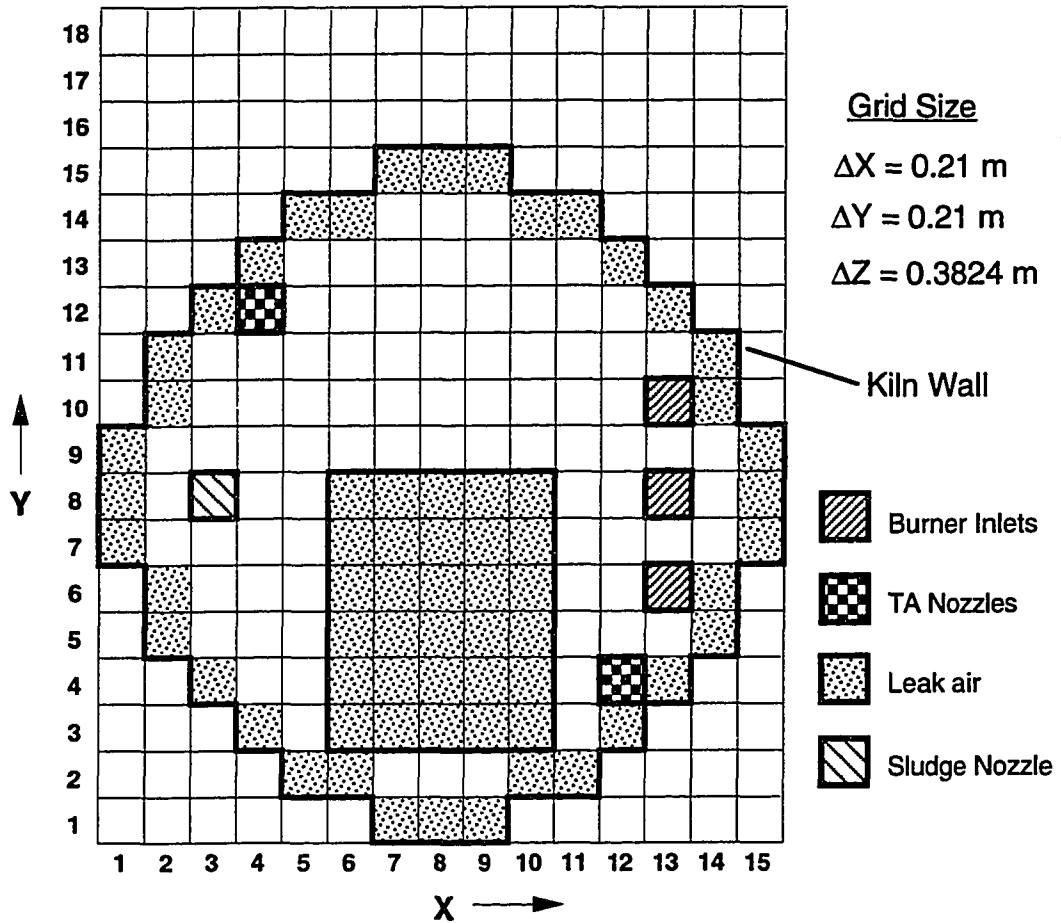


Figure D.2 View of kiln front face computational grid used in Leger et. al (1993c).

front and rear kiln rotary seals, around the edges of the solids loading door, and through various instrument ports in the kiln/afterburner transition section. However, neither the distribution, nor the temperature of the leaks is known; therefore, these values were assumed as indicated in the next paragraph.

Leger et al. (1993c) assumed all of the leak air sources had inlet velocities in the axial flow direction of the kiln, and that the leak air was heated during passage into the kiln from ambient temperatures to 310 K. The perimeter gap at the solids loading

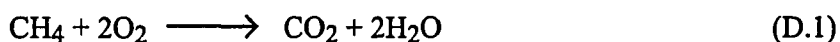
door was assumed to account for 35 percent of the leak air. The gap in the rotary seals is small but encompasses the perimeter of the kiln; therefore, 20 percent of the leak air was assumed to enter through each of the front and rear seals at a temperature of 400 K. The remaining 25 percent represents the combination of any leaks downstream of the kiln, particularly in the kiln-to-afterburner transition section. The transition section leaks were modeled as a 310 K upward flow issuing from the bottom of the transition section.

FLUID PHYSICAL PROPERTIES

The density of the gas was calculated using the ideal gas law, thereby accounting for the effects of buoyant forces that result from the variations in gas density caused by temperature and species concentration. The natural gas from the burners at the field-scale contained a minimum of 95 percent methane by volume and therefore was input as pure methane.

The reaction rate for methane combustion was determined using a combination of a turbulent eddy mixing model presented in Magnussen and Hjertager (1977) and Arrhenius kinetics. However the activation energy for the reaction was decreased by six orders of magnitude due to uncertainty about the kinetic parameters. As a result, the reaction rate was controlled by the turbulent mixing rate.

The combustion reaction was modeled by a one step global reaction shown in Equation D.1. Species conservation equations were solved for nitrogen, oxygen, methane, carbon dioxide, and water vapor. Turbulent effects were modeled using the Algebraic Stress Model (ASM).



Although the effective turbulent viscosity is the overwhelming factor controlling the fluid viscosity, the laminar viscosity was also specified. The combustion gases, which are approximately the same composition as air, were modeled using atmospheric air properties in the laminar viscosity and thermal conductivity calculations. The laminar viscosity was related to temperature by fitting a fourth order polynomial to data from Incropera and DeWitt (1985) over the 300 K to 3,000 K range. In the same manner, the laminar thermal conductivity versus temperature relationship was approximated by a fourth order polynomial using data for air taken over the same temperature range and source. The energy equation was solved in terms of enthalpy, and the temperature was then extracted from the result using the specific heat of the fluid. The enthalpy of the gas was determined by integrating the specific heat from a reference temperature of 298 K to the actual temperature. The gas composition was accounted for in the enthalpy calculation by computing the mixture specific heat as a mass fraction weighted average of the individual, pure component heat capacities. The pure component heat capacities were entered as second order polynomials in temperature as presented by Theodore and Reynolds (1987).

SOLUTION METHOD

The differential equations were solved using a commercially available software package: FLUENT V3.03. The FLUENT code used a control volume-based finite difference method in which the equations were discretized using a quadratic upwind scheme called QUICK. The pressure-linked continuity and momentum equations were solved using the Semi-Implicit Method For Pressure-Linked Equations Consistent (SIMPLEC) algorithm. The resulting matrices were solved using a combined Gauss-Seidel and Thomas TriDiagonal-Matrix Algorithm (TDMA) routine.

The problem was cast as a transient problem with steady state boundary conditions to provide better convergence.

APPENDIX E

KILN WALL HEAT LOSS CALCULATIONS

Previous modeling by Leger et al. (1993c) assumed that the 33 cm thick refractory brick walls of the rotary kiln behave isothermally. To determine the appropriate heat transfer boundary condition, a heat balance was conducted on the rotary kiln. Assuming an outer wall temperature of 320 K (determined by touch), a light wind of 4.5 m/s, an ambient temperature of 300 K, and an exterior wall emissivity of 0.8, convection and radiation losses were calculated to be 24.4 and 18.5 kW, respectively. Heat release from the natural gas support flame (assumed to be pure methane) was calculated to be 4,637 kW. Therefore, the combined radiation and convection losses are less than 1 percent of the total heat loading, hence the isothermal wall assumption of the preceding model (Leger et al, 1993c) was replaced with an adiabatic wall assumption. This boundary condition produces a maximum wall temperature difference between top and bottom of 100° C, which is reasonable considering the rotation and thick, insulating construction of the wall.

APPENDIX F

COMPUTER CODE FOR RADIATION USER SUBROUTINE

```
#if NASA
    FUNCTION USERAC( PRESSR, TEMP, MOLEFR, MASSFR, MOLWTS, LENGTH,
+                 VOLUME, IVALUE, JVALUE, KVALUE, LVALUE, NUMSPC,
+                 ILAMDA, INGRAY )

#else
    FUNCTION USERAC( PRESSR, TEMP, MOLEFR, MASSFR, MOLWTS, LENGTH,
+                 VOLUME, IVALUE, JVALUE, KVALUE, LVALUE, NUMSPC )
#endif

C SCCS ID @(#)userac.F  4.2 2/27/92
C-----
C
C NAME : USERAC
C
C PROGRAM : FLUENT
C VERSION : V3.00
C
C (C) COPYRIGHT BY CREARE.X, INC, 1989
C
C ARGVS                                DESCRIPTION
C
C INPUT : PRESSR - ABSOLUTE PRESSURE
C          TEMP  - TEMPERATURE
C          MOLEFR - MOLE FRACTIONS
C          MASSFR - MASS FRACTIONS
C          MOLWTS - MOLECULAR WEIGHTS
C          LENGTH - LENGTH OF CELL IN RADIATION FLUX DIRECTION
C          VOLUME - VOLUME OF CELL
C          IVALUE - I-INDEX OF CELL
C          JVALUE - J-INDEX OF CELL
C          KVALUE - K-INDEX OF CELL
C          LVALUE - L-INDEX OF CELL
C          NUMSPC - NUMBER OF PRIMARY PHASE SPECIES DEFINED
C          ILAMDA - WAVELENGTH BAND NUMBER
C          INGRAY - =1 => NON-GRAY
C                  =0 => GRAY
C
C OUTPUT : NONE
C
C PURPOSE : THIS FUNCTION RETURNS THE ABSORPTION COEFFICIENT FOR
```

```

C          RADIATION FROM THE MOLE AND/OR MASS FRACTIONS AND
C          THE LOCAL TEMPERATURE AND PRESSURE
C
C          COMMENTS : THE CELL LENGTH, TEMPERATURE AND THE PRESSURE ARE
C                    IN THE USER DEFINED UNITS SYSTEMS AND THE RETURNED
C                    ABSORPTION COEFFICIENT SHOULD BE IN THE USER
C                    SPECIFIED UNITS SYSTEM
C
C          CALLED BY : RXCALC, RYCALC, RZCALC,
C
C-----C
C
C #include "IMPLICIT.INC"
C   To import the delcration size of the arrayys [ARYSIZ]
C   INCLUDE 'SIZE.INC'
C   To determine the cell type [ICELL(ARYSIZ)]
C   #include "BOUNDS.INC"
C   To import the temperatures [T(ARYSIZ)]
C   #include "FLOPRO.INC"
C   For the absorption coef. [ABSR(ARYSIZ)]
C #include "RPFLUX.INC"
C
C          FUNCTION TYPE DECLARATION...                               C
C-----C
C REAL    USERAC
C
C
C-----C
C          ARGUMENT TYPE DECLARATIONS...                             C
C-----C
C
C          IMPLICIT NONE
C          INTEGER NUMSPC
C          INTEGER IVALUE
C          INTEGER JVALUE
C          INTEGER KVALUE
C          INTEGER LVALUE
C
C          REAL    VOLUME
C          REAL    LENGTH
C          REAL    PRESSR
C          REAL    TEMP
C          REAL    MOLWTS(NUMSPC)
C          REAL    MOLEFR(NUMSPC)
C          REAL    MASSFR(NUMSPC)
C
C
C #if NASA
C
C          INTEGER ILAMDA

```

```

      INTEGER INGRAY
#endif
C  %%%%%%%%%%%%%%%%%%%%%%%%%%%%%%%%%%%%%%%%%%%%%%%%%%%%%%%%%%%%%%%%%%%%%%%%%
C
C          rev 16 Feb 95      by Allen Jakway
C  THIS FUNCTION CALCULATES THE ABSORBTIVITY [AS] of
C  soot particles, of a gas with air, CO2, & H2O [AG], and the
C  combined absorptivity [AT] and absorption coef [USERAC].
C  %%%%%%%%%%%%%%%%%%%%%%%%%%%%%%%%%%%%%%%%%%%%%%%%%%%%%%%%%%%%%%%%%%%%%%%%%
C    MBL = MEAN Beam Length
C    FV  = Volume Fraction
C    DLOG = Double Precision natural log, i.e. (ln)
C
C    REAL*8 MBL, A1, A2, G1, G2, AS, AT, AG, FV, USERACDP
C    REAL*8 EG,ABSGP, RSP, VSP, B, RUNIV
C    REAL*8 PH2O, PCO2, P, PI
C    REAL*8 TEMPDP, MOLEFRDP (NUMSPC)
C    REAL  ABSR(ARYSIZ)
C    INTEGER L, ICELL
C
C-----C
C    LOCAL VARIABLE TYPE DECLARATIONS...      C
C-----C
C
C
C    REAL    SMALL
C    PARAMETER ( SMALL = 1.0E-15 )
C
C    P = Atmospheric Pressure in ATM
C    P = 1.D0
C    Calculate the mean beam length
C    MBL = 0.95D0 * 3.18D0
C    Change from single to double precision
C    TEMPDP =TEMP
C    MOLEFRDP =MOLEFR
C    USERACDP =ABSR(LVALUE)
C
C
C    Soot emissivity calculation
C    AS =0.0D0
C    IF (KVALUE .LT. 7) THEN
C    PI = 3.141593D0
C    RUNIV = UNIVERSAL GAS CONSTANT
C    RUNIV = 0.08205D0
C    RSP = The radius of a soot particle
C    RSP = (50.D-9)/2.D0
C    VSP = The volume of a soot particle
C    VSP = (4.D0/3.D0)*PI*RSP**3
C    B = Multiplier to go from mole fract. of C to vol. fract. [FV]
of soot
    B = P*6.022045D23*VSP*1000.D0/(1.D6*RUNIV)

```

```

C
C IF(LVALUE.EQ. 1323) THEN
C   WRITE(*,*) 'TEMP=',TEMP,' T(LVALUE)=' ,T(LVALUE)
C   WRITE(*,*) 'TEMPDP=',TEMPDP,' TEMP=',TEMP
C   WRITE(*,*) 'USERACDP=',USERACDP,' ABSR(LVALUE)=' ,ABSR(LVALUE)
C END IF
C
C Calculate the soot volume fraction
C FV = MOLEFRDP(5) *B / TEMPDP
C
C Calculate the absorbtivity of soot alone {no gas}
C A1 = 1.447D0 -(7.943D-4)*TEMPDP + (7.977D-8)*TEMPDP**2
C A2 = 1.D0 - A1
C G1 = DEXP(13.70D0 + 1.001D0*DLOG(FV))
C G2 = DEXP(14.83D0 + 0.9951D0*DLOG(FV))
C AS = A1*(1.D0-DEXP(-G1*MBL)) + A2*(1.D0-DEXP(-G2*MBL))
C END IF
C
C Now calculate the absorbtivity of the gases alone (no soot)
C Convert from mole fraction to partial pressure
C PH2O = MOLEFRDP(4) * P
C PCO2 = MOLEFRDP(3) * P
C CALL GASRAD(1100.D0,TEMPDP,PH2O,PCO2,MBL,EG,AG,ABSGP)
C
C Now combine to find total absorbtivity of the gas and soot
C mixture
C AT = AS + AG -AS*AG
C
C Now calculate the absorption coef (USERAC)
C IF (AT .EQ. 1.0D0) THEN
C   USERACDP = 10.D0
C ELSE
C   USERACDP = (-DLOG(1.D0-AT))/MBL
C END IF
C USERAC = USERACDP
C
C Output
C WRITE(*,*) 'LVALUE=',LVALUE,' USERAC=',USERAC
C IF (IVALUE.EQ. 9 .AND. JVALUE.EQ.13) THEN
C   IF(KVALUE.GT.5 .AND. KVALUE.LT.18) THEN
C     WRITE(*,*) 'IVALUE=',IVALUE,' JVALUE=',JVALUE,' K=',KVALUE
C     WRITE(*,*) 'TEMPDP=',TEMPDP,' TEMP=',TEMP
C     WRITE(*,*) 'MOLEFR(C)=' ,MOLEFR(5)
C     WRITE(*,*) 'MOLEFR(4)=' ,MOLEFRDP(4) , ' MOLEFR(H2O)=' ,MOLEFR(4)
C     WRITE(*,*) 'MOLEFR(3)=' ,MOLEFRDP(3) , ' MOLEFR(CO2)=' ,MOLEFR(3)
C     WRITE(*,*) 'PH2O=' ,PH2O , ' PCO2=' ,PCO2
C     WRITE(*,*) 'FV',FV,' B',B,' VSP =' ,VSP
C     WRITE(*,*) 'A1',A1,' A2',A2,' G1',G1,' G2',G2
C     WRITE(*,*) 'AS',AS
C     WRITE(*,*) ' USERAC=' ,USERAC
C     WRITE(*,*) 'CURRENT T =' ,TEMP,' NEXT ITERATION'

```

```

C      ENDIF
C      ENDIF
C
C      RETURN
C      END
C *****
C      SUBROUTINE GASRAD(TSO, TG, PH2O, PCO2, L, SUMEM, SUMABS, ABSGP)
C
C      THIS SUBROUTINE CALCULATES THE TOTAL EMISSIVITY [SUMEM] AND
C      ABSORBTIVITY
C      [SUMABS] OF A MIXTURE OF CARBON DIOXIDE, WATER VAPOR AND A
C      NON-PARTICIPATING GAS (AIR). THE PARTIAL PRESSURES OF THE GASEOUS
C      CONSTITUENTS [PH2O & PCO2], THE TEMPERATURE OF THE GAS MIXTURE
C      [TG], AND
C      THE TEMPERATURE OF THE SOURCE OF THE RADIATION [TSO] ARE REQUIRED
C      INPUTS.
C
C
C
C      IMPLICIT REAL*8 (A-H, K, L, N, O-Z)
C      INTEGER V1, V2, V3
C      DIMENSION NUHH(10), NUHC(10), DELTAH1(10), DELTAH2(10),
C      $          DELTAH3(10), DELTAH3(10),
C      $          DELTAHC3(10), DELTAH4(10), DELTAH5(10),
C      $          DELTAC1(10), DELTAC2(10), DELTAC3(10), DELTAC4(10),
C      $          DELTAC5(10), DELTAC6(10), U(10), UO(10), TAUG(15),
C      $          BLKTRNS(25), NU(25), NUL(25), NUU(25), DELNU(15),
C      $          NULP(15), NUUP(15)
C
C      INPUT PARAMETERS
C
C      WRITE(*,*) 'TSO= ', TSO, '   TG= ', TG, '   L= ', L
C      WRITE(*,*) 'PH2O= ', PH2O, '   PCO2= ', PCO2
C      P = 84786.D0/101325.D0
C      PO = 1.D0
C      TO = 100.D0
C
C      HCDK = 1.4388D0
C
C      SPECIFY PARAMETERS FOR H2O
C
C      NUHH(1) = 3652.D0
C      NUHH(2) = 1595.D0
C      NUHH(3) = 3756.D0
C
C      DELTAH1(1) = 0
C      DELTAH1(2) = 0
C      DELTAH1(3) = 0
C      DELTAH2(1) = 0
C      DELTAH2(2) = 1
C      DELTAH2(3) = 0

```

```

DELTAHA3 (1) = 0
DELTAHA3 (2) = 2
DELTAHA3 (3) = 0
DELTAHB3 (1) = 1
DELTAHB3 (2) = 0
DELTAHB3 (3) = 0
DELTAHC3 (1) = 0
DELTAHC3 (2) = 0
DELTAHC3 (3) = 1
DELTAH4 (1) = 0
DELTAH4 (2) = 1
DELTAH4 (3) = 1
DELTAH5 (1) = 1
DELTAH5 (2) = 0
DELTAH5 (3) = 1
C
MH = 3
NH = 1
C
BH = 8.6D0*(T0/TG)**0.5D0 + 0.5D0
C
A0H1 = 5200.D0
A0H2 = 41.2D0
A03HA = 0.19D0
A03HB = 2.3D0
A03HC = 22.4D0
A0H4 = 3.0D0
A0H5 = 2.5D0
C
B0H1 = 0.14311D0
B0H2 = 0.09427D0
B0H3 = 0.13219D0
B0H4 = 0.08169D0
B0H5 = 0.11628D0
C
W0H1 = 28.4D0
W0H2 = 56.4D0
W0H3 = 60.D0
W0H4 = 43.1D0
W0H5 = 32.D0
C
C C02 PARAMETERS
C
NUHC(1) = 1351.D0
NUHC(2) = 667.D0
NUHC(3) = 2396.D0
C
DELTAC1(1) = 0
DELTAC1(2) = 1
DELTAC1(3) = 0
DELTAC2(1) = -1

```


DELTAC2 (2) = 0
 DELTAC2 (3) = 1
 DELTAC3 (1) = 0
 DELTAC3 (2) = -2
 DELTAC3 (3) = 1
 DELTAC4 (1) = 0
 DELTAC4 (2) = 0
 DELTAC4 (3) = 1
 DELTAC5 (1) = 1
 DELTAC5 (2) = 0
 DELTAC5 (3) = 1
 DELTAC6 (1) = 2
 DELTAC6 (2) = 0
 DELTAC6 (3) = 1

C
C

MC = 3
 NC1 = 0.7D0
 NC2 = 0.8D0
 NC3 = 0.8D0
 NC4 = 0.8D0
 NC5 = 0.65D0
 NC6 = 0.65D0

C

BC = 1.3D0

C

AOC1 = 19.D0
 AOC2 = 2.47D-9
 AOC3 = 2.48D-9
 AOC4 = 110.D0
 AOC5 = 4.0D0
 AOC6 = 0.066D0

C

BOC1 = 0.06157D0
 BOC2 = 0.04017D0
 BOC3 = 0.11888D0
 BOC4 = 0.24723D0
 BOC5 = 0.13341D0
 BOC6 = 0.39305D0

C

WOC1 = 12.7D0
 WOC2 = 13.4D0
 WOC3 = 10.1D0
 WOC4 = 11.2D0
 WOC5 = 23.5D0
 WOC6 = 34.5D0

C

C

H2O CALCULATIONS

C

U(1) = HCDK*NUHH(1)/TG
 U(2) = HCDK*NUHH(2)/TG

```

      U(3) = HCDK*NUHH(3)/TG
C
      U0(1) = HCDK*NUHH(1)/T0
      U0(2) = HCDK*NUHH(2)/T0
      U0(3) = HCDK*NUHH(3)/T0
C
C ROTATIONAL BAND
      ALH1 = A0H1
C      WRITE(*,*) 'ALH1',ALH1
C
C 6.3 BAND
      PSITG = 1.D0/(1.D0 - DEXP(-U(2)))
      PSIT0 = 1.D0/(1.D0 - DEXP(-U0(2)))
      ALH2 = ALPHA(DELTAH2,U,U0,A0H2,MH,PSITG,PSIT0)
C      WRITE(*,*) 'ALH2',ALH2
C
C 2.7 (A) BAND
      PSITG = 2.D0/(1.D0 - DEXP(-U(2)))**2.D0
      PSIT0 = 2.D0/(1.D0 - DEXP(-U0(2)))**2.D0
      ALH3A = ALPHA(DELTAH3,U,U0,A03HA,MH,PSITG,PSIT0)
C      WRITE(*,*) 'ALH3A',ALH3A
C
C 2.7 (B) BAND
      PSITG = 1.D0/(1.D0 - DEXP(-U(1)))
      PSIT0 = 1.D0/(1.D0 - DEXP(-U0(1)))
      ALH3B = ALPHA(DELTAH3,U,U0,A03HB,MH,PSITG,PSIT0)
C      WRITE(*,*) 'ALH3B',ALH3B
C
C 2.7 (C) BAND
      PSITG = 1.D0/(1.D0 - DEXP(-U(3)))
      PSIT0 = 1.D0/(1.D0 - DEXP(-U0(3)))
      ALH3C = ALPHA(DELTAH3,U,U0,A03HC,MH,PSITG,PSIT0)
C      WRITE(*,*) 'ALH3C',ALH3C
C
C 2.7 BAND
      ALH3 = ALH3A + ALH3B + ALH3C
C      WRITE(*,*) 'ALH3',ALH3
C
C 1.87 BAND
      PSITG = 1.D0/((1.D0 - DEXP(-U(2)))*(1.D0 - DEXP(-U(3))))
      PSIT0 = 1.D0/((1.D0 - DEXP(-U0(2)))*(1.D0 - DEXP(-U0(3))))
      ALH4 = ALPHA(DELTAH4,U,U0,A0H4,MH,PSITG,PSIT0)
C      WRITE(*,*) 'ALH4',ALH4
C
C 1.38 BAND
      PSITG = 1.D0/((1.D0 - DEXP(-U(1)))*(1.D0 - DEXP(-U(3))))
      PSIT0 = 1.D0/((1.D0 - DEXP(-U0(1)))*(1.D0 - DEXP(-U0(3))))
      ALH5 = ALPHA(DELTAH5,U,U0,A0H5,MH,PSITG,PSIT0)
C      WRITE(*,*) 'ALH5',ALH5
C

```

```

C
C H2O ROTATIONAL BAND
C
      BETAH1 = BOH1*(TG/T0)**(-.5D0)
C
C 6.3 BAND
      TERM1 = 0.D0
      ERR = 1.D0
      V2 = 0
      DO WHILE(ERR.GT.1.D-9)
          TERM = (V2+1)**.5D0*DEXP(-U(2)*V2/2.D0)
          TERM1 = TERM1 + TERM
          ERR = DABS(TERM/TERM1)
          V2 = V2 + 1
      END DO
      PHITG = (1.D0/(1.D0 - DEXP(-U(1)/2.D0)))**2.D0*TERM1**2.D0*
$          (1.D0/(1.D0 - DEXP(-U(3)/2.D0)))**2.D0*
$          (1.D0-DEXP(-U(1)))*(1.D0 - DEXP(-U(2)))**2.D0*
$          (1.D0 - DEXP(-U(3)))
C      WRITE(*,*) 'PHITGH2', PHITG
      TERM1 = 0.D0
      ERR = 1.D0
      V2 = 0
      DO WHILE(ERR.GT.1.D-9)
          TERM = (V2+1)**.5D0*DEXP(-U(2)*V2/2.D0)
          TERM1 = TERM1 + TERM
          ERR = DABS(TERM/TERM1)
          V2 = V2 + 1
      END DO
      PHIT0 = (1.D0/(1.D0 - DEXP(-U(1)/2.D0)))**2.D0*TERM1**2.D0*
$          (1.D0/(1.D0 - DEXP(-U(3)/2.D0)))**2.D0*
$          (1.D0-DEXP(-U(1)))*(1.D0 - DEXP(-U(2)))**2.D0*
$          (1.D0 - DEXP(-U(3)))
C      WRITE(*,*) 'PHIT0H2', PHITG
      BETAH2 = BOH2*(TG/T0)**(-.5D0)*PHITG/PHIT0
C
C 2.7 (A) BAND
      TERM1 = 0.D0
      ERR = 1.D0
      V2 = 0
      DO WHILE(ERR.GT.1.D-9)
          TERM = (V2+1)**.5D0*(V2+2)**.5D0*DEXP(-U(2)*V2/2.D0)
          TERM1 = TERM1 + TERM
          ERR = DABS(TERM/TERM1)
          V2 = V2 + 1
      END DO
      PHITG = 0.5D0*(1.D0/(1.D0-DEXP(-U(1)/2.D0)))**2.D0
$          *TERM1**2.D0*
$          (1.D0/(1.D0-DEXP(-U(3)/2.D0)))**2.D0
$          *(1.D0-DEXP(-U(1)))*
$          (1.D0-DEXP(-U(2)))**3.D0*(1.D0-DEXP(-U(3)))

```

```

C          WRITE(*,*) 'PHITGH3A', PHITG
          TERM1 = 0.D0
          ERR = 1.D0
          V2 = 0
          DO WHILE (ERR.GT.1.D-9)
              TERM = (V2+1)**.5D0*(V2+2)**.5D0*
$              DEXP(-U0(2)*V2/2.D0)
          TERM1 = TERM1 + TERM
          ERR = DABS(TERM/TERM1)
          V2 = V2 + 1
          END DO
          PHIT0 = 0.5D0*(1.D0/(1.D0-DEXP(-U0(1)/2.D0)))**2.D0
$          *TERM1**2.D0*
$          (1.D0/(1.D0-DEXP(-U0(3)/2.D0)))**2.D0
$          *(1.D0-DEXP(-U0(1))) *
$          (1.D0-DEXP(-U0(2)))**3.D0*(1.D0-DEXP(-U0(3)))
C          WRITE(*,*) 'PHIT0H3A', PHIT0
          BETAH3A = BOH3*(TG/T0)**(-.5D0)*PHITG/PHIT0
C
C 2.7 (B) BAND
          TERM1 = 0.D0
          ERR = 1.D0
          V1 = 0
          DO WHILE (ERR.GT.1.D-9)
              TERM = (V1+1)**.5D0*DEXP(-U(1)*V1/2.D0)
              TERM1 = TERM1 + TERM
              ERR = DABS(TERM/TERM1)
              V1 = V1 + 1
          END DO
          PHITG = TERM1**2.D0*(1.D0/(1.D0-DEXP(-U(2)/2.D0)))**2.D0)*
$          (1.D0/(1.D0-DEXP(-U(3)/2.D0)))**2.D0)*
$          (1.D0-DEXP(-U(1)))**2.D0*(1.D0-DEXP(-U(2))) *
$          (1.D0-DEXP(-U(3)))
C          WRITE(*,*) 'PHITGH3B', PHITG
          TERM1 = 0.D0
          ERR = 1.D0
          V1 = 0
          DO WHILE (ERR.GT.1.D-9)
              TERM = (V1+1)**.5D0*DEXP(-U0(1)*V1/2.D0)
              TERM1 = TERM1 + TERM
              ERR = DABS(TERM/TERM1)
              V1 = V1 + 1
          END DO
          PHIT0 = TERM1**2.D0*(1.D0/(1.D0-DEXP(-U0(2)/2.D0)))**2.D0)*
$          (1.D0/(1.D0-DEXP(-U0(3)/2.D0)))**2.D0)*
$          (1.D0-DEXP(-U0(1)))**2.D0*(1.D0-DEXP(-U0(2))) *
$          (1.D0-DEXP(-U0(3)))
C          WRITE(*,*) 'PHIT0H3B', PHIT0
          BETAH3B = BOH3*(TG/T0)**(-.5D0)*PHITG/PHIT0
C
C 2.7 (C) BAND

```

```

TERM1 = 0.D0
ERR = 1.D0
V3 = 0
DO WHILE (ERR.GT.1.D-9)
    TERM = (V3+1)**.5D0*DEXP(-U(3)*V3/2.D0)
    TERM1 = TERM1 + TERM
    ERR = DABS(TERM/TERM1)
    V3 = V3 + 1
END DO
PHITG = (1.D0/(1.D0-DEXP(-U(1)/2.D0)))**2.D0*
$ (1.D0/(1.D0-DEXP(-U(2)/2.D0)))**2.D0*TERM1**2.D0*
$ (1.D0-DEXP(-U(1)))*(1.D0-DEXP(-U(2)))*
$ (1.D0-DEXP(-U(3)))**2.D0
C WRITE(*,*) 'PHITGH3C',PHITG
TERM1 = 0.D0
ERR = 1.D0
V3 = 0
DO WHILE (ERR.GT.1.D-9)
    TERM = (V3+1)**.5D0*DEXP(-U0(3)*V3/2.D0)
    TERM1 = TERM1 + TERM
    ERR = DABS(TERM/TERM1)
    V3 = V3 + 1
END DO
PHIT0 = (1.D0/(1.D0-DEXP(-U0(1)/2.D0)))**2.D0*
$ (1.D0/(1.D0-DEXP(-U0(2)/2.D0)))**2.D0*TERM1**2.D0*
$ (1.D0-DEXP(-U0(1)))*(1.D0-DEXP(-U0(2)))*
$ (1.D0-DEXP(-U0(3)))**2.D0
C WRITE(*,*) 'PHIT0H3C',PHIT0
BETAH3C = B0H3*(TG/T0)**(-.5D0)*PHITG/PHIT0
C
C 2.7 BAND
BETAH3 = (((ALH3A*BETAH3A)**.5D0 + (ALH3B*BETAH3B)**.5D0
$ + (ALH3C*BETAH3C)**.5D0)**2.D0)/ALH3
C
C 1.87 BAND
TERM1 = 0.D0
ERR = 1.D0
V2 = 0
DO WHILE (ERR.GT.1.D-9)
    TERM = (V2+1)**.5D0*DEXP(-U(2)*V2/2.D0)
    TERM1 = TERM1 + TERM
    ERR = DABS(TERM/TERM1)
    V2 = V2 + 1
END DO
TERM2 = 0.0D0
ERR = 1.D0
V3 = 0.D0
DO WHILE (ERR.GT.1.D-9)
    TERM = (V3+1)**.5D0*DEXP(-U(3)*V3/2.D0)
    TERM2 = TERM2 + TERM
    ERR = DABS(TERM/TERM2)

```

```

      V3 = V3 + 1
    END DO
    PHITG = (1.D0/(1.D0-DEXP(-U(1)/2.D0)))**2.D0*TERM1**2.D0*
$      TERM2**2.D0*(1.D0-DEXP(-U(1)))*(1.D0-DEXP(-U(2)))
$      **2.D0*
$      (1.D0-DEXP(-U(3)))**2.D0
C    WRITE(*,*) 'PHITGH4',PHITG
    TERM1 = 0.D0
    ERR = 1.D0
    V2 = 0
    DO WHILE(ERR.GT.1.D-9)
      TERM = (V2+1)**.5D0*DEXP(-U0(2)*V2/2.D0)
      TERM1 = TERM1 + TERM
      ERR = DABS(TERM/TERM1)
      V2 = V2 + 1
    END DO
    TERM2 = 0.0D0
    ERR = 1.D0
    V3 = 0.D0
    DO WHILE(ERR.GT.1.D-9)
      TERM = (V3+1)**.5D0*DEXP(-U0(3)*V3/2.D0)
      TERM2 = TERM2 + TERM
      ERR = DABS(TERM/TERM2)
      V3 = V3 + 1
    END DO
    PHIT0 = (1.D0/(1.D0-DEXP(-U0(1)/2.D0)))**2.D0*TERM1**2.D0*
$      TERM2**2.D0*(1.D0-DEXP(-U0(1)))*(1.D0-DEXP(-U0(2)))
$      **2.D0*
$      (1.D0-DEXP(-U0(3)))**2.D0
C    WRITE(*,*) 'PHIT0H4',PHITG
    BETAH4 = B0H4*(TG/T0)**(-.5D0)*PHITG/PHIT0
C
C 1.38 BAND
    TERM1 = 0.D0
    ERR = 1.D0
    V1 = 0
    DO WHILE(ERR.GT.1.D-9)
      TERM = (V1+1)**.5D0*DEXP(-U(1)*V1/2.D0)
      TERM1 = TERM1 + TERM
      ERR = DABS(TERM/TERM1)
      V1 = V1 + 1
    END DO
    TERM2 = 0.0D0
    ERR = 1.D0
    V3 = 0.D0
    DO WHILE(ERR.GT.1.D-9)
      TERM = (V3+1)**.5D0*DEXP(-U(3)*V3/2.D0)
      TERM2 = TERM2 + TERM
      ERR = DABS(TERM/TERM2)
      V3 = V3 + 1
    END DO

```

```

      PHITG = TERM1**2.D0*(1.D0/(1.D0-DEXP(-U(2)/2.D0)))**2.D0*
$          TERM2**2.D0*(1.D0-DEXP(-U(1)))**2.D0*
$          (1.D0-DEXP(-U(2)))*
$          (1.D0-DEXP(-U(3)))**2.D0
C      WRITE(*,*) 'PHITGH5',PHITG
      TERM1 = 0.D0
      ERR = 1.D0
      V1 = 0
      DO WHILE(ERR.GT.1.D-9)
          TERM = (V1+1)**.5D0*DEXP(-U0(1)*V1/2.D0)
          TERM1 = TERM1 + TERM
          ERR = DABS(TERM/TERM1)
          V1 = V1 + 1
      END DO
      TERM2 = 0.0D0
      ERR = 1.D0
      V3 = 0.D0
      DO WHILE(ERR.GT.1.D-9)
          TERM = (V3+1)**.5D0*DEXP(-U0(3)*V3/2.D0)
          TERM2 = TERM2 + TERM
          ERR = DABS(TERM/TERM2)
          V3 = V3 + 1
      END DO
      PHIT0 = TERM1**2.D0*(1.D0/(1.D0-DEXP(-U0(2)/2.D0)))**2.D0*
$          TERM2**2.D0*(1.D0-DEXP(-U0(1)))**2.D0
$          *(1.D0-DEXP(-U0(2)))*
$          (1.D0-DEXP(-U0(3)))**2.D0
C      WRITE(*,*) 'PHIT0H5',PHITG
      BETAH5 = BOH5*(TG/T0)**(-.5D0)*PHITG/PHIT0
C
C      WRITE(*,*) 'BETAH5',BETAH1,BETAH2,BETAH3,BETAH4,BETAH5
C
      RH = 4.5545D-6
      RHOH = PH2O/(RH*TG)
      X = RHOH*L
      WH1 = WOH1*(TG/T0)**.5D0
      WH2 = WOH2*(TG/T0)**.5D0
      WH3 = WOH3*(TG/T0)**.5D0
      WH4 = WOH4*(TG/T0)**.5D0
      WH5 = WOH5*(TG/T0)**.5D0
C
      TAUH1 = ALH1*X/WH1
      TAUH2 = ALH2*X/WH2
      TAUH3 = ALH3*X/WH3
      TAUH4 = ALH4*X/WH4
      TAUH5 = ALH5*X/WH5
C      WRITE(*,*) 'TAUHS',TAUH1,TAUH2,TAUH3,TAUH4,TAUH5
C
      PEH = ((P/P0)*(1.D0 + (BH - 1.D0)*(PH2O/P)))**NH
      ETAH1 = BETAH1*PEH
      ETAH2 = BETAH2*PEH

```

```

ETAH3 = BETAH3*PEH
ETAH4 = BETAH4*PEH
ETAH5 = BETAH5*PEH
C WRITE(*,*) 'ETAHS',ETAH1,ETAH2,ETAH3,ETAH4,ETAH5
C
IF (TAUH1.LE.1.D0.AND.TAUH1.LE.ETAH1) THEN
    ASTH1 = TAUH1
    AH1 = ASTH1*WH1
    TAUG(1) = TAUH1/ASTH1
ELSE IF (TAUH1.GE.ETAH1.AND.TAUH1.LE.(1.D0/ETAH1)) THEN
    ASTH1 = (4.D0*ETAH1*TAUH1)**.5D0 - ETAH1
    AH1 = ASTH1*WH1
    TAUG(1) = (ETAH1*TAUH1)**.5D0/ASTH1
ELSE IF (TAUH1.GT.(1.D0/ETAH1).AND.ETAH1.LE.1.D0) THEN
    ASTH1 = DLOG(TAUH1*ETAH1) + 2.D0 - ETAH1
    AH1 = ASTH1*WH1
    TAUG(1) = 1.D0/ASTH1
ELSE
    ASTH1 = DLOG(TAUH1) + 1.D0
    AH1 = ASTH1*WH1
    TAUG(1) = 1.D0/ASTH1
ENDIF
IF (TAUG(1).GT.0.9D0) THEN
    TAUG(1) = 0.9D0
ENDIF
DELNU(1) = AH1/(1.D0 - TAUG(1))
C WRITE(*,*) 'AH1',AH1,'TAUG(1)',TAUG(1),'DELNU(1)',DELNU(1)
C
IF (TAUH2.LE.1.D0.AND.TAUH2.LE.ETAH2) THEN
    ASTH2 = TAUH2
    AH2 = ASTH2*WH2
    TAUG(2) = TAUH2/ASTH2
ELSE IF (TAUH2.GE.ETAH2.AND.TAUH2.LE.(1.D0/ETAH2)) THEN
    ASTH2 = (4.D0*ETAH2*TAUH2)**.5D0 - ETAH2
    AH2 = ASTH2*WH2
    TAUG(2) = (ETAH2*TAUH2)**.5D0/ASTH2
ELSE IF (TAUH2.GT.(1.D0/ETAH2).AND.ETAH2.LE.1.D0) THEN
    ASTH2 = DLOG(TAUH2*ETAH2) + 2.D0 - ETAH2
    AH2 = ASTH2*WH2
    TAUG(2) = 1.D0/ASTH2
ELSE
    ASTH2 = DLOG(TAUH2) + 1.D0
    AH2 = ASTH2*WH2
    TAUG(2) = 1.D0/ASTH2
ENDIF
IF (TAUG(2).GT.0.9D0) THEN
    TAUG(2) = 0.9D0
ENDIF
C DELNU(2) = AH2/(1.D0 - TAUG(2))
C WRITE(*,*) 'AH2',AH2,'TAUG(2)',TAUG(2),'DELNU(2)',DELNU(2)

```



```

C
IF (TAUH3.LE.1.D0.AND.TAUH3.LE.ETAH3) THEN
    ASTH3 = TAUH3
    AH3 = ASTH3*WH3
    TAUG(3) = TAUH3/ASTH3
ELSE IF (TAUH3.GE.ETAH3.AND.TAUH3.LE.(1.D0/ETAH3)) THEN
    ASTH3 = (4.D0*ETAH3*TAUH3)**.5D0 - ETAH3
    AH3 = ASTH3*WH3
    TAUG(3) = (ETAH3*TAUH3)**.5D0/ASTH3
ELSE IF (TAUH3.GT.(1.D0/ETAH3).AND.ETAH3.LE.1.D0) THEN
    ASTH3 = DLOG(TAUH3*ETAH3) + 2.D0 - ETAH3
    AH3 = ASTH3*WH3
    TAUG(3) = 1.D0/ASTH3
ELSE
    ASTH3 = DLOG(TAUH3) + 1.D0
    AH3 = ASTH3*WH3
    TAUG(3) = 1.D0/ASTH3
ENDIF
IF (TAUG(3).GT.0.9D0) THEN
    TAUG(3) = 0.9D0
ENDIF

C
DELNU(3) = AH3/(1.D0 - TAUG(3))
C
WRITE(*,*) 'AH3',AH3,'TAUG(3)',TAUG(3),'DELNU(3)',DELNU(3)
C

IF (TAUH4.LE.1.D0.AND.TAUH4.LE.ETAH4) THEN
    ASTH4 = TAUH4
    AH4 = ASTH4*WH4
    TAUG(4) = TAUH4/ASTH4
ELSE IF (TAUH4.GE.ETAH4.AND.TAUH4.LE.(1.D0/ETAH4)) THEN
    ASTH4 = (4.D0*ETAH4*TAUH4)**.5D0 - ETAH4
    AH4 = ASTH4*WH4
    TAUG(4) = (ETAH4*TAUH4)**.5D0/ASTH4
ELSE IF (TAUH4.GT.(1.D0/ETAH4).AND.ETAH4.LE.1.D0) THEN
    ASTH4 = DLOG(TAUH4*ETAH4) + 2.D0 - ETAH4
    AH4 = ASTH4*WH4
    TAUG(4) = 1.D0/ASTH4
ELSE
    ASTH4 = DLOG(TAUH4) + 1.D0
    AH4 = ASTH4*WH4
    TAUG(4) = 1.D0/ASTH4
ENDIF
IF (TAUG(4).GT.0.9D0) THEN
    TAUG(4) = 0.9D0
ENDIF

C
DELNU(4) = AH4/(1.D0 - TAUG(4))
C
WRITE(*,*) 'AH4',AH4,'TAUG(4)',TAUG(4),'DELNU(4)',DELNU(4)
C

IF (TAUH5.LE.1.D0.AND.TAUH5.LE.ETAH5) THEN
    ASTH5 = TAUH5

```

```

      AH5 = ASTH5*WH5
      TAUG(5) = TAUH5/ASTH5
ELSE IF (TAUH5.GE.ETAH5.AND.TAUH5.LE.(1.D0/ETAH5)) THEN
      ASTH5 = (4.D0*ETAH5*TAUH5)**.5D0 - ETAH5
      AH5 = ASTH5*WH5
      TAUG(5) = (ETAH5*TAUH5)**.5D0/ASTH5
ELSE IF (TAUH5.GT.(1.D0/ETAH5).AND.ETAH5.LE.1.D0) THEN
      ASTH5 = DLOG(TAUH5*ETAH5) + 2.D0 - ETAH5
      AH5 = ASTH5*WH5
      TAUG(5) = 1.D0/ASTH5
ELSE
      ASTH5 = DLOG(TAUH5) + 1.D0
      AH5 = ASTH5*WH5
      TAUG(5) = 1.D0/ASTH5
ENDIF
IF (TAUG(5).GT.0.9D0) THEN
      TAUG(5) = 0.9D0
ENDIF
C
      DELNU(5) = AH5/(1.D0 - TAUG(5))
C      WRITE(*,*) 'AH5',AH5, 'TAUG(5)',TAUG(5), 'DELNU(5)',DELNU(5)
C
C      CO2 CALCULATIONS
C
      U(1) = HCDK*NUHC(1)/TG
      U(2) = HCDK*NUHC(2)/TG
      U(3) = HCDK*NUHC(3)/TG
C
      U0(1) = HCDK*NUHC(1)/T0
      U0(2) = HCDK*NUHC(2)/T0
      U0(3) = HCDK*NUHC(3)/T0
C
C      15 BAND
      PSITG = 2.D0/(1.D0 - DEXP(-U(2)))
      PSIT0 = 2.D0/(1.D0 - DEXP(-U0(2)))
      ALC1 = ALPHA(DEL/TAC1,U,U0,A0C1,MC,PSITG,PSIT0)
C      WRITE(*,*) 'ALC1',ALC1
C
C      10.4 BAND
      PSITG = (1.D0-DEXP(-U(1)))*(1.D0/(1.D0-DEXP(-U(1))))**2.D0
      $      - 1.D0)/(1.D0 - DEXP(-U(3)))
      PSIT0 = (1.D0-DEXP(-U0(1)))*(1.D0/(1.D0-DEXP(-U0(1))))**2.D0
      $      - 1.D0)/(1.D0 - DEXP(-U0(3)))
      ALC2 = ALPHA(DEL/TAC2,U,U0,A0C2,MC,PSITG,PSIT0)
C      WRITE(*,*) 'ALC2',ALC2
C
C      9.4 BAND
      ALC3 = ALPHA(DEL/TAC3,U,U0,A0C3,MC,PSITG,PSIT0)
C      WRITE(*,*) 'ALC3',ALC3
C

```

```

C 4.3 BAND
  PSITG = 1.D0/(1.D0 - DEXP(-U(3)))
  PSIT0 = 1.D0/(1.D0 - DEXP(-U0(3)))
  ALC4 = ALPHA(DELTA4,U,U0,A0C4,MC,PSITG,PSIT0)
C
C
C 2.7 BAND
  PSITG = 1.D0/((1.D0 - DEXP(-U(1)))*(1.D0 - DEXP(-U(3))))
  PSIT0 = 1.D0/((1.D0 - DEXP(-U0(1)))*(1.D0 - DEXP(-U0(3))))
  ALC5 = ALPHA(DELTA5,U,U0,A0C5,MC,PSITG,PSIT0)
C
C
C 2.0 BAND
  PSITG = 2.D0/((1.D0 - DEXP(-U(1)))**2.D0*(1.D0 - DEXP(-U(3))))
  PSIT0 = 2.D0/((1.D0 - DEXP(-U0(1)))**2.D0*
$      (1.D0 - DEXP(-U0(3))))
  ALC6 = ALPHA(DELTA6,U,U0,A0C6,MC,PSITG,PSIT0)
C
C
C
C 15 BAND
  TERM1 = 0.D0
  ERR = 1.D0
  V1 = 0
  DO WHILE(ERR.GT.1.D-9)
    TERM = (V1+1)**.5D0*DEXP(-U(1)*V1/2.D0)
    TERM1 = TERM1 + TERM
    ERR = DABS(TERM/TERM1)
    V1 = V1 + 1
  END DO
  TERM2 = 0.D0
  ERR = 1.D0
  V2 = 0.D0
  DO WHILE(ERR.GT.1.D-9)
    TERM = (V2+1)**.5D0*(V2+2)**.5D0*DEXP(-U(2)*V2/2.D0)
    TERM2 = TERM2 + TERM
    ERR = DABS(TERM/TERM2)
    V2 = V2 + 1
  END DO
  PHITG = 0.5D0*TERM1**2.D0*TERM2**2.D0*
$      (1.D0/(1.D0-DEXP(-U(3)/2.D0)))**2.D0*
$      (1.D0-DEXP(-U(1)))**2.D0*(1.D0-DEXP(-U(2)))**3.D0*
$      (1.D0-DEXP(-U(3)))
C      WRITE(*,*) 'PHITG1',PHITG
  TERM1 = 0.D0
  ERR = 1.D0
  V1 = 0
  DO WHILE(ERR.GT.1.D-9)
    TERM = (V1+1)**.5D0*DEXP(-U0(1)*V1/2.D0)
    TERM1 = TERM1 + TERM
    ERR = DABS(TERM/TERM1)

```

```

        V1 = V1 + 1
    END DO
    TERM2 = 0.0D0
    ERR = 1.D0
    V2 = 0.D0
    DO WHILE(ERR.GT.1.D-9)
        TERM = (V2+1)**.5D0*(V2+2)**.5D0*
$           DEXP(-U0(2)*V2/2.D0)
        TERM2 = TERM2 + TERM
        ERR = DABS(TERM/TERM2)
        V2 = V2 + 1
    END DO
    PHIT0 = 0.5D0*TERM1**2.D0*TERM2**2.D0*
$           (1.D0/(1.D0-DEXP(-U0(3)/2.D0)))**2.D0*
$           (1.D0-DEXP(-U0(1)))**2.D0*(1.D0-DEXP(-
U0(2)))**3.D0*
$           (1.D0-DEXP(-U0(3)))
C       WRITE(*,*) 'PHITOC1', PHIT0
C       BETAC1 = BOC1*(TG/T0)**(-.5D0)*PHITG/PHIT0
C
C 10.4 BAND
    TERM1 = 0.D0
    ERR = 1.D0
    V1 = 1
    DO WHILE(ERR.GT.1.D-11)
        TERM = (V1+1)**.5D0*DEXP(-U(1)*V1/2.D0)
        TERM1 = TERM1 + TERM
        ERR = DABS(TERM/TERM1)
        V1 = V1 + 1
    END DO
    TERM2 = 0.0D0
    ERR = 1.D0
    V2 = 0.D0
    DO WHILE(ERR.GT.1.D-11)
        TERM = (V2+1)**.5D0*DEXP(-U(2)*V2/2.D0)
        TERM2 = TERM2 + TERM
        ERR = DABS(TERM/TERM2)
        V2 = V2 + 1
    END DO
    TERM3 = 0.0D0
    ERR = 1.D0
    V3 = 0.D0
    DO WHILE(ERR.GT.1.D-11)
        TERM = (V3+1)**.5D0*DEXP(-U(3)*V3/2.D0)
        TERM3 = TERM3 + TERM
        ERR = DABS(TERM/TERM3)
        V3 = V3 + 1
    END DO
    PHITG = TERM1**2.D0*TERM2**2.D0*TERM3**2.D0*
$           (1.D0-DEXP(-U(2)))**2.D0*
$           (1.D0-DEXP(-U(3)))**2.D0/

```

```

$          (1.D0/(1.D0-DEXP(-U(1)))**2.D0 - 1.D0)
C          WRITE(*,*) 'PHITGC2',PHITG
          TERM1 = 0.D0
          ERR = 1.D0
          V1 = 1
          DO WHILE(ERR.GT.1.D-11)
              TERM = (V1+1)**.5D0*DEXP(-U0(1)*V1/2.D0)
              TERM1 = TERM1 + TERM
              ERR = DABS(TERM/TERM1)
              V1 = V1 + 1
          END DO
          TERM2 = 0.0D0
          ERR = 1.D0
          V2 = 0.D0
          DO WHILE(ERR.GT.1.D-11)
              TERM = (V2+1)**.5D0*DEXP(-U0(2)*V2/2.D0)
              TERM2 = TERM2 + TERM
              ERR = DABS(TERM/TERM2)
              V2 = V2 + 1
          END DO
          TERM3 = 0.0D0
          ERR = 1.D0
          V3 = 0.D0
          DO WHILE(ERR.GT.1.D-11)
              TERM = (V3+1)**.5D0*DEXP(-U0(3)*V3/2.D0)
              TERM3 = TERM3 + TERM
              ERR = DABS(TERM/TERM3)
              V3 = V3 + 1
          END DO
          PHIT0 = TERM1**2.D0*TERM2**2.D0*TERM3**2.D0*
$          (1.D0-DEXP(-U0(2)))**2.D0*
$          (1.D0-DEXP(-U0(3)))**2.D0/
$          (1.D0/(1.D0-DEXP(-U0(1)))**2.D0 - 1.D0)
C          WRITE(*,*) 'PHITOC2',PHIT0
          BEIAC2 = BOC2*(TG/T0)**(-.5D0)*PHITG/PHIT0
C
C 9.4 BAND
          BEIAC3 = BOC3*(TG/T0)**(-.5D0)*PHITG/PHIT0
C
C 4.3 BAND
          TERM1 = 0.D0
          ERR = 1.D0
          V2 = 0
          DO WHILE(ERR.GT.1.D-9)
              TERM = (V2+1)**.5D0*DEXP(-U(2)*V2/2.D0)
              TERM1 = TERM1 + TERM
              ERR = DABS(TERM/TERM1)
              V2 = V2 + 2
          END DO
          TERM2 = 0.0D0
          ERR = 1.D0

```

```

V3 = 0.D0
DO WHILE(ERR.GT.1.D-9)
    TERM = (V3+1)**.5D0*DEXP(-U(3)*V3/2.D0)
    TERM2 = TERM2 + TERM
    ERR = DABS(TERM/TERM2)
    V3 = V3 + 1
END DO
PHITG = (1.D0-DEXP(-U(1)))*(1.D0-DEXP(-U(2)))*
$      (1.D0-DEXP(-U(3)))**2.D0/(1.D0-DEXP(-
U(1)/2.D0))**2.D0
$      *TERM1**2.D0*TERM2**2.D0
C      WRITE(*,*) 'PHITGC4', PHITG
    TERM1 = 0.D0
    ERR = 1.D0
    V2 = 0
    DO WHILE(ERR.GT.1.D-9)
        TERM = (V2+1)**.5D0*DEXP(-U(2)*V2/2.D0)
        TERM1 = TERM1 + TERM
        ERR = DABS(TERM/TERM1)
        V2 = V2 + 2
    END DO
    TERM2 = 0.0D0
    ERR = 1.D0
    V3 = 0.D0
    DO WHILE(ERR.GT.1.D-9)
        TERM = (V3+1)**.5D0*DEXP(-U(3)*V3/2.D0)
        TERM2 = TERM2 + TERM
        ERR = DABS(TERM/TERM2)
        V3 = V3 + 1
    END DO
    PHIT0 = (1.D0-DEXP(-U(1)))*(1.D0-DEXP(-U(2)))*
$      (1.D0-DEXP(-U(3)))**2.D0/(1.D0-DEXP(-
U(1)/2.D0))**2.D0
$      *TERM1**2.D0*TERM2**2.D0
C      WRITE(*,*) 'PHIT0C4', PHIT0
    BETAC4 = BOC4*(TG/T0)**(-.5D0)*PHITG/PHIT0
C
C 2.7 BAND
    TERM1 = 0.D0
    ERR = 1.D0
    V1 = 0
    DO WHILE(ERR.GT.1.D-9)
        TERM = (V1+1)**.5D0*DEXP(-U(1)*V1/2.D0)
        TERM1 = TERM1 + TERM
        ERR = DABS(TERM/TERM1)
        V1 = V1 + 1
    END DO
    TERM2 = 0.0D0
    ERR = 1.D0
    V2 = 0.D0
    DO WHILE(ERR.GT.1.D-9)

```

```

        TERM = (V2+1)**.5D0*DEXP(-U(2)*V2/2.D0)
        TERM2 = TERM2 + TERM
        ERR = DABS(TERM/TERM2)
        V2 = V2 + 1
    END DO
    TERM3 = 0.0D0
    ERR = 1.D0
    V3 = 0.D0
    DO WHILE(ERR.GT.1.D-9)
        TERM = (V3+1)**.5D0*DEXP(-U(3)*V3/2.D0)
        TERM3 = TERM3 + TERM
        ERR = DABS(TERM/TERM3)
        V3 = V3 + 1
    END DO
    PHITG = TERM1**2.D0*TERM2**2.D0*TERM3**2.D0*
$      (1.D0-DEXP(-U(1)))**2.D0*
$      (1.D0-DEXP(-U(2)))**2.D0*
$      (1.D0-DEXP(-U(3)))**2.D0
C      WRITE(*,*) 'PHITGC5',PHITG
    TERM1 = 0.D0
    ERR = 1.D0
    V1 = 0
    DO WHILE(ERR.GT.1.D-9)
        TERM = (V1+1)**.5D0*DEXP(-U0(1)*V1/2.D0)
        TERM1 = TERM1 + TERM
        ERR = DABS(TERM/TERM1)
        V1 = V1 + 1
    END DO
    TERM2 = 0.0D0
    ERR = 1.D0
    V2 = 0.D0
    DO WHILE(ERR.GT.1.D-9)
        TERM = (V2+1)**.5D0*DEXP(-U0(2)*V2/2.D0)
        TERM2 = TERM2 + TERM
        ERR = DABS(TERM/TERM2)
        V2 = V2 + 1
    END DO
    TERM3 = 0.0D0
    ERR = 1.D0
    V3 = 0.D0
    DO WHILE(ERR.GT.1.D-9)
        TERM = (V3+1)**.5D0*DEXP(-U0(3)*V3/2.D0)
        TERM3 = TERM3 + TERM
        ERR = DABS(TERM/TERM3)
        V3 = V3 + 1
    END DO
    PHIT0 = TERM1**2.D0*TERM2**2.D0*TERM3**2.D0*
$      (1.D0-DEXP(-U0(1)))**2.D0*
$      (1.D0-DEXP(-U0(2)))**2.D0*
$      (1.D0-DEXP(-U0(3)))**2.D0
C      WRITE(*,*) 'PHIT0C5',PHIT0

```

```

      BETAC5 = B0C5*(TG/T0)**(-.5D0)*PHITG/PHIT0
C
C 2.0 BAND
      TERM1 = 0.D0
      ERR = 1.D0
      V1 = 0
      DO WHILE(ERR.GT.1.D-9)
          TERM = (V1+1)**.5D0*(V1+2)**.5D0*DEXP(-U(1)*V1/2.D0)
          TERM1 = TERM1 + TERM
          ERR = DABS(TERM/TERM1)
          V1 = V1 + 1
      END DO
      TERM2 = 0.0D0
      ERR = 1.D0
      V2 = 0.D0
      DO WHILE(ERR.GT.1.D-9)
          TERM = (V2+1)**.5D0*DEXP(-U(2)*V2/2.D0)
          TERM2 = TERM2 + TERM
          ERR = DABS(TERM/TERM2)
          V2 = V2 + 1
      END DO
      TERM3 = 0.0D0
      ERR = 1.D0
      V3 = 0.D0
      DO WHILE(ERR.GT.1.D-9)
          TERM = (V3+1)**.5D0*DEXP(-U(3)*V3/2.D0)
          TERM3 = TERM3 + TERM
          ERR = DABS(TERM/TERM3)
          V3 = V3 + 1
      END DO
      PHITG = 0.5D0*TERM1**2.D0*TERM2**2.D0*TERM3**2.D0*
$          (1.D0-DEXP(-U(1)))**3.D0*
$          (1.D0-DEXP(-U(2)))**2.D0*
$          (1.D0-DEXP(-U(3)))**2.D0
C      WRITE(*,*) 'PHITG6',PHITG
      TERM1 = 0.D0
      ERR = 1.D0
      V1 = 0
      DO WHILE(ERR.GT.1.D-9)
$          TERM = (V1+1)**.5D0*(V1+2)**.5D0*
          DEXP(-U0(1)*V1/2.D0)
          TERM1 = TERM1 + TERM
          ERR = DABS(TERM/TERM1)
          V1 = V1 + 1
      END DO
      TERM2 = 0.0D0
      ERR = 1.D0
      V2 = 0.D0
      DO WHILE(ERR.GT.1.D-9)
          TERM = (V2+1)**.5D0*DEXP(-U0(2)*V2/2.D0)
          TERM2 = TERM2 + TERM

```



```

      ERR = DABS (TERM/TERM2)
      V2 = V2 + 1
END DO
TERM3 = 0.0D0
ERR = 1.0D0
V3 = 0.0D0
DO WHILE (ERR.GT.1.D-9)
      TERM = (V3+1)**.5D0*DEXP(-U0(3)*V3/2.D0)
      TERM3 = TERM3 + TERM
      ERR = DABS (TERM/TERM3)
      V3 = V3 + 1
END DO
PHIT0 = 0.5D0*TERM1**2.D0*TERM2**2.D0*TERM3**2.D0*
$      (1.D0-DEXP(-U0(1)))**3.D0*
$      (1.D0-DEXP(-U0(2)))**2.D0*
$      (1.D0-DEXP(-U0(3)))**2.D0
C      WRITE(*,*) 'PHIT0C6', PHIT0
BETAC6 = B0C6*(TG/T0)**(-.5D0)*PHITG/PHIT0
C
C      WRITE(*,*) 'BETACS', BETAC1, BETAC2, BETAC3, BETAC4, BETAC5, BETAC6
C
RC = 1.8643D-6
RHOC = PCO2/(RC*TG)
X = RHOC*L
WC1 = W0C1*(TG/T0)**.5D0
WC2 = W0C2*(TG/T0)**.5D0
WC3 = W0C3*(TG/T0)**.5D0
WC4 = W0C4*(TG/T0)**.5D0
WC5 = W0C5*(TG/T0)**.5D0
WC6 = W0C6*(TG/T0)**.5D0
C
TAUC1 = ALC1*X/WC1
TAUC2 = ALC2*X/WC2
TAUC3 = ALC3*X/WC3
TAUC4 = ALC4*X/WC4
TAUC5 = ALC5*X/WC5
TAUC6 = ALC6*X/WC6
C      WRITE(*,*) 'TAUCS', TAUC1, TAUC2, TAUC3, TAUC4, TAUC5, TAUC6
C
PEC1 = ((P/P0)*(1.D0 + (BC - 1.D0)*(PCO2/P)))**NC1
PEC2 = ((P/P0)*(1.D0 + (BC - 1.D0)*(PCO2/P)))**NC2
PEC3 = ((P/P0)*(1.D0 + (BC - 1.D0)*(PCO2/P)))**NC3
PEC4 = ((P/P0)*(1.D0 + (BC - 1.D0)*(PCO2/P)))**NC4
PEC5 = ((P/P0)*(1.D0 + (BC - 1.D0)*(PCO2/P)))**NC5
PEC6 = ((P/P0)*(1.D0 + (BC - 1.D0)*(PCO2/P)))**NC6
C
ETAC1 = BETAC1*PEC1
ETAC2 = BETAC2*PEC2
ETAC3 = BETAC3*PEC3
ETAC4 = BETAC4*PEC4
ETAC5 = BETAC5*PEC5

```

```

ETAC6 = BETAC6*PEC6
C WRITE(*,*) 'ETACS',ETAC1,ETAC2,ETAC3,ETAC4,ETAC5,ETAC6
C
IF (TAUC1.LE.1.D0.AND.TAUC1.LE.ETAC1) THEN
    ASTC1 = TAUC1
    AC1 = ASTC1*WC1
    TAUG(6) = TAUC1/ASTC1
ELSE IF (TAUC1.GE.ETAC1.AND.TAUC1.LE.(1.D0/ETAC1)) THEN
    ASTC1 = (4.D0*ETAC1*TAUC1)**.5D0 - ETAC1
    AC1 = ASTC1*WC1
    TAUG(6) = (ETAC1*TAUC1)**.5D0/ASTC1
ELSE IF (TAUC1.GT.(1.D0/ETAC1).AND.ETAC1.LE.1.D0) THEN
    ASTC1 = DLOG(TAUC1*ETAC1) + 2.D0 - ETAC1
    AC1 = ASTC1*WC1
    TAUG(6) = 1.D0/ASTC1
ELSE
    ASTC1 = DLOG(TAUC1) + 1.D0
    AC1 = ASTC1*WC1
    TAUG(6) = 1.D0/ASTC1
ENDIF
IF (TAUG(6).GT.0.9D0) THEN
    TAUG(6) = 0.9D0
ENDIF
C
DELNU(6) = AC1/(1.D0 - TAUG(6))
C WRITE(*,*) 'AC1',AC1,'TAUG(6)',TAUG(6),'DELNU(6)',DELNU(6)
C
IF (TAUC2.LE.1.D0.AND.TAUC2.LE.ETAC2) THEN
    ASTC2 = TAUC2
    AC2 = ASTC2*WC2
    TAUG(7) = TAUC2/ASTC2
ELSE IF (TAUC2.GE.ETAC2.AND.TAUC2.LE.(1.D0/ETAC2)) THEN
    ASTC2 = (4.D0*ETAC2*TAUC2)**.5D0 - ETAC2
    AC2 = ASTC2*WC2
    TAUG(7) = (ETAC2*TAUC2)**.5D0/ASTC2
ELSE IF (TAUC2.GT.(1.D0/ETAC2).AND.ETAC2.LE.1.D0) THEN
    ASTC2 = DLOG(TAUC2*ETAC2) + 2.D0 - ETAC2
    AC2 = ASTC2*WC2
    TAUG(7) = 1.D0/ASTC2
ELSE
    ASTC2 = DLOG(TAUC2) + 1.D0
    AC2 = ASTC2*WC2
    TAUG(7) = 1.D0/ASTC2
ENDIF
IF (TAUG(7).GT.0.9D0) THEN
    TAUG(7) = 0.9D0
ENDIF
C
DELNU(7) = AC2/(1.D0 - TAUG(7))
C WRITE(*,*) 'AC2',AC2,'TAUG(7)',TAUG(7),'DELNU(7)',DELNU(7)
C

```

```

IF (TAUC3.LE.1.D0.AND.TAUC3.LE.ETAC3) THEN
  ASTC3 = TAUC3
  AC3 = ASTC3*WC3
  TAUG(8) = TAUC3/ASTC3
ELSE IF (TAUC3.GE.ETAC3.AND.TAUC3.LE.(1.D0/ETAC3)) THEN
  ASTC3 = (4.D0*ETAC3*TAUC3)**.5D0 - ETAC3
  AC3 = ASTC3*WC3
  TAUG(8) = (ETAC3*TAUC3)**.5D0/ASTC3
ELSE IF (TAUC3.GT.(1.D0/ETAC3).AND.ETAC3.LE.1.D0) THEN
  ASTC3 = DLOG(TAUC3*ETAC3) + 2.D0 - ETAC3
  AC3 = ASTC3*WC3
  TAUG(8) = 1.D0/ASTC3
ELSE
  ASTC3 = DLOG(TAUC3) + 1.D0
  AC3 = ASTC3*WC3
  TAUG(8) = 1.D0/ASTC3
ENDIF
IF(TAUG(8).GT.0.9D0) THEN
  TAUG(8) = 0.9D0
ENDIF
C
DELNU(8) = AC3/(1.D0 - TAUG(8))
C
WRITE(*,*) 'AC3',AC3,'TAUG(8)',TAUG(8),'DELNU(8)',DELNU(8)
C
IF (TAUC4.LE.1.D0.AND.TAUC4.LE.ETAC4) THEN
  ASTC4 = TAUC4
  AC4 = ASTC4*WC4
  TAUG(9) = TAUC4/ASTC4
ELSE IF (TAUC4.GE.ETAC4.AND.TAUC4.LE.(1.D0/ETAC4)) THEN
  ASTC4 = (4.D0*ETAC4*TAUC4)**.5D0 - ETAC4
  AC4 = ASTC4*WC4
  TAUG(9) = (ETAC4*TAUC4)**.5D0/ASTC4
ELSE IF (TAUC4.GT.(1.D0/ETAC4).AND.ETAC4.LE.1.D0) THEN
  ASTC4 = DLOG(TAUC4*ETAC4) + 2.D0 - ETAC4
  AC4 = ASTC4*WC4
  TAUG(9) = 1.D0/ASTC4
ELSE
  ASTC4 = DLOG(TAUC4) + 1.D0
  AC4 = ASTC4*WC4
  TAUG(9) = 1.D0/ASTC4
ENDIF
IF(TAUG(9).GT.0.9D0) THEN
  TAUG(9) = 0.9D0
ENDIF
C
DELNU(9) = AC4/(1.D0 - TAUG(9))
C
WRITE(*,*) 'AC4',AC4,'TAUG(9)',TAUG(9),'DELNU(9)',DELNU(9)
C
IF (TAUC5.LE.1.D0.AND.TAUC5.LE.ETAC5) THEN
  ASTC5 = TAUC5
  AC5 = ASTC5*WC5

```

```

      TAUG(10) = TAUC5/ASTC5
ELSE IF (TAUC5.GE.ETAC5.AND.TAUC5.LE.(1.D0/ETAC5)) THEN
      ASTC5 = (4.D0*ETAC5*TAUC5)**.5D0 - ETAC5
      AC5 = ASTC5*WC5
      TAUG(10) = (ETAC5*TAUC5)**.5D0/ASTC5
ELSE IF (TAUC5.GT.(1.D0/ETAC5).AND.ETAC5.LE.1.D0) THEN
      ASTC5 = DLOG(TAUC5*ETAC5) + 2.D0 - ETAC5
      AC5 = ASTC5*WC5
      TAUG(10) = 1.D0/ASTC5
ELSE
      ASTC5 = DLOG(TAUC5) + 1.D0
      AC5 = ASTC5*WC5
      TAUG(10) = 1.D0/ASTC5
ENDIF
IF (TAUG(10).GT.0.9D0) THEN
      TAUG(10) = 0.9D0
ENDIF
C
DELNU(10) = AC5/(1.D0 - TAUG(10))
C
WRITE(*,*) 'AC5',AC5,'TAUG(10)',TAUG(10),'DELNU(10)',DELNU(10)
C
IF (TAUC6.LE.1.D0.AND.TAUC6.LE.ETAC6) THEN
      ASTC6 = TAUC6
      AC6 = ASTC6*WC6
      TAUG(11) = TAUC6/ASTC6
ELSE IF (TAUC6.GE.ETAC6.AND.TAUC6.LE.(1.D0/ETAC6)) THEN
      ASTC6 = (4.D0*ETAC6*TAUC6)**.5D0 - ETAC6
      AC6 = ASTC6*WC6
      TAUG(11) = (ETAC6*TAUC6)**.5D0/ASTC6
ELSE IF (TAUC6.GT.(1.D0/ETAC6).AND.ETAC6.LE.1.D0) THEN
      ASTC6 = DLOG(TAUC6*ETAC6) + 2.D0 - ETAC6
      AC6 = ASTC6*WC6
      TAUG(11) = 1.D0/ASTC6
ELSE
      ASTC6 = DLOG(TAUC6) + 1.D0
      AC6 = ASTC6*WC6
      TAUG(11) = 1.D0/ASTC6
ENDIF
IF (TAUG(11).GT.0.9D0) THEN
      TAUG(11) = 0.9D0
ENDIF
C
DELNU(11) = AC6/(1.D0 - TAUG(11))
C
WRITE(*,*) 'AC6',AC6,'TAUG(11)',TAUG(11),'DELNU(11)',DELNU(11)
C
C
C
C
PAUSE
C
NU(1) = 0.D0
NU(2) = DELNU(1)
NU(3) = 1600.D0 - 0.5D0*DELNU(2)
NU(4) = 1600.D0 + 0.5D0*DELNU(2)

```

```

NU(5) = 3760.D0 - 0.5D0*DELNU(3)
NU(6) = 3760.D0 + 0.5D0*DELNU(3)
NU(7) = 5350.D0 - 0.5D0*DELNU(4)
NU(8) = 5350.D0 + 0.5D0*DELNU(4)
NU(9) = 7250.D0 - 0.5D0*DELNU(5)
NU(10) = 7250.D0 + 0.5D0*DELNU(5)
NU(11) = 667.D0 - 0.5D0*DELNU(6)
NU(12) = 667.D0 + 0.5D0*DELNU(6)
NU(13) = 960.D0 - 0.5D0*DELNU(7)
NU(14) = 960.D0 + 0.5D0*DELNU(7)
NU(15) = 1060.D0 - 0.5D0*DELNU(8)
NU(16) = 1060.D0 + 0.5D0*DELNU(8)
NU(17) = 2410.D0 - DELNU(9)
NU(18) = 2410.D0
NU(19) = 3660.D0 - 0.5D0*DELNU(10)
NU(20) = 3660.D0 + 0.5D0*DELNU(10)
NU(21) = 5200.D0 - 0.5D0*DELNU(11)
NU(22) = 5200.D0 + 0.5D0*DELNU(11)
DO 17 I=1,22
C      WRITE(*,*) 'NU(I)',NU(I)
17    CONTINUE
C
NULP(1) = NU(1)
NULP(2) = NU(3)
NULP(3) = NU(5)
NULP(4) = NU(7)
NULP(5) = NU(9)
NULP(6) = NU(11)
NULP(7) = NU(13)
NULP(8) = NU(15)
NULP(9) = NU(17)
NULP(10) = NU(19)
NULP(11) = NU(21)
C
NUUP(1) = NU(2)
NUUP(2) = NU(4)
NUUP(3) = NU(6)
NUUP(4) = NU(8)
NUUP(5) = NU(10)
NUUP(6) = NU(12)
NUUP(7) = NU(14)
NUUP(8) = NU(16)
NUUP(9) = NU(18)
NUUP(10) = NU(20)
NUUP(11) = NU(22)
C
NUL(1) = NU(1)
NUL(2) = NU(2)
NUL(3) = NU(3)
NUL(4) = NU(4)
NUL(5) = NU(5)

```

```

NUL(6) = NU(6)
NUL(7) = NU(7)
NUL(8) = NU(8)
NUL(9) = NU(9)
NUL(10) = NU(10)
NUL(11) = NU(11)
NUL(12) = NU(12)
NUL(13) = NU(13)
NUL(14) = NU(14)
NUL(15) = NU(15)
NUL(16) = NU(16)
NUL(17) = NU(17)
NUL(18) = NU(18)
NUL(19) = NU(19)
NUL(20) = NU(20)
NUL(21) = NU(21)
C
NUU(1) = NU(2)
NUU(2) = NU(3)
NUU(3) = NU(4)
NUU(4) = NU(5)
NUU(5) = NU(6)
NUU(6) = NU(7)
NUU(7) = NU(8)
NUU(8) = NU(9)
NUU(9) = NU(10)
NUU(10) = NU(11)
NUU(11) = NU(12)
NUU(12) = NU(13)
NUU(13) = NU(14)
NUU(14) = NU(15)
NUU(15) = NU(16)
NUU(16) = NU(17)
NUU(17) = NU(18)
NUU(18) = NU(19)
NUU(19) = NU(20)
NUU(20) = NU(21)
NUU(21) = NU(22)
C
C
C ORDER LIMITS
C
C
DO 60 J=1,21
DO 50 I=1,21
    IF(NU(I).LT.NU(I+1)) GOTO 50
    TEMPN = NU(I)
    NU(I) = NU(I+1)
    NU(I+1) = TEMPN
50 CONTINUE
60 CONTINUE

```

C

```

NUL(1) = NU(1)
NUL(2) = NU(2)
NUL(3) = NU(3)
NUL(4) = NU(4)
NUL(5) = NU(5)
NUL(6) = NU(6)
NUL(7) = NU(7)
NUL(8) = NU(8)
NUL(9) = NU(9)
NUL(10) = NU(10)
NUL(11) = NU(11)
NUL(12) = NU(12)
NUL(13) = NU(13)
NUL(14) = NU(14)
NUL(15) = NU(15)
NUL(16) = NU(16)
NUL(17) = NU(17)
NUL(18) = NU(18)
NUL(19) = NU(19)
NUL(20) = NU(20)
NUL(21) = NU(21)

```

C

```

NUU(1) = NU(2)
NUU(2) = NU(3)
NUU(3) = NU(4)
NUU(4) = NU(5)
NUU(5) = NU(6)
NUU(6) = NU(7)
NUU(7) = NU(8)
NUU(8) = NU(9)
NUU(9) = NU(10)
NUU(10) = NU(11)
NUU(11) = NU(12)
NUU(12) = NU(13)
NUU(13) = NU(14)
NUU(14) = NU(15)
NUU(15) = NU(16)
NUU(16) = NU(17)
NUU(17) = NU(18)
NUU(18) = NU(19)
NUU(19) = NU(20)
NUU(20) = NU(21)
NUU(21) = NU(22)

```

C

```
DO 18 I=1,22
```

C

```
WRITE(*,*) NU(I)
```

18

```
CONTINUE
```

C

```
CALCULATE TRANSMISSIVITY, EMISSIVITY, AND ABSORPTIVITY
```

C

```
DO 70 I=1,22
```

```

      BLKTRNS(I) = 1.DO
      DO 80 J=1,11
          IF(NU(I) .GE. NULP(J) .AND. NU(I) .LT. NUUP(J))
              THEN
          BLKTRNS(I) = BLKTRNS(I)*TAUG(J)
          ENDIF
80      CONTINUE
C      WRITE(*,*) I, 'BLKTRNS(I)', BLKTRNS(I)
C
C      CONTINUE
C      PAUSE
C
      SUMABS = 0.DO
      SUMEM = 0.DO
      SUMABSPN = 0.DO
      SUMABSPD = 0.DO
C
      DO 100 I=1,21
          TDNU = TG/NUL(I)
          TDNUP1 = TG/NUU(I)
          DELF = F(TDNU) - F(TDNUP1)
          SUMEM = SUMEM + (1.DO - BLKTRNS(I))*DELF
          TDNU = TSO/NUL(I)
          TDNUP1 = TSO/NUJ(I)
          DELF = F(TDNU) - F(TDNUP1)
          SUMABS = SUMABS + (1.DO - BLKTRNS(I))*DELF
          NUA = (NUU(I)+NUL(I))/2.DO
          TDNU = TG/NUA
          SUMABSPN = SUMABSPN + (1.DO-BLKTRNS(I))**2.DO*
          $           B(TDNU,NUA)*(NUU(I) - NUL(I))
          SUMABSPD = SUMABSPD + (1.DO-BLKTRNS(I))*
          $           B(TDNU,NUA)*(NUU(I) - NUL(I))
100     CONTINUE
C
      ABSGP = SUMABSPN/SUMABSPD
C      WRITE(*,*) 'SUMEM', SUMEM, 'SUMABS', SUMABS, 'ABSGP', ABSGP
      RETURN
      END
C %%%%%%%%%%% FUNCTION DECLARATIONS %%%%%%%%%%%
C
      FUNCTION ALPHA(DEL,U,U0,ALPH0,M,PSITG,PSIT0)
      IMPLICIT REAL*8(A-H,K,L,N,O-Z)
      DIMENSION DEL(10),U(10),U0(10)
C
      SUM1 = 0.DO
      SUM2 = 0.DO
      HCDK = 14388.DO
C
      DO 10 I=1,M
          SUM1 = SUM1 + U(I)*DEL(I)
          SUM2 = SUM2 + U0(I)*DEL(I)

```



```

10  CONTINUE
C
NUM = (1.D0 - DEXP(-SUM1))*PSITG
DENOM = (1.D0 - DEXP(-SUM2))*PSITO
IF(NUM.EQ.DENOM) THEN
    ALPHA = ALPHO
    GOTO 20
ENDIF
ALPHA = ALPHO*NUM/DENOM
$
C
20  RETURN
    END
C
C
C
FUNCTION F(TDNU)
IMPLICIT REAL*8(A-H,M,O-Z)
IF(TDNU.LT.0.1230D0) THEN
    F = 0.D0
C
    WRITE(*,*) 'F1',F
ELSE IF(TDNU.GE.0.1230D0.AND.TDNU.LE.0.783D0) THEN
    M0 = -.465826D0
    M1 = 15.7476D0
    M2 = -211.9D0
    M3 = 1458.58D0
    M4 = -5659.26D0
    M5 = 13589.9D0
    M6 = -20796.2D0
    M7 = 19826.1D0
    M8 = -10753.8D0
    M9 = 2536.15D0
    F = M0 + M1*TDNU + M2*TDNU**2.D0 + M3*TDNU**3.D0 +
$
$
$
$
$
$
$
$
$
$
    WRITE(*,*) 'F2',F
C
ELSE IF(TDNU.LT.0.825D0.AND.TDNU.GT.0.783D0) THEN
    F = 0.85D0 + (TDNU-0.783D0)*
$
$
$
$
$
$
$
$
$
$
    WRITE(*,*) 'F3',F
C
ELSE IF(TDNU.LE.1.87D0.AND.TDNU.GE.0.825D0) THEN
    M0 = 0.705509D0
    M1 = -0.493321D0
    M2 = 2.00283D0
    M3 = -2.03645D0
    M4 = 0.873569D0
    M5 = -0.138617D0
    F = M0 + M1*TDNU + M2*TDNU**2.D0 + M3*TDNU**3.D0 +
$
$
$
$
$
$
$
$
$
$
    M4*TDNU**4.D0 + M5*TDNU**5.D0

```

```
C          WRITE(*,*) 'F4',F
ELSE IF (TDNU.GT.1.87D0) THEN
  F = 1.D0
C          WRITE(*,*) 'F5',F
ENDIF
RETURN
END

C
C
FUNCTION B(TDNU,NUA)
IMPLICIT REAL*8(A-H,M,O-Z)
HCDK = 1.4388D0
HC2 = 6.6262D-34*(2.9979D10)**2.D0
PI = 3.14D0
B = 2.D0*PI*HC2*NUA**3.D0/(DEXP(HCDK/TDNU) - 1.D0)
RETURN
END
```

APPENDIX G

GOVERNING DIFFERENTIAL EQUATIONS USED IN THE NUMERICAL MODEL

For the case of turbulent flows FLUENT solves the Reynolds averaged (Stanisic, 1985) Navier-Stokes equations along with the Reynolds averaged governing differential equations of continuity, energy, and species, as well as the turbulent parameters of dissipation rate, ϵ , and turbulent kinetic energy, κ , in a discretized form for its control volume-based, finite difference solution technique. The terms shown in Table G.1 are for steady state conditions and correspond to the κ - ϵ model of turbulence. The generic steady state transport equation in differential form corresponding to Table G.1 follows.

$$\frac{\partial(\bar{\rho}\tilde{u}\phi)}{\partial x} + \frac{\partial(\bar{\rho}\tilde{v}\phi)}{\partial y} + \frac{\partial(\bar{\rho}\tilde{w}\phi)}{\partial z} - \frac{\partial}{\partial x} \left(\Gamma_{\phi} \frac{\partial \phi}{\partial x} \right) - \frac{\partial}{\partial y} \left(\Gamma_{\phi} \frac{\partial \phi}{\partial y} \right) - \frac{\partial}{\partial z} \left(\Gamma_{\phi} \frac{\partial \phi}{\partial z} \right) = S_{\phi}$$

Where:

ϕ Represents the dependent variable

Γ_{ϕ} Represents the diffusion coefficient

S_{ϕ} Represents the source term

and the “ \sim ” overlining represents Favre averaging (however, as density fluctuations are assumed negligible it has no significance for this work).

Table G.1 Reynolds Averaged Governing Equations for Numerical Model
Showing κ - ϵ Turbulence Model Terms.

Equation	ϕ	Γ_ϕ	S_ϕ
Continuity	1	0	0
X Momentum	\tilde{u}	μ_e $-\frac{\partial \bar{P}}{\partial x} + \frac{\partial}{\partial x} \left(\mu_e \frac{\partial \tilde{u}}{\partial x} \right) + \frac{\partial}{\partial y} \left(\mu_e \frac{\partial \tilde{v}}{\partial x} \right) + \frac{\partial}{\partial z} \left(\mu_e \frac{\partial \tilde{w}}{\partial x} \right) + \bar{\rho} g_x - \frac{2}{3} \bar{\rho} \tilde{k}$	
Y Momentum	\tilde{v}	μ_e $-\frac{\partial \bar{P}}{\partial y} + \frac{\partial}{\partial x} \left(\mu_e \frac{\partial \tilde{u}}{\partial y} \right) + \frac{\partial}{\partial y} \left(\mu_e \frac{\partial \tilde{v}}{\partial y} \right) + \frac{\partial}{\partial z} \left(\mu_e \frac{\partial \tilde{w}}{\partial y} \right) + \bar{\rho} g_y - \frac{2}{3} \bar{\rho} \tilde{k}$	
Z Momentum	\tilde{w}	μ_e $-\frac{\partial \bar{P}}{\partial z} + \frac{\partial}{\partial x} \left(\mu_e \frac{\partial \tilde{u}}{\partial z} \right) + \frac{\partial}{\partial y} \left(\mu_e \frac{\partial \tilde{v}}{\partial z} \right) + \frac{\partial}{\partial z} \left(\mu_e \frac{\partial \tilde{w}}{\partial z} \right) + \bar{\rho} g_z - \frac{2}{3} \bar{\rho} \tilde{k}$	
Turbulent Energy	$\tilde{\kappa}$	$\frac{\mu_e}{\sigma_\kappa}$	$G - \bar{\rho} \tilde{\epsilon}$
Dissipation Rate	$\tilde{\epsilon}$	$\frac{\mu_e}{\sigma_\epsilon}$	$\left(\frac{\tilde{\epsilon}}{\tilde{\kappa}} \right) (C_1 G - C_2 \bar{\rho} \tilde{\epsilon})$
Species mass Fraction	\tilde{f}	$\frac{\mu_e}{\sigma_f}$	R_f
Enthalpy	\tilde{h}	$\frac{\mu_e}{\sigma_h}$	$S_h + S_r$

Where:

R_f Represents net rate of production through chemical reaction

S_h Represents the source of enthalpy due to chemical reaction

S_r Represents the source of enthalpy due to radiation

σ_f Is the turbulent Schmidt number

σ_h Is the turbulent Prandtl number

C_1 and C_2 Are empirical turbulence constants

σ_κ and σ_ϵ Are "Prandtl" numbers governing the turbulent diffusion of κ and ϵ

μ_e Is the effective viscosity = $\mu + \mu_t$

and

$$G = \mu_e \left\{ 2 \left[\left(\frac{\partial \tilde{u}}{\partial x} \right)^2 + \left(\frac{\partial \tilde{v}}{\partial y} \right)^2 + \left(\frac{\partial \tilde{w}}{\partial z} \right)^2 \right] + \left(\frac{\partial \tilde{u}}{\partial y} + \frac{\partial \tilde{v}}{\partial x} \right)^2 + \left(\frac{\partial \tilde{u}}{\partial z} + \frac{\partial \tilde{w}}{\partial x} \right)^2 + \left(\frac{\partial \tilde{v}}{\partial z} + \frac{\partial \tilde{w}}{\partial y} \right)^2 \right\}$$

APPENDIX H

NUMERICAL MODEL BOUNDARY CONDITIONS AND MISCELLANEOUS SOLUTION INFORMATION

KEY FOR THE LISTING OF THE NUMERICAL MODEL SPECIFICATIONS

In the computer program printout the following designations hold:

<u>Zone</u>	<u>defines</u>
W1	walls
I1	top kiln burner
I2	middle kiln burner
I3	bottom kiln burner
I6	sludge lance
I8	top kiln turbulence air inlet
I9	bottom kiln turbulence air inlet
ID	solids loading chute door
IJ	front rotary seal leak air, lower
IK	front rotary seal leak air, burner side
IL	front rotary seal leak air, non-burner side
IM	front rotary seal leak air, top
IS	sump (transition section) and rear rotary seal leak
IR	rear rotary seal leak air, burner side
IT	rear rotary seal leak air, top
IU	rear rotary seal leak air, non-burner side

1) TA-ON DATA FROM JAKWAY ET AL. (1995A, 1995B) COARSE GRID

BASE INFILTRATION AIR DISTRIBUTION
1% SOOT FOR 1ST 1/3 OF KILN
KA8K & L.LP
FROM KA8H1.CAS AND KA8K.DAT ON 27 MARCH 95

- UNITS SYSTEM -

INDEX	PROPERTY	UNITS	S.I. CONVERSION FACTOR
1	DIMENSIONLESS	DIMENSIONLESS	1.000E+00
2	MASS	KILOGRAMS	1.000E+00
3	LENGTH	METERS	1.000E+00
4	TIME	SECONDS	1.000E+00
5	VELOCITY	METERS/SEC	1.000E+00
6	FORCE	NEWTONS	1.000E+00
7	ACCELERATION	METERS/SEC/SEC	1.000E+00
8	ENERGY	JOULES	1.000E+00
9	POWER	WATTS	1.000E+00
10	MASS FLOW RATE	KILOGRAMS/SEC	1.000E+00
11	TEMPERATURE	KELVIN	1.000E+00
12	ENTHALPY	JOULES/KILOGRAM	1.000E+00
13	PRESSURE	PASCALS	1.000E+00
14	DENSITY	KILOGRAMS/CU.M	1.000E+00
15	VISCOSITY	KG/M-SEC.	1.000E+00
16	K.E. OF TURBLNCE	M.SQ/SEC/SEC	1.000E+00
17	K.E. DISS. RATE	M.SQ/SEC/SEC/SEC	1.000E+00
18	SPEC. HEAT CAP.	JOULES/KG-K	1.000E+00
19	THERMAL CONDUCT.	WATTS/M-K	1.000E+00
20	DIFFUSIVITY	M.SQ/SEC.	1.000E+00
21	ACTIVATION ENRGY	JOULES/KGMOL	1.000E+00
22	ANGLE	RADIANS	1.000E+00
23	HEAT FLUX	WATTS/M.SQ.	1.000E+00
24	PARTICLE DIAM.	METERS	1.000E+00
25	MOMENTUM TR RATE	KG.M/SEC/SEC	1.000E+00
26	HEAT TRANSF COEF	WATTS/M.SQ-K	1.000E+00
27	PERMEABILITY	M.SQ.	1.000E+00
28	(INTERNAL MISC.)	UNDEFINED	1.000E+00
29	VOLUME. FLOWRATE	CU.M/SEC.	1.000E+00
30	AREA	M.SQ.	1.000E+00
31	ARRHENIUS FACTOR	CONSISTENT UNITS	1.000E+00
32	INERTIAL FACTOR	PER METER	1.000E+00
33	VOL. HEAT RATE	WATTS/CU.M.	1.000E+00
34	ABSORB./SCATTER.	PER METER	1.000E+00
35	ANGULAR VELOCITY	RADIANS/SECOND	1.000E+00
36	MOL. SIZE PARM.	ANGSTROMS	1.000E+00
37	PRESSURE GRAD.	PASCALS/METER	1.000E+00
38	MUSHY ZONE CON.	KG/CU.M.-SEC	1.000E+00
39	SURFACE TENSION	NEWTONS/METER	1.000E+00
40	SURF. TEN. GRAD.	NEWTONS/M-K	1.000E+00
41	CONTACT RESIST.	M.SQ.-K/WATT	1.000E+00

- GEOMETRY -

BOUNDARY FITTED COORDINATES

NI = 17 NJ = 17 NK = 34

CELL TYPES: K = 1

J	I=	2	4	6	8	10	12	14	16		
17		W1	W1	W1	W1	W1	W1	W1	W1	W1	17
16		W1	IL	IL	IL	IL	IL	IL	IL	IL	16
15		W1	IL	W1	W1	W1	W1	W1	W1	W1	15
14		W1	IL	W1	I8	W1	W1	W1	W1	W1	14
13		W1	IL	W1	W1	W1	W1	W1	W1	W1	13
12		W1	IL	W1	W1	W1	W1	W1	W1	W1	12
11		W1	IL	W1	W1	W1	W1	W1	W1	W1	11
10		W1	IL	W1	W1	W1	W1	W1	W1	I1	10
9		W1	IL	W1	W1	W1	W1	W1	W1	W1	9
8		W1	IL	W1	W1	ID	ID	ID	ID	I2	8
7		W1	IL	W1	I6	W1	ID	ID	ID	W1	7
6		W1	IL	W1	W1	ID	ID	ID	ID	I3	6
5		W1	IL	W1	W1	ID	ID	ID	ID	W1	5
4		W1	IL	W1	W1	ID	ID	ID	ID	I9	4
3		W1	IL	W1	W1	W1	W1	W1	W1	W1	3
2		W1	I1	J1	J1	J1	J1	J1	J1	J1	2
1		W1	W1	W1	W1	W1	W1	W1	W1	W1	1
J	I=	2	4	6	8	10	12	14	16		

CELL TYPES: K = 2 to 18 & 21 to 33

J	I=	2	4	6	8	10	12	14	16		
17		W1	W1	W1	W1	W1	W1	W1	W1	17	
16		W1	W1	16
15		W1	W1	15
14		W1	W1	14
13		W1	W1	13
12		W1	W1	12
11		W1	W1	11
10		W1	W1	10
9		W1	W1	9
8		W1	W1	8
7		W1	W1	7
6		W1	W1	6
5		W1	W1	5
4		W1	W1	4
3		W1	W1	3
2		W1	W1	2
1		W1	W1	W1	W1	W1	W1	W1	W1	W1	1
J	I=	2	4	6	8	10	12	14	16		


```

CELL TYPES: K = 19
  J I= 2  4  6  8 10 12 14 16
17 WLLLLLLLLLLLLLLLLLLLLLLLLLLLLLW 17
16 IU . . . . . . . . . . . . . . .IR 16
15 IU . . . . . . . . . . . . . . .IR 15
14 IU . . . . . . . . . . . . . . .IR 14
13 IU . . . . . . . . . . . . . . .IR 13
12 IU . . . . . . . . . . . . . . .IR 12
11 IU . . . . . . . . . . . . . . .IR 11
10 IU . . . . . . . . . . . . . . .IR 10
 9 IU . . . . . . . . . . . . . . .IR  9
 8 IU . . . . . . . . . . . . . . .IR  8
 7 IU . . . . . . . . . . . . . . .IR  7
 6 IU . . . . . . . . . . . . . . .IR  6
 5 IU . . . . . . . . . . . . . . .IR  5
 4 IU . . . . . . . . . . . . . . .IR  4
 3 IU . . . . . . . . . . . . . . .IR  3
 2 IU . . . . . . . . . . . . . . .IR  2
 1 WLISISISISISISISISISISISISISW  1
  J I= 2  4  6  8 10 12 14 16

```

```

CELL TYPES: K = 20
  J I= 2  4  6  8 10 12 14 16
17 WLWLWLWLWLWLWLWLWLWLWLWLWLWL 17
16 W1 . . . . . . . . . . . . . . .W1 16
15 W1 . . . . . . . . . . . . . . .W1 15
14 W1 . . . . . . . . . . . . . . .W1 14
13 W1 . . . . . . . . . . . . . . .W1 13
12 W1 . . . . . . . . . . . . . . .W1 12
11 W1 . . . . . . . . . . . . . . .W1 11
10 W1 . . . . . . . . . . . . . . .W1 10
 9 W1 . . . . . . . . . . . . . . .W1  9
 8 W1 . . . . . . . . . . . . . . .W1  8
 7 W1 . . . . . . . . . . . . . . .W1  7
 6 W1 . . . . . . . . . . . . . . .W1  6
 5 W1 . . . . . . . . . . . . . . .W1  5
 4 W1 . . . . . . . . . . . . . . .W1  4
 3 W1 . . . . . . . . . . . . . . .W1  3
 2 W1 . . . . . . . . . . . . . . .W1  2
 1 WLISISISISISISISISISISISISW  1
  J I= 2  4  6  8 10 12 14 16

```

CELL TYPES: K = 34

```

J I= 2  4  6  8 10 12 14 16
17 W1W1W1W1W1W1W1W1W1W1W1W1W1W1W1W1W1 17
16 W1 0 0 0 0 0 0 0 0 0 0 0 0 0 0 OW1 16
15 W1 0 0 0 0 0 0 0 0 0 0 0 0 0 0 OW1 15
14 W1 0 0 0 0 0 0 0 0 0 0 0 0 0 0 OW1 14
13 W1 0 0 0 0 0 0 0 0 0 0 0 0 0 0 OW1 13
12 W1 0 0 0 0 0 0 0 0 0 0 0 0 0 0 OW1 12
11 W1 0 0 0 0 0 0 0 0 0 0 0 0 0 0 OW1 11
10 W1 0 0 0 0 0 0 0 0 0 0 0 0 0 0 OW1 10
 9 W1 0 0 0 0 0 0 0 0 0 0 0 0 0 0 OW1  9
 8 W1 0 0 0 0 0 0 0 0 0 0 0 0 0 0 OW1  8
 7 W1 0 0 0 0 0 0 0 0 0 0 0 0 0 0 OW1  7
 6 W1 0 0 0 0 0 0 0 0 0 0 0 0 0 0 OW1  6
 5 W1 0 0 0 0 0 0 0 0 0 0 0 0 0 0 OW1  5
 4 W1 0 0 0 0 0 0 0 0 0 0 0 0 0 0 OW1  4
 3 W1 0 0 0 0 0 0 0 0 0 0 0 0 0 0 OW1  3
 2 W1 0 0 0 0 0 0 0 0 0 0 0 0 0 0 OW1  2
 1 W1W1W1W1W1W1W1W1W1W1W1W1W1W1W1W1W1  1
J I= 2  4  6  8 10 12 14 16

```

- CHEMICAL SPECIES DEFINITIONS -

```

TOTAL NUMBER OF CHEMICAL SPECIES = 6
NUMBER OF GAS PHASE SPECIES      = 6
NUMBER OF SURFACE SPECIES         = 0
NUMBER OF SPECIES EQUATIONS SOLVED = 5

```

SPECIES NUMBER	SPECIES NAME	SPECIES TYPE
1	CH4	GAS PHASE
2	O2	GAS PHASE
3	CO2	GAS PHASE
4	H2O	GAS PHASE
5	CARBON (S)	GAS PHASE
6	N2	GAS PHASE - (NOT SOLVED)

- REACTION STOICHIOMETRY DEFINITION -

SPECIES NAME	REACTION NO. 1
CH4	1.000E+00
O2	2.000E+00
CO2	-1.000E+00
H2O	-2.000E+00
CARBON (S)	0.000E+00
N2	0.000E+00

- REACTION RATE CONSTANTS -

PARAMETER	REACTION NO. 1
TYPE	GAS PHASE
LAW	ARRH./MIX.
ARRHENTIUS	
PRE-EXP.	1.000E+12
ACTIVATION	
ENERGY	1.000E+02
TEMP. EXP.	0.000E+00
CONSTANT-A	4.000E+00
CONSTANT-B	5.000E-01
SPEC. EXP.	
CH4	1.000E+00
O2	1.000E+00

- MULTI-GRID PARAMETERS -

PRESSURE IS SOLVED BY MULTI-GRID METHOD.
 TERMINATION CRITERION: 0.1000000047E-02
 RESIDUAL REDUCTION RATE: 0.9999999747E-04
 MAX. LEVEL OF BLOCK CORRECTIONS IN I-DIR.: 0
 MAX. LEVEL OF BLOCK CORRECTIONS IN J-DIR.: 0
 MAX. LEVEL OF BLOCK CORRECTIONS IN K-DIR.: 2

ENTHALPY IS SOLVED BY MULTI-GRID METHOD.
 TERMINATION CRITERION: 0.1000000047E-02
 RESIDUAL REDUCTION RATE: 0.9999999747E-04
 MAX. LEVEL OF BLOCK CORRECTIONS IN I-DIR.: 0
 MAX. LEVEL OF BLOCK CORRECTIONS IN J-DIR.: 0
 MAX. LEVEL OF BLOCK CORRECTIONS IN K-DIR.: 2

MAXIMUM NO. OF FINE GRID ITERATIONS: 30
 MAXIMUM NO. OF ITERATIONS PER LEVEL: 200
 COARSE GRID SPACING IN I-DIRECTION: 3
 COARSE GRID SPACING IN J-DIRECTION: 3
 COARSE GRID SPACING IN K-DIRECTION: 2
 MONITOR MG SOLVER: NO
 MAX.-MG-LEVEL: 4

- VELOCITY BOUNDARY CONDITIONS -

ZONE	U-VEL.	V-VEL.	W-VEL.
W1	0.00E+00	0.00E+00	0.00E+00
I1	-2.23E+00	-8.00E-01	1.14E+01
I2	-4.18E-01	0.00E+00	2.15E+00
I3	-2.35E+00	8.44E-01	1.21E+01
I6	0.00E+00	0.00E+00	3.85E-01
I8	6.23E+00	2.58E+00	1.63E+01
I9	-1.26E+01	5.23E+00	1.63E+01
ID	0.00E+00	0.00E+00	1.99E+00
IJ	0.00E+00	0.00E+00	1.52E+00
IK	0.00E+00	0.00E+00	1.81E+00
IL	0.00E+00	0.00E+00	1.16E+00
IM	0.00E+00	0.00E+00	2.62E+00
IR	-4.06E-01	0.00E+00	0.00E+00
IS	0.00E+00	3.87E-01	0.00E+00
IT	0.00E+00	-4.60E-01	0.00E+00
IU	4.06E-01	0.00E+00	0.00E+00

- TURBULENCE BOUNDARY CONDITIONS -

- TWO EQUATION MODEL -

ZONE	TURB.-INTEN.	CHAR.-LENGTH
W1	SET	SET
I1	1.000E+01	2.500E-01
I2	1.000E+01	2.500E-01
I3	1.000E+01	2.500E-01
I6	1.000E+01	2.000E-01
I8	1.000E+01	2.000E-01
I9	1.000E+01	2.000E-01
ID	1.000E+01	5.000E-01
IJ	1.000E+01	1.000E-01
IK	1.000E+01	1.000E-01
IL	1.000E+01	1.000E-01
IM	1.000E+01	1.000E-01
IR	1.000E+01	1.000E-01
IS	1.000E+01	5.000E-01
IT	1.000E+01	1.000E-01
IU	1.000E+01	1.000E-01

- CHEMICAL SPECIES BOUNDARY CONDITIONS (*) -

ZONE	CH4	O2	CO2	H2O	CARBON (S)
W1	LINK CUT	LINK CUT	LINK CUT	LINK CUT	LINK CUT
I1	1.8380E-01	1.6220E-01	2.0000E-04	4.1700E-02	1.8400E-03
I2	0.0000E+00	2.0450E-01	2.9300E-04	2.4000E-02	0.0000E+00
I3	2.1870E-01	1.5520E-01	2.0000E-04	4.0600E-02	2.1900E-03
I6	0.0000E+00	0.0000E+00	1.0000E-06	1.0000E+00	0.0000E+00
I8	0.0000E+00	2.0450E-01	2.9300E-04	2.4000E-02	0.0000E+00
I9	0.0000E+00	2.0450E-01	2.9300E-04	2.4000E-02	0.0000E+00
ID	0.0000E+00	2.0450E-01	2.9300E-04	2.4000E-02	0.0000E+00
IJ	0.0000E+00	2.0450E-01	2.9300E-04	2.4000E-02	0.0000E+00
IK	0.0000E+00	2.0450E-01	2.9300E-04	2.4000E-02	0.0000E+00
IL	0.0000E+00	2.0450E-01	2.9300E-04	2.4000E-02	0.0000E+00
IM	0.0000E+00	2.0450E-01	2.9300E-04	2.4000E-02	0.0000E+00
IR	0.0000E+00	2.0450E-01	2.9300E-04	2.4000E-02	0.0000E+00
IS	0.0000E+00	2.0450E-01	2.9300E-04	2.4000E-02	0.0000E+00
IT	0.0000E+00	2.0450E-01	2.9300E-04	2.4000E-02	0.0000E+00
IU	0.0000E+00	2.0450E-01	2.9300E-04	2.4000E-02	0.0000E+00

(*) - MOLE FRACTIONS

- TEMPERATURE BOUNDARY CONDITIONS -

ZONE	TEMPERATURE
W1	HEAT FLUX
I1	3.0740E+02
I2	3.0730E+02
I3	3.0730E+02
I6	4.3300E+02
I8	3.0600E+02
I9	3.0600E+02
ID	4.0000E+02
IJ	5.0000E+02
IK	5.0000E+02
IL	5.0000E+02
IM	5.0000E+02
IR	5.0000E+02
IS	3.5000E+02
IT	5.0000E+02
IU	5.0000E+02

- GRAVITATIONAL ACCELERATIONS -

X = 0.000E+00
Y = -9.810E+00
Z = 0.000E+00

- SPECIAL TEMPERATURE BOUNDARIES -

ZONE	HEAT FLUX BOUNDARY	HEAT FLUX VALUE	EXT. H-T BOUNDARY	EXTERNAL HEAT TRANSFER COEFF.
W1	Y	0.0000E+00	N	N/A
EXT. TEMP.	ZONE	EXT. RAD BOUNDARY	T-INFINITY	EXT. EMISS.
N/A	W1	N	N/A	N/A

- TURBULENCE MODEL CONSTANTS -

C1 = 1.4E+00
 C2 = 1.9E+00
 CMU = 9.0E-02

- WALL FUNCTION TURBULENCE MODEL CONSTANTS -

WALL ZONE CAPP ELOG
 W1 4.187E-01 9.793E+00

- ZONAL EMISSIVITIES (DTRM) -

ZONE	EMISSIVITY
W1	8.0000E-01
O	8.0000E-01
I1	1.0000E-02
I2	1.0000E-02
I3	1.0000E-02
I6	1.0000E-02
I8	1.0000E-02
I9	1.0000E-02
ID	1.0000E-02
IJ	1.0000E-02
IK	1.0000E-02
IL	1.0000E-02
IM	1.0000E-02
IR	1.0000E-02
IS	1.0000E-02
IT	1.0000E-02
IU	1.0000E-02

- RADIATION MODEL CONSTANTS -

ABSORPTION COEFFICIENT	=	COMPUTED
SCATTERING COEFFICIENT	=	1.000E-08
CARBON DIOXIDE SPECIES	=	CO2
WATER VAPOR SPECIES	=	H2O
EMITTER TEMPERATURE	=	1.103E+03
MEAN BEAM LENGTH	=	3.020E+00
NUMBER OF RADIATING SURFACES	=	2370
NUMBER OF RAYS IN THETA	=	4
NUMBER OF RAYS IN PHI	=	4

- USER DEFINED PROPERTIES -

FLUID VISCOSITY	-	NO
FLUID DENSITY	-	NO
FLUID SPECIFIC HEAT	-	NO
FLUID THERMAL CONDUCTIVITY	-	NO
TURBULENT VISCOSITY	-	NO
ABSORPTION COEFFICIENT	-	YES
SCATTERING COEFFICIENT	-	NO

- USER DEFINED SOURCE TERMS -

X-MOMENTUM EQUATION	-	NO
Y-MOMENTUM EQUATION	-	NO
Z-MOMENTUM EQUATION	-	NO
PRESSURE CORRECTION EQUATION	-	NO
TURBULENT K.E. EQUATION	-	NO
TURB. K.E. DISSIPATION EQUATION	-	NO
ENTHALPY EQUATION	-	NO
SPECIES EQUATIONS	-	NO

- USER STARTUP SUBROUTINE IS NOT ACTIVE -

- USER DEFINED ADJUSTMENTS -

X-MOMENTUM EQUATION	-	NO
X-MOMENTUM EQUATION	-	NO
X-MOMENTUM EQUATION	-	NO
X-MOMENTUM EQUATION	-	NO

- USER DEFINED REAL VARIABLES -

USER DEFINED REAL VARIABLE, USPAR1 - 0.00000E+00
 USER DEFINED REAL VARIABLE, USPAR2 - 0.00000E+00
 USER DEFINED REAL VARIABLE, USPAR3 - 0.00000E+00
 USER DEFINED REAL VARIABLE, USPAR4 - 0.00000E+00
 USER DEFINED REAL VARIABLE, USPAR5 - 0.00000E+00
 USER DEFINED REAL VARIABLE, USPAR6 - 0.00000E+00
 USER DEFINED REAL VARIABLE, USPAR7 - 0.00000E+00
 USER DEFINED REAL VARIABLE, USPAR8 - 0.00000E+00
 USER DEFINED REAL VARIABLE, USPAR9 - 0.00000E+00

- USER DEFINED INTEGER VARIABLES -

USER DEFINED INTEGER VARIABLE, IUFLG1 - 0
 USER DEFINED INTEGER VARIABLE, IUFLG2 - 0
 USER DEFINED INTEGER VARIABLE, IUFLG3 - 0
 USER DEFINED INTEGER VARIABLE, IUFLG4 - 0
 USER DEFINED INTEGER VARIABLE, IUFLG5 - 0
 USER DEFINED INTEGER VARIABLE, IUFLG6 - 0
 USER DEFINED INTEGER VARIABLE, IUFLG7 - 0
 USER DEFINED INTEGER VARIABLE, IUFLG8 - 0
 USER DEFINED INTEGER VARIABLE, IUFLG9 - 0

- PROPERTY CALCULATION OPTIONS -

COMPOSITION DEPENDENT VISCOSITY - NO
 COMPOSITION DEPENDENT THERMAL CONDUCTIVITY - NO
 COMPOSITION DEPENDENT SPECIFIC HEAT - YES
 ANY PROPERTY COMPUTED USING KINETIC THEORY - NO
 ENABLE USER SPECIFIED MIXING LAWS - NO

- DENSITY IS COMPUTED FROM THE IDEAL GAS LAW
 - THE OPERATING PRESSURE = 1.0132E+05

- SPECIES MOLECULAR WEIGHTS -

SPECIES NAME	MOLECULAR WEIGHT
CH4	1.6040E+01
O2	3.2000E+01
CO2	4.4010E+01
H2O	1.8020E+01
CARBON (S)	1.2000E+01
N2	2.8010E+01

- SPECIFIC HEAT DEFINITION -

SPECIFIC HEAT FOR CH4 :

$$CP = 7.435E+02 + 5.260E+00*T**1 - 1.757E-03*T**2 + 2.077E-07*T**3$$

SPECIFIC HEAT FOR O2 :

$$CP = 8.071E+02 + 4.178E-01*T**1 - 1.658E-04*T**2 + 2.524E-08*T**3$$

SPECIFIC HEAT FOR CO2 :

$$CP = 6.015E+02 + 1.002E+00*T**1 - 4.394E-04*T**2 + 6.556E-08*T**3$$

SPECIFIC HEAT FOR H2O :

$$CP = 1.638E+03 + 6.611E-01*T**1 + 2.983E-05*T**2 - 3.000E-08*T**3$$

SPECIFIC HEAT FOR CARBON (S) :

$$CP = 5.185E+00 + 2.691E+00*T**1 - 8.622E-04*T**2 + 1.845E-07*T**3$$

SPECIFIC HEAT FOR N2 :

$$CP = 9.482E+02 + 2.694E-01*T**1 - 5.374E-05*T**2 + 1.657E-09*T**3$$

$$ENIHALPY REFERENCE TEMPERATURE = 2.9815E+02$$

- MIXTURE THERMAL CONDUCTIVITY DEFINITION -

$$K = 3.089E-02 - 6.055E-05*T**1 + 2.046E-07*T**2 - 1.342E-10*T**3 + 2.984E-14*T**4$$

- MIXTURE VISCOSITY DEFINITION -

$$VISCOSITY = 4.204E-06 + 5.555E-08*T**1 - 2.518E-11*T**2 + 9.074E-15*T**3 - 1.160E-18*T**4$$

- FORMATION ENIHALPY INFORMATION -

SPECIES NAME	FORMATION ENIHALPY	REFERENCE TEMPERATURE
CH4	-7.4873E+07	2.9815E+02
O2	0.0000E+00	2.9815E+02
CO2	-3.9352E+08	2.9815E+02
H2O	-2.4183E+08	2.9815E+02
CARBON (S)	0.0000E+00	2.9815E+02
N2	0.0000E+00	2.9815E+02

REFERENCE PRESSURE LOCATION :

I = 2
 J = 2
 K = 2

- SOLUTION CONTROL PARAMETERS -

SOLVER MARCHING DIRECTION	- K-DIRECTION
SOLVER SWEEP DIRECTION	- I-DIRECTION
ALTERNATE SWEEP DIRECTION	- YES
SOLUTION METHOD	- SIMPLEC
ALLOW PATCHING OF BOUNDARY VALUES	- NO
CONVERGENCE/DIVERGENCE CHECK ON	- NO
MINIMUM RESIDUAL SUM	- 1.000E-03
MINIMUM ENTHALPY RESIDUAL	- 1.000E-06
NORMALIZE RESIDUALS	- YES
CONTINUITY CHECK	- NO
TEMPERATURE CHANGE LIMITER	- 1.000E+00
CALCULATE Y PLUS ITERATIVELY	- NO
REYNOLDS STRESS TURBULENCE MODEL	- NO
RNG TURBULENCE MODEL	- NO
INCLUDE BUOYANCY TERMS IN TURB. MODEL	- NO
MONITOR SOLVER	- NO
COMPRESSIBLE FLOW	- NO
SUPERSONIC INFLOW	- NO
SUPERSONIC OUTFLOW	- NO
FIX VARIABLE OPTION ENABLED	- NO
SET PRESSURE REFERENCE LOCATION	- NO
VISCOUS DISSIPATION	- NO
INCLUDE SPECIES DIFF. EFFECTS IN ENTH.	- NO

DIFFERENCING SCHEME - POWER LAW

VARIABLE	SOLVED	BLOCK CORRECT	NO. SWEEPS	UNDERRELAX 1	RESIDUAL AT 4838 ITERATIONS
PRESSURE	YES	NO	30	6.0000E-01	5.3751E-07
U-VELOCITY	YES	NO	10	3.0000E-01	4.3547E-05
V-VELOCITY	YES	NO	1	3.0000E-01	1.1037E-05
W-VELOCITY	YES	NO	1	3.0000E-01	5.2237E-06
TURB. K.E.	YES	NO	1	3.0000E-01	5.4224E-06
K.E. DISS.	YES	NO	1	3.0000E-01	2.2432E-06
ENIHALPY	YES	NO	30	6.0000E-01	9.9817E-07
CH4	YES	NO	30	4.0000E-01	3.6277E-04
O2	YES	NO	1	4.0000E-01	3.6365E-07
CO2	YES	NO	1	4.0000E-01	1.1585E-06
H2O	YES	NO	1	4.0000E-01	7.3627E-07
CARBON (S)	YES	NO	30	4.0000E-01	1.2731E-06
PROPERTIES	YES	N/A	N/A	N/A	N/A
VISCOSITY	N/A	N/A	N/A	3.0000E-01	N/A
TEMPERATURE	N/A	N/A	N/A	6.0000E-01	N/A
RADIATION	YES	N/A	N/A	N/A	N/A

RADIATION SOLVED EVERY 5 ITERATIONS
 MAXIMUM NUMBER OF DIRM ITERATIONS = 10
 DIRM ITERATION TOLERANCE = 1.0000E-03

```

*****
*
*           FLUENT (V4.25) Fluid Flow Modeling
*
*   Copyright (C) 1984, 1989, 1991, 1994 by Fluent Inc.
*   All rights reserved. No part of this code may be
*   reproduced or otherwise used in any form without express
*   written permission from Fluent Inc. Use of this code is
*   subject to terms of the license agreement.
*   FLUENT, FLUENT/BFC, FLUENT/PC, and FLUENT/CVD
*   are registered trademarks of:
*
*           Fluent Inc.
*           Centerra Resource Park
*           10 Cavendish Court
*           Lebanon, New Hampshire 03766 USA
*           (800) 445-4454
*           15000 Cells, 10 Species Equations Available
*****

```


CELL TYPES: K = 2 to 27

J	I=	2	4	6	8	10	12	14	16	
17	W2W2W2W2W2W2W2W2W2W2W2W2W2W2W2W2									17
16	W2W2W2W2	16
15	W2W2	15
14	W2W2	14
13	W2W2	13
12	W2W2	12
11	W2W2	11
10	W2W2	10
9	W2W2	9
8	W2W2	8
7	W2W2	7
6	W2W2	6
5	W2W2	5
4	W2W2	4
3	W2W2	3
2	W2W2W2W2	2
1	W2W2W2W2W2W2W2W2W2W2W2W2W2W2W2W2									1

J I= 2 4 6 8 10 12 14 16

CELL TYPES: K = 28

J	I=	2	4	6	8	10	12	14	16	
17	W2W2TTTTTTTTTTTTTTTTTTTTTTTTTTTTW2W2									17
16	W2W2W2W2	16
15	IUIR	15
14	IUIR	14
13	IUIR	13
12	IUIR	12
11	IUIR	11
10	IUIR	10
9	IUIR	9
8	IUIR	8
7	IUIR	7
6	IUIR	6
5	IUIR	5
4	IUIR	4
3	IUIR	3
2	W2W2W2W2	2
1	W2W2ISISISISISISISISISISISISISW2W2									1

J I= 2 4 6 8 10 12 14 16

CELL TYPES: K = 29

J	I=	2	4	6	8	10	12	14	16	
17	W2W2W2W2W2W2W2W2W2W2W2W2W2W2W2W2									17
16	W2W2W2W2	16
15	W2W2	15
14	W2W2	14
13	W2W2	13
12	W2W2	12
11	W2W2	11
10	W2W2	10
9	W2W2	9
8	W2W2	8
7	W2W2	7
6	W2W2	6
5	W2W2	5
4	W2W2	4
3	W2W2	3
2	W2W2W2W2	2
1	W2W2ISISISISISISISISISISISW2W2									1

J I= 2 4 6 8 10 12 14 16

CELL TYPES: K = 30 to 42

J	I=	2	4	6	8	10	12	14	16	
17	W2W2W2W2W2W2W2W2W2W2W2W2W2W2W2W2									17
16	W2W2W2W2	16
15	W2W2	15
14	W2W2	14
13	W2W2	13
12	W2W2	12
11	W2W2	11
10	W2W2	10
9	W2W2	9
8	W2W2	8
7	W2W2	7
6	W2W2	6
5	W2W2	5
4	W2W2	4
3	W2W2	3
2	W2W2W2W2	2
1	W2W2W2W2W2W2W2W2W2W2W2W2W2W2W2W2									1

J I= 2 4 6 8 10 12 14 16

- VELOCITY BOUNDARY CONDITIONS -

ZONE	U-VEL.	V-VEL.	W-VEL.
W1	0.00E+00	0.00E+00	0.00E+00
W2	0.00E+00	0.00E+00	0.00E+00
I1	-2.24E+00	-8.04E-01	1.15E+01
I2	-4.16E-01	0.00E+00	2.14E+00
I3	-2.33E+00	8.37E-01	1.20E+01
I6	0.00E+00	0.00E+00	3.86E-01
I8	6.29E+00	2.61E+00	1.64E+01
I9	-1.27E+01	5.28E+00	1.64E+01
ID	0.00E+00	0.00E+00	1.99E+00
IJ	0.00E+00	0.00E+00	1.57E+00
IK	0.00E+00	0.00E+00	1.86E+00
IL	0.00E+00	0.00E+00	1.18E+00
IM	0.00E+00	0.00E+00	2.70E+00
IR	-4.67E-01	0.00E+00	0.00E+00
IS	0.00E+00	4.51E-01	0.00E+00
IT	0.00E+00	-5.35E-01	0.00E+00
IU	4.67E-01	0.00E+00	0.00E+00

- CHEMICAL SPECIES BOUNDARY CONDITIONS (*) -

ZONE	CH4	O2	CO2	H2O	CARBON (S)
W1	LINK CUT	LINK CUT	LINK CUT	LINK CUT	LINK CUT
W2	LINK CUT	LINK CUT	LINK CUT	LINK CUT	LINK CUT
I1	1.8380E-01	1.6200E-01	2.0000E-04	4.1700E-02	1.8400E-03
I2	0.0000E+00	2.0450E-01	2.9280E-04	2.4000E-02	0.0000E+00
I3	2.1870E-01	1.5500E-01	2.0000E-04	4.0600E-02	2.1900E-03
I6	0.0000E+00	0.0000E+00	1.0000E-06	1.0000E+00	0.0000E+00
I8	0.0000E+00	2.0450E-01	2.9300E-04	2.4000E-02	0.0000E+00
I9	0.0000E+00	2.0450E-01	2.9300E-04	2.4000E-02	0.0000E+00
ID	0.0000E+00	2.0450E-01	2.9300E-04	2.4000E-02	0.0000E+00
IJ	0.0000E+00	2.0450E-01	2.9300E-04	2.4000E-02	0.0000E+00
IK	0.0000E+00	2.0450E-01	2.9300E-04	2.4000E-02	0.0000E+00
IL	0.0000E+00	2.0450E-01	2.9300E-04	2.4000E-02	0.0000E+00
IM	0.0000E+00	2.0450E-01	2.9300E-04	2.4000E-02	0.0000E+00
IR	0.0000E+00	2.0450E-01	2.9300E-04	2.4000E-02	0.0000E+00
IS	0.0000E+00	2.0450E-01	2.9300E-04	2.4000E-02	0.0000E+00
IT	0.0000E+00	2.0450E-01	2.9300E-04	2.4000E-02	0.0000E+00
IU	0.0000E+00	2.0450E-01	2.9300E-04	2.4000E-02	0.0000E+00

(*) - MOLE FRACTIONS

- TEMPERATURE BOUNDARY CONDITIONS -

ZONE	TEMPERATURE
W1	HEAT FLUX
W2	HEAT FLUX
I1	3.0920E+02
I2	3.0600E+02
I3	3.0914E+02
I6	4.3300E+02
I8	3.0600E+02
I9	3.0600E+02
ID	4.0000E+02
IJ	5.0000E+02
IK	5.0000E+02
IL	5.0000E+02
IM	5.0000E+02
IR	5.0000E+02
IS	3.5000E+02
IT	5.0000E+02
IU	5.0000E+02

- SPECIAL TEMPERATURE BOUNDARIES -

ZONE	HEAT FLUX BOUNDARY	HEAT FLUX VALUE	EXT. H-T BOUNDARY	EXTERNAL HEAT TRANSFER COEFF.	EXT. TEMP.
W1	Y	0.00E+00	N	N/A	N/A
W2	Y	0.00E+00	N	N/A	N/A

ZONE	EXT. RAD BOUNDARY	T-INFINITY	EXT. EMISS.
W1	N	N/A	N/A
W2	N	N/A	N/A

VARIABLE	SOLVED	BLOCK CORRECT	NO. SWEEPS	UNDERRELAX 1	RESIDUAL AT 2000 ITERATIONS
PRESSURE	YES	NO	30	6.0000E-01	4.5908E-06
U-VELOCITY	YES	NO	10	3.0000E-01	2.1135E-05
V-VELOCITY	YES	NO	1	3.0000E-01	5.6471E-06
W-VELOCITY	YES	NO	1	3.0000E-01	3.5671E-06
TURB. K.E.	YES	NO	1	3.0000E-01	3.9119E-07
K.E. DISS.	YES	NO	1	3.0000E-01	3.2921E-07
ENIHALPY	YES	NO	30	6.0000E-01	2.5749E-06
CH4	YES	NO	30	4.0000E-01	1.1699E-04
O2	YES	NO	1	4.0000E-01	1.0947E-07
CO2	YES	NO	1	4.0000E-01	2.4017E-07
H2O	YES	NO	1	4.0000E-01	1.6366E-07
CARBON (S)	YES	NO	30	4.0000E-01	4.2001E-07
PROPERTIES	YES	N/A	N/A	N/A	N/A
VISCOSITY	N/A	N/A	N/A	3.0000E-01	N/A
TEMPERATURE	N/A	N/A	N/A	7.0000E-01	N/A
RADIATION	YES	N/A	N/A	N/A	N/A

RADIATION SOLVED EVERY 5 ITERATIONS

MAXIMUM NUMBER OF DIRM ITERATIONS = 10

DIRM ITERATION TOLERANCE = 1.0000E-03

3) TA-OFF DATA FROM JAKWAY ET AL. (1995A, 1995B) COARSE GRID

BASE INFILTRATION AIR DISTRIBUTION,
1% SOOT FOR 1ST 1/3 OF KILN
KA9B.LP, CREATED FROM KA9B.CAS & .DAT ON 4 MAY95

This section contains only the differences with the model case presented in section H-1 of this appendix.

- GEOMETRY -

BOUNDARY FITTED COORDINATES

NI = 17 NJ = 17 NK = 34

- VELOCITY BOUNDARY CONDITIONS -

ZONE	U-VEL.	V-VEL.	W-VEL.
W1	0.00E+00	0.00E+00	0.00E+00
I1	-2.23E+00	-8.00E-01	1.14E+01
I2	-4.18E-01	0.00E+00	2.15E+00
I3	-2.35E+00	8.44E-01	1.21E+01
I6	0.00E+00	0.00E+00	3.85E-01
I8	0.00E+00	0.00E+00	0.00E+00
I9	0.00E+00	0.00E+00	0.00E+00
ID	0.00E+00	0.00E+00	2.16E+00
IJ	0.00E+00	0.00E+00	1.63E+00
IK	0.00E+00	0.00E+00	1.95E+00
IL	0.00E+00	0.00E+00	1.25E+00
IM	0.00E+00	0.00E+00	2.83E+00
IR	-4.37E-01	0.00E+00	0.00E+00
IS	0.00E+00	4.17E-01	0.00E+00
IT	0.00E+00	-4.95E-01	0.00E+00
IU	4.37E-01	0.00E+00	0.00E+00

- CHEMICAL SPECIES BOUNDARY CONDITIONS (MOLE FRACTIONS) -

ZONE	CH4	O2	CO2	H2O	CARBON (S)
W1	LINK CUT	LINK CUT	LINK CUT	LINK CUT	LINK CUT
I1	1.8380E-01	1.6220E-01	2.0000E-04	4.1700E-02	1.8400E-03
I2	0.0000E+00	2.0450E-01	2.9300E-04	2.4000E-02	0.0000E+00
I3	2.1870E-01	1.5520E-01	2.0000E-04	4.0600E-02	2.1900E-03
I6	0.0000E+00	0.0000E+00	1.0000E-06	1.0000E+00	0.0000E+00
I8	0.0000E+00	2.0450E-01	2.9300E-04	2.4000E-02	0.0000E+00
I9	0.0000E+00	2.0450E-01	2.9300E-04	2.4000E-02	0.0000E+00
ID	0.0000E+00	2.0450E-01	2.9300E-04	2.4000E-02	0.0000E+00
IJ	0.0000E+00	2.0450E-01	2.9300E-04	2.4000E-02	0.0000E+00
IK	0.0000E+00	2.0450E-01	2.9300E-04	2.4000E-02	0.0000E+00
IL	0.0000E+00	2.0450E-01	2.9300E-04	2.4000E-02	0.0000E+00
IM	0.0000E+00	2.0450E-01	2.9300E-04	2.4000E-02	0.0000E+00
IR	0.0000E+00	2.0450E-01	2.9300E-04	2.4000E-02	0.0000E+00
IS	0.0000E+00	2.0450E-01	2.9300E-04	2.4000E-02	0.0000E+00
IT	0.0000E+00	2.0450E-01	2.9300E-04	2.4000E-02	0.0000E+00
IU	0.0000E+00	2.0450E-01	2.9300E-04	2.4000E-02	0.0000E+00

- TEMPERATURE BOUNDARY CONDITIONS -

ZONE	TEMPERATURE
W1	HEAT FLUX
I1	3.0740E+02
I2	3.0730E+02
I3	3.0730E+02
I6	4.3300E+02
I8	3.0600E+02
I9	3.0600E+02
ID	4.0000E+02
IJ	5.0000E+02
IK	5.0000E+02
IL	5.0000E+02
IM	5.0000E+02
IR	5.0000E+02
IS	3.5000E+02
IT	5.0000E+02
IU	5.0000E+02

VARIABLE	SOLVED	BLOCK CORRECT	NO. SWEEPS	UNDERRELAX 1	RESIDUAL AT 1020 ITERATIONS
PRESSURE	YES	NO	30	6.0000E-01	5.0541E-07
U-VELOCITY	YES	NO	10	3.0000E-01	3.7573E-05
V-VELOCITY	YES	NO	1	3.0000E-01	7.6067E-06
W-VELOCITY	YES	NO	1	3.0000E-01	4.8676E-06
TURB. K.E.	YES	NO	1	3.0000E-01	8.9371E-07
K.E. DISS.	YES	NO	1	3.0000E-01	4.5345E-07
ENTHALPY	YES	NO	30	6.0000E-01	7.7974E-07
CH4	YES	NO	30	4.0000E-01	2.4824E-04
O2	YES	NO	1	4.0000E-01	8.9696E-08
CO2	YES	NO	1	4.0000E-01	1.7838E-07
H2O	YES	NO	1	4.0000E-01	1.3404E-07
CARBON (S)	YES	NO	30	4.0000E-01	2.8547E-07
PROPERTIES	YES	N/A	N/A	N/A	N/A
VISCOSITY	N/A	N/A	N/A	3.0000E-01	N/A
TEMPERATURE	N/A	N/A	N/A	6.0000E-01	N/A
RADIATION	YES	N/A	N/A	N/A	N/A

4) TA-ON DATA FROM LEGER ET AL. (1991A, 1993A, 1993B), COARSE GRID

BASE INFILTRATION AIR DISTRIBUTION,
 1% SOOT FOR 1ST 1/3 OF KILN
 KA8W.CAS AND DAT 21 MAY 95.
 LP ON 27 AUG 95

This section contains only the differences with the model case presented in section H-1 of this appendix.

- VELOCITY BOUNDARY CONDITIONS -

ZONE	U-VEL.	V-VEL.	W-VEL.
W1	0.00E+00	0.00E+00	0.00E+00
I1	-2.26E+00	-8.12E-01	1.16E+01
I2	-4.10E-01	0.00E+00	2.11E+00
I3	-2.33E+00	8.38E-01	1.20E+01
I6	0.00E+00	0.00E+00	3.86E-01
I8	7.79E+00	3.23E+00	2.04E+01
I9	-1.58E+01	6.54E+00	2.04E+01
ID	0.00E+00	0.00E+00	1.99E+00
IJ	0.00E+00	0.00E+00	1.52E+00
IK	0.00E+00	0.00E+00	1.81E+00
IL	0.00E+00	0.00E+00	1.16E+00
IM	0.00E+00	0.00E+00	2.63E+00
IR	-4.07E-01	0.00E+00	0.00E+00
IS	0.00E+00	3.87E-01	0.00E+00
IT	0.00E+00	-4.60E-01	0.00E+00
IU	4.06E-01	0.00E+00	0.00E+00

- CHEMICAL SPECIES BOUNDARY CONDITIONS (*) -

ZONE	CH4	O2	CO2	H2O	CARBON (S)
W1	LINK CUT	LINK CUT	LINK CUT	LINK CUT	LINK CUT
I1	1.9260E-01	1.6060E-01	2.0000E-04	4.0800E-02	1.8400E-03
I2	0.0000E+00	2.0450E-01	2.9300E-04	2.4000E-02	0.0000E+00
I3	2.3560E-01	1.5440E-01	2.0000E-04	2.7300E-02	2.1900E-03
I6	0.0000E+00	0.0000E+00	1.0000E-06	1.0000E+00	0.0000E+00
I8	0.0000E+00	2.0450E-01	2.9300E-04	2.4000E-02	0.0000E+00
I9	0.0000E+00	2.0450E-01	2.9300E-04	2.4000E-02	0.0000E+00
ID	0.0000E+00	2.0450E-01	2.9300E-04	2.4000E-02	0.0000E+00
IJ	0.0000E+00	2.0450E-01	2.9300E-04	2.4000E-02	0.0000E+00
IK	0.0000E+00	2.0450E-01	2.9300E-04	2.4000E-02	0.0000E+00
IL	0.0000E+00	2.0450E-01	2.9300E-04	2.4000E-02	0.0000E+00
IM	0.0000E+00	2.0450E-01	2.9300E-04	2.4000E-02	0.0000E+00
IR	0.0000E+00	2.0450E-01	2.9300E-04	2.4000E-02	0.0000E+00
IS	0.0000E+00	2.0450E-01	2.9300E-04	2.4000E-02	0.0000E+00
IT	0.0000E+00	2.0450E-01	2.9300E-04	2.4000E-02	0.0000E+00
IU	0.0000E+00	2.0450E-01	2.9300E-04	2.4000E-02	0.0000E+00

(*) - MOLE FRACTIONS

- TEMPERATURE BOUNDARY CONDITIONS -

ZONE	TEMPERATURE
W1	HEAT FLUX
I1	3.0910E+02
I2	3.0730E+02
I3	3.0730E+02
I6	4.3300E+02
I8	3.0600E+02
I9	3.0600E+02
ID	4.0000E+02
IJ	5.0000E+02
IK	5.0000E+02
IL	5.0000E+02
IM	5.0000E+02
IR	5.0000E+02
IS	3.5000E+02
IT	5.0000E+02
IU	5.0000E+02

VARIABLE	SOLVED	BLOCK CORRECT	NO. SWEEPS	UNDERRELAX 1	RESIDUAL AT 961 ITERATIONS
PRESSURE	YES	NO	30	6.0000E-01	3.5715E-07
U-VELOCITY	YES	NO	10	3.0000E-01	3.9129E-05
V-VELOCITY	YES	NO	1	3.0000E-01	1.3635E-05
W-VELOCITY	YES	NO	1	3.0000E-01	5.8008E-06
TURB. K.E.	YES	NO	1	3.0000E-01	8.1869E-06
K.E. DISS.	YES	NO	1	3.0000E-01	1.9579E-06
ENIHALPY	YES	NO	30	6.0000E-01	9.9547E-07
CH4	YES	NO	30	4.0000E-01	1.9978E-04
O2	YES	NO	1	4.0000E-01	4.4787E-07
CO2	YES	NO	1	4.0000E-01	1.2841E-06
H2O	YES	NO	1	4.0000E-01	8.7358E-07
CARBON (S)	YES	NO	30	4.0000E-01	1.4400E-06
PROPERTIES	YES	N/A	N/A	N/A	N/A
VISCOSITY	N/A	N/A	N/A	3.0000E-01	N/A
TEMPERATURE	N/A	N/A	N/A	6.0000E-01	N/A
RADIATION	YES	N/A	N/A	N/A	N/A

RADIATION SOLVED EVERY 5 ITERATIONS

MAXIMUM NUMBER OF DTRM ITERATIONS = 10

DTRM ITERATION TOLERANCE = 1.0000E-03

5) TA-OFF DATA FROM LEGER ET AL. (1991A, 1993A, 1993B) COARSE GRID

BASE INFILTRATION AIR DISTRIBUTION,
1% SOOT FOR 1ST 1/3 OF KILN
KA8X.CAS AND DAT 21 MAY 95.
LP ON 27 AUG 95

This section contains only the differences with the model case presented in section H-1 of this appendix.

- VELOCITY BOUNDARY CONDITIONS -

ZONE	U-VEL.	V-VEL.	W-VEL.
WL	0.00E+00	0.00E+00	0.00E+00
I1	-2.15E+00	-7.74E-01	1.11E+01
I2	-4.10E-01	0.00E+00	2.11E+00
I3	-2.12E+00	7.61E-01	1.09E+01
I6	0.00E+00	0.00E+00	2.45E-01
I8	0.00E+00	0.00E+00	0.00E+00
I9	0.00E+00	0.00E+00	0.00E+00
ID	0.00E+00	0.00E+00	1.61E+00
IJ	0.00E+00	0.00E+00	1.21E+00
IK	0.00E+00	0.00E+00	1.45E+00
IL	0.00E+00	0.00E+00	9.25E-01
IM	0.00E+00	0.00E+00	2.10E+00
IR	-3.25E-01	0.00E+00	0.00E+00
IS	0.00E+00	3.10E-01	0.00E+00
IT	0.00E+00	-3.68E-01	0.00E+00
IU	3.25E-01	0.00E+00	0.00E+00

- CHEMICAL SPECIES BOUNDARY CONDITIONS (*) -

ZONE	CH4	O2	CO2	H2O	CARBON (S)
W1	LINK CUT	LINK CUT	LINK CUT	LINK CUT	LINK CUT
I1	1.5590E-01	1.6790E-01	2.0000E-04	4.2700E-02	1.8400E-03
I2	0.0000E+00	2.0400E-01	2.9300E-04	2.4000E-02	0.0000E+00
I3	1.5760E-01	1.7000E-01	2.0000E-04	3.0500E-02	2.1900E-03
I6	0.0000E+00	0.0000E+00	1.0000E-06	1.0000E+00	0.0000E+00
I8	0.0000E+00	2.0450E-01	2.9300E-04	2.4000E-02	0.0000E+00
I9	0.0000E+00	2.0450E-01	2.9300E-04	2.4000E-02	0.0000E+00
ID	0.0000E+00	2.0450E-01	2.9300E-04	2.4000E-02	0.0000E+00
IJ	0.0000E+00	2.0450E-01	2.9300E-04	2.4000E-02	0.0000E+00
IK	0.0000E+00	2.0450E-01	2.9300E-04	2.4000E-02	0.0000E+00
IL	0.0000E+00	2.0450E-01	2.9300E-04	2.4000E-02	0.0000E+00
IM	0.0000E+00	2.0450E-01	2.9300E-04	2.4000E-02	0.0000E+00
IR	0.0000E+00	2.0450E-01	2.9300E-04	2.4000E-02	0.0000E+00
IS	0.0000E+00	2.0450E-01	2.9300E-04	2.4000E-02	0.0000E+00
IT	0.0000E+00	2.0450E-01	2.9300E-04	2.4000E-02	0.0000E+00
IU	0.0000E+00	2.0450E-01	2.9300E-04	2.4000E-02	0.0000E+00

(*) - MOLE FRACTIONS

- TEMPERATURE BOUNDARY CONDITIONS -

ZONE	TEMPERATURE
W1	HEAT FLUX
I1	3.0930E+02
I2	3.0600E+02
I3	3.0750E+02
I6	4.3300E+02
I8	3.0600E+02
I9	3.0600E+02
ID	4.0000E+02
IJ	5.0000E+02
IK	5.0000E+02
IL	5.0000E+02
IM	5.0000E+02
IR	5.0000E+02
IS	3.5000E+02
IT	5.0000E+02
IU	5.0000E+02

VARIABLE	SOLVED	BLOCK CORRECT	NO. SWEEPS	UNDERRELAX 1	RESIDUAL AT 974 ITERATIONS
PRESSURE	YES	NO	30	6.0000E-01	3.9602E-07
U-VELOCITY	YES	NO	10	3.0000E-01	4.2599E-05
V-VELOCITY	YES	NO	1	3.0000E-01	1.0678E-05
W-VELOCITY	YES	NO	1	3.0000E-01	5.8918E-06
TURB. K.E.	YES	NO	1	3.0000E-01	6.2791E-06
K.E. DISS.	YES	NO	1	3.0000E-01	2.8232E-06
ENIHALPY	YES	NO	30	6.0000E-01	9.8728E-07
CH4	YES	NO	30	4.0000E-01	4.2840E-04
O2	YES	NO	1	4.0000E-01	5.3595E-07
CO2	YES	NO	1	4.0000E-01	1.6965E-06
H2O	YES	NO	1	4.0000E-01	1.0851E-06
CARBON (S)	YES	NO	30	4.0000E-01	1.7105E-06
PROPERTIES	YES	N/A	N/A	N/A	N/A
VISCOSITY	N/A	N/A	N/A	3.0000E-01	N/A
TEMPERATURE	N/A	N/A	N/A	6.0000E-01	N/A
RADIATION	YES	N/A	N/A	N/A	N/A

RADIATION SOLVED EVERY 5 ITERATIONS

MAXIMUM NUMBER OF DIRM ITERATIONS = 10

DIRM ITERATION TOLERANCE = 1.0000E-03

VITA

Allen Lee Jakway was born at the venerable Baptist Hospital in New Orleans on the 27th of February in 1962. He attended Lakeview elementary after which his parents sacrificed to get him into St. John Lutheran for Junior High. For high school he attended Benjamin Franklin magnet. A full scholarship convinced him to stay at home and attend the University of New Orleans where he earned his Bachelor of Science degree in Mechanical Engineering graduating *cum laude* at the top of his engineering class. Chevron Chemical in Belle Chasse, Louisiana employed him for the next several years where he first became interested in the environmental area of engineering. Throughout this time, the author was active in his church particularly in the youth group where he was introduced to singing and acting in musicals. A four year fellowship offer then attracted the author to Baton Rouge to attend Louisiana State University. Summers spent in Utah and New Mexico conducting research have been particularly rewarding as have the experiences of delivering professional conference presentations in Baton Rouge, New Orleans, Boston, and Seattle. After graduation, the author plans to fulfill a long time dream of seeing this country at a relaxed and more intimate pace by bicycling and camping across this continent.

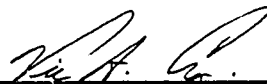
DOCTORAL EXAMINATION AND DISSERTATION REPORT

Candidate: Allen Lee Jakway

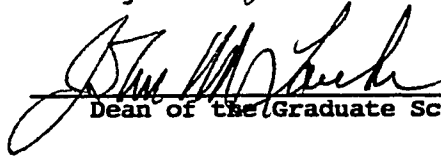
Major Field: Mechanical Engineering

Title of Dissertation: Experimental and Numerical-Modeling Studies of a Field-Scale Hazardous Waste Rotary Kiln Incinerator

Approved:

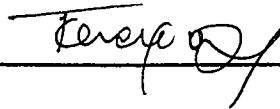

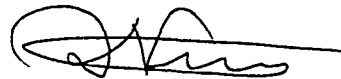
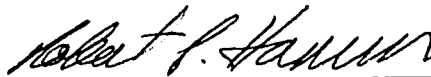
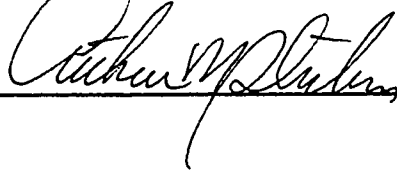


Major Professor and Chairman



Dean of the Graduate School

EXAMINING COMMITTEE:



Date of Examination:

09/29/95